Investigations of Ferrocenyl-Functionalized Organotin Chalcogenide and Oxide Complexes

DISSERTATION

Zur Erlangung des akademischen Grades eines

Doktors der Naturwissenschaften

(Dr. rer. nat.)

dem Fachbereich Chemie der Philipps-Universität Marburg

vorgelegt von Diplom-Chemiker

Zhiliang You

aus Suzhou V. R. China

Marburg/Lahn 2014

Hochschulkennziffer: 1180

Die vorliegende Arbeit entstand in der Zeit von Juni 2010 bis Juli 2014 unter Anleitung von Prof. Dr. Stefanie Dehnen am Fachbereich Chemie der Philipps-Universität Marburg.

Vom Fachbereich Chemie der Philipps-Universität Marburg als Dissertation am 08. Dezember 2014 angenommen.

1. Gutachter: Prof. Dr. Stefanie Dehnen
2. Gutachter: Prof. Dr. Jörg Sundermeyer

Tag der Mündlichen Prüfung: 10. Dezember 2014

Meinen Eltern gewidmet

“I don´t know anything, but I do know that everything is interesting if you go into it deeply enough.”

Richard Feynman

白日依山尽　黄河入海流

欲穷千里目　更上一层楼

——登鹳雀楼

王之涣

Contents

1 Introduction

1.1 Compounds with binary or ternary inorganic chalcogenidometalate anions

The chemistry of group 14 chalcogenidometalates with according anions $[T_yE_z]^{q-}$ (T = Sn, Ge; E = S, Se, Te; q charge) and alkali, alkaline earth metal or ammonium cations have been intensively investigated since the middle of last century due to the wide range of properties such as semiconductivity, photoconductivity, non-linear optics, catalysis and ion exchange capability.[1] Chalcongenidotretelates, in particular, can be synthesized by reactions in solution at ambient temperature, in high-temperature melt or by solid-state reactions, where the products exhibit versatile structural features. These range from monomeric through oligomeric to polymeric framework structures, which can be characterized in detail by means of modern analysis methods, particularly the X-ray diffraction and Raman spectroscopy.[2] The combination of transition metal ions with chalcogenidotetrelates yields ternary chalcogenidometalates anions with the general composition of $[M_xT_yE_z]^{q-}$ (M = transition metal), representing a class of compounds with combined or mixed properties derived from the corresponding parent compounds, such as, respective opto-electronic or magnetic behavior, attracting increasing attention.[3]

1.1.1 Compounds with binary inorganic chalcogenidotetrelate anions

The simplest and fundamental binary chalcogenidotetrelate units are the tetrahedral *ortho*-anions $[TE_4]^{4-}$ (T = Ge, Sn; E = S, Se), which can be isolated from aqueous solutions. These units are stable in strongly alkaline solutions, but condense to oligomeric units such as $[Sn_2S_7]^{6-}$, $[Sn_2S_6]^{4-}$ and $[Sn_4S_{10}]^{4-}$ or polymeric chains $[(SnS_3)^{2-}]_n$ through the corner- or edge-connections on lowering the pH value. The corresponding condensation pathways, established by Krebs and co-workers,[2c] are shown in Figure 1.1, for the $[SnS_4]^{4-}$ anion for instance.

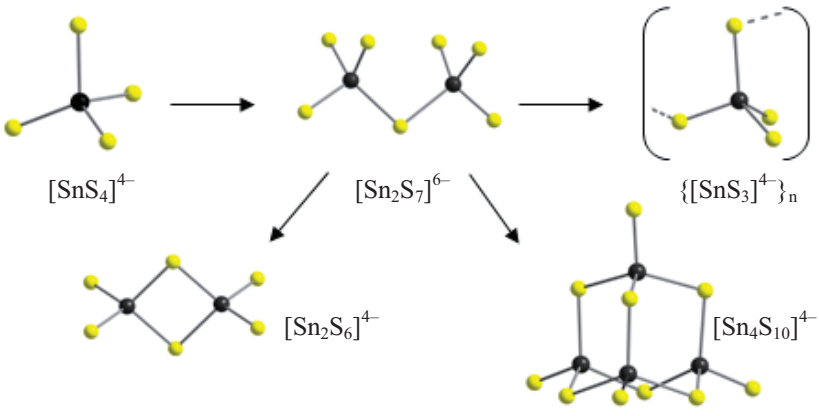

Figure 1.1 Condensation pathways of the $[SnS_4]^{4-}$ anions in aqueous solution.

For the successful isolation of pure phases with polymeric structures, such as infinite chains, sheets or frameworks, condensations under hydro-(solvo)thermal conditions are usually chosen. Due to the complexity of the hydro(solvo)thermal reactions, designing or predicting the structures and compositions of the reaction products is impossible, however, due to the intensive research in this area during the last decades, a number of chalcogenidometalate compounds have been synthesized. A variety of (often interdependent) factors, which can influence the reactions, have been discovered. These include the counter cation size and charge, solvent polarity and temperature, besides the previously mentioned pH value, and their impact on the reactions has been reviewed by Sheldrick.[2b] For instance, in the extensive work of Ozin *et al*., a series of hexagonal-shaped sheets of 24-atom rings with the general composition of $\{[Sn_3S_7]^{2-}\}_n$ (Figure 1.2) were obtained in the presence of $[Et_4N]^+$, $DABCOH^+$ (protonated 1,8-diazabicyclooctane) and a mixed cationic system of $[NH_4]^+/[Et_4N]^+$, while the reactions in the presence of $[^nPr_4N]^+$ and $[^nBu_4N]^+$ yielded elliptical-shaped sheets of 32-atom rings with the general composition of $\{[Sn_4S_9]^{2-}\}_n$. Both types of structures are based on *semi*-cube-like (SC) units $[Sn_3S_4]$, and can be further extended through the linkage of each of all Sn atoms by two μ-S atoms each. The different counterions play a structure-directing role, not only leading to the formation of two different structures, but also resulting in a variety of different void spaces within and between the thiostannte sheets in the same structure due to different counterion sizes.[4]

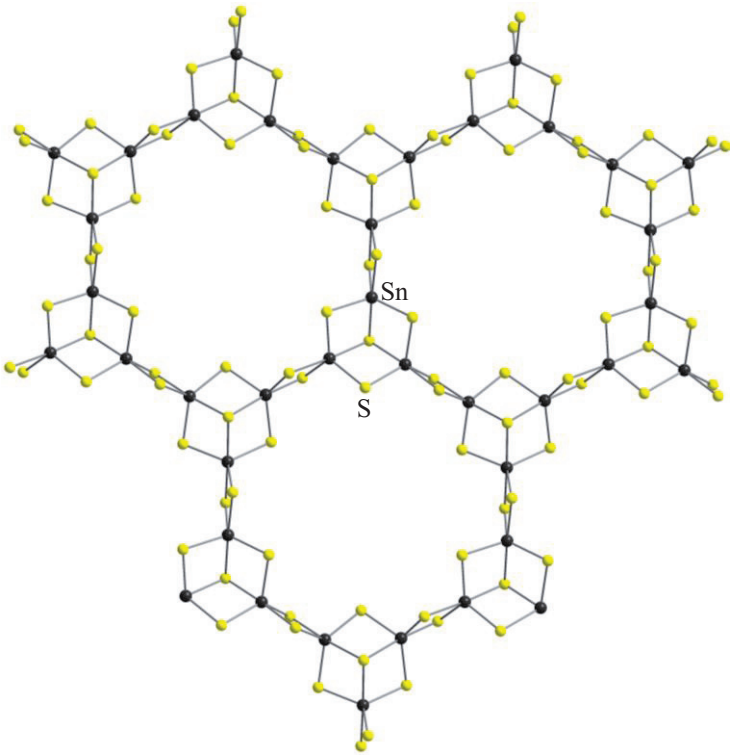

Figure 1.2 Fragment of one sheet of $\{[Sn_3S_7]^{2-}\}_n$.[4]

Compared to water or organic solvents, ionic liquids are advantageous because of negligible vapor pressure, high thermal stability, wide liquidus range and the ability to dissolve a variety of materials,[5] and have therefore been recently increasingly employed in the synthesis of zeolites,[6] metal-organic frameworks,[7] and nanomaterials.[8] Starting with $[Ge_4Se_{10}]^{4-}$, in the presence of $SnCl_4 \cdot 5H_2O$, the largest main-group element polyanion, so-called "zeoball" consisting of 192 Sn/Ge/Se atoms, was synthesized in our group with the use of the ionic liquids (Figure 1.3).[9]

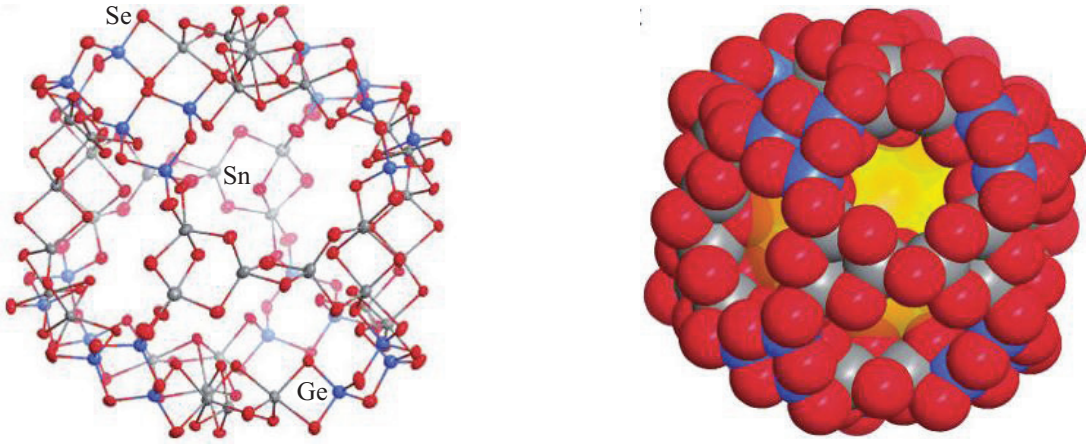

Figure 1.3 Structure of the polyanionic "zeoball" $[Sn_{36}Ge_{24}Se_{132}]^{24-}$ (left) and its corresponding space-filling model (right).[9]

1.1.2 Compounds with ternary inorganic chalcogenidometalate anions

Many compounds with ternary inorganic chalcogenidometalate anions that combine the transition metal atoms with atoms of group 14 and 16 elements have been efficiently generated by metathesis reactions of binary chalcogenidotetrelat building units like the monomeric $[TE_4]^{4-}$, dimeric $[T_2E_6]^{4-}$, or the adamantane-like $[T_4E_{10}]^{4-}$ anions with transition metal ions under ambient conditions in solution.[3c,d,10] The advantage of this synthetic methodology over hydro(solo)thermal reactions with separate sources of the three components,[11] is that the chalcogenidotetrelate units usually maintain their structures under the mild reaction conditions; hence, they can coordinate to the transition metal cations through the terminal chalcogenide ligands under formation of ternary molecular anions or nanostructured or mesostructured derivatives with well-defined spatial separation of the transition metal atoms. For instance, the *ortho*-chalcogenidostannte anions $[SnE_4]^{4-}$ (E = S, Se and Te) react with transition metal cations M^{2+} (M = Co, Zn, Mn, Cd, Hg) in water and/or in alcoholic solution to form a series of *P*1- and *T*3-type ternary clusters, three of which are shown as example in Figure 1.4.[12] On the other hand, reactions of the adamantane-like anions $[T_4E_{10}]^{4-}$ (T = Ge, Sn; E = S, Se) with different transition metal cations analogously led to the formation of a family of ternary porous open-framework compounds, one of which is shown in Figure 1.5.[3c,d]

To examine and confirm the mentioned combination or mixture of physical properties, investigations of the optical absorption behaviors were carried out on diverse series of structurally well-defined compounds, like the *P*1-type clusters, by UV-visible spectroscopy. This showed that the electronic excitation energies are finely tunable by variation of the involved atoms. As shown in Figure 1.6, the family of compounds with ternary *P*1-type clusters $[K_{10}(ROH)_n][M_4(\mu_4\text{-}E)(SnE_4)_4]$ (M = Hg, Mn, Cd, Zn; E = Se, Te), posses well-defined, sharp optical absorptions associated with

their electronic excitation energies. Substituting the selenide atoms with telluride atoms in the compounds leads to a strong red shift of the absorption; further fine-tuning can be achieved by exchanging the transition metal ions in the ternary anions.[12a,c]

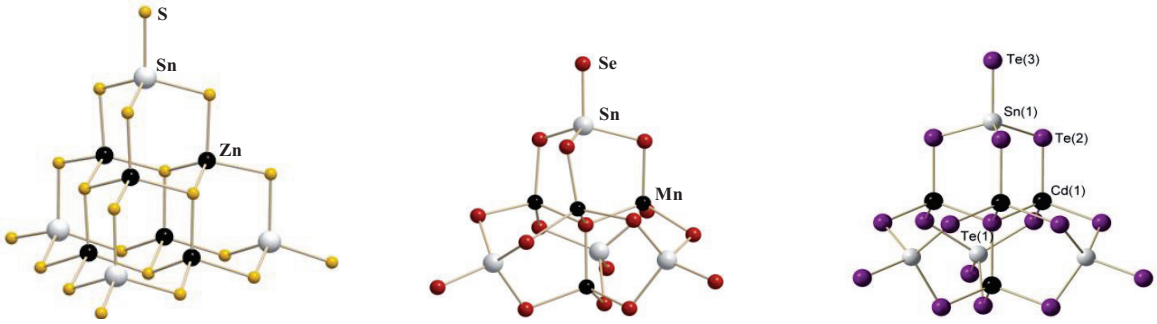

Figure 1.4 Binary $[SnE_4]^{4-}$ anion-based ternary *P*1 (center and right) and *T*3 (left) clusters.[12]

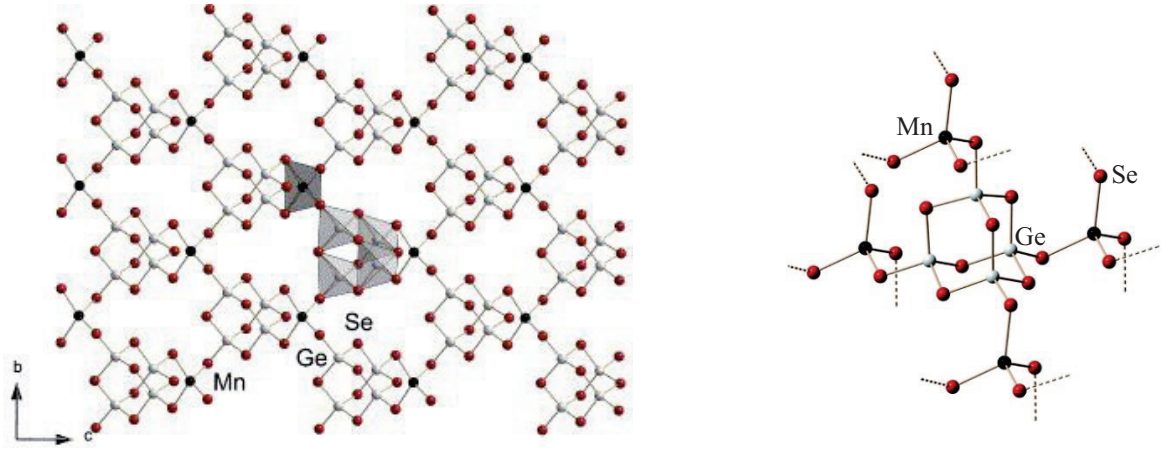

Figure 1.5 Ternary Mn/Ge/Se open-framework-structures based on binary adamantane-type anions $[Ge_4Se_{10}]^{4-}$: Fragment illustrating the coordination of an individual $[Ge_4Se_{10}]^{4-}$ unit to the transition metal cation Mn^{4+} (right); network arrangement in the crystal structure (left), solvent molecules are omitted for clarity.[3b]

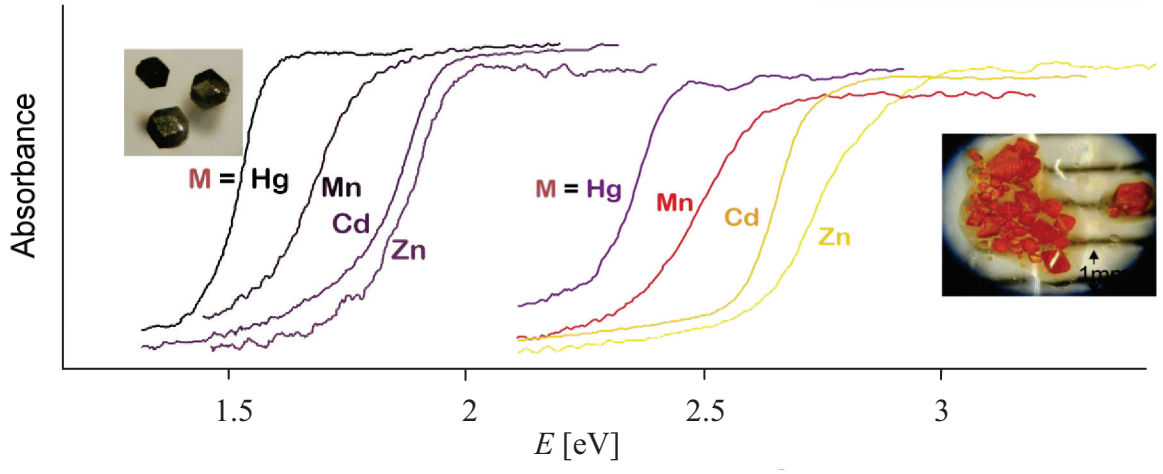

Figure 1.6 Solid state UV-visible spectra of the compounds $[K_{10}(ROH)_n][M_4(\mu_4\text{-}E)(SnE_4)_4]$ for M = Hg, Mn, Cd, Zn; E = Se (right) or Te (left), R = H, (n = 20) or R = H, Me (n = 16.5, 0.5).[3d,12a,c]

1.2 Binary and ternary organo-functionalized chalcogenidotetrelate compounds

Introduction of organic functionalities to binary chalcogenidotetrelate cages leads to the formation of corresponding hybrid complexes with an inorganic chalcogenidotetrelate core and an organic ligand shell. These do not only possess the interesting properties derived from the inorganic core, but also improved stabilities, solubilities, as well as reactivities in the case of functionalized compounds with reactive organic groups. Carbonyl groups, for example, are reactive toward hydrazine, as well as towards terminal hydrazine derivatives, hydrazones, or hydrazides.[13] Thus the organic shell can be further extended to yield new compounds or networks, in which the inorganic core can be conserved or undergo fragmentation and/or re-arrangement processes.[13a,b,d]

1.2.1 Binary organo-functionalized chalcogenidotetrelate compounds

Since 1903, a large number of binary, organo-functinalized chalcogenidotetrelate compounds have been synthesized, usually through the reaction of mono-substituted tetrel halogenide compounds RTX_3 (R = organic ligand; T = Si, Sn, Ge; X = Cl, Br) with chalcogenide sources (chalcogenide salts of alkali metals, H_2S or silylated chalcogenides $[(R_3Si)]_2E$). These exhibit mainly one of two structural modifications of the same $[T_4E_6]$ core, namely the adamantane-like (AD) or the douple-decker-like (DD) cage. Until 2009, the compounds were substituted with unreactive organic groups (R = Me, Ph, CF_3, C_6F_5, $C(SiMe_3)_3$),[14] most of them possess an AD topology. The structural investigations of these $[(RT)_4E_6]$ compounds indicated that the DD topology is kinetically preferred and can be converted to the AD variant at elevated temperature, which is especially facile for the heavier element analogs (Scheme 1.1).[15]

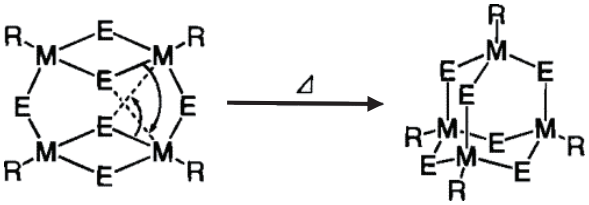

Scheme 1.1 Conversion of a double-decker like cage (DD) to an adamantane-like cage (AD) at elevated temperature.[15]

During the past five years, our group has successfully synthesized and characterized a series of AD or DD cage compounds $[(R^fT)_4E_6]$, functionalized with reactive organic groups (R^f = functional organic ligand like $R^1 = C_2H_4COO(H)$ or $R^2 = CMe_2CH_2C(Me)O$; T/E = Sn/S; Ge/S; Ge/Te). These compounds were prepared from R^fTCl_3 precursors with chalcogenide salts of alkali metals, thus *via* a similar route like the synthesis of compounds with unreactive organic groups.[13d,16] Investigations on the structural preferences of these compounds have been carried out by DFT calculations, revealing that the DD topology is energetically preferred with respect to the AD one for the Sn/S system due to the formation of five-membered rings upon O→Sn back-coordination from the

functional groups of the ligands to the tin atoms. On the other hand, for the Ge/S system the O→Ge back-coordination is not energetically favored, with insignificant energy differences between DD and AD calculated by DFT, such that the two conformers may compete and/or co-exist in solution.[13d,16b] For the heavier elementary Ge/Te system, despite the isolation of the AD cluster, a new type of structural topology noradamantane (NA) with a T–T bond has been introduced, thermodynamically favored over the DD cluster for certain ligands R^f.[17] Another organo-functionalized chalcogenidotetrelate with a *semi*-cube-like (SC) core has been generated with control of the stoichiometry of the reactants and by using less polar solvents, exhibiting a very strong stability in the gas phase.[16a] All structure types are illustrated in Figure 1.7.

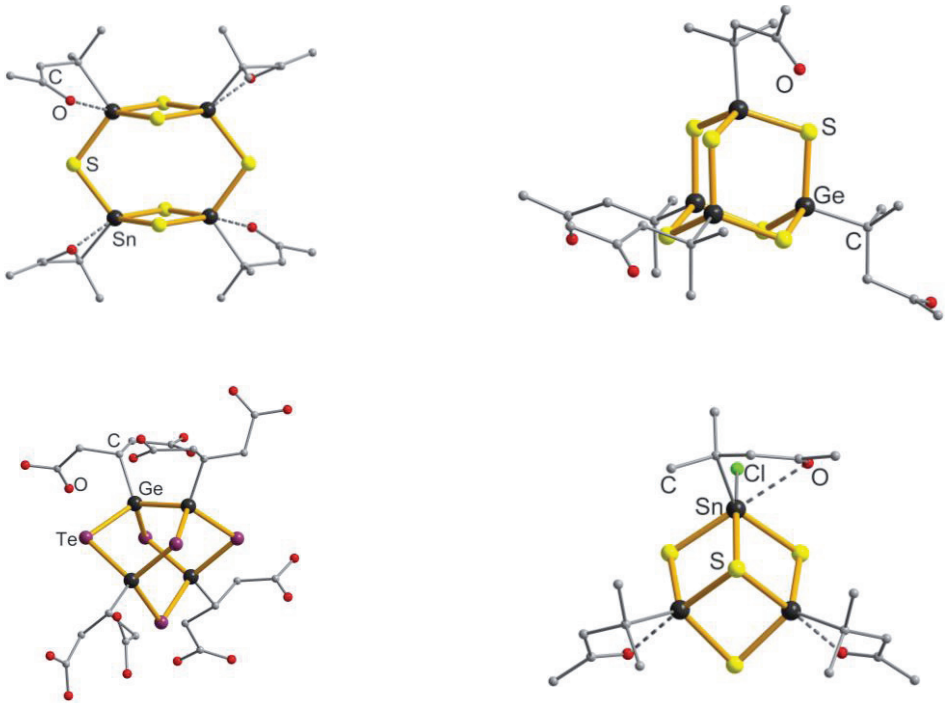

Figure 1.7 Examples of the DD ([$(R^2Sn)_4S_6$], top left), AD ([$(R^2Ge)_4S_6$], top right), NA ([$(R^4Ge)_4Te_5$], bottom left) and SC ([$(R^2Sn)_3S_4Cl$], bottom right) types of organo-functionalized chalcogenidotetrelate clusters with reactive organic groups, $R^2 = CMe_2CH_2C(Me)O$; $R^4 = CH(CH_2COOH)_2$. H atoms are omitted for clarity.

1.2.2 Ternary organo-functionalized chalcogenidotetrelate compounds

Similar to the synthesis of the ternary inorganic chalcogenidotetrelate clusters, the binary organo-functionalized chalcogenidotetrelate compounds mentioned in the last section can be used as precursors for the preparation of corresponding ternary compounds with transition metal cations. However, the lack of terminal chalcogenide ligand in the organo-decorated compounds (with formal replacement of the terminal $-E^-$ by R^f) requires another synthetic approach that affords reactive chalcogenide sites.

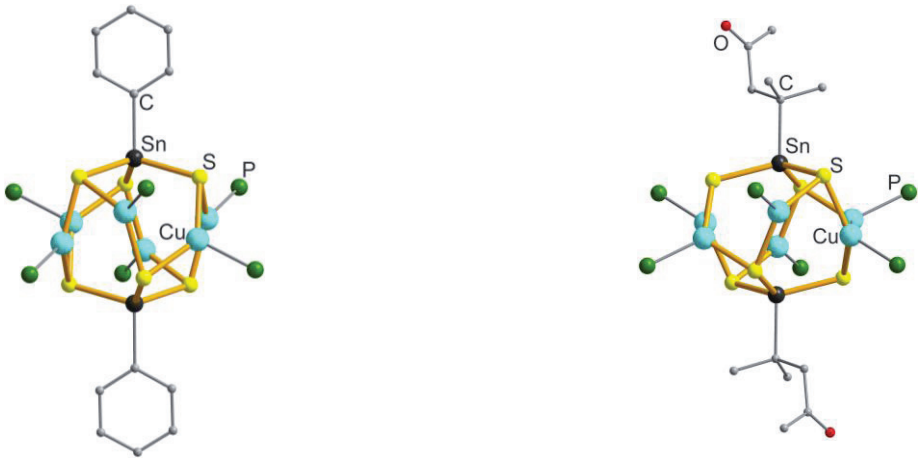

Figure 1.8 Ternary organo-functionalized chalcogenidotetrelate compounds: $[(PhSn)_2(CuPMe_2Ph)_6S_6]$ (left) and $[(R^2Sn)_2(CuPPh_3)_6S_6]$ (right). H atoms are omitted for clarity.

The *Merzweile*r group synthesized the first example of a ternary organo-functionalized chalcogenidotetrelate compound $[(PhSn)_2(CuPMe_2Ph)_6S_6]$ (Figure 1.8, left) upon *in-situ* formation of a $[PhSnS_3]^{3-}$ anion, prepared from the binary AD cluster $[(PhSn)_4S_6]$ and Na_2S in a mixture of water and THF.[14a] This reaction route was proven to be very effective; hence, a series of ternary transition metal chalcogenidotetrelate compounds was prepared in the meantime, including compounds with reactive organic groups. For example, the ternary compound $[(R^2Sn)_2(CuPPh_3)_6S_6]$ was generated by the treatment of the corresponding binary DD cluster $[(R^2Sn)_4S_6]$ with $Na_2S{\cdot}9H_2O$ and ensuing reaction with $[Cu(PPh_3)_3Cl]$, shown in figure 1.8 (right).[13d]

1.2.3 Extension of the reactive organic ligand shell

The introduction of the reactive organic groups into chalcogenidotetrelate compounds arose the opportunity to further extend the organic shell with suitable building blocks, due to an improved solubility in organic solvents and the reactivity of the organic groups. According studies were undertaken recently in our group.

For instance, the carbonyl group of the ligand R^2 in the DD cage $[(R^2Sn)_4S_6]$ (**A**) is reactive towards hydrazine hydrate, forming the reactive hydrazone ligand $CMe_2CH_2C(Me)=NNH_2$ (R^3), as well as towards terminal hydrazine derivatives, hydrazones or hydrazides.[13a,b,d] Dependent on the steric demand of the resulting ligand and their ability to realize intramolecular N→Sn back-coordination, the new organotin sulfide compounds either maintain the original DD topology or undergo fragmentation and/or re-arrangements of the Sn/S skleton. The latter occurred, for instance, at the formation of a double-SC-like (DSC) $[Sn_6S_{10}]$ cluster, or at the synthesis of a DSC cluster-based cavitand upon reaction with corresponding bis-hydrazine.[13a,b,d] Furthermore, by treatment of the

DSC cluster-based cavitand $[R^6{}_4Sn_{12}S_{20}]$ (R^6 = {$[CMe_2CH_2C(Me)=N–NH]_2C_{10}H_6$}) with $HSnCl_3 \cdot 2Et_2O$, a SC cluster-based capsule $[R^6{}_3Sn_6S_8][(SnCl_3)_2]$ was obtained, indicating the pH-sensitivity of inorganic core of such organo-functionalized compounds, similar to the observations with purely inorganic chalcogenidotetralate compounds.[13b] Figures 1.9 and 1.10 illustrate these structural changes.

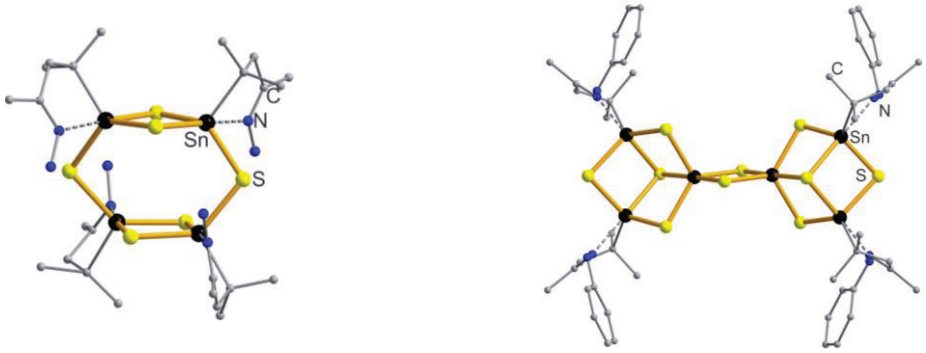

Figure 1.9 Molecular structures of the DD cluster $[(R^3Sn)_4S_6]$ (left, $R^3 = CMe_2CH_2C(Me)=NNH_2$) and of the DSC cluster $[(R^5Sn)_4Sn_2S_{10}]$ (right, $R^5 = CMe_2CH_2C(Me)NNHPh$). H atoms are omitted for clarity.

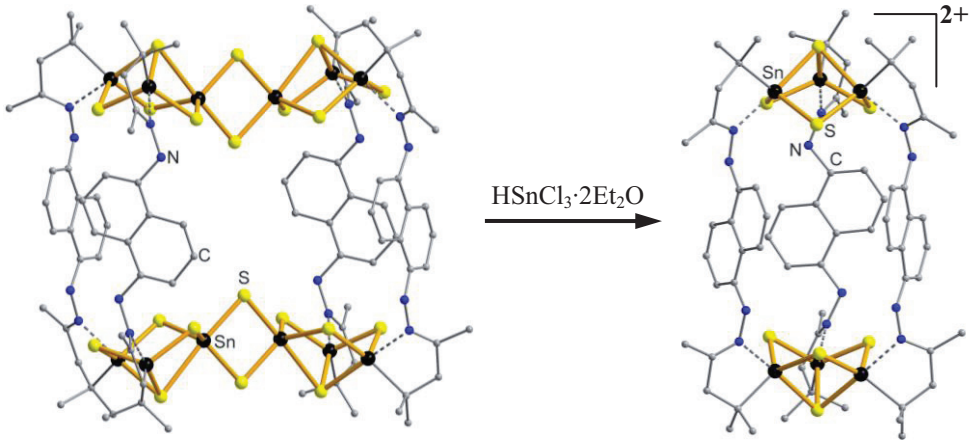

Figure 1.10 Acidification of the DSC cluster-based cavitand $[R^6{}_4Sn_{12}S_{20}]$ with $HSnCl_3 \cdot 2Et_2O$ leading to the SC cluster-based capsule $[R^6{}_3Sn_6S_8]^{2+}$, R^6 = {$[CMe_2CH_2C(Me)=N–NH]_2C_{10}H_6$}. H atoms are omitted for clarity.

Moreover, treatment of the $[(R^1Ge)_4S_6]$ cluster with $MnCl_2 \cdot 4H_2O$ under solvothermal conditions in a MeOH/DMF mixture led to formation of a coordination framework based on an organo-functionalized chalcogenidotetrelate cluster, in which the carboxylate groups at the four ligands of the $[(R^1Ge)_4S_6]$ clusters are linked *via* O→Mn coordinations to the transition-metal ions Mn^{2+}.[18]

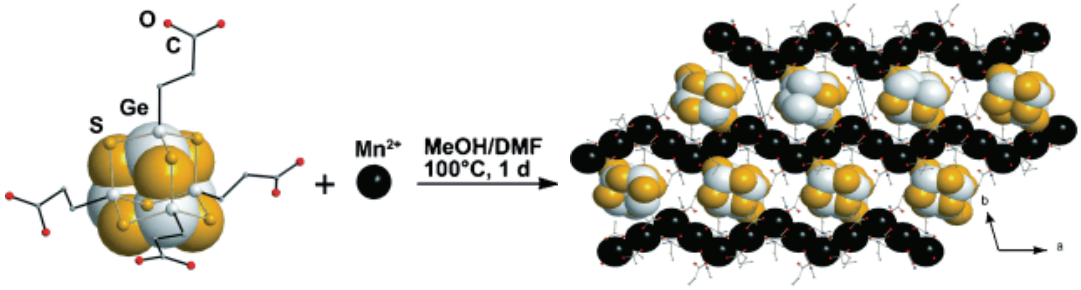

Figure 1.11 Scheme of the reaction of the $[(R^1Ge)_4S_6]$ cluster with Mn^{2+} in a MeOH/DMF mixture at 100°C (Ge, S and Mn atoms in space filling representation), yielding the three-dimensional framework $[Mn_2\{OOCC_2H_4Ge)_4S_6\}(MeOH)(DMF)_2]$. H atoms are omitted for clarity.[18]

1.3 Chalcogenidometalate-based metal-organic frameworks

Metal-organic frameworks (MOFs) are organic-inorganic hybrid compounds, basically consisting of metal ions or metalate clusters as inorganic units coordinated by often rigid organic molecules to form one-, two-, or three-dimensional structures. These compounds have attracted increasing interest due to their intriguing structures and wide potential applications in a variety of areas, including gas storage, separations, catalysis, magnetism and non-linear optics.[19]

Compared to the metal ions holding little directional information, metalate clusters with well-defined geometries can act as building blocks maintaining their structural integrity throughout the formation process to direct the assembly of the target MOFs with suitable organic linkers. A variety of synthetic approaches for the construction of novel metalate cluster-based MOFs have been developed in the last decades. The key approach is the design of organic and inorganic building blocks with desired architectures, as well as chemical and physical properties, which are then transferred to the resulting MOFs materials.[19e,20]

Chalcogenidometalte compounds comprising inorganic or organo-functionalized chalcogenidotetrelate clusters mentioned above, with their special optic and/or electronic properties, could be suitable building blocks for the synthesis of a new class of metalate cluster-based MOFs. However, few examples have been known to date in which chalcogenidometalte units are assembled with organic ligands to form this class MOFs. Beside the organic coordination framework based on an organo-functionalized chalcogenidotetrelate cluster mentioned in the previous section, the *Feng* group has recently synthesized two nanostructured cadmium chalcogenide cluster-based MOFs under solvothermal conditions, by assembling a $[Cd_{32}S_{14}(SPh)_{36}]$ cluster with two different bifunctional pyridine ligands.[21] One of them is shown in Figure 1.12. Here, the four corners of the tetrahedral clusters are linked by bifunctional 4,4′-trimethylenedipyridine (TMDPy) ligands through N→Cd coordinations.

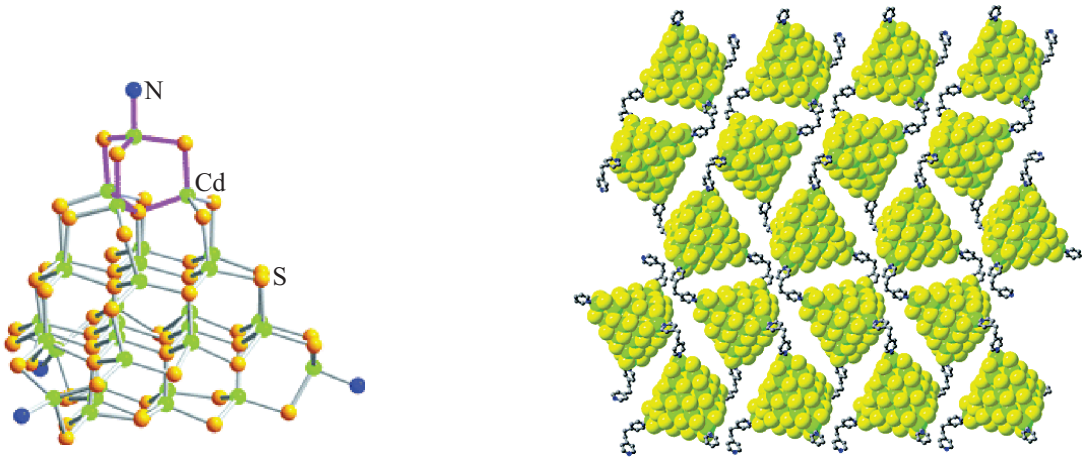

Figure 1.12 Network of tetrahedral clusters $[Cd_{32}S_{14}(SPh)_{36}]$ (left) stabilized by 4,4´-trimethylenedipyridine (TMDPy) through metal-ligand coordination bonds resulting in a metal-organic framework (right).[21]

1.4 Ferrocenyl-linked metal coordination compounds or frameworks and metalate cluster-based multiferrocenyl compounds

Ferrocene is known for its well-developed, highly adaptable synthetic chemistry and its one electron redox activity. For this, it is a favorable component for sensors, conducting, magnetic and electro-optical materials.[22] Many different kinds of coordination compounds have been synthesized by the assembly of bifunctional ferrocenyl ligands (fC) with metal ions or complexes, exhibiting a variety of topologies. They range from macrocylic rings or squares through one-dimensional chains to two- and three-dimensional MOFs. Two examples are shown in Figure 1.13. One of them is a macrocylic square, which was synthesized by the reaction of the bifunctional ferrocenyl hydrazide-hydrazone ligand $[(C_5H_4N)CH{=}N{-}NHC(O)]_2fC$ with $[Ni(BF_4)_2]$ in basic methanolic solution.[23] The marocyclic square contains four Ni cations, joined together through four bifunctional ferrocenyl ligands and displaying octahedral coordination spheres. The other compound is a two-dimensional MOF, generated by reflux of a toluene solution of 1,1´-ferrocenedicarboxylic acid $(COOH_2)fC$ and trimethyltin hydroxide.[24]

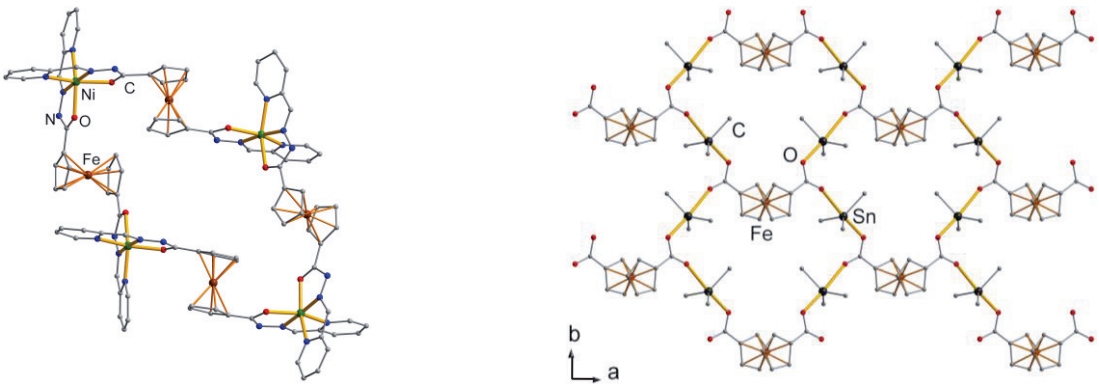

Figure 1.13 Macrocyclic square (left) and two dimensional MOF (right), generated through the assembly of bifunctional ferrocenyl ligands with metal complexes. Solvent molecules and H atoms are omitted for clarity.

However, metalate cluster-based multiferrocenyl compounds, as well as metalate clusters functionalized with ferrocenyl units are rare, hence, only few examples have been reported until now. These have been mainly synthesized by two different approaches. One of them is the attachment of ferrocene units to preferred metalate clusters, such as polyoxometalates (POMs).[25]

As shown in Figure 1.14, a ferrocenyl-modified hexamolybdate cluster has been obtained by attachment of a ferrocenyl terminated acetylene ligand to a hexamolybdate cluster. The connection through an extended π-conjugated bridge was realized by using a Pd-catalyzed coupling reaction of the monoiodo-functionalized cluster substrate.

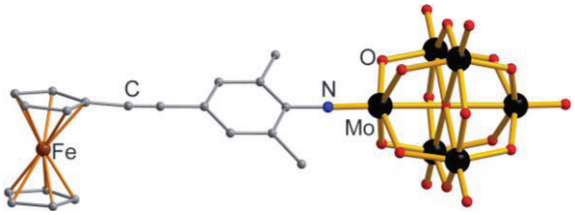

Figure 1.14 Molecular structure of the ferrocenyl unit modified hexamolybdate cluster. H atoms are omitted for clarity.

The second approach is the formation of the cluster by reaction of a ferrocenyl-substituted reagent with a suitable metal compound. For instance, two tinoxide cluster-based multiferrocenyl compounds were synthesized by treatment of mono- or bis-functionalized ferrocene carboxylic acids with the corresponding organotin oxides (Figure 1.15).[26] Both of the compounds possess (poly-)cyclic tinoxide units surrounded by six ferrocenyl moieties:, they belong to the largest tinoxide cluster-based multiferrocenyl compounds.

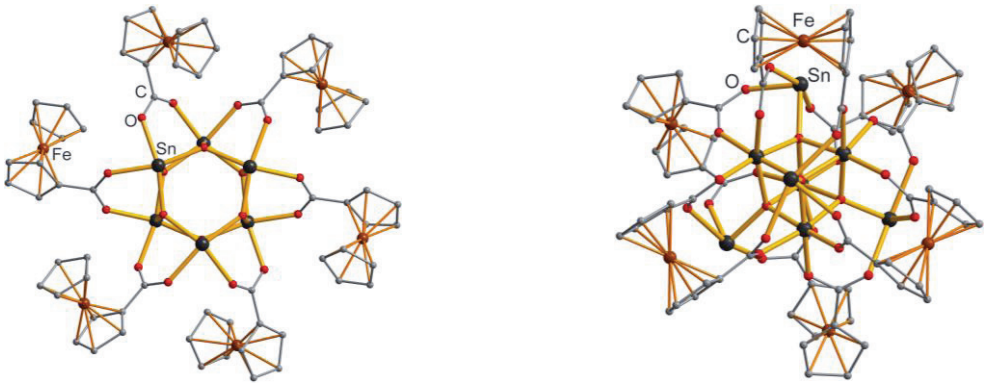

Figure 1.15 Two tinoxide cluster-based multiferrocenyl compounds. H atoms are omitted for clarity.

In the same way, chalcogenide cluster-based multiferrocenyl compounds were generated, mainly by treatment of according metal compounds with silylated chalcogenidoferrocenes like mono-

substituted TMSSeFc, $TMSSH_2CFc$, or bis-substituted derivatives $(SeTMS)_2fC$, established by the *Corrigan* group. Two examples are showed in Figure 1.16. The Cd/Se cluster is surrounded by six ferrocenyl units which derived from the silylated selenoferrocene TMSSeFc. While the latter exhibits a molecular AD topology, the shown Ag/S cluster, with its thirty-six ferrocenyl units, reaches the nanoscale level.[27]

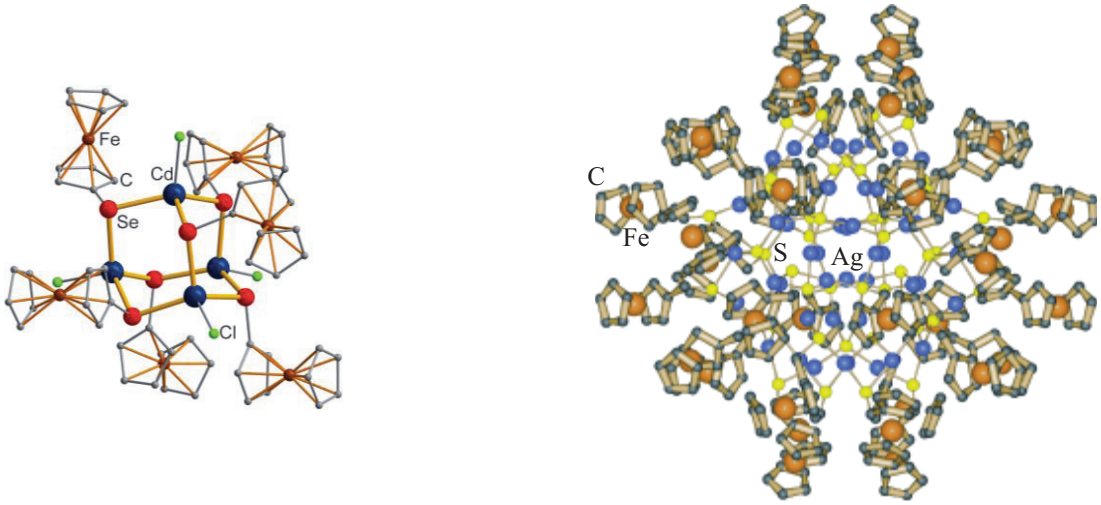

Figure 1.16 Multiferrocenyl compounds based on Cd/Se cluster (left) and on Ag/S cluster [27a] (right). H atoms are omitted for clarity.

Besides, a similar ferrocenyl-substituted AD chalcogenide cluster $[(FcSn)_4S_6]$ has also been synthesized in our group, however, by direct treatment of $FcSnCl_3$ with Na_2S in THF, similar to the synthesis of other organo-functionalized binary chalcogenidotetrelate compounds mentioned above. A similar reaction in aqueous acetone solution generates the salt-like compound $Na_3[(FcSn)_3S_6]$, which can further react with $[Ni(acac)_2]$ to form a ferrocenyl-substituted ternary thiostannate complex (Figure 1.16).[28]

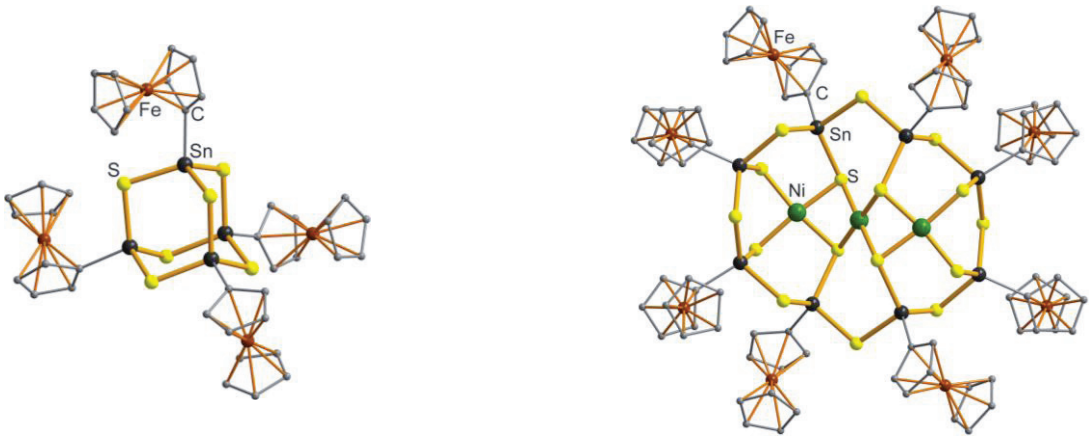

Figure 1.17 Multiferrocenyl compounds based on a binary AD thiostannate cluster $[Sn_4S_6]$ (left), or on a ternary nickel thiostannate cluster $[Ni_3Sn_8S_{14}]$ (right). H atoms are omitted for clarity.

1.5 Preliminary work

The extension of a DD tiostannate cage $[(R^2Sn)_4S_6]$ (**A**, Figure 1.7) with mono- (Fc) and bis-functionalized (fC) ferrocenyl units war part of the work in my diploma thesis.

Compound **IC-1a** $[(R^{Fc}Sn)_4Sn_2S_{10}]$ (R^{Fc} = $CMe_2CH_2C(Me)=N-N=C(Me)Fc$) (Figure 1.18; see also section 3.1.2), which is mentioned in this thesis, was already synthesized and crystallographically characterized in my diploma thesis.

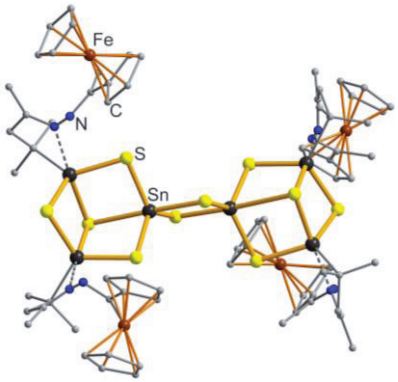

Figure 1.18 Molecular structure of the DSC cluster **IC-1a** $[(R^{Fc}Sn)_4Sn_2S_{10}]$ (R^{Fc} = $CMe_2CH_2C(Me)=N-N=C(Me)Fc$). H atoms are omitted for clarity.

2 Motivation

Organic-inorganic hybrid compounds with their special properties, derived from the combination of organic and inorganic building blocks, currently belong to the most actively investigated materials. Our recent work on the design of organo-functionalized chalcogenidotetrelate clusters aims at the combination of the directed incorporation of chalcogenide moieties in molecular or supramolecular hybrid compounds, as well as in contemporary metal-organic framework chemistry.[13,16a,17,18] The combination of chalcogenide complexes or clusters with organic decoration or linkage thus confers the possible use of these compounds due to the specific opto-electronic characteristics of the inorganic nodes derived from binary or ternary *semi*-conductor chalcogenide moieties.

Ferrocene, because of its well-established synthetic chemistry and remarkable and reversible redox activity, is a favorable component for electronically useful materials.[22] The major aim of this thesis was to design reliable synthetic approaches to attach ferrocenyl units to organotin chalcogenide clusters, and to study the influence of this specific organometallic ligands on the structural, and optical and electrochemical properties of the resulting ensemble.

Since organo-functionalized chalcogenidotetrelate clusters that are decorated with reactive organic groups enable further derivatization, thereby extending their organic shells with appropriate organic ligands mentioned above, a very promising approach could be further functionalization of such chalcogenidotetrelate clusters with mono- (Fc) and bis-substituted (fC) ferrocenyl ligands. A direct functionalization of Sn/S clusters with ferrocenyl units was previously achieved by the treatment of ferrocenyl-substituted tin chloride ($FcSnCl_3$) with sulfide sources. Hence according reactions with other chalcogenide sources could be an alternative way.

The structural, optical and electrochemical properties of the products were to be examined for instance by XRD, ESI-MS, NMR, UV-visible spectroscopy, and cyclic (CV) and differential pulse (DPV) voltammetry.

3 Cumulative Section

3.1 Functionalization of DD clusters $[(R^fSn)_4S_6]$ with ferrocenyl units

An effective way to attach ferrocenyl units to an inorganic chalcogenidotetrelate cage is provided by the functionalization of organo-decorated chalcogenidotetrelate cages with mono- (Fc) and bis-substituted (fC) ferrocenyl ligands. Such chalcogenide cages, especially the Sn/S cages with reactive organic groups R^2 und R^3, can extend the organic ligand shell through condensation reactions with suitable organic compounds such as those mentioned in the introductory section. Thus, three ferrocenyl ligands $[NH_2–N=C(Me)]Fc$,[29] $[NH_2–NHC(O)]_2fC$,[30] and $[OC(H)]_2fC$[31] were synthesized according to the reported methods and reacted with two different Sn/S cages $[(R^FSn)_4S_6]$ (**A**, $R^f = R^2$; **B**, $R^f = R^3$), as reported in this section.

Reactions of two fC ligands led to the attachment of the ferrocenyl units to the corresponding $[(R^fSn)_4S_6]$ cages. Both compounds exhibit a criss-cross-type intramolecular bridging mode of the metal-organic spacer around the inorganic Sn/S cores, while the latter retain their DD topology from $[(R^fSn)_4S_6]$ during the reactions. However, they exhibit slight differences in structural details due to the two different ways of attachment, which also cause different electrochemical stabilities of both compounds.

Differently, the reaction of a mono-functionalized ferrocenyl ligand was accompanied by the re-arrangement of the Sn/S core to form a DSC cage, surrounded by four metal-organic ligands. As confirmed by NMR spectroscopy and by CV and DPV, these show different ligand dynamics in solution than in the solid state. The degradation of the DSC cage by addition different amounts of HCl led to the formation of binuclear or mononuclear species, the latter of which can act as a precursor to formation/recovery of the binuclear species or the DSC cage, respectively

3.1.1 Modification of Sn/S cages with bis-functionalized ferrocenyl units

Zhiliang You,[a] Dieter Fenske[b] and Stefanie Dehnen*[a]

[a]*Fachbereich Chemie, Philipps-Universität Marburg, Hans-Meerwein-Straße, D-35043 Marburg, Germany*

[b]*Institut für Anorganische Chemie der Universität Karlsruhe, Engesserstrasse 15, Geb. 30.45, 76131 Karlsruhe, Germany*

Appeared in

Dalton Trans. **2013**, *42*, 8179–8182 (Front Cover).

Author contributions

Z. You conceived the project and carried out the synthesis and characterization, refined and described the crystal structure, and co-wrote the manuscript. D. Fenske measured and collected the crystal data of compound **1** and proof-read the manuscript. S. Dehnen supervised the work and co-wrote the manuscript.

Abstract

Bis-functionalized ferrocenyl units have been attached to organofunctionalized $[(R^fSn)_4S_6]$ double-decker clusters as criss-cross-type intramolecular straps. Two different ways of linking result in different crystal structures and different electrochemical stabilities of the resulting compounds.

Dalton Transactions

An international journal of inorganic chemistry

www.rsc.org/dalton

Volume 42 | Number 23 | 21 June 2013 | Pages 8149–8520

ISSN 1477-9226

RSC Publishing

COVER ARTICLE

Dehnen *et al.*

Modification of Sn/S cages with bis-functionalized ferrocenyl units

1477-9226(2013)42:23;1-N

Dalton Transactions

RSC Publishing

COMMUNICATION

View Article Online
View Journal | View Issue

Modification of Sn/S cages with bis-functionalized ferrocenyl units†

Cite this: *Dalton Trans.*, 2013, **42**, 8179

Received 8th February 2013,
Accepted 18th February 2013

DOI: 10.1039/c3dt50386k

www.rsc.org/dalton

Zhiliang You,[a] Dieter Fenske[b] and Stefanie Dehnen*[a]

Bis-functionalized ferrocenyl units have been attached to organo-functionalized $[(R^FSn)_4S_6]$ double-decker clusters as criss-cross-type intramolecular straps. Two different ways of linking result in different crystal structures and different electrochemical stabilities of the resulting compounds.

The design of organo-functionalized metal chalcogenide cages aims at the combination of the directed incorporation of chalcogenide moieties in molecular or supramolecular hybrid compounds,[1] as well as in contemporary metal–organic framework chemistry.[2] The combination of chalcogenide complexes or clusters with organic decoration or linkage thus expands the possible use of these compounds by the specific opto-electronic characteristics of the inorganic nodes, which formally derive from binary or ternary solids, thus from semi-conductors, ionic conductors or metallic conductors.[3]

In the course of our recent work on group 14 chalcogenide cages, we have reported on the generation of tin or germanium chalcogenide clusters from precursors R^FTCl_3 with terminal keto or carboxyl groups (T = Ge or Sn; R^F = functional organic ligand: $R^1 = C_2H_4COOH$, $R^2 = CMe_2CH_2C(Me)O$).[4] Functionalization by R^1 allows metal coordination upon deprotonation.[5] Clusters with R^2 are reactive towards hydrazine, forming the reactive hydrazone ligand $CMe_2CH_2C(Me)=NNH_2$ (R^3), as well as towards terminal hydrazine derivatives, hydrazones or hydrazides.[4a,6] Currently, we have demonstrated that bis-functionalized organic spacers R^{bis} may be used for intramolecular linkage, that may include reactions to give ternary complexes[7] or a re-arrangement of the inorganic cage into macro-cavitands or macro-capsules.[6a]

We have been interested in whether the attachment of transition metal moieties might also work *via* coupling reactions. Since the decoration of clusters or nanoparticles by ferrocenyl units evolved as an attractive modification of the underlying structures,[8] bis-functionalized ferrocenyl (fC) moieties were used in corresponding reactions with $[(R^3Sn)_4S_6]$ or $[(R^2Sn)_4S_6]$. Herein we report on the observations that were made upon the installation of two different fC-containing spacers, R^{fC1} = $[CMe_2CH_2C(Me)=N–N=C(H)]_2fC$ and R^{fC2} = $[CMe_2CH_2C(Me)=N–NHC(O)]_2fC$, that were introduced by two different reactions shown in eqn (1) and (2), and in Scheme 1.

$$\left[(R^3Sn)_4S_6\right] + [OC(H)]_2fC \xrightarrow{a} \left[(R^{fC1}Sn_2)_2S_4\right](\mathbf{1}) \quad (1)$$

$$\left[(R^2Sn)_4S_6\right] + [H_2N–NHC(O)]_2fC \xrightarrow{a} \left[(R^{fC2}Sn_2)_2S_4\right](\mathbf{2}) \quad (2)$$

a: CH_2Cl_2 / CH_3OH, 17.5 h, reflux.

Both compounds were characterized by standard analysis techniques (see ESI†). Besides the different synthetic approach to form the bridges in compounds **1** and **2** that led to the presence of a CH group between the Cp rings and the N–N unit in

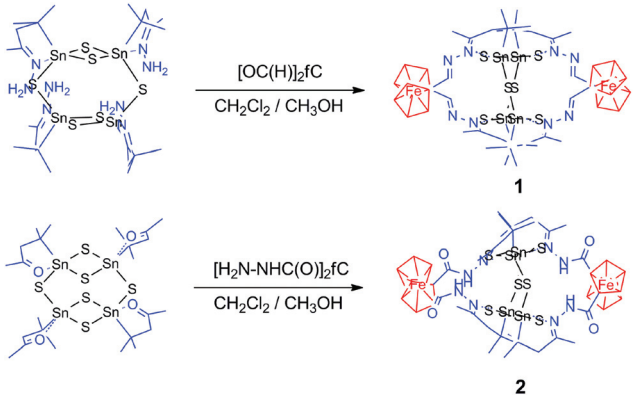

Scheme 1 Synthesis of the title compounds **1** and **2** with bis-functionalized ferrocenyl (fC) spacers involved in intramolecular bridges.

[a]*Philipps-Universität Marburg, Fachbereich Chemie, Hans-Meerwein-Strasse, D-35043 Marburg, Germany. E-mail: dehnen@chemie.uni-marburg.de; Fax: +49 6421 2825653; Tel: +49 6421 2825751*

[b]*Institut für Anorganische Chemie der Universität Karlsruhe, Engesserstrasse 15, Geb. 30.45, 76131 Karlsruhe, Germany. E-mail: dieter.fenske@aoc1.uni-karlsruhe.de; Fax: (+49) 721-608-8440*

†Electronic supplementary information (ESI) available: Synthetic details for **1**·$3CH_2Cl_2$ and **2**·$5CH_2Cl_2$, X-ray diffraction, spectroscopic/-metric data, electrochemical and quantum chemical details. CCDC 911480 (**1**) and 911481 (**2**). For ESI and crystallographic data in CIF or other electronic format see DOI: 10.1039/c3dt50386k

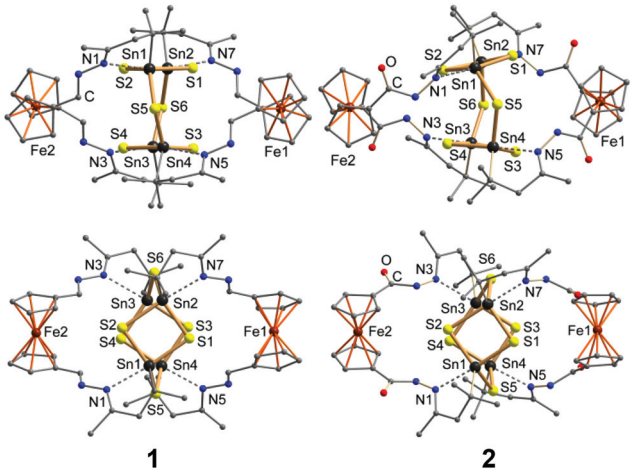

Fig. 1 Molecular structures of **1** (using the example of one of two symmetry-independent molecules) and **2**, each viewed in two different orientations (top and bottom) to emphasize the different conformations.

1, in contrast to a CO group at this place in **2**, the resulting spacers differ in the nature of the N–N unit itself. In **1**, the N–N bond is part of a bis-hydrazone and therefore fixed by two N=C double bonds; in **2**, it represents an N–NH moiety that was introduced with the ferrocenyl hydrazide.

These apparently slight differences seem to be the base for a dramatic difference in the molecular structures of **1** and **2** that were elucidated by single-crystal X-ray diffraction (Fig. 1).‡

Both molecules exhibit a criss-cross-type intramolecular bridging mode of the metal–organic spacer, such as observed previously for 1,2-$[CMe_2CH_2C(Me)N{=}N]_2C_6H_4$ that comprises a purely organic bridge.[6b] As emphasized in Fig. 1, the $[Sn_4S_6]$ unit, which was introduced as a near D_{2h}-symmetric cage in the precursors $[(R^3Sn)_4S_6]$ or $[(R^2Sn)_4S_6]$ (Sn–$S_{four\text{-}ring}$ 238.92(15)–251.41(8) pm, Sn–S_{bridge} 240.91(8)–243.32(10) pm, Sn–C 217.2(3)–218.8(3) pm, Sn···O 261.4(1)–267.2(1) pm, Sn···N 234.1(3)–239.0(2) pm; Sn–$S_{four\text{-}ring}$–Sn 86.89(5)–90.20(3)°, Sn–S_{bridge}–Sn 105.12(4)–107.65(4)°),[4b] retains its geometry with only small changes in **1** (Sn–$S_{four\text{-}ring}$ 238.46(17)–250.71(18) pm, Sn–S_{bridge} 240.6(2)–242.29(18) pm, Sn–C 216.6(8)–220.7(7) pm, Sn···N 246.9(8)–254.7(6) pm; Sn–$S_{four\text{-}ring}$–Sn 88.57(6)–89.10(6)°, Sn–S_{bridge}–Sn 107.90(7)–109.74(7)°), while it undergoes a significant distortion in **2** (Sn–$S_{four\text{-}ring}$ 238.91(19)–249.59(19) pm, Sn–S_{bridge} 242.01(19)–243.6(2) pm, Sn–C 215.9(7)–217.5(8) pm, Sn···N 234.3(6)–243.7(6) pm; Sn–$S_{four\text{-}ring}$–Sn 86.85(7)–88.09(6)°, Sn–S_{bridge}–Sn 111.51(7)–111.92(8)°) – visible in the angles around the bridging S atoms and the following S···S distances: S2···S4 396 pm and S1···S3 402 pm in **1**, *versus* S2···S4 372 pm and S1···S3 478 pm in **2**; the deformation gives rise to intramolecular NH···S hydrogen bond formation in **2** (Fig. S8†).

The size and conformational rigidity of an organic intramolecular bridge has been shown to play a crucial role in the design of binary tetrelchalcogenide cages:[6] a C=N···N=C "bite" in the range of 380–667 pm allowed for three different conformers of the topologically maintained $[(R^{bis}Sn_2)_2S_6]$ cage, whereas "bites" larger than 850 pm would lead to a re-arrangement into cavitand-type molecules $[(R^{bis}Sn_2)_4Sn_4S_{20}]$. Thus far, "bites" in between did not lead to isolable products. It thus remained questionable whether medium-sized bridges would still enable intramolecular bridging of $[Sn_4S_6]$ units, as for the criss-cross-type bridging mode of $[CMe_2CH_2C(Me){=}N{-}N{=}C(H)]_2C_6H_4$,[6b] or whether a deformation/deconstruction/re-arrangement of the cages was the case, as for longer spacers like $CMe_2CH_2C(Me){=}N{-}N(H)]_2CO$ (N···N 380 pm),[6a] or whether it might result in intermolecular bridging.

Indeed, the bis-functionalized fC linkers used herein have the spacer length in question, and thus lead to N···N spacer lengths in the corresponding range: in **1**, the final C=N···N=C "bite" of the spacer amounts to 731–737 pm (N1···N3, N5···N7 for molecule A, see Fig. 1, or N10···N12 or N14···N16 for molecule B, see ESI†), whereas in **2**, both "straps" differ, and show C=N···N=C distances of 629 pm (N1···N3) or 755 pm (N5···N7), respectively.

As we learn from our study, the intermediate spacer length still allows for a criss-cross-type bridging; however, the results also indicate high conformational flexibility of the pretty long linkers which enables the adjustment to specific requirements of the crystal structure, such as crystallization of compounds with symmetric or asymmetric bridges, respectively. Neither DFT calculations nor NMR studies (see ESI†) indicate the preservation of the asymmetric conformation of **2** in isolated form or solution, thus more effective packing of the asymmetric clusters of **2** in comparison with a symmetric alternative seems to be preferable.

The successful attachment of ferrocene units to the Sn/S double-decker cages prompted us to study the electrochemical properties of **1** and **2**, which was realized in DCM solutions of the title compounds (0.1 M TBFP) using cyclic and differential pulse voltammetry (CV and DPV) at 25 °C. The two ferrocene redox centers in each of the compounds are connected *via* organic and inorganic moieties, and hence show large Fe···Fe distances of 12.2 Å (**1**) or 12.4 Å (**2**), respectively. According to previous investigations with multiple redox centers that are well-separated, the ferrocene units should behave identically with no interaction between them. Thus, a single current–potential CV curve would be expected which is similar to that observed with a single one-electron electroactive center, but with a magnitude determined by the total number of redox centers.[9]

Indeed, as shown in Fig. 2a and 2b, compound **1** undergoes a single-step oxidation ($\mathbf{1}/\mathbf{1}^{2+}$) at E_{pa} = 466 mV, confirmed by an analysis of the diagnostic criteria of CV, *i.e.* the difference between two peak potentials ΔE_p and the ratio of peak currents i_{pa}/i_{pc} (120/2 mV and 0.85, respectively, at 100 mV s^{-1}).[10]

However, the electrochemical investigation of **2** indicated that the replacement of the [HC=N–N=C] linking pattern in **1** by the [O=C–NH–N=C] moiety in **2** resulted in significantly different cyclic voltammograms (Fig. 3).

For **2**, the voltammograms scanned between −200 and 1100 mV (Fig. 3a) indicate the occurrence of an irreversible (see Table S4 in the ESI†) redox process, obviously comprised

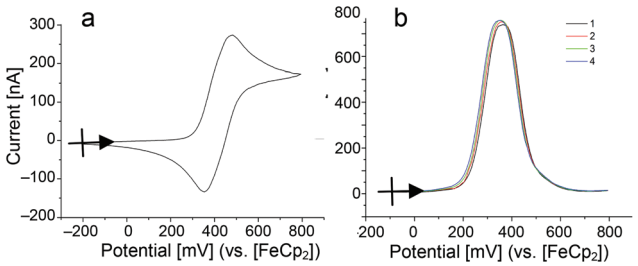

Fig. 2 Cyclic and differential pulse voltammograms,[11] recorded at a platinum electrode on a CH_2Cl_2 solution of **1** (1.03 mM) in the presence of TBFP (0.1 M). Scan ranges and rates: CV, (a) −200 to 800 mV, 100 mV s^{-1}; DPV, (b) −100 to 800 mV, 10 mV s^{-1}. Pulse amplitude for DPV: 50 mV.

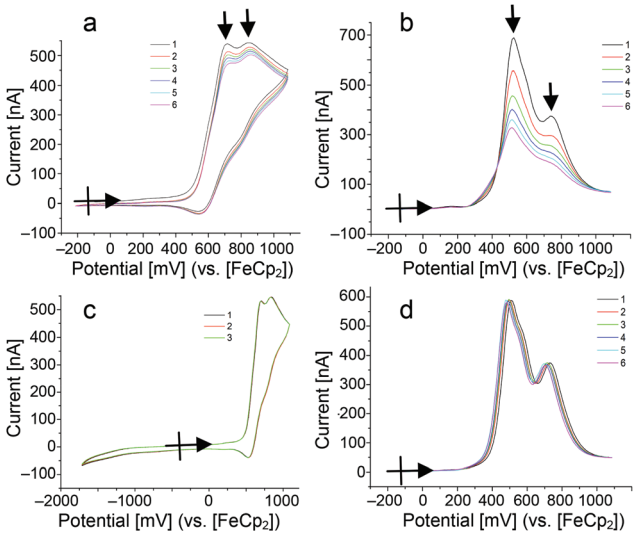

Fig. 3 Cyclic and differential pulse voltammograms,[11] recorded at a platinum electrode on a CH_2Cl_2 solution of **2** (1.07 mM) in the presence of TBFP (0.1 M). Scan ranges and rates: CV, (a) −200 to 1100 mV, 100 mV s^{-1}; (c) −1700 to 1100 mV, 100 mV s^{-1}; DPV, (b) −200 to 1100 mV, 10 mV s^{-1}; (d) −110 to 1100 mV, 10 mV s^{-1}. Pulse amplitude for DPV: 50 mV.

of two oxidation steps, which was further confirmed by the DPV measurements (Fig. 3b). The first anodic peak potential, which can be surely assigned to the ferrocenyl moieties, is observed at E^1_{pa} = 706 mV, pointing out that the electron attracting power of the [O═C–NH–N═C] group attached to the fC units in **2** is significantly stronger than that of the [HC═N–N═C] units in **1** (466 mV). The second anodic peak potential is found at E^2_{pa} = 836 mV, with half the intensity of the first one. Additionally, a broad shoulder was observed between the two steps in the DPV diagram.

The decrease of the intensity of the oxidation peaks in the successive scans both in CV and DVP reveals a passivation of the platinum electrode that results most probably from the formation of sulfide anions that start to poison the electrode,[12] causing the shoulder and the second oxidation peak in the DPV. Accordingly, as the scan range in the reverse sweep is expanded to −1700 mV, the poisoned electrode can be recovered by reduction, and the shape of the wave remains the same in the successive scans (Fig. 3c and 3d). However, the mentioned decomposition of the sample persists, as indicated by the two redox steps, the shoulder and the non-equivalent intensities of the peaks. We do not know the exact processes that occur, but oxidative decomposition of organotin compounds is known[13] and may induce further fragmentation.

For **1**, the corresponding poisoning of the electrode indicating (partial) decomposition of the compound is not visible according to the successive DPV measurements of **1** that exhibit only arbitrary and minor changes from cycle to cycle. Thus, the different ways of attachment of the fC groups to the organo-functionalized Sn/S cores do not only result in different structural details, but do also affect the electrochemical properties of the resulting compounds. Besides different oxidation potentials of the fC moieties, the stability of the Sn/S cage seems to be affected, as well, which is further supported by analysis of the fC-free double-decker cluster $[(R^2Sn)_4S_6]$, that is electrochemically inert in the range −100 to 1300 mV (Fig. S10†).

The differences in the electronic situation can also be monitored by the different solid state UV-visible spectra (see ESI†) that show broad maxima around 514 and 270 nm (**1**) or 500 and 273 nm (**2**), respectively, and a smooth shoulder around 401 nm (**1**) or 357 nm (**2**), respectively. The low-frequency maximum and the shoulder are assigned to the fC-units,[14] while the high-frequency maximum is assigned to p(S)→p(Sn) charge transfer, as observed for related Sn/S clusters.[5b] In comparison with pure ferrocene (maxima at 445 and 328 nm)[14] the values are red-shifted, as expected for electron-withdrawing substituents like C═O or C═N, but more pronounced for the azine C═N–N═C group in **1** due to the extended π-conjugation.[15]

Conclusions

The attachment of bis-functionalized ferrocenyl linkers to organo-functionalized $[(R^FSn)_4S_6]$ double-decker clusters is accessible by two different ways of linking that result in both different structural and different electrochemical stabilities of the resulting compounds.

Notes and references

‡Data were collected on a diffractometer equipped with a STOE imaging plate detector system (IPDS2T), using MoKα radiation with graphite monochromatization (λ = 0.71073 Å). Structure solution was performed by Sir-2004[16] with full-matrix least squares refinement against F^2 using SHELXL-97 software.[17] Crystal data for **1**·$3CH_2Cl_2$: single crystals from an MeOH / CH_2Cl_2 mixture upon layering by *n*-pentane, $[(R^{fC1}Sn_2)_2S_4]\cdot 3CH_2Cl_2$, orthorhombic, space group $P2_12_12_1$, a = 12.60540(10) Å, b = 25.6456(2) Å, c = 41.9115(4) Å, V = 13548.9(2) Å^3, T = 180(2) K, Z = 8, μ = 2.330 mm^{-1}, 22 698 independent reflections (R_{int} = 0.0315). The final R_1 = 0.0396 ($I > 2\sigma(I)$), wR_2 = 0.1081 for all data and GooF = 1.036. Crystal data for **2**·$5CH_2Cl_2$: single crystals from CH_2Cl_2 solution upon layering by *n*-pentane, $[(R^{fC2}Sn_2)_2S_4]\cdot 5CH_2Cl_2$, monoclinic, space group $P2_1/c$, a = 15.731 Å, b = 24.753 Å, c = 21.079 Å, β = 111.58°, V = 7632.5 Å^3, T = 100(2) K, Z = 4, μ = 2.219 mm^{-1}, 16 134 independent reflections (R_{int} = 0.1320). The final R_1 = 0.0431 ($I > 2\sigma(I)$), wR_2 = 0.1058 for all data and GooF = 0.816.

1 (*a*) X. Bu, N. Zheng and P. Feng, *Chem.–Eur. J.*, 2004, **10**, 3356; (*b*) P. Feng, X. Bu and N. Zheng, *Acc. Chem. Res.*, 2005, **38**, 293; (*c*) N. Zheng, H. Lu, X. Bu and P. Feng, *J. Am. Chem. Soc.*, 2006, **128**, 4528.
2 (*a*) H. Li, M. Eddaoudi, M. O'Keeffe and O. M. Yaghi, *Nature*, 1999, **402**, 276; (*b*) H. L. Li, A. Laine, M. O'Keeffe and O. M. Yaghi, *Science*, 1999, **283**, 1145; (*c*) E. Antonova, C. Nather, P. Kogerler and W. Bensch, *Angew. Chem., Int. Ed.*, 2011, **50**, 764.
3 (*a*) N. Zheng, X. Bu, J. Lauda and P. Feng, *Chem. Mater.*, 2006, **18**, 4307; (*b*) Q. Zhang, T. Wu, X. Bu, T. Tran and P. Feng, *Chem. Mater.*, 2008, **20**, 4170.
4 (*a*) Z. H. Fard, C. Müller, T. Harmening, R. Pöttgen and S. Dehnen, *Angew. Chem., Int. Ed.*, 2009, **48**, 4441; (*b*) Z. H. Fard, L. Xiong, C. Müller, M. Hołyńska and S. Dehnen, *Chem.–Eur. J.*, 2009, **15**, 6595.
5 (*a*) Z. Hassanzadeh Fard, R. Clerac and S. Dehnen, *Chem.–Eur. J.*, 2010, **16**, 2050; (*b*) Z. Hassanzadeh Fard, M. Hołynska and S. Dehnen, *Inorg. Chem.*, 2010, **49**, 5748.
6 (*a*) Z. Hassanzadeh Fard, M. R. Halvagar and S. Dehnen, *J. Am. Chem. Soc.*, 2010, **132**, 2848; (*b*) M. R. Halvagar, Z. Hassanzadeh Fard and S. Dehnen, *Chem.–Eur. J.*, 2011, **17**, 4371.
7 M. R. Halvagar, Z. Hassanzadeh Fard and S. Dehnen, *Chem. Commun.*, 2010, **46**, 4716.
8 (*a*) H. B. Yang, K. Ghosh, Y. Zhao, B. H. Northrop, M. M. Lyndon, D. C. Muddiman, H. S. White and P. J. Stang, *J. Am. Chem. Soc.*, 2008, **130**, 839; (*b*) S. Ahmar, D. G. MacDonald, N. Vijayaratnam, T. L. Battista, M. S. Workentin and J. F. Corrigan, *Angew. Chem., Int. Ed.*, 2010, **49**, 4422.
9 G. Ferguson, C. Glidewell, G. Opromolla, C. M. Zakaria and P. Zanello, *J. Organomet. Chem.*, 1996, **517**, 183.
10 J. Heinze, *Angew. Chem., Int. Ed. Engl.*, 1984, **23**, 831.
11 *Electrochemical Methods: Fundamentals and Application*, ed. A. J. Bard, L. R. Faulkner, VCH, New York, 2nd edn, 2001.
12 (*a*) S. Kapusta, A. Viehbeck, S. M. Wilhelm and N. Hackerman, *J. Electroanal. Chem.*, 1983, **153**, 157; (*b*) R. Mohtadi, W. K. Lee and J. W. Van Zee, *Appl. Catal., B*, 2005, **56**, 37.
13 (*a*) C. L. Wong and J. K. Kochi, *J. Am. Chem. Soc.*, 1979, **101**, 5593; (*b*) S. Fukuzumi, C. L. Wong and J. K. Kochi, *J. Am. Chem. Soc.*, 1980, **102**, 2928.
14 L. Kaplan, W. L. Kester and J. J. Katz, *J. Am. Chem. Soc.*, 1952, **74**, 5531.
15 T. H. Barr and W. E. Watts, *J. Organomet. Chem.*, 1968, **15**, 177.
16 M. C. Burla, R. Caliandro, M. Camalli, B. Carrozzini, G. L. Cascarano, L. De Caro, C. Giacovazzo, G. Polidori and R. Spagna, *J. Appl. Crystallogr.*, 2005, **38**, 381.
17 G. W. Sheldrick, Bruker AXS Inc., Madison WI, 1997.

Electronic Supplementary Material (ESI) for Dalton Transactions

Modification of Sn/S Cages with Bisfunctionalized Ferrocenyl Units

Zhiliang You, Dieter Fenske, Stefanie Dehnen*

Fachbereich Chemie, Philipps-Universität Marburg,

Hans-Meerwein-Straße, D-35043Marburg, Germany

email: dehnen@chemie.uni-marburg.de

SUPPORTING INFORMATION

1. Experimental Syntheses Details

***General*:** All reaction steps were carried out under Ar atmosphere. All solvents were dried and freshly distilled prior to use. Organotin sulfide clusters $[(R^{2,3}Sn)_4S_6]$ (R^2= $CMe_2CH_2C(Me)O$, R^3 = $CMe_2CH_2C(Me)=NNH_2$) and 1,1´-diformylferrocene $fC[C(O)H]_2$ were prepared according to the reported methods.[1][2] The synthesis of ferrcene-1,1´-dicaboxylic acid hydrazide $fC[C(O)NH\text{-}NH_2]_2$ was slightly modified (see below).[3] Oxalyl chloride ($C_2O_2Cl_2$) and hydrazine monohydrate 64-65% ($N_2H_4{\cdot}H_2O$) were purchased from Aldrich.

^{1}H NMR, ^{13}C NMR and ^{119}Sn NMR measurements were carried out using a Bruker DRX 400 MHz spectrometer at 25ºC. In ^{1}H and ^{13}C NMR, the chemical shifts were quoted in ppm relative to the residual protons of deuterated solvents. In ^{119}Sn NMR, Me_4Sn was used as internal standard.

Infrared (IR) spectra were recorded on a Bruker TENSOR 37 FT-IR-Spektrometer.

Mass spectrometry (MS) was performed on a Finnigan MAT 95S. The Electrospray Ionisation (ITMS-ESI) spectra were obtained by using solvent as the carrier gas.

UV/Vis spectra were recorded on a Perkin- Elmer Cary 5000 UV/Vis/NIR spectrometer in the range of 800–200 nm employing the double-beam technique. The samples were prepared as suspension in nujol oil between two quartz plates.

Synthesis of Ferrcen-1,1′-dicaboxylic acid hydrazine

A mixture of ferrocene dicarboxylic acid fC[COOH]$_2$ (0.424 g, 1.55 mmol) in dichloromethane (DCM, 15.0 mL) was cooled with an ice bath. Oxalyl chloride (5.00 mL, 59.1 mmol) was then slowly added and the reaction mixture was then heated under reflux for 3 h. After removing the solvent and excess oxalyl chloride under vacuum, the resulted carboxylic chloride was dissolved in THF (15.0 mL), and added dropwise to a solution of hydrazine monohydrate (5.00 mL, 105 mmol) in ethanol (15.0 mL). The mixture was then stirred for 3 h at room temperature and heated under reflux for 18 h. Dark insoluble decomposition products formed in the heat, which were removed by filtration. The filtrate was then evaporated in vacuo until a precipitate formed. The resulting yellow solid was washed several times with ethanol and dried in vacuo. Yield: 0.240 g, 51.3%.

MS (ESI): *m/z* = 303.1([M+H]$^+$), 325.1 ([M+Na]$^+$). Elemental analysis, calculated (%) for $C_{12}H_{14}N_4O_2Fe_1$: C 47.71, H 4.67, N 18.55; found: C 47.17, H 4.70, N 18.51.

*Synthesis of [($R^{fCl}Sn_2$)$_2S_6$]·3CH_2Cl_2, {**1**·3CH_2Cl_2, R^{fCl} = [$CMe_2CH_2C(Me)$=N–N=C(H)]$_2$fC]}*

fC[C(O)H]$_2$ (0.0097 g, 0.04 mmol) and [(R^3Sn)$_4S_6$] (0.0224g, 0.02 mmol) were suspended in a solvent mixture of methanol (MeOH, 3 mL) and DCM (3 mL). The mixture was heated under reflux for 17.5 h and then filtered. The filtrate was layered with *n*-pentane (1:1). Red block-shape crystals of **1** were obtained within 3 weeks. Yield: 0.0171 g, 55.7% (calculated on basis of [(R^3Sn)$_4S_6$])

^{1}**H** NMR (400 MHZ, CD_2Cl_2, 25°C): *δ/ppm* = 1.35, 1.52 (ss, 24H; ***Me***$_2$C), 2.09 (s, 12H; ***Me***), 2.58 (dd, 8H; C***H***$_2$), 4.30, 4.63, 4.79, 5.25 (4m, 4x4H; Cp-***H***), 9.55 (s, 4H, ***H***-C=N-); ^{13}**C** NMR (100 MHZ, CD_2Cl_2, 25°C): *δ/ppm* = 19.66 (N=C***C***H$_3$), 25.41, 25.99 ((***C***H$_3$)$_2$C), 36.03 (***C***Me$_2$), 50.87 (***C***H$_2$), 65.33, 70.19, 71.45, 76.04 (H***C***-Cp)), 79.98 (-***C***-Cp), 163.54 (Cp(H)***C***=N), 169.41 (Me(CH$_2$)***C***=N); ^{119}**Sn** NMR (149 MHz, CD_2Cl_2): *δ/ppm* = –64.6; MS (ESI): *m/z* = 1530.7 ([M+H]$^+$); IR cm^{-1}: 3078.17 (C-H of Cp), 1633.59, 1591.16 (C=N), 1139.85 (N-N). Elemental analysis, calculated (%) for $C_{49}H_{66}N_8Cl_2Fe_2S_6Sn_4$: C 36.40, H 4.13, N 6.93, S 11.90; found: C 36.75, H 4.24, N 6.84, S 11.47. Note that only two solvent molecules remained after the drying process in high vacuum for 6 hours prior to the analysis.

*Synthesis of [($R^{fC2}Sn_2)_2S_6$]·5CH_2Cl_2, {**2**·5CH_2Cl_2, R^{fC2} = [$CMe_2CH_2C(Me)$=N–NHC(O)]$_2$fC]}*

fC[C(O)NH-NH_2]$_2$ (0.025 g, 0.083 mmol) and [($R^2Sn)_4S_6$] (0.044g, 0.0413 mmol) were suspended in a solvent mixture of MeOH (5.00 mL) and DCM (5.00 mL). The mixture was heated under reflux for 17.5 h. Dark insoluble decomposition products formed in the heat, which was removed by filtration. The filtrate was evaporated in vacuo. The resulting yellow solid was dissolved in DCM (6.00 mL), and layered with *n*-pentane (1:1). Orange block-shape crystals of **2** were obtained within 10 days. Yield: 0.0340 g, 51.6% (calculated on basis of [($R^2Sn)_4S_6$])

^{1}**H** NMR (400 MHZ, CD_2Cl_2, 25°C): *δ/ppm* = 1.35, 1.52 (ss, 24H; ***Me***$_2$C), 1.89 (s, 12H; ***Me***), 2.76 (dd, 8H; C***H***$_2$), 4.41, 4.55, 4.75, 5.43 (4m, 4x4H; Cp-***H***), 9.10 (s, 4H, ***H***-NC=O); ^{13}**C** NMR (100 MHZ, CD_2Cl_2, 25°C): *δ/ppm* = 21.85 (N=C***C***H_3), 26.74, 27.28 (($\boldsymbol{C}H_3)_2$C), 36.18 (***C***Me_2), 52.16 (***C***H_2), 68.11, 71.51, 73.30, 74.01 (H***C***-Cp)), 77.82 (-***C***-Cp), 165.48 (Cp***C***=O-NH), 173.29 (Me(CH_2)***C***=N); ^{119}**Sn** NMR (149 MHz, CD_2Cl_2): *δ/ppm* = –78.3; MS (ESI): *m/z* = 1618.8 ([M+Na]$^+$); IR cm^{-1}: 3313.47 (N-H), 3053.10 (C-H of Cp), 1685.67 (C=O), 1664.45 (C=N), 1168.78 (N-N). Elemental analysis, calculated (%) for $C_{49}H_{66}N_8O_4Cl_2Fe_2S_6Sn_4$: C 35.01, H 3.96, N 6.67, S 11.45; found: C 35.80, H 4.25, N 6.34, S 11.26. Note that only one solvent molecule remained after the drying process in high vacuum for 6 hours prior to the analysis.

2. Spectrometry and Spectroscopy

ESI mass spectra:

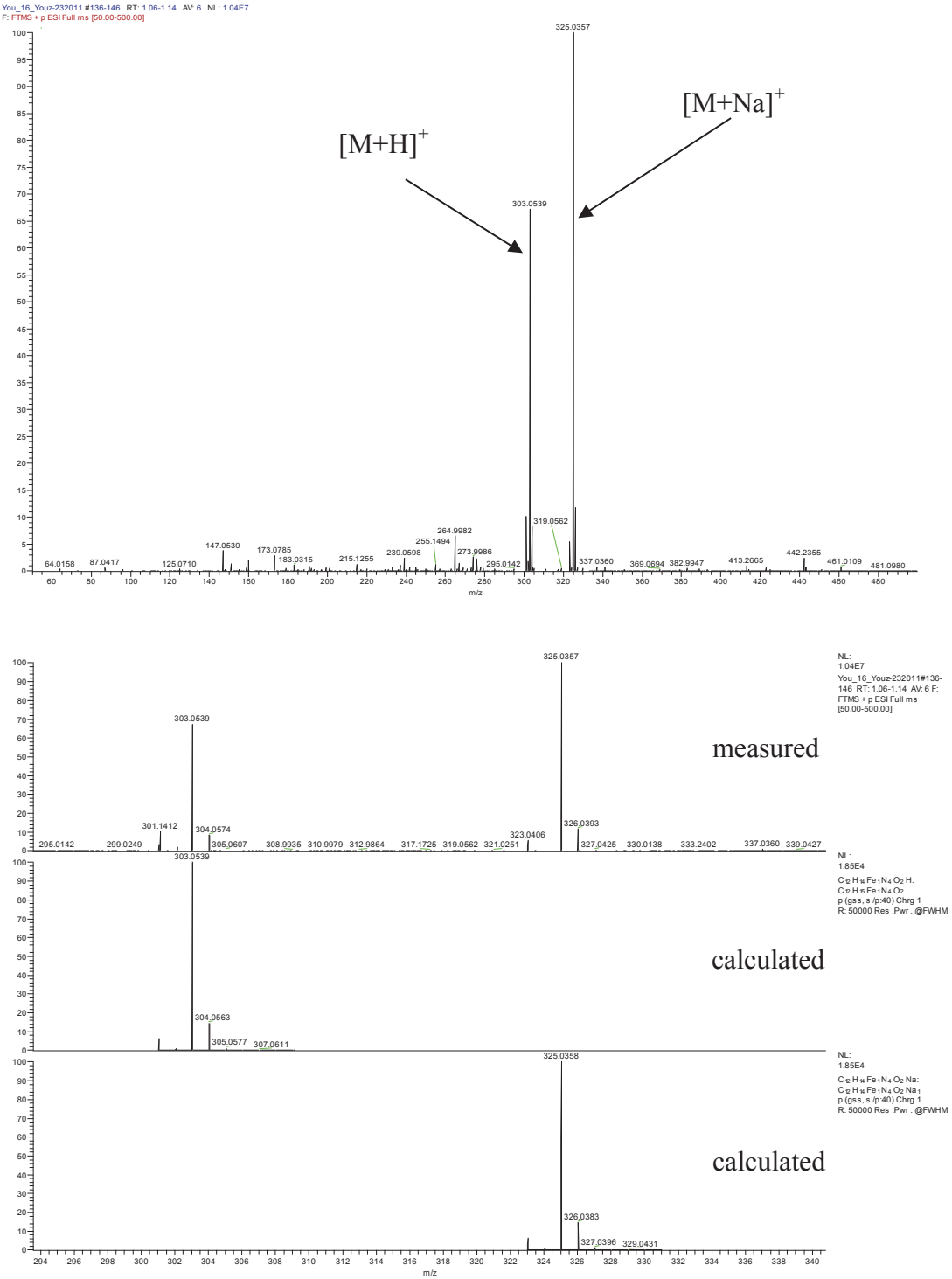

Figure S1. ESI mass spectrum of **fC[C(O)NH-NH$_2$]$_2$**.

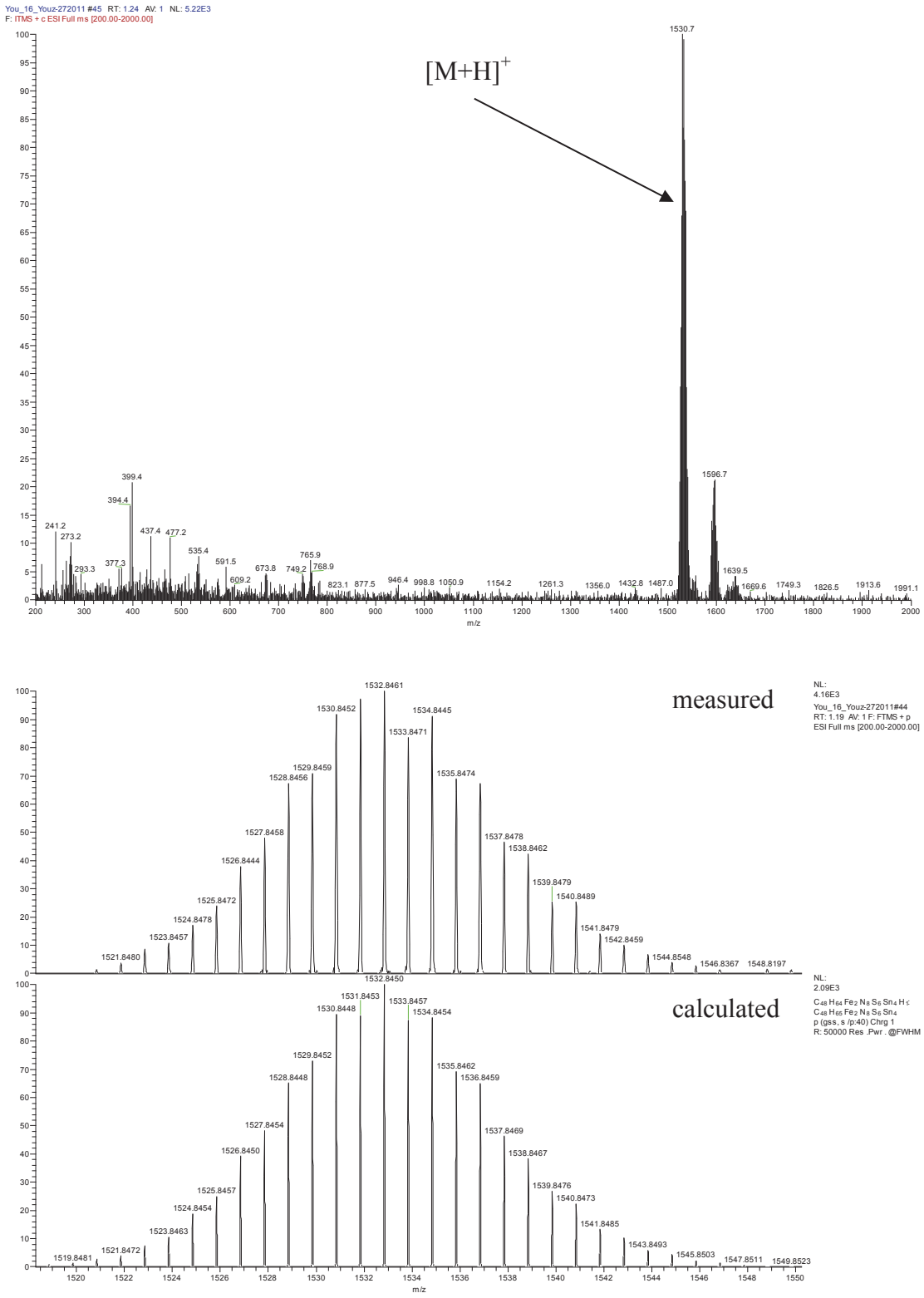

Figure S2. ESI mass spectrum of **1**.

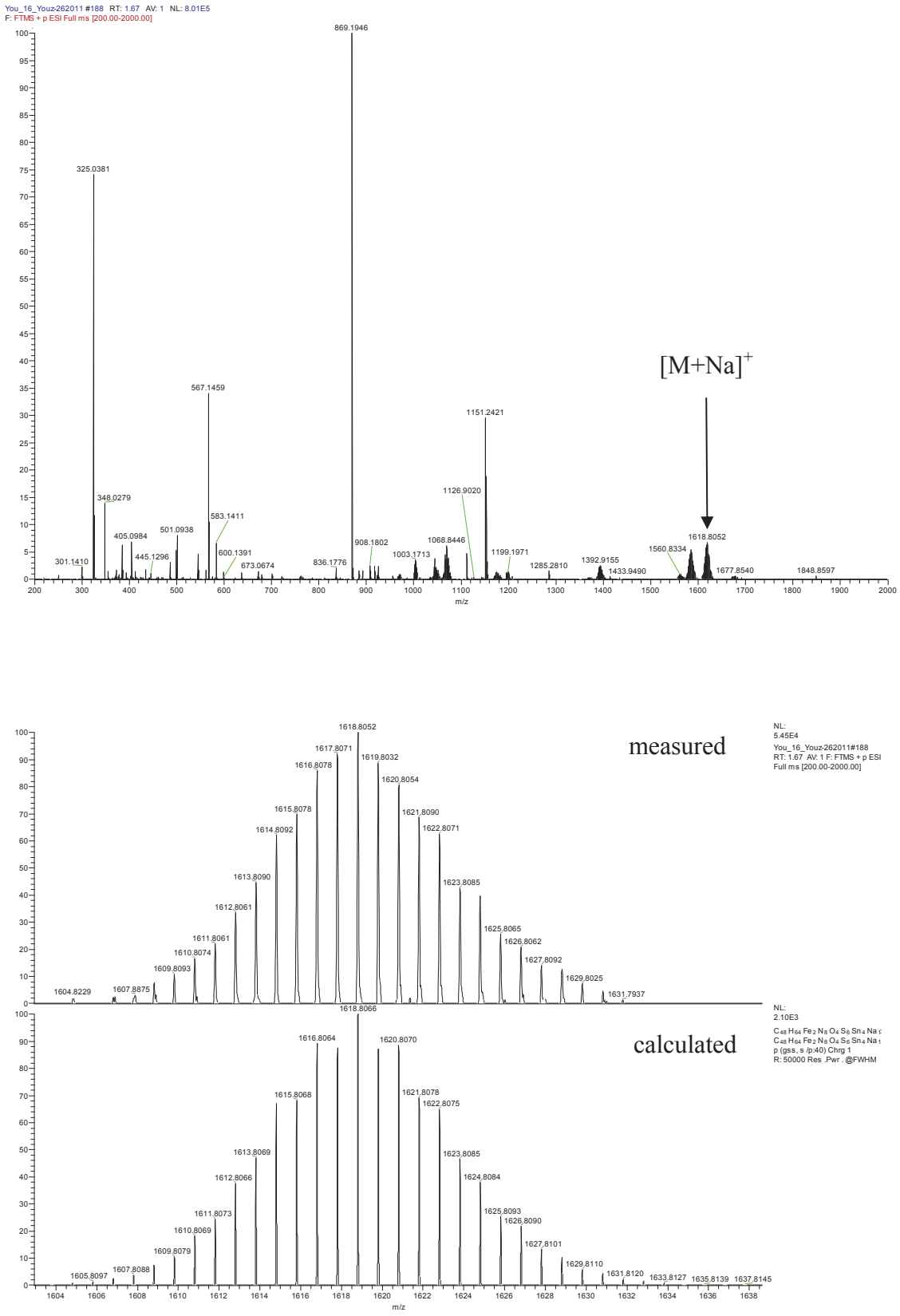

Figure S3. ESI mass spectrum of **2**.

Temperature-dependent ^{1}H NMR spectra of 2:

The conformational difference between the two ferrocene units in **2** (see molecular structure) is offset in solution. However, the structures with co-planar Cp rings and their binding chains (C=O double bond) are rigid, neither the Cp rings nor the attached organic chains can freely rotate. In such rigid conformation, the four protons of the same Cp ring are chemically non-equivalent. Hence, there are four separate signals. Additionally, one signal, which belongs to proton H9 (see figure S4), is shifted downfield due to the anisotropy that results in a closer proximity of the electron pair at the adjacent O atom.

In order to examine the potential influence of conformational changes at the spacers on the cage geometry, we carried out ^{1}H NMR measurements at different temperatures. For this, a solution of **2** in tetrachloroethan-d_2 was heated up to 370 K. The increased temperatures should result the increasing of the flexibility both of the Cp rings and the chains that attach them to the Sn/S cluster. As a result, the Sn/S cluster should become higher symmetric, leading to identical signals between chemical identical protons. In fact, no considerable changes were observed. We therefore conclude that the conformational peculiarities observed for **2** are not maintained in solution.

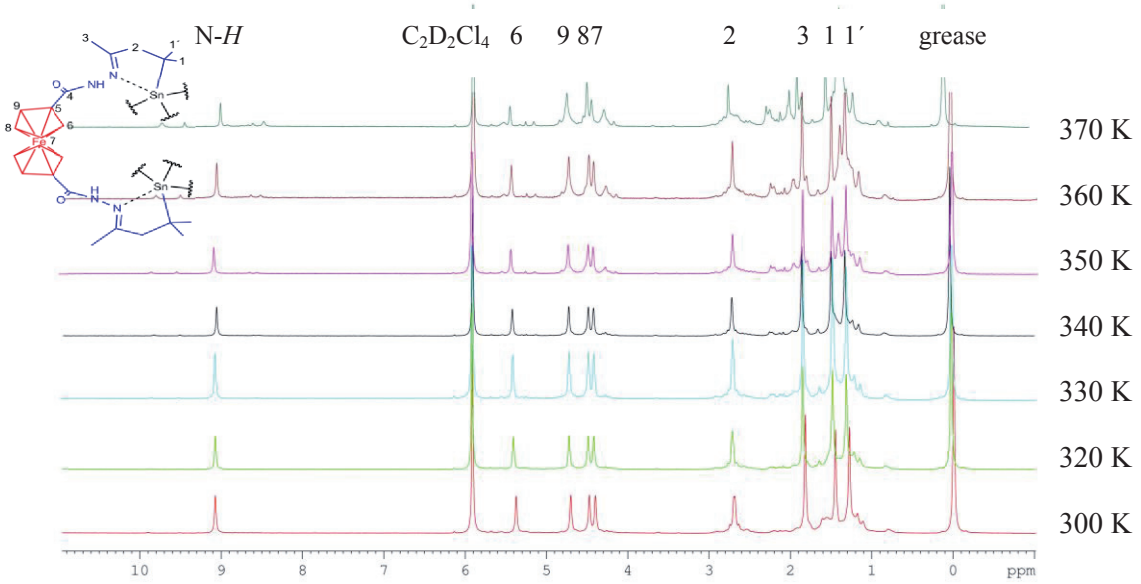

Figure S4. ^{1}H NMR spectra of **2** in tetrachloroethan-d_2 ($C_2D_2Cl_4$) with increasing measuring temperature (300 ~ 370 K).

UV-visible spectra:

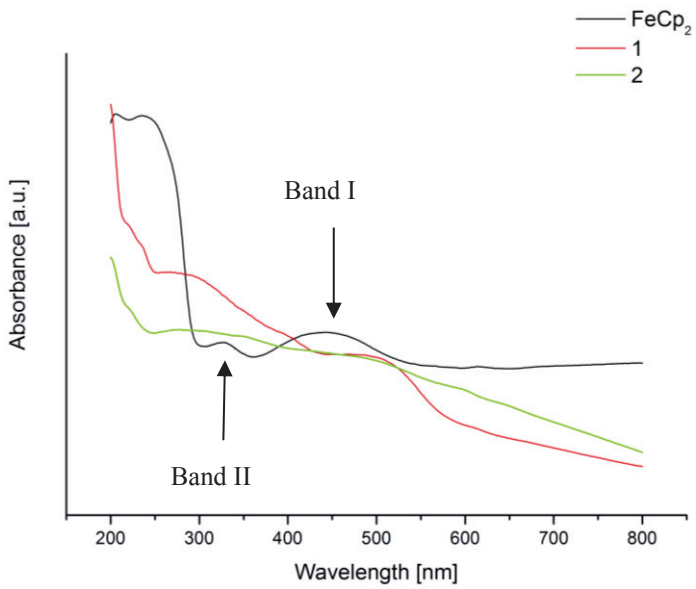

Figure. S**5** Solid-state UV-visible spectra of compounds **1** (red), **2** (green) and ferrocene (black), recorded as suspensions of single crystals in nujol oil.

The spectrum of ferrocene in the solid state displays two significant broad absorption bands, I at 445, and II at 328 nm, similar to the values recordred in ethanol solution (band I at 400, and II at 325 nm).[4]

Compound **1** has two distinct broad maxima at 514 and 270 nm, which can be assigned to the fC-containing organic spacer ($[CMe_2CH_2C(Me)=N–N=C(H)]_2fC$) and to a p(S)→p(Sn) charge transfer of the Sn-S-skeleton, respectively, according to similar reported values.[5,6] Compared with band I of pure ferrocene, the absorption band of the ferrocene units in **1** has a notable redshift of 69 nm, which is probably caused by the presence of the carbonyl substituent on ferrocene.[5] The according redshift of band I in compound **2** (about 55 nm) is smaller than observed for **1**. The absorption band at 273 nm can be also assigned to a p(S)→p(Sn) charge transfer. In both compounds, the second ferrocene-derived band II is observed, but the absorption is very weak, complicating an accurate estimate of their positions (ca. 401 nm in **1** and ca. 357 nm in **2**). For explanations, see the main manuscript text.

3. X-ray diffraction measurement, structure solution and refinement details

Data were collected on a diffractometer equipped with a STOE imaging plate detector system IPDS2T, using MoKa radiation with graphite monochromatization (λ = 0.71073 Å) at 100 K. The structure solution was performed by Sir-2004,[7] full-matrix-least-squares refinement against F^2, using SHELXS-97 and SHELXL-97 software.[8] Details of the data collections and refinements are given in Table S1. Selected bond lengths and bond angles are provided in Tables S2 and S3.

Table S1. Crystallographic and refinement details of **1** and **2**.

Compound	**1**·3CH_2Cl_2	**2**·5CH_2Cl_2
Chemical formula	$C_{51}H_{70}Cl_6Fe_2N_8S_6Sn_4$	$C_{53}H_{74}Cl_{10}Fe_2N_8O_4S_6Sn_4$
Formula Mass/g·mol^{-1}	1786.81	2020.52
Crystal color and shape	red block	orange block
Crystal size /mm^3	0.28×0.11×0.05	0.17×0.09×0.08
Crystal system	Orthorhombic	Monoclinic
a/Å	12.605	15.731
b/Å	25.646	24.753
c/Å	41.912	21.079
β/°	90.00	111.58
V/Å3	13548.9	7632.5
Space group	$P2_12_12_1$	$P2_1/c$
Z	8	4
Radiation type	Mo Kα	Mo Kα
Abs. coefficient, μ/mm^{-1}	2.330	2.219
Abs. correction type	numerical	numerical
min/max transmission	0.743/0.890	0.7042/0.8425
2θ range /deg	2.50-50.00	2.66-53.54
No. of reflections measured	77481	75937
No. of independent reflections	22698	16134
R_{int}	0.0315	0.1320
R_1 ($I > 2\sigma(I)$) / $wR(F^2)$ (all data)	0.0396/0.1081	0.0431/0.1058
Goodness of fit on F^2	1.036	0.816
Largest diff. peak/hole /e$^-$·Å^{-3}	1.233/-0.726	1.454/-1.231

*Compound **1***:

All non-H atoms were refined employing anisotropic displacement parameters. Disordered dichlormethane molecules were refined using PART and SAME constraints.

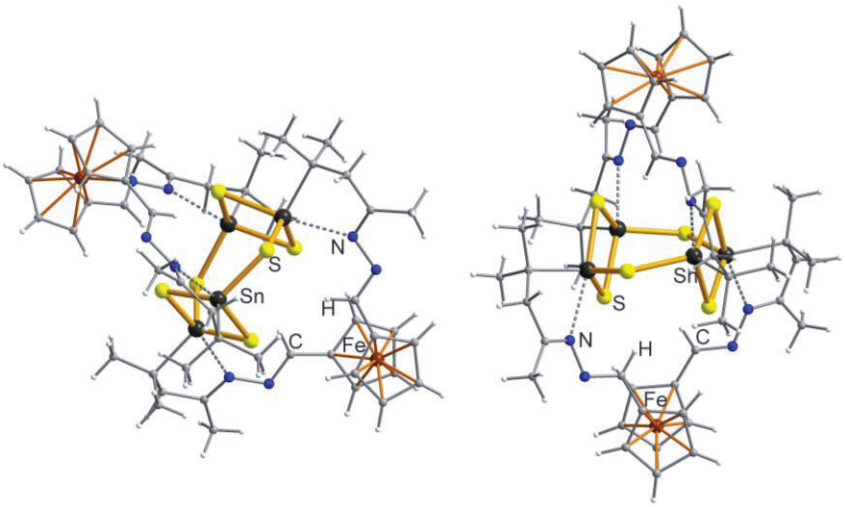

A **B**

Figure S6. Molecular structures of the two independent molecules A (left) and B (right) in **1**.

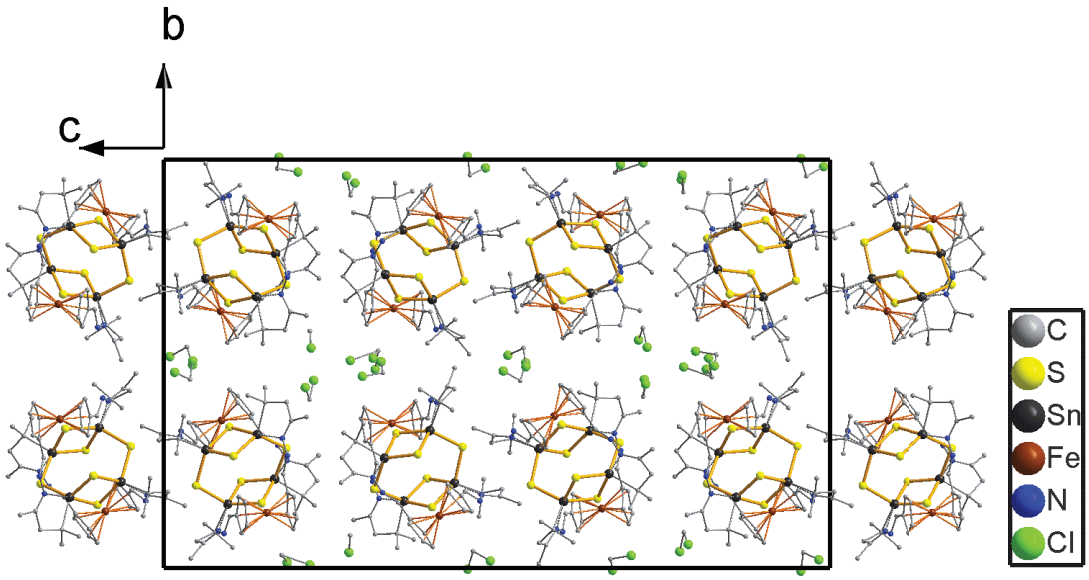

Figure S7. Packing of the molecules of **1**·3CH_2Cl_2 in the crystal, viewed along the crystallographic *a* axis. H atoms are omitted for clarity.

Table S2. Selected bond lengths [pm], bond angles [°] in **1**·3CH_2Cl_2.

S(1)-Sn(1)	248.7(2)	Sn(2)-C(49)	218.8(8)
S(1)-Sn(2)	239.21(19)	Sn(3)-C(73)	216.6(8)
S(2)-Sn(1)	238.60(18)	Sn(4)-C(70)	219.8(8)
S(2)-Sn(2)	249.1(2)	Sn(5)-C(25)	217.4(7)
S(3)-Sn(3)	249.16(18)	Sn(6)-C(1)	217.8(8)
S(3)-Sn(4)	239.30(18)	Sn(7)-C(46)	220.7(7)
S(4)-Sn(3)	238.48(19)	Sn(8)-C(22)	218.7(7)
S(4)-Sn(4)	250.71(18)	Sn(1)-N(1)	253.8(9)
S(5)-Sn(1)	240.74(19)	Sn(2)-N(7)	246.9(8)
S(5)-Sn(4)	240.82(19)	Sn(3)-N(3)	254.7(6)
S(6)-Sn(3)	241.12(18)	Sn(4)-N(5)	248.3(6)
S(6)-Sn(2)	241.5(2)	Sn(5)-N(14)	250.2(6)
S(7)-Sn(6)	238.91(18)	Sn(6)-N(12)	253.1(5)
S(7)-Sn(5)	249.83(17)	Sn(7)-N(16)	248.8(6)
S(8)-Sn(5)	239.28(18)	Sn(8)-N(10)	250.7(6)
S(8)-Sn(6)	248.70(17)	Sn(2)-S(1)-Sn(1)	88.84(7)
S(9)-Sn(7)	249.6(2)	Sn(1)-S(2)-Sn(2)	88.89(7)
S(9)-Sn(8)	238.46(17)	Sn(4)-S(3)-Sn(3)	88.75(6)
S(10)-Sn(7)	239.08(17)	Sn(3)-S(4)-Sn(4)	88.57(6)
S(10)-Sn(8)	249.02(19)	Sn(1)-S(5)-Sn(4)	108.46(7)
S(11)-Sn(6)	242.29(18)	Sn(3)-S(6)-Sn(2)	109.74(7)
S(11)-Sn(7)	241.02(19)	Sn(6)-S(7)-Sn(5)	88.92(6)
S(12)-Sn(5)	241.0(2)	Sn(5)-S(8)-Sn(6)	89.10(6)
S(12)-Sn(8)	240.6(2)	Sn(8)-S(9)-Sn(7)	88.79(6)
Sn(1)-C(94)	217.6(9)	Sn(7)-S(10)-Sn(8)	88.79(6)

*Compound **2***:

All non-H atoms were refined employing anisotropic displacement parameters. An EADP constraint was used for the atom pair C49 C52. A disordered dichlormethane molecule was refined using PART and SAME constraints, and the C–Cl bond lengths were restrained to 1.76(2) Å with a DFIX restraint.

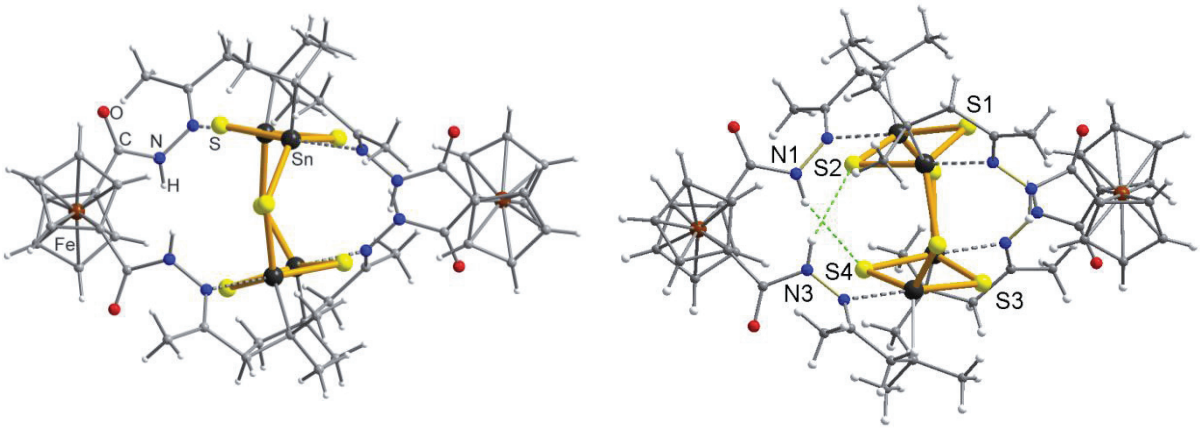

Figure S8. Molecular structure of **2** (left) and illustration of intramolecular hydrogen bonding (right).

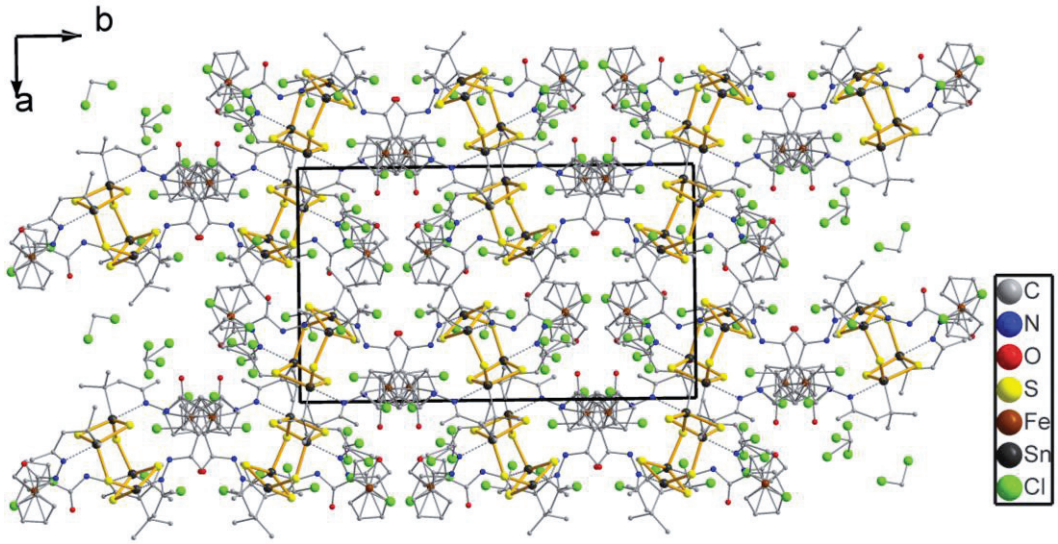

Figure S9. Packing of the molecules of **2**·5CH_2Cl_2 in the crystal, viewed along the crystallographic *c* axis. H atoms are omitted for clarity.

Table S3. Selected bond lengths [pm], bond angles [°] in **2**·5CH_2Cl_2.

S(1)-Sn(3)	239.3(2)	C(22)-Sn(2)	217.5(8)
S(1)-Sn(1)	248.25(19)	C(27)-Sn(1)	215.9(7)
S(2)-Sn(2)	238.91(19)	C(46)-Sn(4)	216.6(7)
S(2)-Sn(4)	249.1(2)	N(1)-Sn(3)	240.6(6)
S(3)-Sn(1)	241.5(2)	N(4)-Sn(2)	234.3(6)
S(3)-Sn(3)	249.59(19)	N(5)-Sn(1)	243.7(6)
S(4)-Sn(4)	241.32(19)	N(8)-Sn(4)	241.9(6)
S(4)-Sn(2)	248.5(2)	Sn(3)-S(1)-Sn(1)	88.09(6)
S(5)-Sn(2)	243.11(19)	Sn(2)-S(2)-Sn(4)	87.24(7)
S(5)-Sn(1)	243.6(2)	Sn(1)-S(3)-Sn(3)	87.29(6)
S(6)-Sn(3)	242.01(19)	Sn(4)-S(4)-Sn(2)	86.85(7)
S(6)-Sn(4)	242.8(2)	Sn(2)-S(5)-Sn(1)	111.92(8)
C(3)-Sn(3)	217.4(8)	Sn(3)-S(6)-Sn(4)	111.51(7)

4. Electrochemical measurements

All electrochemical measurements – cyclic and differential pulse voltammetry (CV and DPV) – were recorded under Ar atmosphere at 25 °C, using 0.1 mol/L [*n*-Bu_4N][PF_6] as the supporting electrolyte. The potentials were referenced internally to ferrocene, added at the end of the experiments. Working and counter electrodes: Pt; scan rate: 100 mV/s; pulse amplitude for DPV: 50 mV.

Table S4. Electrochemical characteristics for the oxidation process of the complexes **1** and **2** in DCM solution. (Measured at 100 mV/s, *vs*. [$FeCp_2$] in mV)

Complex	E_{pa}^1	E_{pa}^2	ΔE_p^1	ΔE_p^2	i_{pa}^1/i_{pc}^1	i_{pa}^2/i_{pc}^2
1	466	-	120	-	0.85	-
2	706	836	180	-	1.76	-

To investigate the electrochemical behavior of the double-decker cluster itself, we have performed a DVP analysis of the fC-free precursor [$(R^2Sn)_4S_6$] (Figure S10; R^2 = $CMe_2CH_2C(Me)O$). It indicates that the Sn/S framework itself is stable in the respective bias range.

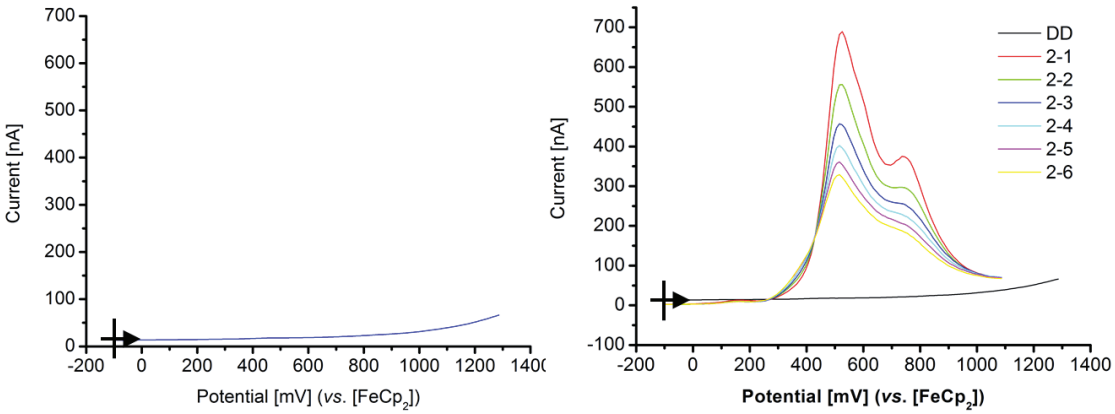

Figure S10. : DVP of $1.05 \cdot 10^{-3}$ mol/L of $[(R^2Sn)_4S_6]$ ("DD", $R^2 = CMe_2CH_2C(Me)O$) in DCM along with 0.1 mol/L $[NBu_4][PF_6]$ (left), and comparison of the DVP of $[(R^2Sn)_4S_6]$ with that observed for **2** (right; see also Figure 2b in the main manuscript), in the range of –100 - 1300 mV, scan rate 10 mV/s, pulse amplitude 50 mV.

5. Quantum chemical analyses

Density functional theory (DFT) investigations were undertaken employing the program system TURBOMOLE (Version 6.2),[9] using the BP86 functional,[10] and def2-TZVP basis sets.[11] For Sn atoms, an effective core potential (ECP-28) was applied.[12] The molecules of **1** and **2** were investigated by simultaneous optimization of the electronic and geometric structures, starting out from the geometries observed experimentally in the crystal structures without application of symmetry restrictions (C_1 symmetry). Both molecules converged into near D_{2d} symmetric structures, thus the unsymmetric conformation of **2** did not turn out to be a systematic feature upon attachment of the very fC ligand, but to be due to secondary effects within the crystal structure.

6. References for the Supporting Information

[1] Z. H. Fard, L. Xiong, C. Müller, M. Hołynska, S. Dehnen, *Chem. Eur. J.* **2009**, *15*, 6595.

[2] A. Connell, P. J. Holliman, I. R. Butler, L. Male, S. J. Coles, P. N. Horton, M. B. Hursthouse, W. Clegg, L. Russo, *J. Organomet. Chem.* **2009**, *694*, 2020.

[3] Q. B. Song, Z. L. Lu, X. L. Wu, Y. X. Ma, *Transition Met. Chem.* **1994**, *19*, 503; S. Top, S. Masi, G. Jaouen, *Eur. J. Inorg. Chem.* **2002**, 1848.

[4] L. Kaplan, W. L. Kester, J. J. Katz, *J. Am. Chem. Soc.* **1952**, *74*, 5531.

[5] T. H. Barr, W. E. Watts, *J. Organomet. Chem.* **1968**, *15*, 177.

[6] Z. H. Fard, M. Hołynska, S. Dehnen, *Inorg. Chem.* **2010**, *49*, 5748.

[7] M. C. Burla, R. Caliandro, M. Camalli, B. Carrozzini, G. L. Cascarano, L. De Caro, C. Giacovazzo, G. Polidori, R. Spagna, *J. Appl. Crystallogr.* **2005**, *38*, 381.

[8] G. W. Sheldrick, Bruker AXS Inc., Madison WI, **1997**.

[9] TURBOMOLE GmbH **2011**. TURBOMOLE is a development of University of Karlsruhe and Forschungszentrum Karlsruhe 1989-2007, TURBOMOLE GmbH since 2007.

[10] A. D. Becke, *Phys. Rev. A* **1988,** *38*, 3098; J. P. Perdew, *Phys. Rev. B* **1996**, *33*, 8822.

[11] F. Weigend, R. Ahlrichs, *Phys. Chem. Chem. Phys.* **2005**, *7,* 3297, F. Weigend, *Phys. Chem. Chem. Phys.* **2006**, *8*, 1057.

[12] H. Stoll, B. Metz, M. Dolg, *J. Comput. Chem*. **2002**, *23*, 767.

3.1.2 Directed formation of a ferrocenyl-decorated organotin sulfide complex and its controlled degradation

Zhiliang You and Stefanie Dehnen*

Fachbereich Chemie and Wissenschaftliches Zentrum für Materialwissenschaften, Philipps-Universität Marburg, Hans-Meerwein-Straße, D-35043 Marburg, Germany

---

Appeared in

Inorg. Chem. **2013**, *52*, 12332–12334.

Author contributions

Z. You conceived the project and carried out the synthesis and characterization, refined and described the crystal structure, co-wrote the manuscript. S. Dehnen supervised the work and co-wrote the manuscript.

Abstract

Attachment of ferrocenyl (Fc) units to an organo-functionalized precursor yielded the Fc-decorated complex $[(R^{Fc}Sn)_4Sn_6S_{10}]$ [**1**; R^{Fc} = $CMe_2CH_2C(Me)=N-N=C(Me)Fc$], which shows different ligand dynamics in solution than in the solid state, as confirmed by NMR spectroscopy and by cyclic and differential pulse voltammetry. The addition of different amounts of hydrochloric acid to a solution of **1** produced the derivatives $[(R^{Fc}SnCl_2)_2S]$ (**2**) and $[R^{Fc}SnCl_3 \cdot HCl]$ (**3**), the latter of which acts as a precursor to the formation/recovery of **2** or **1**, respectively.

Inorganic Chemistry

Communication

pubs.acs.org/IC

Directed Formation of a Ferrocenyl-Decorated Organotin Sulfide Complex and Its Controlled Degradation

Zhiliang You and Stefanie Dehnen*

Fachbereich Chemie and Wissenschaftliches Zentrum für Materialwissenschaften, Philipps-Universität Marburg, Hans-Meerwein-Straße, D-35043 Marburg, Germany

Supporting Information

ABSTRACT: Attachment of ferrocenyl (Fc) units to an organo-functionalized precursor yielded the Fc-decorated complex $[(R^{Fc}Sn)_4Sn_6S_{10}]$ [**1**; R^{Fc} = $CMe_2CH_2C(Me)$=N−N=C(Me)Fc], which shows different ligand dynamics in solution than in the solid state, as confirmed by NMR spectroscopy and by cyclic and differential pulse voltammetry. The addition of different amounts of hydrochloric acid to a solution of **1** produced the derivatives $[(R^{Fc}SnCl_2)_2S]$ (**2**) and $[R^{Fc}SnCl_3{\cdot}HCl]$ (**3**), the latter of which acts as a precursor to the formation/recovery of **2** or **1**, respectively.

Different types of organo-decorated main-group metal chalcogenide complexes have been investigated for many years because of their properties that derive from the combination of an inorganic (semi)metal chalcogenide core and an organic ligand shell.[1] Concerning group 14 chalcogenides, first studies were dedicated to syntheses and structures,[2,3] whereas recent developments focus more on the stabilities, functionalization, and resulting properties of the corresponding inorganic−organic complexes or networks.[4]

We have recently reported the synthesis and characterization of adamantane-type or double-decker-type (DD) $[(R^fT)_4S_6]$ or defect-heterocubane-type (SC) $[(R^fT)_3S_4]^q$ complexes [R^f = functional organic ligand like R^1 = $C_2H_4COO(H)$ or R^2 = $CMe_2CH_2C(Me)O$; T = Ge or Sn; q = possible charge], which were prepared from precursors R^fTCl_3.[5] Complexes with R^2 are reactive toward hydrazine, as well as toward terminal hydrazine derivatives, hydrazones, or hydrazides.[5a,6,7] The DD-type thiostannate complex $[(R^2Sn)_4S_6]$ (**A**) undergoes a structural rearrangement upon reaction with terminal hydrazine derivatives, resulting in the formation of a double-SC (DSC) $[Sn_6S_{10}]$ topology, as in $[(R^4Sn)_4Sn_2S_{10}]$ [**B**; R^4 = $CMe_2CH_2C(Me)$=NNHPh].[5a,6] Aiming at a deeper understanding and control of the synthesis, reactivity, and physicochemical properties of organo-functionalized chalcogenide complexes, we currently concentrate on the attachment of new ligands to known complex topologies and study their directed degradation as well as interconversion between different forms.

The work has been extended by the introduction of ferrocenyl (Fc) ligands to study their influence on the structural and electrochemical properties of the decorated $[Sn_4S_6]$ complexes. Whereas the first experiments were undertaken with bis-substituted intramolecular (fC) linkers,[8] the current investigations were undertaken with the monosubstituted Fc substituents presented herein (Scheme 1).

Scheme 1. Synthesis of Compounds 1−3 by Stepwise Reactions Starting from Precursor Complex A

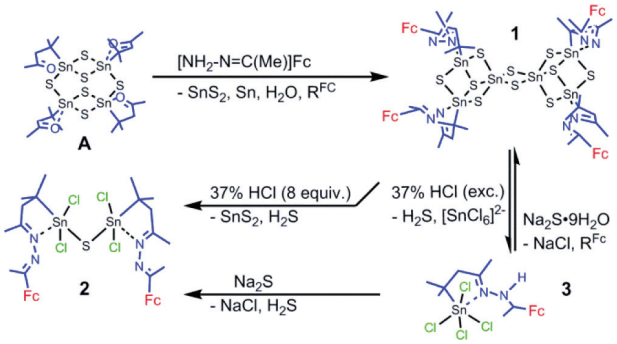

Derivatization of **A** with 4 equiv of H_2NN=C(Me)Fc was accompanied by rearrangement of the Sn/S core to form a DSC-type cage in $[(R^{Fc}Sn)_4Sn_2S_{10}]$ [**1**; R^{Fc} = $CMe_2CH_2C(Me)$=N−N=C(Me)Fc]. Previous studies of this rearrangement suggested that its occurrence or suppression is highly dependent on the steric demand of the ligand and its ability to form an intramolecular N → Sn coordination. Thus, the R^{Fc} ligand with a terminal Fc group seems to be bulky enough in this regard.

The treatment of **1** with 8 equiv of concentrated hydrochloric acid (37% HCl) yielded 2 equiv of the sulfide-bridged, dinuclear complex $[(R^{Fc}SnCl_2)_2S]$ (**2**) besides H_2S (4 equiv) and SnS_2 (2 equiv); by the addition of excess acid, the novel organotin chloride complex $[R^{Fc}SnCl_3{\cdot}HCl]$ (**3**) was obtained besides H_2S (10 equiv) and $[SnCl_6]^{2-}$ (2 equiv). The reaction of **3** with 2 equiv of $Na_2S{\cdot}9H_2O$ in a water/acetone mixture regenerated **1**, while the addition of anhydrous Na_2S in tetrahydrofuran (THF), however, led to the formation of **2** (Scheme 1). All three compounds were characterized by standard analytical techniques and single-crystal X-ray diffraction [see the Supporting Information (SI), Table S1].

The $[Sn_4S_6]$ core of the DD cage in **A** was rearranged during the reaction, yielding **1**, as observed in the case of **B**.[5a,6] In **1**, however, the $[Sn_6S_{10}]$ skeleton is connected to four Fc units via Schiff-base ligands (Figure 1). Two conformational isomers, **1a** and **1b**, were isolated upon two different reaction pathways at

Received: September 10, 2013
Published: October 14, 2013

   dx.doi.org/10.1021/ic4022992 | *Inorg. Chem.* 2013, 52, 12332−12334

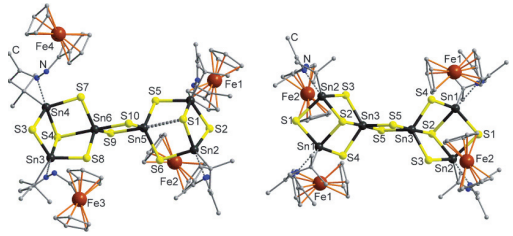

Figure 1. Molecular structures (without H atoms) of **1a** (left) and **1b** (right).

different crystallization conditions. Both crystallize in the space group $P\bar{1}$ but with different unit cells. Additionally, **1b** possesses molecular inversion symmetry, whereas **1a** exhibits no molecular symmetry.

Most of the bond lengths and angles within the $[Sn_6S_{10}]$ cores in **1a** and **1b** differ only marginally and agree with reported values (see the SI, Tables S2 and S3).[5a] The only notable exception is one unusually large Sn−S distance (Sn5···S1 3.007 Å) in **1a**, which is clearly associated with the solid state because ^{119}Sn NMR in solution produces only two signals (see the SI, Figure S12). This asymmetry of the Sn/S core in **1a** is accompanied by an asymmetric situation of the Fc-terminated ligands.

In the C_i-symmetric molecule of **1b**, the distances between the two Fe ions that belong to the same SC are naturally equal (Fe1···Fe2 6.1 Å), whereas for **1a**, this is obviously not the case. Here, two distances are observed (Fe1···Fe2 11.1 Å and Fe3···Fe4 6.3 Å), due to the different orientations of the Fc units, that are free to rotate about the C_{Cp}−C(Me) and/or N−N bonds of the Schiff-base ligand (see the SI, Scheme S1).

The different orientations of the Fc units in **1a** are obviously offset in solution, as confirmed by ^{1}H NMR spectra. Thus, the orientation of the Fc units in **1** seems to be highly flexible; the conformers realized in **1a** and **1b** are believed to be the result of the most effective packing of the molecules during crystallization, as indicated by intermolecular hydrogen-bonding interactions that can only be observed in the case of **1b** (see the SI, Figure S1).

The presence of four Fc units in close proximity to each other prompted us to investigate the electrochemical behavior of **1**. Cyclic and differential pulse voltammetry (CV and DPV) was performed in a CH_2Cl_2 solution in the presence of of tetra-*n*-butylammonium hexafluorophosphate (TBFP; 0.1 M) at 25 °C (Figure 2). As shown in Figure 2, compound **1** undergoes two oxidation steps, which are almost overlapped in the CV ($E^1_{1/2}$ = 435 mV and $E^2_{1/2}$ = 615 mV at a scan rate of 100 mV/s) but sufficiently well separated in the DPV curve. The nearly equal intensities of the two peaks in the DPV graph suggest that each of

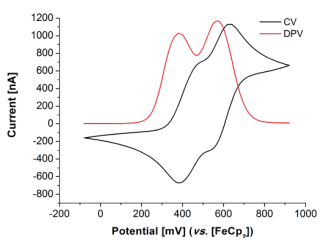

Figure 2. Cyclic and differential pulse voltammograms, recorded at a platinum electrode in a CH_2Cl_2 solution of **1** (1.61 mM), in the presence of TBFP (0.1 M). Scan ranges and rates: CV, −100 to +900 mV, 400 mV/s; DPV, −100 to +900 mV, 10 mV/s. Pulse amplitude 50 mV.

the two oxidations should involve the same number of (two) electrons.

The two-step oxidation of **1** indicates the existence of an electronic communication between the Fc units. According to previous investigations with multiple redox centers,[8,9] Fc units of different SC units are not likely to interact owing to the large Fe··· Fe distance (**1a**, 13.0−14.5 Å; **1b**, 15.6−20.1 Å); they should thus behave identically. However, two vicinal Fc units that are located at the same SC moiety seem to communicate as a consequence of the flexibility of their relative orientations, as demonstrated in the different conformers (**1a** and **1b**). The comproportionation constant K_{comp}, which is a guide to the extent of electronic communication, was calculated on the basis of the separation between the formal electrode potentials of the two oxidation processes,[10] revealing that the electronic communication is relatively large (1.49×10^{12}) in spite of a small potential separation (see the SI, Table S7).

Electrospray ionization mass spectrometry in the positive ion mode, ESI-MS (+), of a methanolic solution of **1** not only exhibited the molecular peak of **1** (m/z 2325.63, $[M]^+$) but also provided deeper insight into the deconstruction or (re)assembly of Fc-ligated S/Sn cages in the gas phase. Three further species were identified, with the predominant peak according to $[(R^{Fc}Sn)_3S_4]^+$ (m/z 1452.96, $[M-R^{Fc}-3(SnS_2)]^+$); the composition belongs most probably to a SC-type fragment, which was also detected as the predominant peak in the positive-ion ESI-MS of **2**. Hence, this very stable structural motif forms from different sources under ESI-MS conditions. Compound **3**, in contrast, is unstable in the gas phase, exhibiting three decomposition products ($[HR^{Fc}SnCl_3]^+$, $[R^{Fc}SnCl_2]^+$, and $[R^{Fc}]^+$). The weak peak at m/z 1004.95 can be assigned to the oxo complex $[(R^{Fc}SnCl_2)_2O]^+$, which forms upon hydrolysis of **3** under ESI-MS conditions (see the SI, Figure S11).

Compound **2** crystallizes with two independent molecules in the asymmetric unit that exhibit nearly identical structural parameters (see the SI, Tables S4 and S5). An intermolecular Cl···H−C hydrogen bond (2.82 Å) interconnects the two molecules (see the SI, Figure S4). Depending on the chosen synthetic pathway, the asymmetric unit of **2** contains solvent molecules $\{[(R^{Fc}SnCl_2)_2S]\cdot 3CHCl_3$ (**2a**); Figure 3, left} or

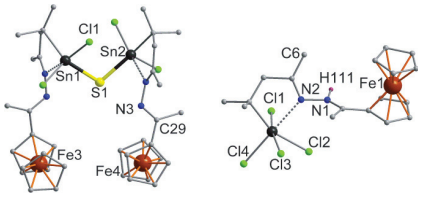

Figure 3. Molecular structures of **2a** (one of two independent molecules, left) and **3** (right). Solvent and H atoms (except the one labeled) are omitted for clarity.

cocrystallized with the byproduct $\{[(R^{Fc}SnCl_2)_2S]\cdot H_2S$ (**2b**)$\}$. Compound **3** crystallizes in the orthorhombic space group $Pna2_1$, with four molecules in the unit cell (Figure 3, right).

The pentacoordinated Sn atoms retain their organometallic decoration during degradation by HCl addition in both compounds. In **2**, two of three S^{2-} ligands per Sn atom in **1** were replaced by Cl^- ligands, with one remaining S atom acting as a bridge to form the dinuclear complex. The addition of excess HCl, however, resulted in complete degradation by formation of the mononuclear complex **3**. Here, 1 equiv of HCl is caught

dx.doi.org/10.1021/ic4022992 | *Inorg. Chem.* 2013, 52, 12332−12334

between two molecules through an intermolecular hydrogen bond Sn−Cl···H−N (see the SI, Figures S8 and S18), thereby converting the pentacoordinated Sn atom into a hexacoordinated one, similar to other organotin tri/tetrahalides with intramolecular coordination by a donor atom.[11]

The different reactions of **3** with Na_2S (see above) reflect the influence of the solvents: using the more polar water/acetone mixture, the reaction back to **1** was completed within a few minutes, with a distinct color change from purple via red to yellow; in THF, in contrast, the reaction stopped at an intermediate step (namely, upon formation of **2**), because the color of the suspension was still purple-red after stirring for 18 h.

We demonstrated the direct formation of a Fc-decorated organotin sulfide complex displaying electronic communication of vicinal Fc units, which can be split into di- or mononuclear organotin complexes by the addition of HCl. Future research is dedicated to the reactivity of the fragments toward chalcogenide compounds.

■ ASSOCIATED CONTENT

Ⓢ Supporting Information

X-ray data (CIF), details of syntheses, analyses (IR, Raman, ESI-MS, ^{1}H, ^{13}C, and ^{119}Sn NMR, and EDX), and electrochemical measurements. Figures S1−S25, Scheme S1, and Tables S1−S10. This material is available free of charge via the Internet at http://pubs.acs.org.

■ AUTHOR INFORMATION

Corresponding Author

*E-mail: dehnen@chemie.uni-marburg.de.

Notes

The authors declare no competing financial interest.

■ ACKNOWLEDGMENTS

The authors thank the Deutsche Forschungsgemeinschaft for financial support of this work within the framework of SFB 1083.

■ REFERENCES

(1) Dehnen, S.; Melullis, M. *Coord. Chem. Rev.* **2007**, *251*, 1259.

(2) (a) Pfeiffer, P.; Lehnardt, R. *Ber. Dtsch. Chem. Ges.* **1903**, *36*, 3027. (b) Dörfelt, C.; Janeck, A.; Kobelt, D.; Paulus, E. F.; Scherer, H. *J. Organomet. Chem.* **1968**, *14*, P22. (c) Kobelt, D.; Paulus, E. F.; Scherer, H. *Acta Crystallogr.* **1972**, *B28*, 2323. (d) Davies, A. G.; Smith, L.; Smith, P. J. *J. Organomet. Chem.* **1972**, *39*, 279. (e) Berwe, H.; Haas, A. *Chem. Ber.* **1987**, *120*, 1175. (f) Benno, R. H.; Fritchie Junior, C. J. *J. Chem. Soc., Dalton Trans.* **1973**, 543. (g) Haas, A.; Kutsch, H.-J.; Krüger, C. *Chem. Ber.* **1987**, *120*, 1045. (h) Dakternieks, D.; Jurkschat, K.; Wu, H.; Tiekink, E. R. T. *Organometallics* **1993**, *12*, 2788. (i) Weidenbruch, M.; Schlaefke, J.; Schäfer, A.; Peters, K.; von Schnering, H.-G.; Marsmann, H. *Angew. Chem., Int. Ed.* **1994**, *33*, 1846. (j) Unno, M.; Kawai, Y.; Shioyama, H.; Matsumoto, H. *Organometallics* **1997**, *16*, 4428. (k) Mehring, M.; Schürmann, M.; Reuter, H.; Dakternieks, D.; Jurkschat, K. *Angew. Chem., Int. Ed.* **1997**, *36*, 1112. (l) Zobel, B.; Schürmann, M.; Jurkschat, K.; Dakternieks, D.; Duthie, A. *Organometallics* **1998**, *17*, 4096. (m) Wraage, K.; Pape, T.; Herbst-Irmer, R.; Noltemeyer, M.; Schmidt, H.-G.; Roesky, H. W. *Eur. J. Inorg. Chem.* **1999**, 869.

(3) (a) Wagner, C.; Raschke, C.; Merzweiler, K. *Appl. Organomet. Chem.* **2004**, *18*, 147. (b) Bouška, M.; Dostál, L.; Padělková, Z.; Lyčka, A.; Herres-Pawlis, S.; Jurkschat, K.; Jambor, R. *Angew. Chem., Int. Ed.* **2012**, *51*, 3478. (c) Wagner, M.; Zöller, T.; Hiller, W.; Prosenc, M. H.; Jurkschat, K. *Chem.—Eur. J.* **2013**, *19*, 9463.

(4) (a) Davies, A. G. *Organotin Chemistry*, 2nd completely revised and updated ed.; Wiley-VCH: New York, 2004. (b) Feng, P.; Bu, X.; Zheng, N. *Acc. Chem. Res.* **2005**, *38*, 293. (c) Bu, X.; Zheng, N.; Feng, P. *Chem.—Eur. J.* **2004**, *10*, 3356.

(5) (a) Hassanzadeh Fard, Z.; Xiong, L.; Müller, C.; Hołyńska, M.; Dehnen, S. *Chem.—Eur. J.* **2009**, *15*, 6595. (b) Hassanzadeh Fard, Z.; Müller, C.; Harmening, T.; Pöttgen, R.; Dehnen, S. *Angew. Chem., Int. Ed.* **2009**, *48*, 4441. (c) Eußner, J. P.; Barth, B. E. K.; Leusmann, E.; You, Z.; Rinn, N.; Dehnen, S. *Chem.—Eur. J.* **2013**, *19*, DOI: 10.1002/chem.201301521.

(6) (a) Fard, Z. H.; Halvagar, M. R.; Dehnen, S. *J. Am. Chem. Soc.* **2010**, *132*, 2848. (b) Halvagar, M. R.; Fard, Z. H.; Dehnen, S. *Chem.—Eur. J.* **2011**, *17*, 4371.

(7) Halvagar, M. R.; Hassanzadeh Fard, Z.; Xiong, L.; Dehnen, S. *Inorg. Chem.* **2009**, *48*, 7373.

(8) You, Z.; Fenske, D.; Dehnen, S. *Dalton Trans.* **2013**, *42*, 8179.

(9) (a) MacDonald, D. G.; Eichhöfer, A.; Campana, C. F.; Corrigan, J. F. *Chem.—Eur. J.* **2011**, *17*, 5890. (b) Ferguson, G.; Glidewell, C.; Opromolla, G.; Zakaria, C. M.; Zanello, P. *J. Organomet. Chem.* **1996**, *517*, 183.

(10) Richardson, D. E.; Taube, H. *Inorg. Chem.* **1981**, *20*, 1278.

(11) (a) Jambor, R.; Růžička, A.; Brus, J.; Císařová, I.; Holeček, J. *Inorg. Chem. Commun.* **2001**, *4*, 257. (b) Novák, P.; Císařová, I.; Kolářová, L.; Růžička, A.; Holeček, J. *J. Organomet. Chem.* **2007**, *692*, 4287.

(12) (a) Fox, O. D.; Dalley, N. K.; Harrison, R. G. *J. Am. Chem. Soc.* **1998**, *120*, 7111. (b) Fang, H. C.; Zhu, J. Q.; Zhou, L. J.; Jia, H. Y.; Li, S. S.; Gong, X.; Li, S. B.; Cai, Y. P.; Thallapally, P. K.; Liu, J.; Exarhos, G. J. *Cryst. Growth Des.* **2010**, *10*, 3277. (c) Chen, M.; Chen, S. S.; Okamura, T. A.; Su, Z.; Chen, M. S.; Zhao, Y.; Sun, W. Y.; Ueyama, N. *Cryst. Growth Des.* **2011**, *11*, 1901.

Directed Formation of a Ferrocenyl-Decorated Organotin Sulfide Complex and Its Controlled Degradation

Zhiliang You and Stefanie Dehnen*

Fachbereich Chemie, Philipps-Universität Marburg,

Hans-Meerwein-Straße, D-35043Marburg, Germany

email: dehnen@chemie.uni-marburg.de

SUPPORTING INFORMATION

1. Experimental Syntheses Details

***General*:** All reaction steps were carried out under Ar atmosphere. All solvents were dried and freshly distilled prior to use. Organotin sulfide clusters $[(R^2Sn)_4S_6]$ (R^2 = $CMe_2CH_2C(Me)O$) and acetylferrocene hydrazone $[NH_2\text{-}N{=}C(Me)]Fc$ were prepared according to the reported methods.[1,2]

^1H NMR, ^{13}C NMR and ^{119}Sn NMR measurements were carried out using a Bruker DRX 400 MHz spectrometer at 25ºC. In ^1H and ^{13}C NMR spectra, the chemical shifts were quoted in ppm relative to the residual protons of deuterated solvents. In ^{119}Sn NMR, Me_4Sn was used as internal standard.

Infrared (IR) spectra were recorded on a Bruker TENSOR 37 FT-IR spectrometer.

Mass spectrometry (MS) was performed on a Finnigan MAT 95S. The Electrospray Ionisation (ITMS-ESI) spectra were obtained by using solvent as the carrier gas.

By-products given in Scheme 1 were analyzed as follows: The presence of Sn and S in the $Sn+SnS_2$ precipitate was determined by means of energy-dispersive X-ray spectroscopy (EDX) and wet chemical analysis following standard protocols (for details of the EDX technique, see chapter 5 below); organic leaving groups and $[SnCl_6]^{2-}$ were detected by means of ^1H, ^{13}C and ^{119}Sn NMR spectra, respectively. H_2S was identified by its characteristic smell upon opening the Schlenk tube. NaCl was gained in single-crystalline form as large colorless cubes and identified by means of single-crystal X-ray diffraction. The release of water could not be verified, but is strongly suggested due to its plausibility.

Synthesis of ***1a*** *[(R^{Fc}Sn)$_4$S$_8${Sn(μ-S)$_2$}]· 5CH_2Cl_2,{**1**·5CH_2Cl_2, R^{Fc} = [$CMe_2CH_2C(Me)$=N–N=C(Me)]Fc}*

[NH_2-N=C(Me)]Fc (0.040 g, 0.165 mmol) and [(R^2Sn)$_4$S$_6$] (0.044 g, 0.041 mmol) were solved in 10 mL of CH_2Cl_2. The solution was heated under reflux for 17 h. Red block-shape crystals of **1a** were obtained within 2 days by layering the reaction solution with *n*-hexane (1:1) at room temperature.

Yield: 0.046 g, 49.0% (calculated on basis of [NH_2-N=C(Me)]Fc)

Synthesis of ***1b*** *[(R^{Fc}Sn)$_4$S$_8${Sn(μ-S)$_2$}]· 6CH_2Cl_2,{**1**·6CH_2Cl_2, R^{Fc} = [$CMe_2CH_2C(Me)$=N–N=C(Me)]Fc}*

A solution of $Na_2S\cdot 9H_2O$ (0.0855 g, 0.356 mmol) in acetone/water (14 mL, 8:6) was added slowly into a mixture of **3** (0.104 g, about 0.178 mmol) in 6 mL of acetone at –5°C. The mixture was stirred for 20 min at room temperature. The yellow-brown powder was collected on a glass frit, washed with water, and dried under vacuum. Red crystals of **1b** were obtained by layering a solution of the powder in CH_2Cl_2 with *n*-pentane (1:1) at –15°C.

Yield: 0.073 g, 70.2% (calculated on basis of **3**)

^{1}**H** NMR (400 MHZ, CD_2Cl_2, 25°C): δ/ppm = 1.37 (s, 6H; ***Me***$_2$C), 1.85 (s, 3H; ***Me***(Cp)C=N), 2.06 (s, 3H, ***Me***C=N), 2.71 (s, 2H, C***H***$_2$), 4.24 (s, 5H, $Cp_{unsubst.}$-***H***), 4.34, 4.64, (2xm, 2x2H, $Cp_{subst.}$-***H***); ^{13}**C** NMR (100 MHZ, CD_2Cl_2, 25°C): *δ/ppm* = 17.80 (N=C***C***H$_3$), 19.87(N=C***C***H$_3$(Cp)), 26.50 ((***C***H$_3$)$_2$C), 39.354 (***C***Me$_2$), 50.48 (***C***H$_2$), 68.25, 70.11, 70.64, (H***C***-Cp)), 82.31 (-***C***-Cp), 162.80 (Cp(H)***C***=N), 162.99 (Me(CH$_2$)***C***=N); ^{119}**Sn** NMR (149 MHz, CD_2Cl_2): *δ/ppm* = –95.32; –108.34 ; MS-ESI: *m/z* = 2325.63 ([M]$^+$); *m/z* = 2002.50 ([M−R^{Fc}]$^+$); *m/z* = 1636.81 ([M−R^{Fc}−2(SnS_2)]$^+$); *m/z* = 1452.96 ([M−R^{Fc}−3(SnS_2)]$^+$); IR (KBr, Nujol mull in polyethylene windows): ῡ/cm^{-1} = 3435.6 (w), 3090.9 (w), 2934.9 (w), 2849.4 (m), 1621.2 (s), 1596.0 (s), 1476.0 (m), 1455.3 (m), 1380.8 (m), 1364.8 (s), 1295.3 (s), 1245.1 (w), 1213.6 (m), 1140.0 (m), 1121.7 (s), 1105.1 (s), 1018.8 (m), 999.9 (m), 891.6 (m), 817.9 (s), 517.4 (m), 479.7 (s), 436.7 (w), 361.5 (s), 343.8 (s), 317.3 (s), 290.0 (s), 262.3 (s), 198.5(m), 174.8 (m), 144.2 (w), 107.7 (w).

*Synthesis of **2a** [($R^{Fc}SnCl_2)_2S$]· H_2S,{**2**·3$CHCl_3$, R^{Fc} = [$CMe_2CH_2C(Me)$=N–N=C(Me)]Fc}*

A solution of 37% HCl (0.0302 g, 0.310 mmol of HCl) in 1.5 mL of MeOH was added to a solution of **1** (0,090 g, 0.0387 mmol) in 15 mL of CH_2Cl_2 at 0°C. Upon the addition, the clear red solution turned to a purple-red mixture. After 10 h stirring at room temperature, the mixture was filtered, and the deep red filtrate was evaporated in vacuum. The resulting oily solid was dissolved in 8 mL of $CHCl_3$, and layered with *n*-pentane (1:1). Red block-shape crystals of **2a** were obtained within 10 days.

Yield: 0.0092 g, 5.60% (calculated on basis of **1**)

*Synthesis of **2b** [($R^{Fc}SnCl_2)_2S$]· H_2S,{**2**·H_2S, R^{Fc} = [$CMe_2CH_2C(Me)$=N–N=C(Me)]Fc}*

Anhydrous Na_2S (0.0138 g, 0.164 mmol) and **3** (0.048 g, 0.082 mmol) were suspended in 20 mL of THF. After 18 h stirring at room temperature, the mixture was filtered. The red filtrate was evaporated in vacuum, dissolved in 6 mL of CH_2Cl_2 and layered with *n*-pentane (1:1). Red block-shape crystals of **2b** were obtained within 3 days.

Yield: 0.0041 g, 9.54% (calculated on basis of **3**)

^{1}**H** NMR (400 MHZ, CD_2Cl_2, 25°C): δ/ppm = 1.43, 1.55 (ss, 6H; ***Me***$_2$C), 1.89 (s, 3H; ***Me***(Cp)C=N), 2.12 (s, 3H, ***Me***C=N), 2.87 (s, 2H, C***H***$_2$), 4.31 (s, 5H, $Cp_{unsubst.}$-***H***), 4.38, 4.72, (2xm, 2x2H, $Cp_{subst.}$-***H***); ^{119}**Sn** NMR (149 MHz, CD_2Cl_2): *δ/ppm* = –84.05; MS-ESI: *m/z* = 1452.96 ([($R^{Fc}Sn)_3S_4]^+$); IR (KBr, Nujol mull in polyethylene windows): ϋ/cm^{-1} = 3089.0 (w, br), 2965.5 (w, br), 2861.0 (w, br), 2366.3 (w), 2350.2 (w), 1680.3 (s), 1596.5 (s), 1469.9 (m), 1443.4 (m), 1421.1 (m), 1369.7 (s), 1294.9 (m), 1210.6 (w), 1114.2 (s), 1005.5 (s), 889.6 (m), 823.7 (s), 738.9 (m), 666.65 (w), 519.6 (m), 480.8 (vs), 443.1 (m), 375.1 (s), 344.7 (s), 311.1 (vs), 251.2 (vs, br), 200.80 (s), 170.3(vs), 153.7 (m), 126.4 (vs, br), 98.8 (s), 68.13 (vs), 60.6 (s), 45.9 (vs, sh), 33.98 (vs, sh).

*Synthesis of **3** [$HR^{Fc}SnCl_4$], {R^{Fc} = [$CMe_2CH_2C(Me)$=N–N=C(Me)]Fc}*

[NH_2-N=C(Me)]Fc (0.040 g, 0.165 mmol) and [($R^2Sn)_4S_6$] (0.044 g, 0.041 mmol) were solved in 10 mL of CH_2Cl_2. The solution was heated under reflux for 17 h, then

1 mL, thus an excess of 37% HCl (water solution) were added by using a syringe. Upon the addition, the red solution turned to dark purple-red. After 10 min stirring, the solvent was removed under reduced pressure, and the resulting purple powder was dried for another 4 h under high vacuum. The powder, the identity of which was proven by ^{1}H and ^{119}Sn-NMR, is sufficiently clean for further reactions (Fig. S6). Sinlge-crystals of **3** were obtained within 1 day upon layering the reaction mixture with THF.

Yield: 0.018 g, 18.6% (crystals calculated on basis of [NH_2-N=C(Me)]Fc)

^{1}**H** NMR(400 MHz; DMSO-d_6; 25^{o}C): δ/ppm = 1.26 (s, 6H; ***Me***$_2$C), 1.94 (s, 3H; ***Me***(Cp)C=N), 2.15 (s, 3H, ***Me***C=N), 2.70 (s, 2H, C***H***$_2$), 4.30 (s, 5H, *Cp*$_{unsubst.}$-***H***), 4.46, 4.74, (2xm, 2x2H, *Cp*$_{subst.}$-***H***); ^{13}**C** NMR (100 MHz, DMSO-d_6, 25^{o}C): δ/ppm = 17.24 (N=C***C***H3), 20.07(N=C***C***H3(Cp)), 26.90 ((***C***H3)2C), 48.85 (***C***H2), 69.74 (***C***Me2) 67.69, 69.21, 70.34, (H***C***-Cp)), 81.39 (-***C***-Cp), 164.85 (Cp(H)***C***=N), 164.99 (Me(CH2)***C***=N); ^{119}**Sn** NMR (149 MHz, DMSO-d_6): δ/ppm = −417.91; MS-ESI: *m/z* = 1004.95 ([(M-HCl-Cl)$_2$O]$^+$) *m/z* = 548.94 ([M-Cl]$^+$); *m/z* = 512.96 ([M−HCl−Cl]$^+$); *m/z* = 323.2 ([M-$HSnCl_4$]$^+$); IR (KBr, Nujol mull in polyethylene windows): ϑ/cm^{-1} = 3414.4 (m), 3196.9 (w), 3093.7 (s), 2983.3 (m), 2952.1 (m), 2854.6 (m), 1600.6 (s), 1483.5 (m), 1436.2 (m), 1412.6 (m), 1379.3 (s), 1324.4 (m), 1254.0 (m), 1219.0 (m), 1133.9 (m), 1106.7 (m), 1042.4 (m), 1017.7 (m), 1001.4 (m), 892.4 (m), 857.2 (m), 829.2 (s), 779.1 (m), 723.7 (m), 639.3 (m), 518.4 (m), 495.1 (m), 477.3 (s), 440.8 (m), 374.7 (m), 320.7 (s), 293.1 (s), 250.1 (s), 206.1 (s), 154.3 (s).

2. X-ray diffraction measurement, structure solution and refinement details

Data were collected on a diffractometer equipped with a STOE imaging plate detector system IPDS2T, using MoKα radiation with graphite monochromatization (λ = 0.71073 Å) at 100 K. The structure solution and refinement was performed by Sir-2004,[3a] full-matrix-least-squares refinement against *F*2 was done using SHELXL-97 software.[3b] Details of the data collections and refinements are given in Table S1. Selected bond lengths and bond angles are provided in tables S2-S6. Structural details are illustrated in Figures S1-S8.

Table S1. Crystal and structure refinement data.

Compound	**1a:** **1**·5CH_2Cl_2	**1b**: **1**·6CH_2Cl_2	**2a**: **2**·3$CHCl_3$	**2b**: **2**·H_2S	**3**
Chemical formula	$C_{77}H_{102}Cl_{10}Fe_4N_8S_{10}Sn_6$	$C_{78}H_{104}Cl_{12}Fe_4N_8S_{10}Sn_6$	$C_{75}H_{95}Cl_{17}Fe_4N_8S_2Sn_4$	$C_{72}H_{92}Cl_8Fe_4N_8S_3Sn_4$	$C_{18}H_{24}Cl_4Fe_1N_2Sn_1$
Formula Mass/g·mol^{-1}	2750.31	2835.24	2473.52	2147.48	284.73
Crystal color and shape	red block	Red block	Orange-red block	Yellow needle	Purple plate
Crystal size /mm^3	0.34x0.08x0.06	0.40x0.38x0.36	0.16x0.16x0.09	0.17x0.05x0.05	0.40x0.20x0.06
Crystal system	Triclinic	Triclinic	Monoclinic	Monoclinic	Orthorhombic
a/Å	10.925	14.477	16.402	17.603	25.781
b/Å	21.491	14.948	17.897	17.958	10.253
c/Å	21.736	15.913	17.528	25.862	8.229
α/°	91.95	65.48	90.00	90.00	90.00
β/°	99.80	78.88	115.99	94.608	90.00
γ/°	96.02	61.08	90.00	90.00	90.00
V/Å3	4993.9	2742.2	4625.0	8149	2175.1
Space group	$P\bar{1}$	$P\bar{1}$	$P2_1$	$P2_1/c$	$Pna2_1$
Z	2	2	2	4	4
Abs. coefficient, *μ*/mm^{-1}	2.556	2.377	2.252	2.281	2.312
Abs. correction type	psi-scan	numerical	gaussian	gaussian	numerical
min/max transmission	0.4769/0.8617	0.4498/0.4815	0.7146/0.8230	0.6978/0.8945	0.4582/0.8737
2θ range /deg	2.62-50.00	2.82-53.44	2.76-53.5	2.32-52.18	5.88-53.44
No. of reflections measured	40505	40772	24319	25668	7460
No. of independent reflections	17515	11284	14387	15877	2641
Flack x parameter [4]	–	–	0.11(5)	–	0.06(5)
R_{int}	0.0527	0.1241	0.1503	0.0854	0.0835
R_1 ($I > 2\sigma(I)$) / $wR(F^2)$ (all data)	0.0350/0.0675	0.0383/0.100	0.0837/0.2065	0.0448/0.0786	0.0419/0.0959
Goodness of fit on F^2	0.800	0.934	0.912	0.843	0.811
Largest diff. peak/hole /e$^-$·Å^{-3}	3.329/-0.920	1.934/-1.940	1.283/-1.381	0.844/-0.831	1.575/-1.216

*Compound **1***:

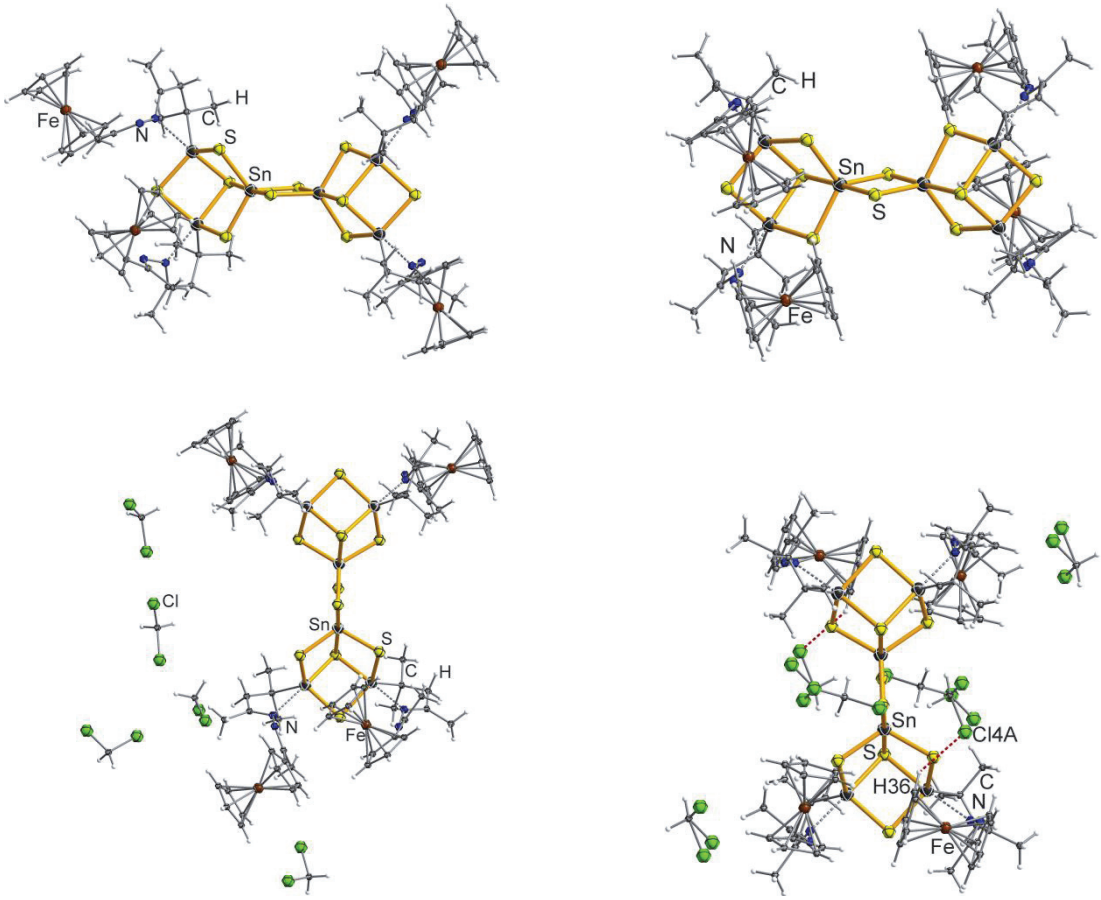

1a **1b**

Figure S1. Molecular structures of **1a** (left) and **1b** (right), each viewed in two different orientations (top and bottom) to emphasize the different conformations. Intermolecular hydrogen bonding (red) between Cl and H atoms in **1b** is illustrated.

Scheme S1. Formation of conformers upon rotation of the Fc-terminated ligands about their C_{Cp}–C(Me) and/or N–N bonds.

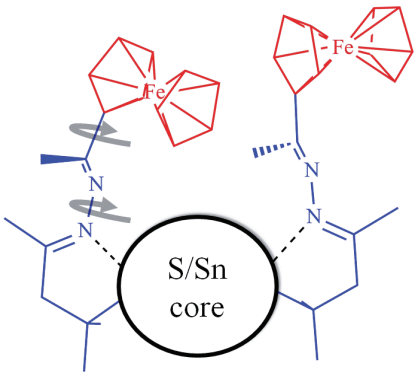

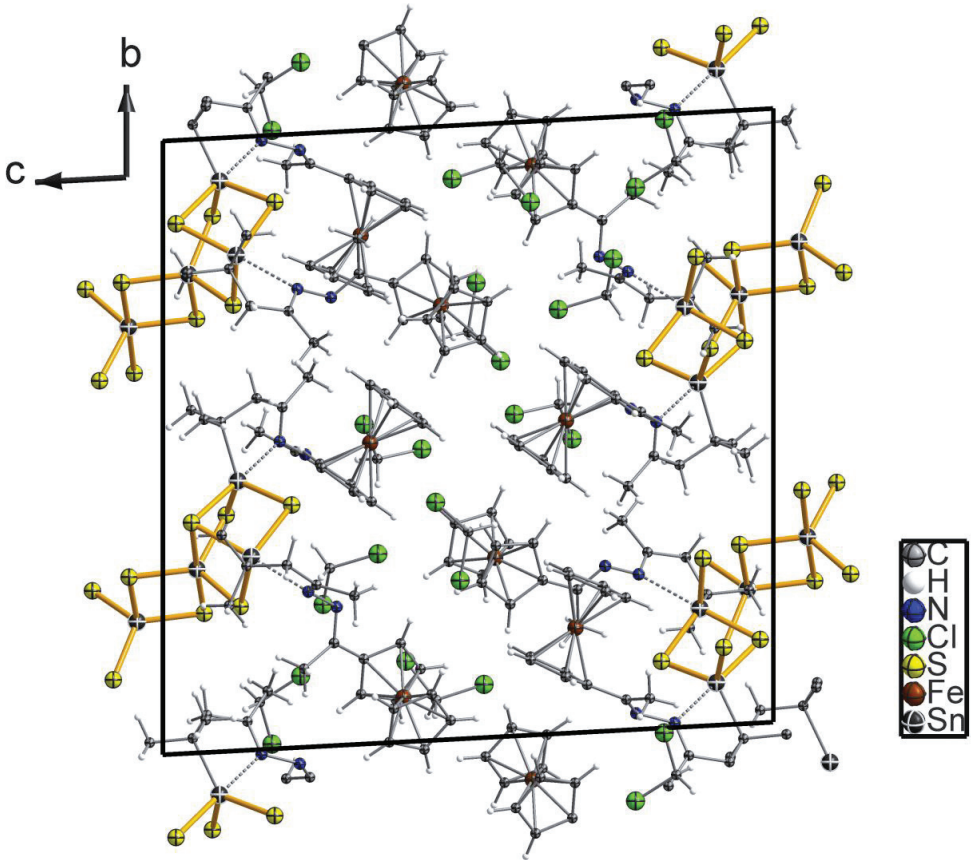

Figure S2. Packing of the molecules of **1**a in the crystal, viewed along the crystallographic *a* axis.

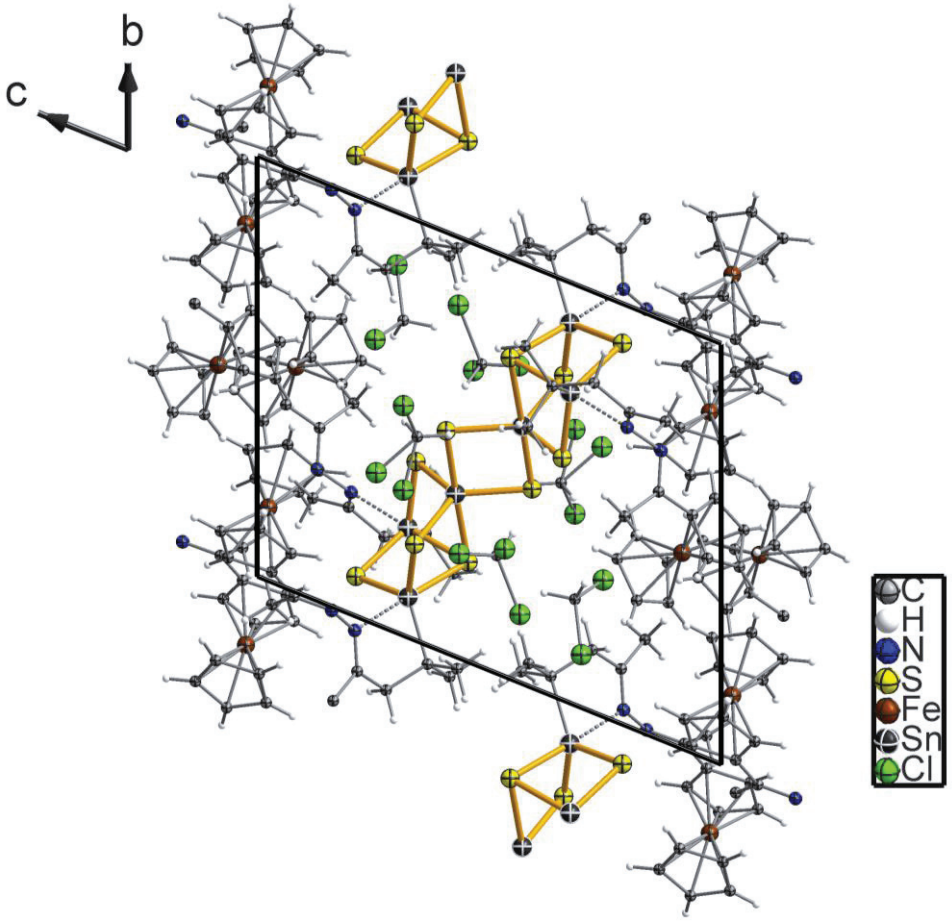

Figure S3. Packing of the molecules of **1b** in the crystal, viewed along the crystallographic *a* axis.

Table S2. Selected bond lengths [Å], bond angles [°] in **1a**.

S(1)-Sn(1)	2.4820(16)	S(10)-Sn(6)	2.5113(17)
S(1)-Sn(2)	2.5067(18)	Sn(1)-C(1)	2.185(6)
S(1)-Sn(5)	3.007 (gelesen)	Sn(2)-C(19)	2.180(5)
S(2)-Sn(1)	2.4106(17)	Sn(3)-C(37)	2.176(6)
S(2)-Sn(2)	2.4266(15)	Sn(4)-C(56)	2.184(5)
S(3)-Sn(4)	2.4218(16)	Sn(1)-N(1)	2.570(4)
S(3)-Sn(3)	2.4250(17)	Sn(2)-N(3)	2.345(5)
S(4)-Sn(3)	2.5354(16)	Sn(3)-N(5)	2.428(4)
S(4)-Sn(4)	2.5351(18)	Sn(4)-N(7)	2.402(5)
S(4)-Sn(6)	2.7327(17)	Sn(1)-S(1)-Sn(2)	83.91(5)
S(5)-Sn(5)	2.3999(16)	Sn(1)-S(2)-Sn(2)	87.18(5)
S(5)-Sn(1)	2.4000(16)	Sn(4)-S(3)-Sn(3)	88.77(5)
S(6)-Sn(5)	2.4023(17)	Sn(3)-S(4)-Sn(4)	83.92(5)
S(6)-Sn(2)	2.4153(16)	Sn(3)-S(4)-Sn(6)	85.20(5)
S(7)-Sn(4)	2.3945(16)	Sn(4)-S(4)-Sn(6)	83.50(5)
S(7)-Sn(6)	2.4189(18)	Sn(5)-S(5)-Sn(1)	97.21(6)
S(8)-Sn(3)	2.3996(16)	Sn(5)-S(6)-Sn(2)	96.64(6)
S(8)-Sn(6)	2.4268(16)	Sn(4)-S(7)-Sn(6)	93.67(6)
S(9)-Sn(6)	2.3942(17)	Sn(3)-S(8)-Sn(6)	95.37(5)
S(9)-Sn(5)	2.4669(17)	Sn(6)-S(9)-Sn(5)	87.93(6)
S(10)-Sn(5)	2.3651(17)	Sn(5)-S(10)-Sn(6)	87.54(6)

Table S3. Selected bond lengths [Å], bond angles [°] in **1b**.

S(1)-Sn(1)	2.4237(10)	Sn(1)-C(1)	2.181(4)
S(1)-Sn(2)	2.4242(11)	Sn(2)-C(19)	2.184(4)
S(2)-Sn(1)	2.5247(10)	Sn(1)-N(1)	2.434(3)
S(2)-Sn(2)	2.5387(10)	Sn(2)-N(3)	2.428(3)
S(2)-Sn(3)	2.7767(11)	Sn(1)-S(1)-Sn(2)	89.17(3)
S(3)-Sn(2)	2.4030(11)	Sn(1)-S(2)-Sn(2)	84.46(3)
S(3)-Sn(3)	2.4238(11)	Sn(1)-S(2)-Sn(3)	84.03(3)
S(4)-Sn(1)	2.3925(11)	Sn(2)-S(2)-Sn(3)	83.83(3)
S(4)-Sn(3)	2.4271(11)	Sn(2)-S(3)-Sn(3)	94.87(4)
S(5)-Sn(3)	2.3891(10)	Sn(1)-S(4)-Sn(3)	94.99(4)
S(5)-Sn(3′)	2.4982(11)	Sn(3)-S(5)-Sn(3′)	88.70(3)

Compound ***2***:

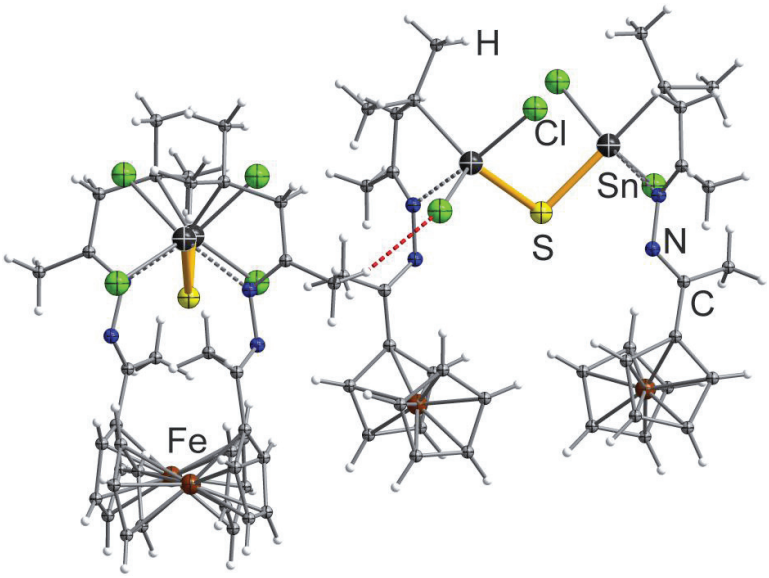

Figure S4. Molecular structures of the two independent molecules in **2a** (as an example of similar situations in **2a** and **2b**) and illustration of intermolecular hydrogen bonding between Cl and H (red).

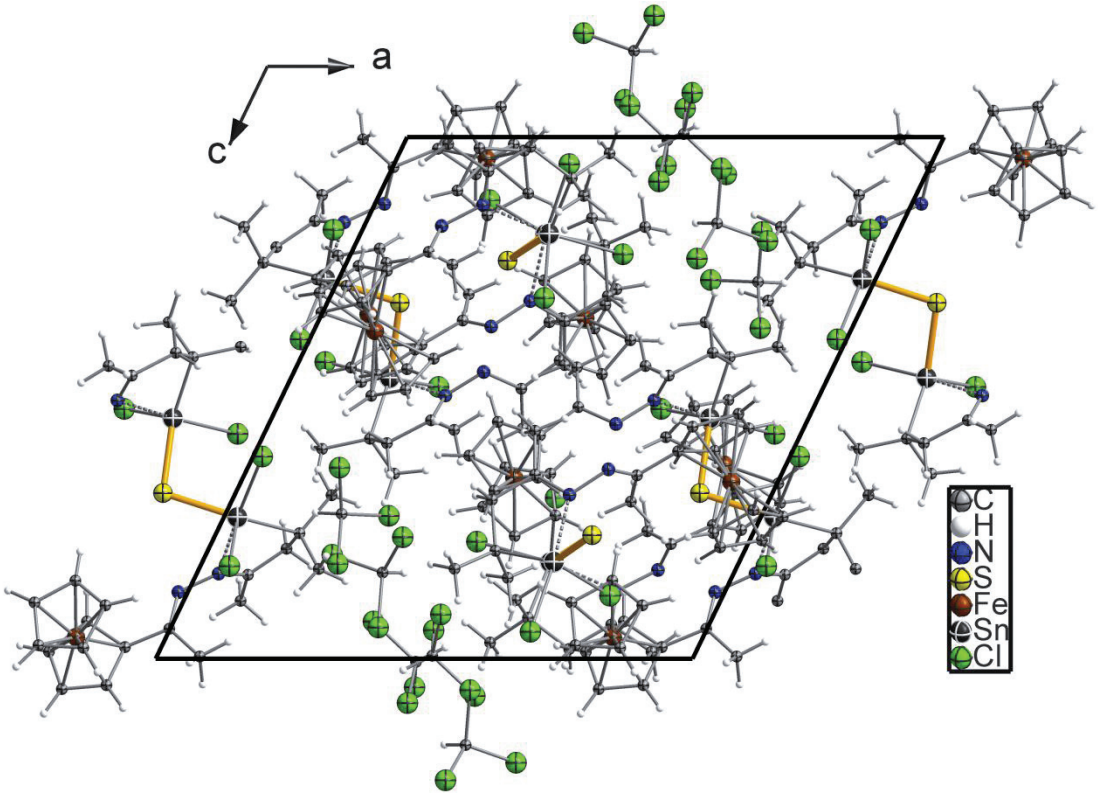

Figure S5. Packing of the molecules of **2a** in the crystal, viewed along the crystallographic *b* axis.

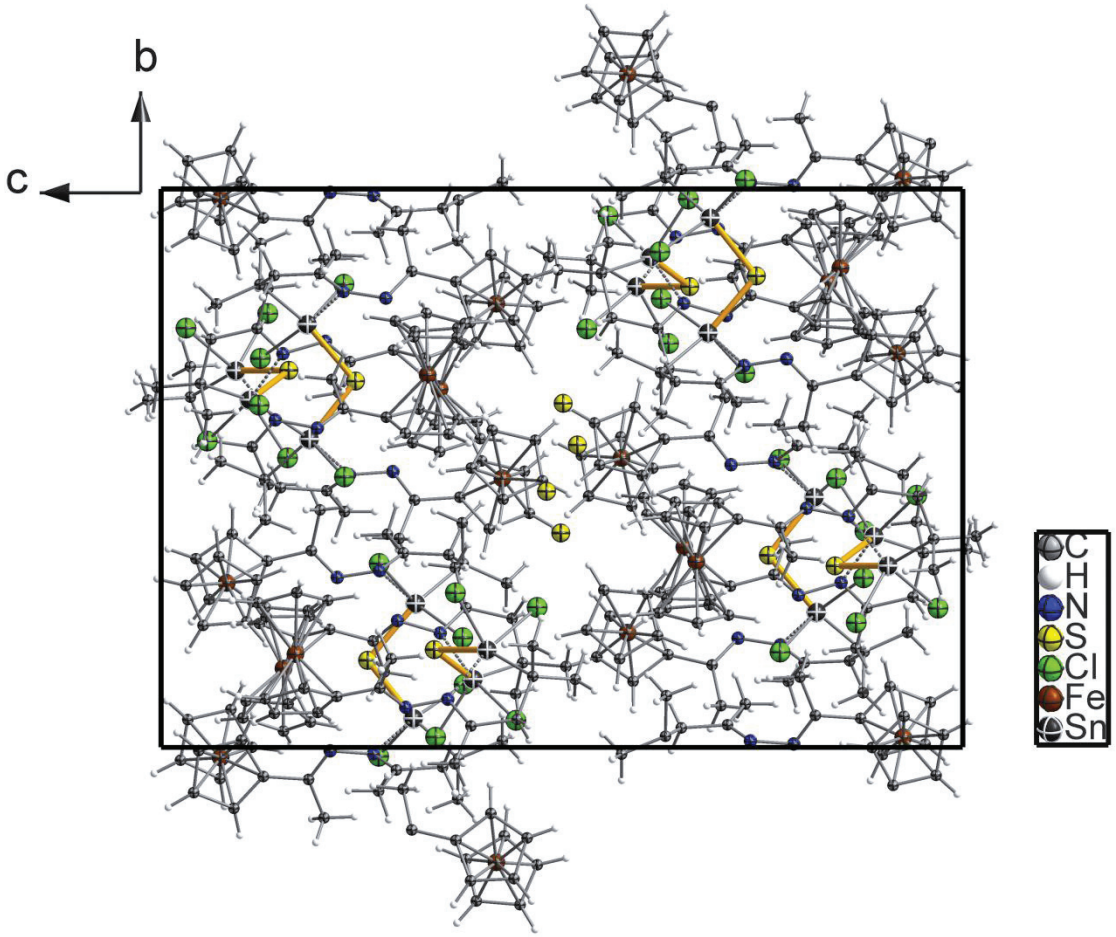

Figure S6. Packing of the molecules of **2b** in the crystal, viewed along the crystallographic *a* axis.

Table S4. Selected bond lengths [Å], bond angles [°] in **2a**.

S(1)-Sn(2)	2.371(6)	Sn(4)-Cl(7)	2.471(5)
S(1)-Sn(1)	2.389(5)	Sn(1)-C(16)	2.20(2)
S(2)-Sn(3)	2.380(5)	Sn(2)-C(34)	2.09(2)
S(2)-Sn(4)	2.416(6)	Sn(3)-C(52)	2.190(18)
Sn(1)-Cl(2)	2.376(6)	Sn(4)-C(70)	2.18(2)
Sn(1)-Cl(1)	2.465(6)	N(2)-Sn(1)	2.41(2)
Sn(2)-Cl(4)	2.353(5)	N(4)-Sn(2)	2.372(18)
Sn(2)-Cl(3)	2.465(5)	N(6)-Sn(3)	2.336(18)
Sn(3)-Cl(5)	2.364(6)	N(8)-Sn(4)	2.425(16)
Sn(3)-Cl(6)	2.466(6)	Sn(2)-S(1)-Sn(1)	100.23(17)
Sn(4)-Cl(8)	2.374(6)	Sn(3)-S(2)-Sn(4)	104.88(16)

Table S5. Selected bond lengths [Å], bond angles [°] in **2b**.

S(1)-Sn(2)	2.385(2)	Cl(8)-Sn(4)	2.474(2)
S(1)-Sn(1)	2.397(2)	Sn(1)-C(16)	2.200(7)
S(2)-Sn(3)	2.371(2)	Sn(2)-C(34)	2.182(8)
S(2)-Sn(4)	2.407(2)	Sn(3)-C(52)	2.210(7)
Cl(1)-Sn(1)	2.379(2)	Sn(4)-C(70)	2.203(8)
Cl(2)-Sn(1)	2.478(2)	N(2)-Sn(1)	2.352(6)
Cl(3)-Sn(2)	2.479(2)	N(4)-Sn(2)	2.389(6)
Cl(4)-Sn(2)	2.368(2)	N(6)-Sn(3)	2.343(6)
Cl(5)-Sn(3)	2.360(2)	N(8)-Sn(4)	2.392(7)
Cl(6)-Sn(3)	2.499(2)	Sn(2)-S(1)-Sn(1)	101.44(8)
Cl(7)-Sn(4)	2.394(2)	Sn(3)-S(2)-Sn(4)	98.75(8)

*Compound **3***:

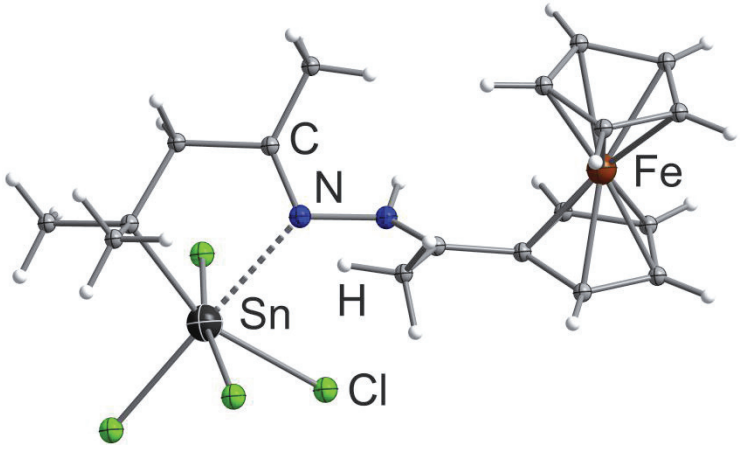

Figure S7. Molecular structure of **3**.

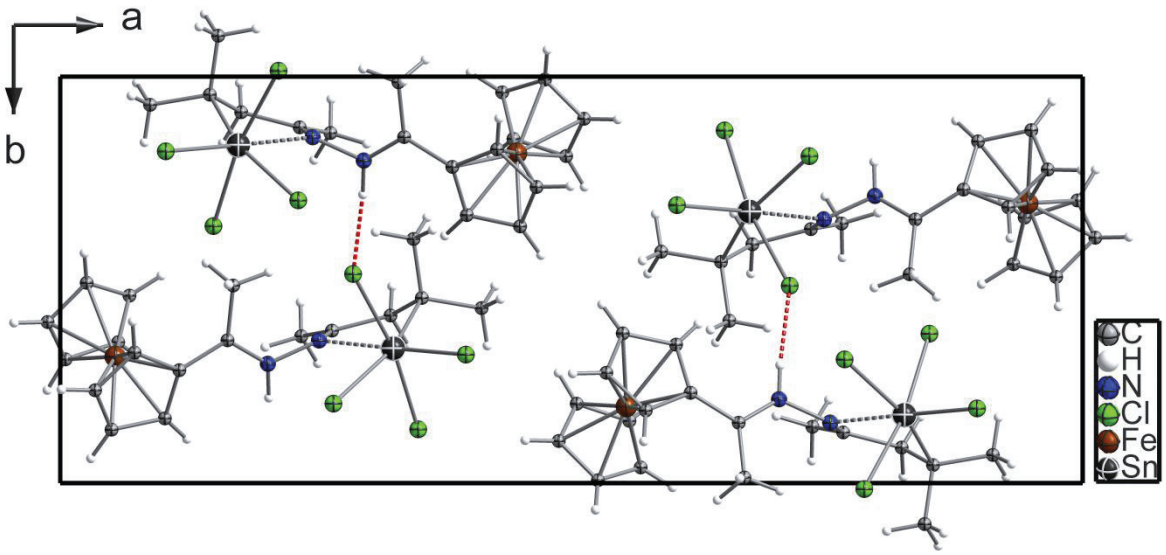

Figure S8. Packing of the molecules of **3** in the crystal, viewed along the crystallographic *c* axis and illustration of intermolecular hydrogen bonding between Cl and H (red).

Table S6. Selected bond lengths [Å], bond angles [°] in **3**.

Cl(1)-Sn(1)	2.483(3)	Cl(1)-Sn(1)-Cl(3)	170.07(9)
Cl(2)-Sn(1)	2.382(3)	Cl(2)-Sn(1)-Cl(3)	84.54(9)
Cl(3)-Sn(1)	2.539(3)	Cl(2)-Sn(1)-Cl(4)	96.79(11)
Cl(4)-Sn(1)	2.404(3)	Cl(2)-Sn(1)-Cl(1)	86.22(9)
C(3)-Sn(1)	2.201(10)	Cl(4)-Sn(1)-Cl(1)	94.60(10)
N(2)-Sn(1)	2.428(9)	Cl(4)-Sn(1)-Cl(3)	90.10(9)

3. Electrochemical measurements on compound 1

Electrochemical measurements – cyclic and differential pulse voltammetry (CV and DPV) – were recorded under Ar atmosphere at 25°C, using 0.1 mol/L [nBu$_4$N][PF$_6$] as the supporting electrolyte. The potentials (Table S7) were referenced internally to ferrocene, added at the end of the experiments. Working and counter electrodes: Pt; scan rate: 100 mV/s; pulse amplitude for DPV: 50 mV.

Table S7. Electrochemical characteristics for the oxidation process of **1** in DCM solution. (Measured at 100 mV/s, *vs*. [FeCp$_2$] in mV)

Complex	E_{pa}^1	E_{pa}^2	ΔE_p^1	ΔE_p^2	$E_{1/2}^1$	$E_{1/2}^2$	$\Delta E_{1/2}$	K_{comp}
1	470	650	70	70	435	615	180	1.49 x10^{12}

4. Spectrometry and Spectroscopy

The ESI (+) mass spectrum of **1** is shown in Figure S9 (A-E).

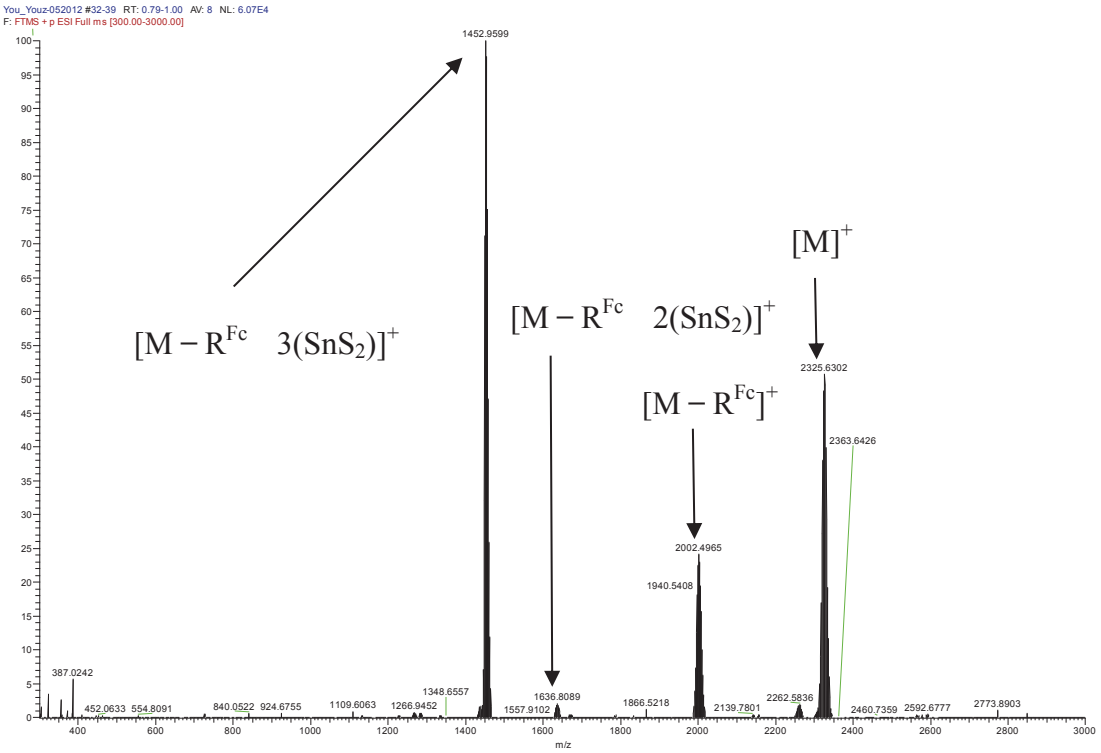

A

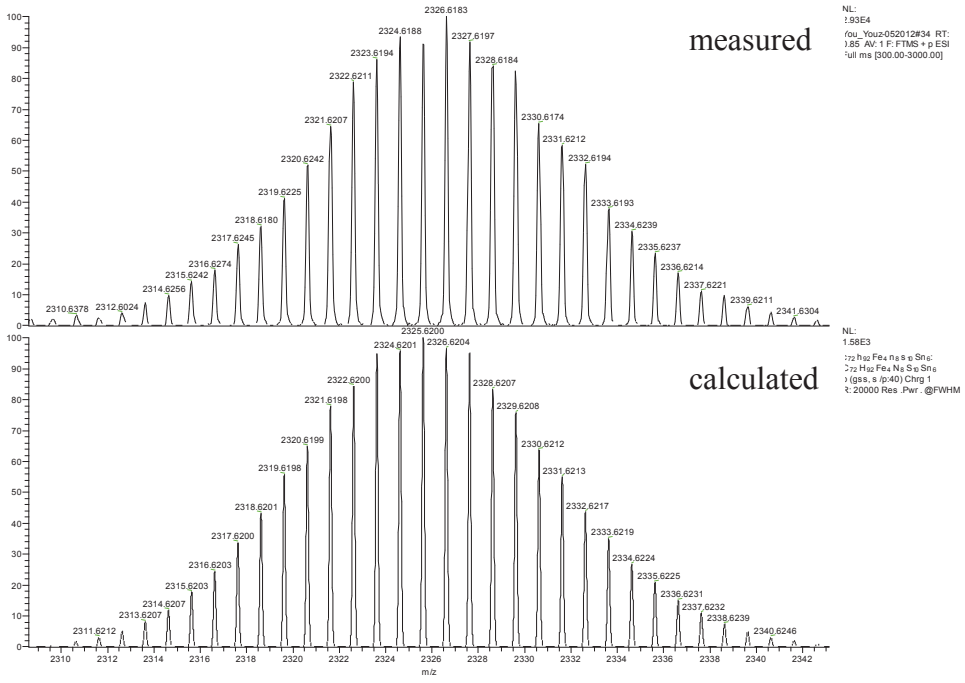

B: ($[M]^+$)

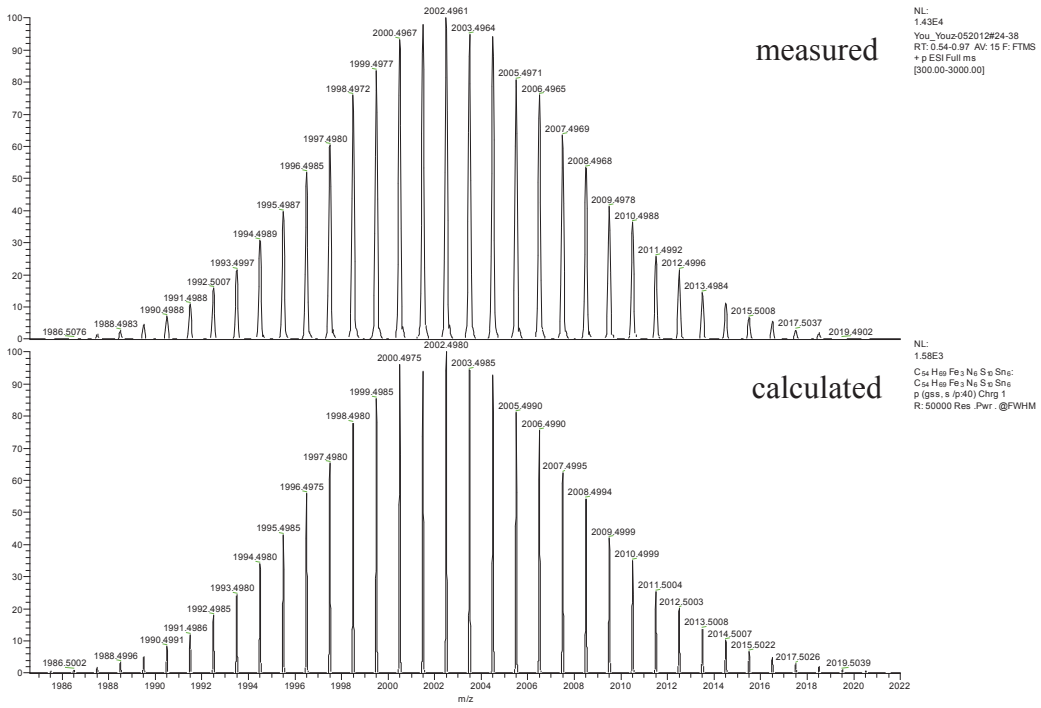

C: ($[M - R^{Fc}]^+$)

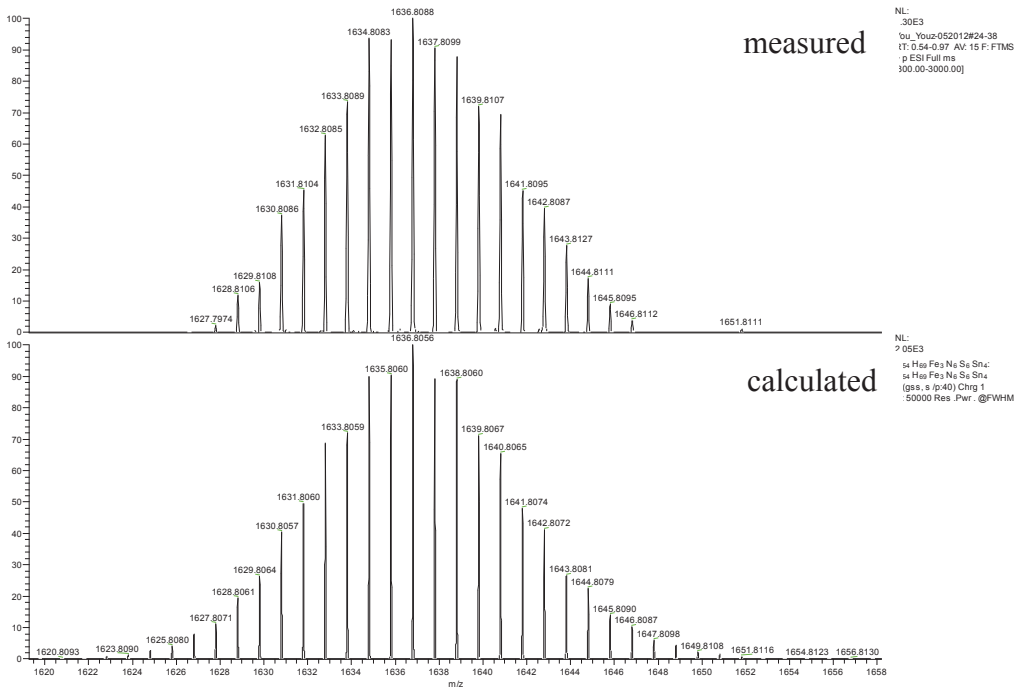

D: ($[M - R^{Fc} - 2(SnS_2)]^+$)

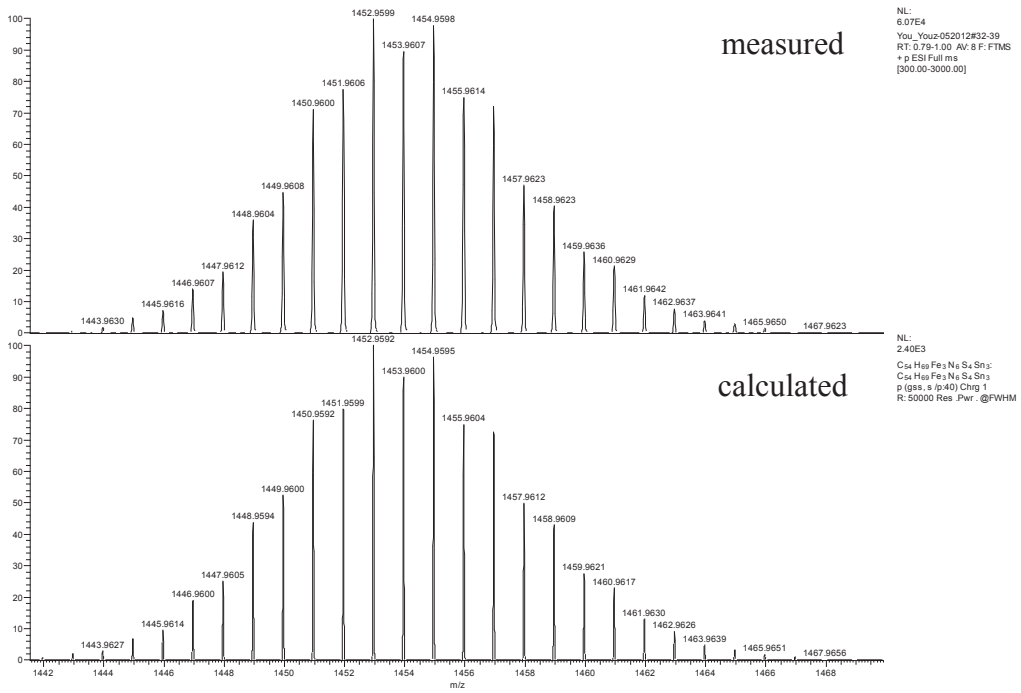

E: $([M - R^{Fc} - 3(SnS_2)]^+)$

Figure S9. ESI mass spectra of **1**, overview (**A**), *m/z* = 2325.63 ($[M]^+$) (**B**); *m/z* = 2002.50 ($[M-R^{Fc}]^+$) (**C**); *m/z* = 1636.81 ($[M-R^{Fc}-2(SnS_2)]^+$) (**D**); *m/z* = 1452.96 ($[M-R^{Fc}-3(SnS_2)]^+$) (**E**).

The ESI (+) mass spectrum of **2** is shown in Figure S10 (A-B).

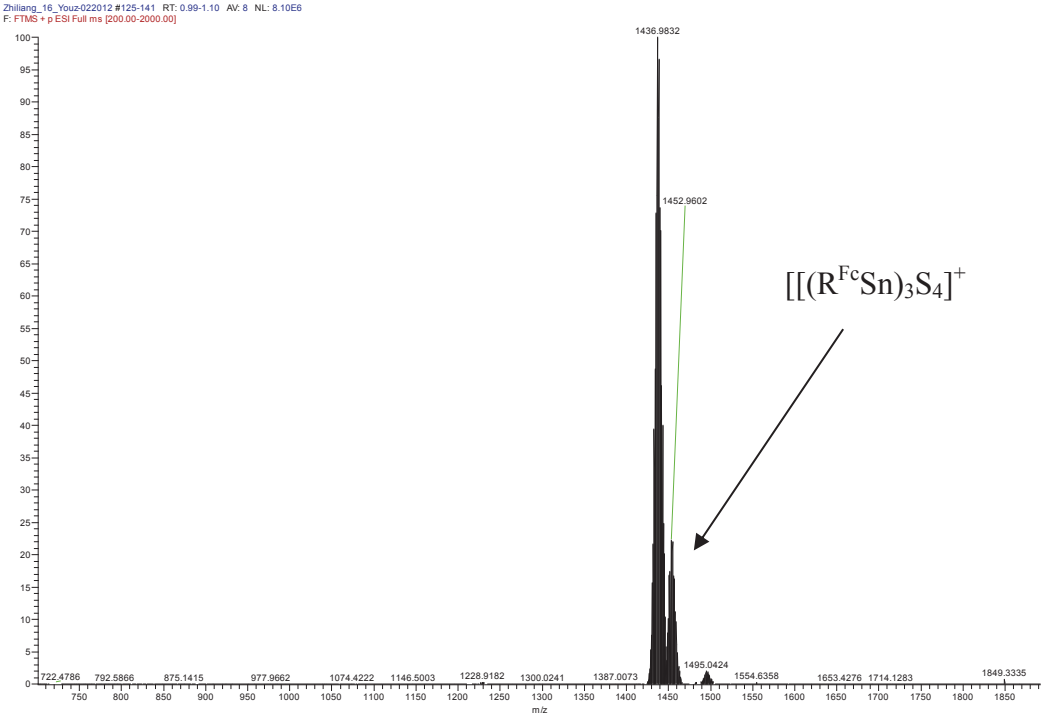

A

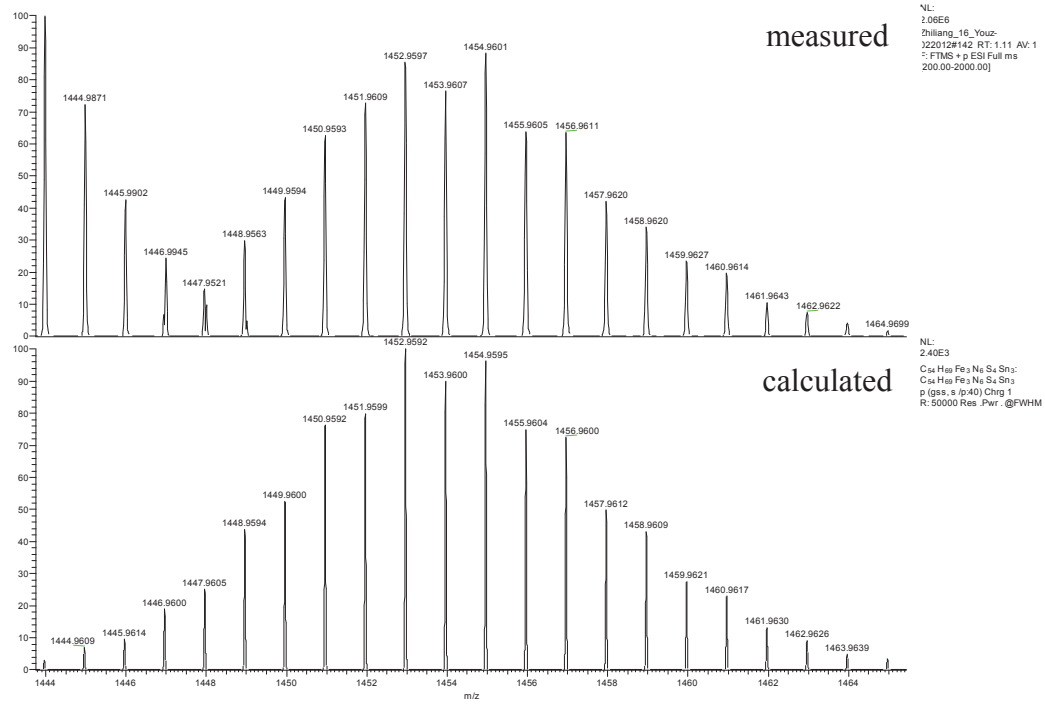

B

Figure S10. ESI mass spectra of **2**: overview (**A**), *m/z* = 1452.96 ($[(R^{Fc}Sn)_3S_4]^+$) (**B**).

The ESI (+) mass spectrum of **3** is shown in Figure S11 (A-E).

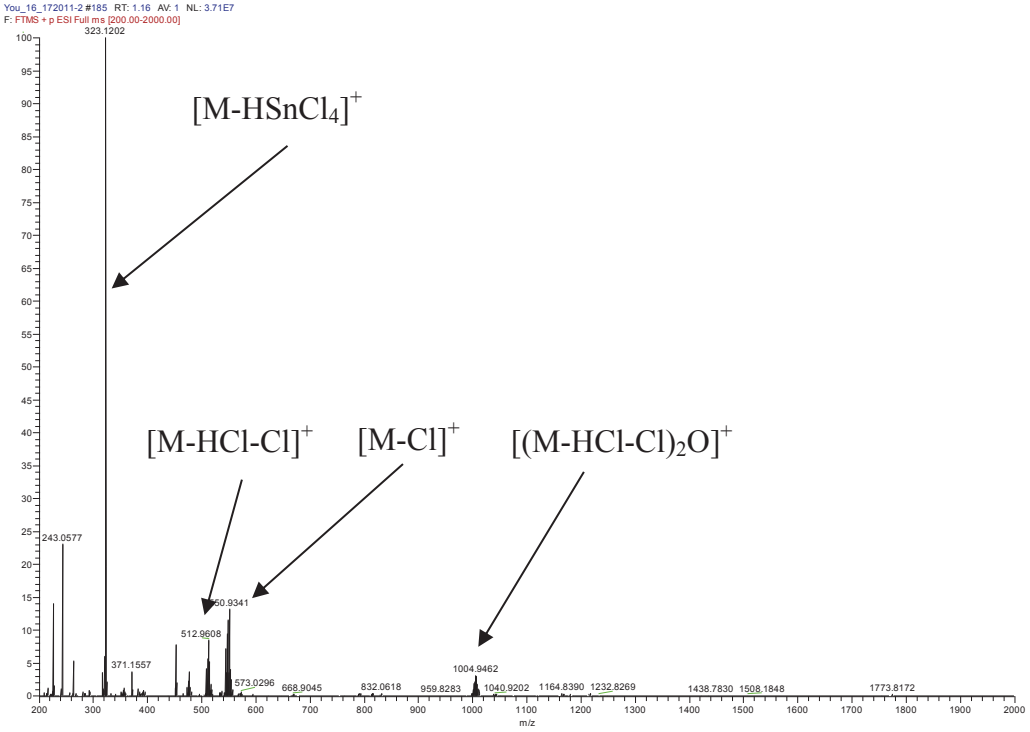

A

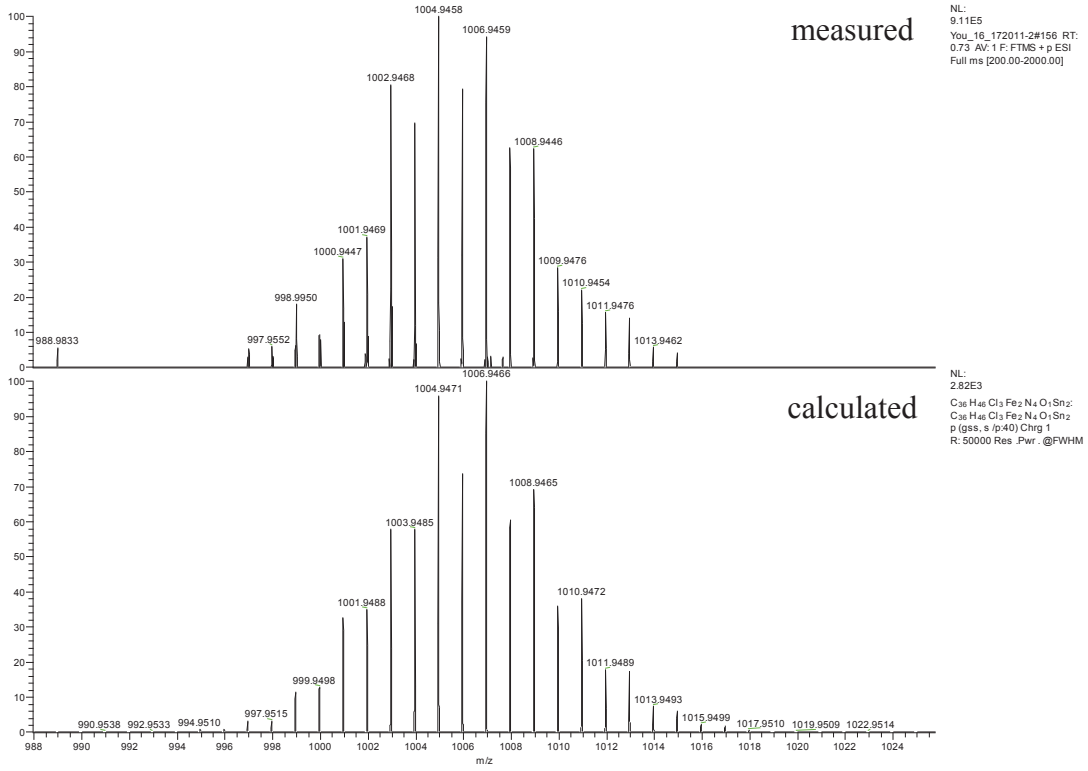

B: $[(M\text{-}HCl\text{-}Cl)_2O]^+$

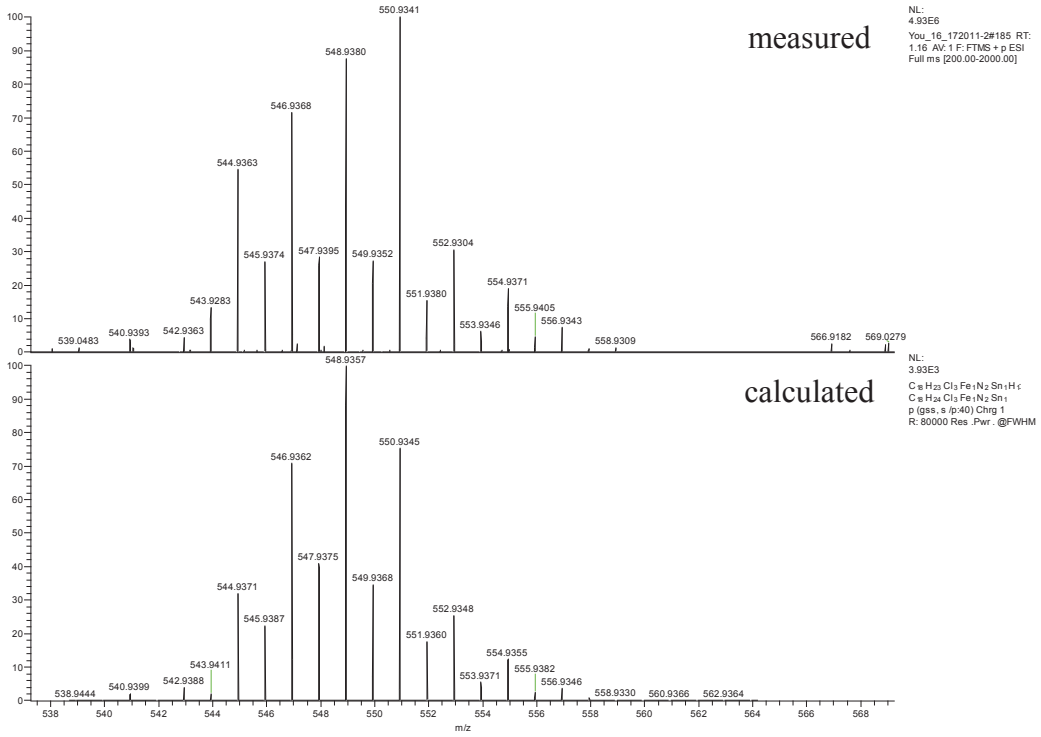

C: $[M\text{-}Cl]^+$

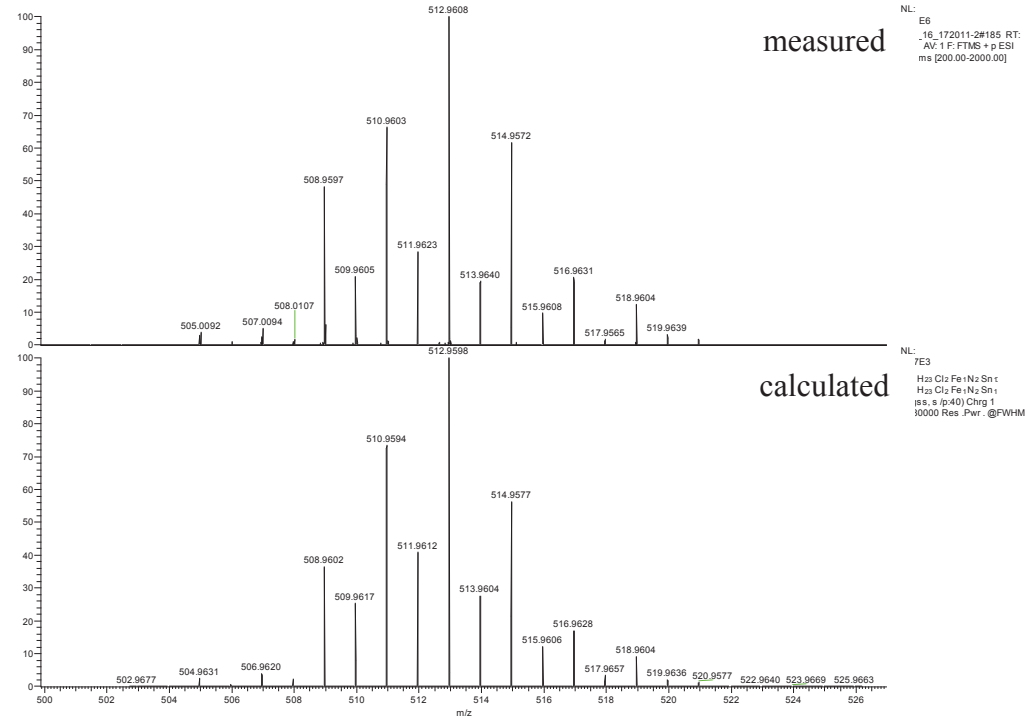

D: $[M\text{-}HCl\text{-}Cl]^{\cdot+}$

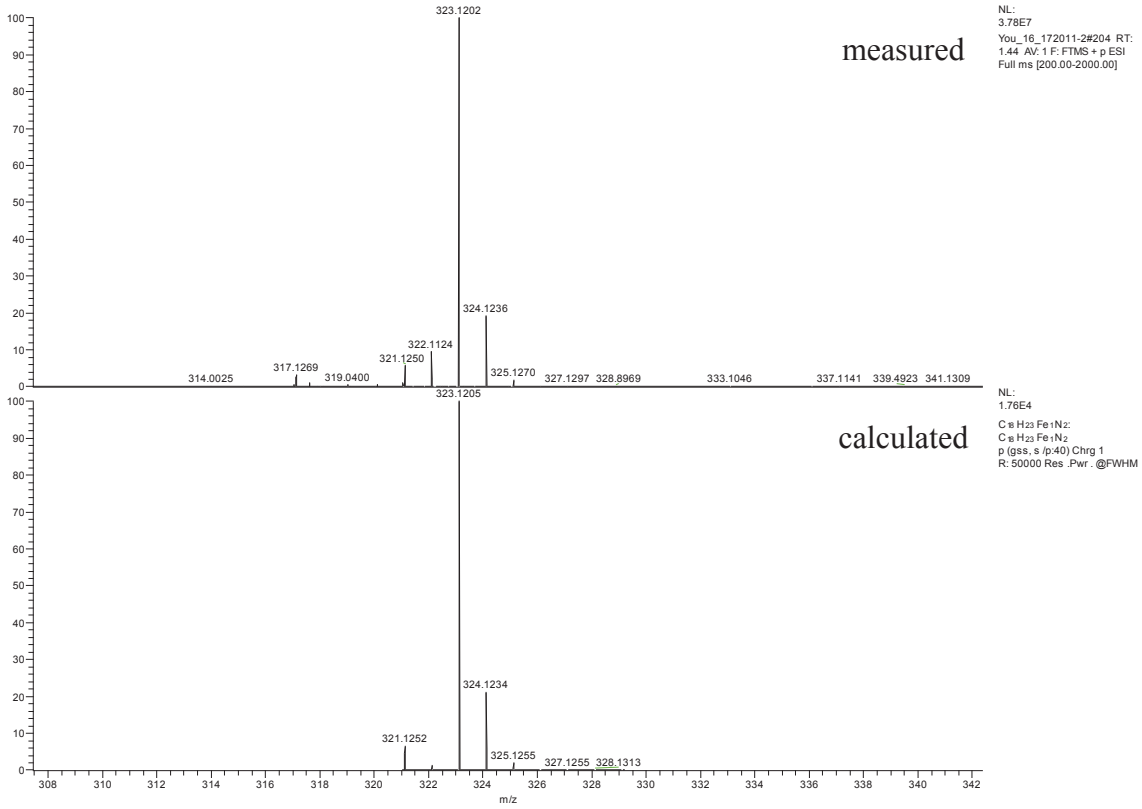

E: $[M\text{-}HSnCl_4]^+$

Figure S11. ESI mass spectra of **3**: overview (**A**), *m/z* = 1004.95 ($[(M\text{-}HCl\text{-}Cl)_2O]^+$) (B), *m/z* = 548.94 ($[M\text{-}Cl]^+$) (C), *m/z* = 512.96 ($[M-HCl-Cl]^+$) (D), *m/z* = 323.2 ($[M\text{-}HSnCl_4]^+$) (E).

The ^{119}Sn NMR spectrum of **1a** is shown in Figure S12.

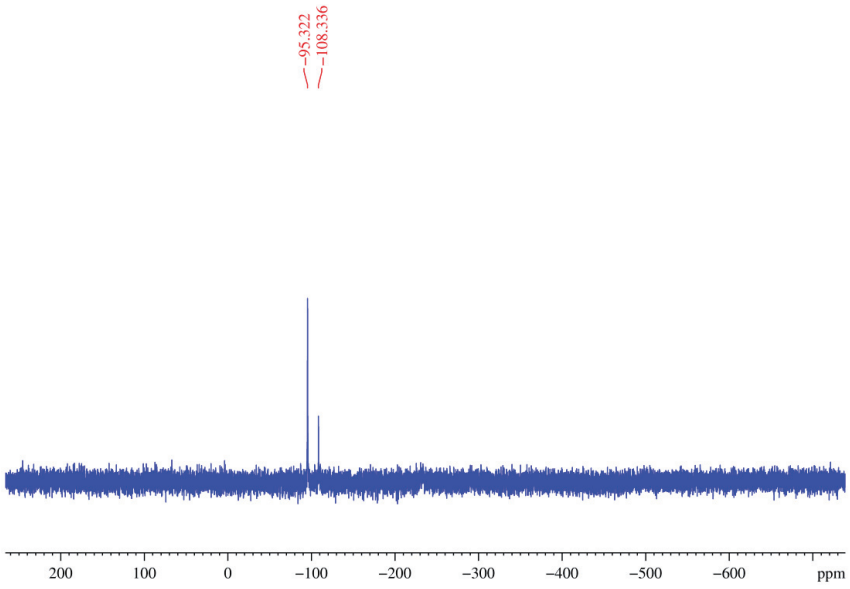

Figure S12. ^{119}Sn-NMR spectrum of **1a** in CD_2Cl_2.

Figures S13-S17 provide further information of the NMR analysis of **3**.

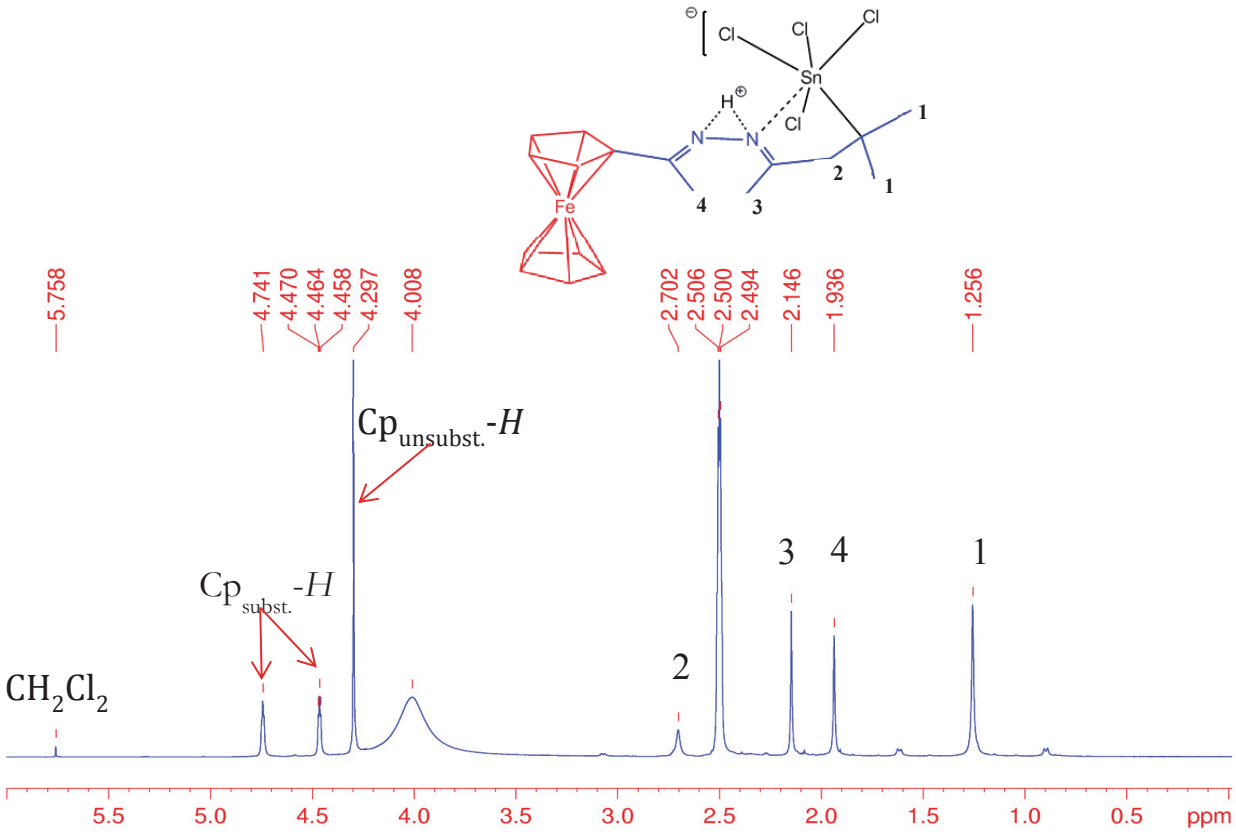

Figure S13. ^{1}H-NMR spectrum of **3** in DMSO-d_6.

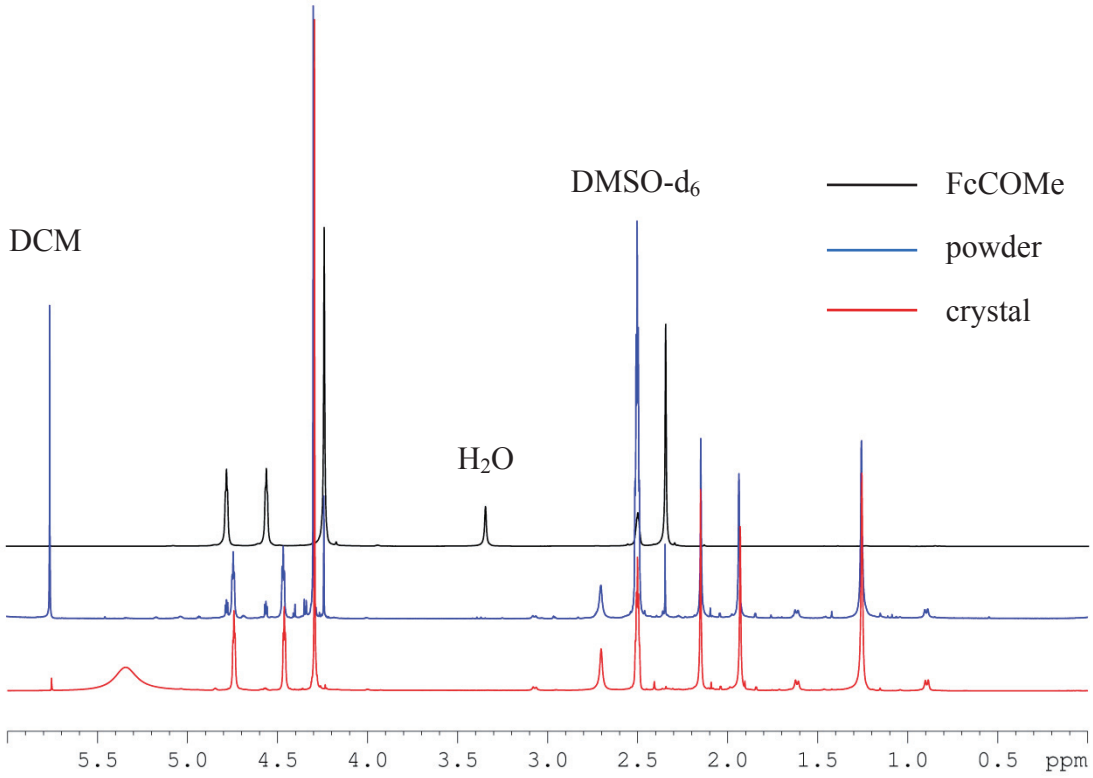

Figure S14. ^{1}H-NMR spectrum of powder of **3** (blue curve), in comparison with crystals of **3** (red curve) and acetylferrocene (FcCOMe, black curve).

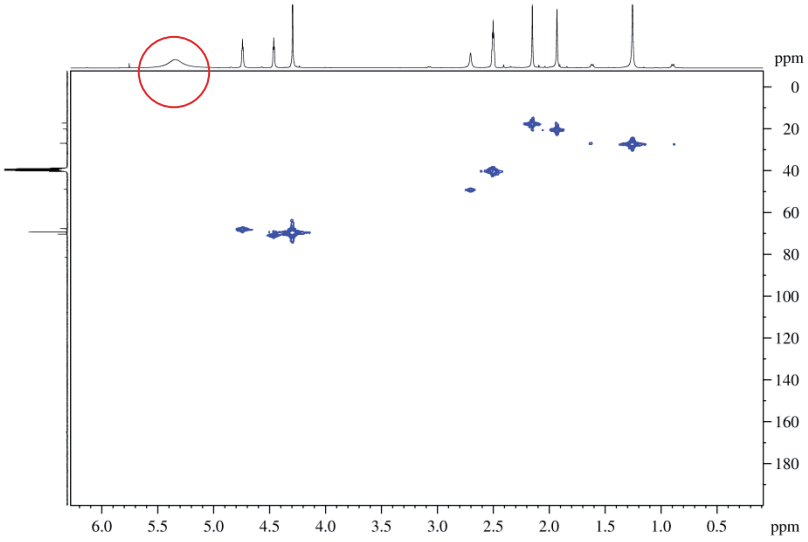

Figure S15. 2D-NMR: HMQC of **3** in DMSO-d^{6}, no corresponding direct C-H coupling of HCl could be found.

A comparison of ^{1}H NMR spectra of solutions of the powder obtained directly from the reaction without further work-up, acetylferrocene and single-crystals of **3** (Figure S14) indicates that the crude product contains only small amounts of of acetylferrocene (FcCOMe), which probably stems from the decomposition of the Schiff-base ligands C=N−N=C under the acidic condition. The ^{1}H NMR signal of the proton (H111, 5.35 ppm) is expectedly broad, indicating a fluctuation between the neighboring N atoms in solution. A 2D-NMR (HMQC) spectrum shows that the proton is not connected to any C atom (Figure S15).

With decreasing concentration of the compound dissolved in DMSO, the proton seems to be released to the solution owing its big affinity to DMSO, as detected by ^{1}H-NMR measurements. Figure S16 monitors the concentration dependency.

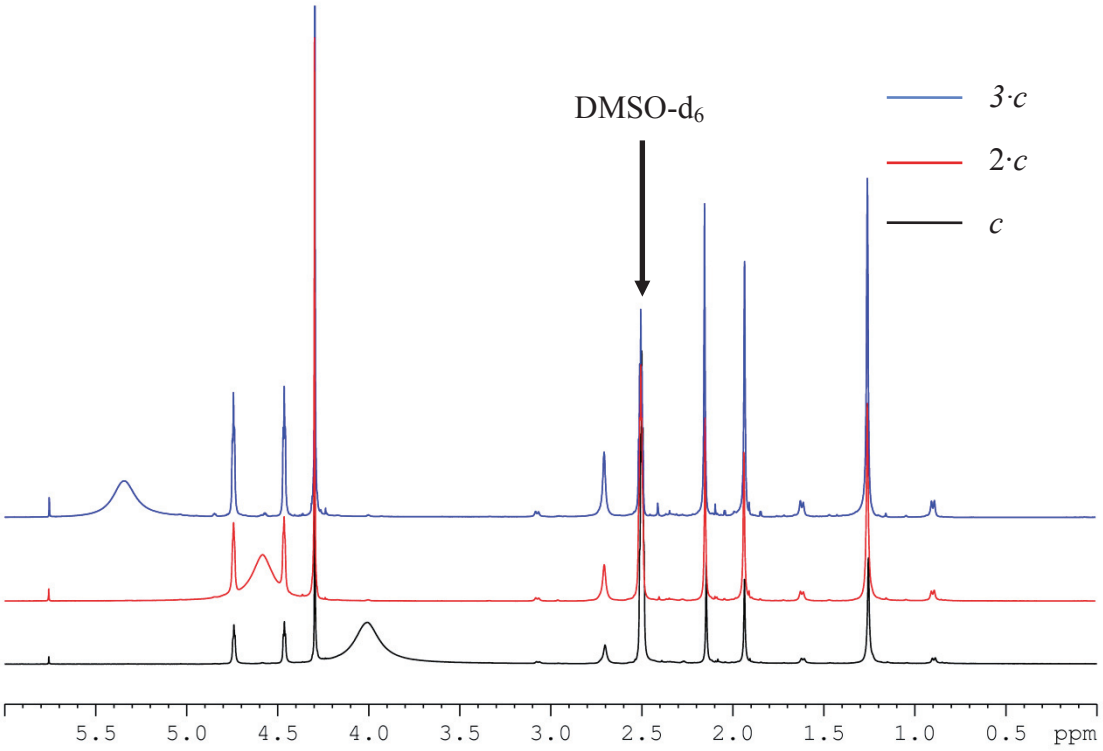

Figure S16. ^{1}H-NMR spectrum of **3** in DMSO-d$_6$ with different concentrations, black curve with a concentration of *c*, red curve with a concentration of 2·*c* and blue curve with a concentration of 3·*c*.

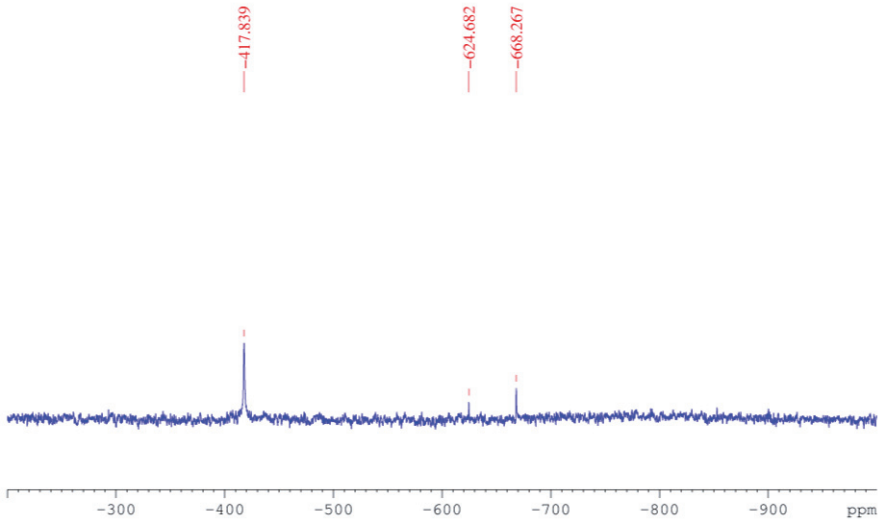

Figure S17. ^{119}Sn-NMR spectrum of the powder of **3** in DMSO-d_6.

The ^{119}Sn-NMR analysis of the powder (Figure S17) shows a relatively strong peak at −417.84 ppm, which is in agreement with the measurement on pure single-crystals of **3**. Besides, two other peaks at –624.68 and –668.27 ppm, respectively, can be assigned to two species of the by-product anion $[SnCl_6]^{2-}$, which was probably formed upon replacement of chloride anions with DMSO-d_6 according to previous investigations.[5]

The structure analysis for single-crystals of **3** (see also Chapter 2) is in agreement with the NMR studies, but shows a static picture regarding the proton. An additional chloride ligand completes the octahedral coordination environment of the tin atom in **3**, producing a total negative charge of the molecule. No counter cation was detected, but we have found residual electron density between N1 and Cl3, treated here as a proton (H111) connected to N1. The bond length N1−H111 (1.10 Å) seems obviously longer than the default (X-Ray) value of N− H (0.87 Å) suggested in SHELXL. However, a quite short distance between H111 and Cl3 (2.15 Å) was observed, in between the sum of covalent and van der Waals radii.[6] Thus, the situation can be viewed as one molecule of HCl being caught between two organotin trichloride molecules in a Sn–Cl···H–N fashion (Figure S18); the hydrogen bonds hereby cause the extension of both the N–H contact as well as the significantly longer Sn–Cl3 bond (2.539(3)) in comparison with others (Sn–Cl1, Sn-Cl2, Cl4 2.483(3), 2.382(3), 2.404(3)). Continuation of this pattern leads to the formation of a one-dimensional coordination polymer.

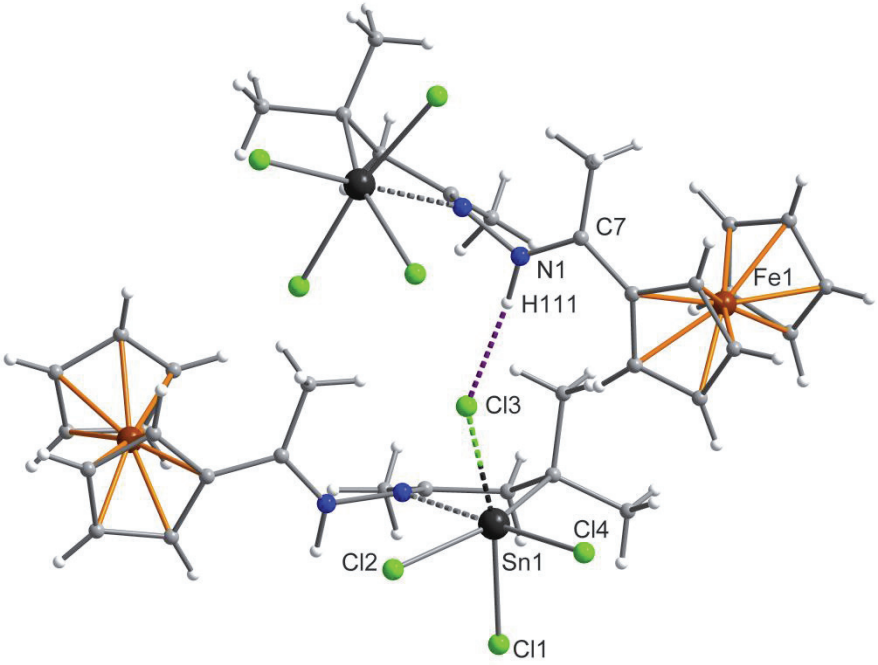

Figure S18. Intermolecular hydrogen bond Sn–Cl···H–N (purple dashed line) between two molecules of compound **3**.

5. UV-visible spectra

UV/Vis spectra (Figure S19) were recorded on a Perkin-Elmer Cary 5000 UV/vis/NIR spectrometer in the range of 800–200 nm employing the double-beam technique. The samples were prepared as solution in CH_2Cl_2.

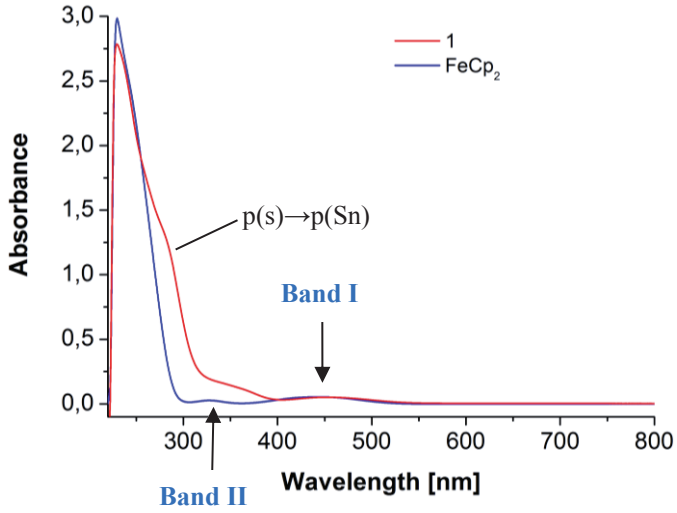

Figure S19. UV/Vis spectra of **1** (red curve) and ferrocene (blue curve).

The spectrum of ferrocene (blue curve) displays two significant absorption bands, **I** at 444.17 nm, and **II** at 328.00 nm, similar to the values recorded in ethanol solution (band **I** at 400, and **II** at 325 nm).[7] Besides the two absorption bands, which are slightly red shifted, compound **1** possesses the third absorption band at about 283 nm, which can be assigned to a p(S)→p(Sn) charge transfer of the Sn-S-skeleton according to similar reported values.[8]

6. Energy dispersive X-ray (EDX) spectroscopy:

EDX analyses were performed using the EDX device Voyager 4.0 of Noran Instruments coupled with the electron microscope CamScan CS 4DV. Data acquisition was performed with an acceleration voltage of 20 kV and 100 s accumulation time. For the analyses, multiple single crystals were used and the data recorded both various times on one single crystal and various times on other single crystals. Figures S20, S22 and S23 show the EDX spectra, Tables S8-S10 summarize the data. Figure S21 provides an SEM image of a single crystal of **2**.

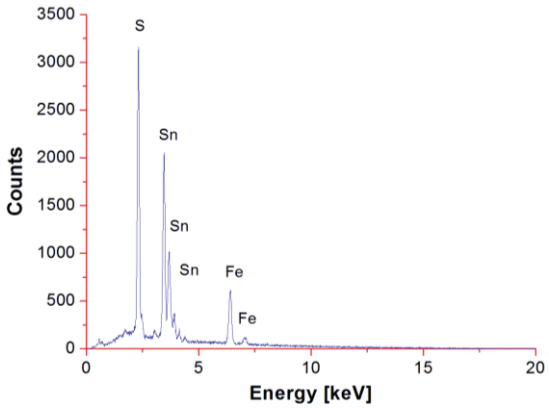

Figure S20. EDX analysis of **1**.

Table S8. EDX analysis of **1**.

Element	k-ratio (calc.)	ZAF	Atom %	Atomic ratio obs. (calc.)	Element Wt %	Wt % Err. (1-Sigma)
S-K	0.2060	1.215	49.57	9.91(10.00)	25.01	+/- 0.24
Sn-L	0.4850	1.194	30.99	6.20(6.00)	57.89	+/- 0.85
Fe-K	0.1590	1.075	19.44	3.89(4.00)	17.09	+/- 0.89
Total			100	20	100	

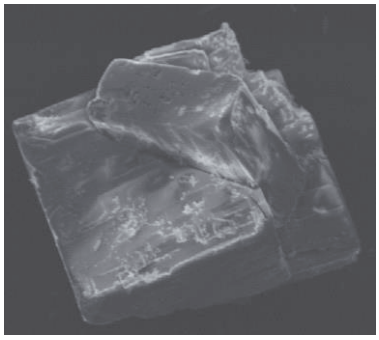

Figure S21. SEM image of a single crystal of **2**.

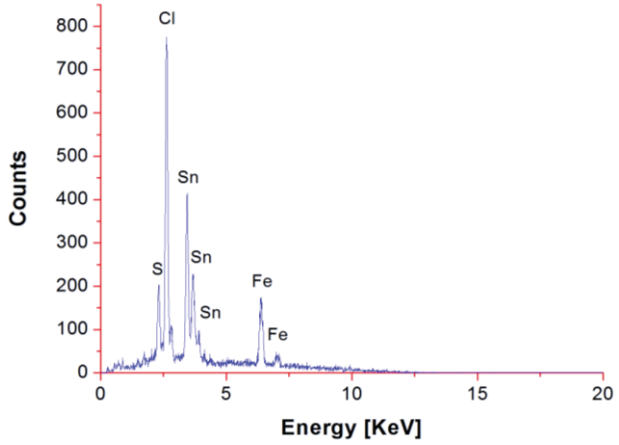

Figure S22. EDX analysis of **2**.

Table S9. EDX analysis of **2**.

Element	k-ratio (calc.)	ZAF	Atom %	Atomic ratio obs. (calc.)	Element Wt %	Wt % Err. (1-Sigma)
S-K	0.0446	1.185	9.87	0.89(1.00)	5.28	+/- 0.28
Sn-L	0.3909	1.242	24.52	2.21(2.00)	48.56	+/- 1.49
Fe-K	0.1873	1.074	21.59	1.94(2.00)	20.12	+/- 0.59
Cl-K	0.2221	1.172	44.02	3.96(4.00)	26.04	+/- 0.47
Total			100	9	100	

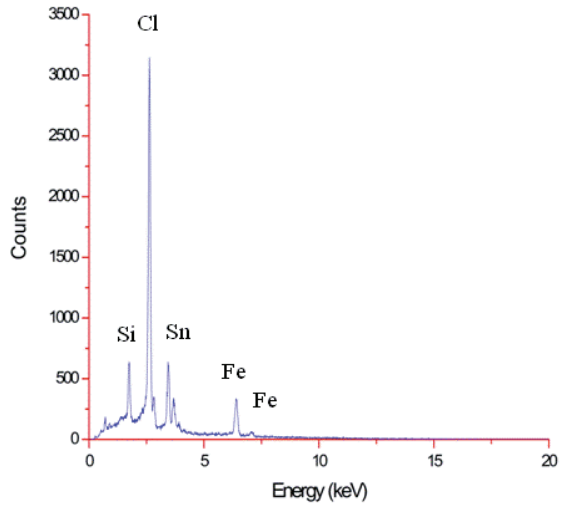

Figure S23. EDX analysis of **3**.

Table S10. EDX analysis of **3**.

Element	k-ratio (calc.)	ZAF	Atom %	Atomic ratio obs. (calc.)	Element Wt %	Wt % Err. (1-Sigma)
Cl-K	0.4326	1.096	68.99	4.14(4.00)	47.41	+/- 0.43
Sn-L	0.2652	1.354	15.61	0.936(1.00)	35.91	+/- 1.10
Fe-K	0.1523	1.095	15.40	0.924(1.00)	16.68	+/- 0.65
Total			100	6	100	

6. Raman Spectroscopy

Raman spectra (Figures S24-S25) were recorded on a Labram HR 800 Raman spectrometer with a 632.8 nm red laser in the range of 50-3000 cm^{-1}. The beam was focused on the sample through a confocal microscope using a 50× objective lens.

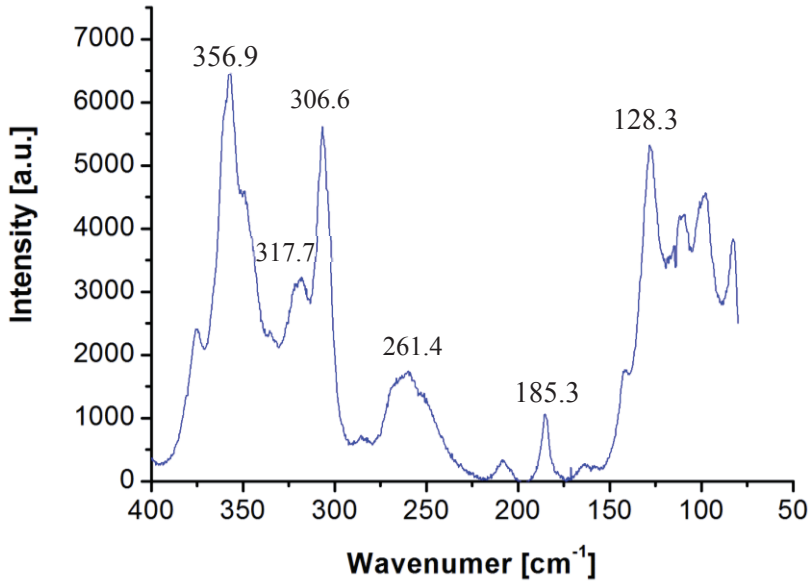

Figure S24. Single-crystal Raman spectrum of **1**.

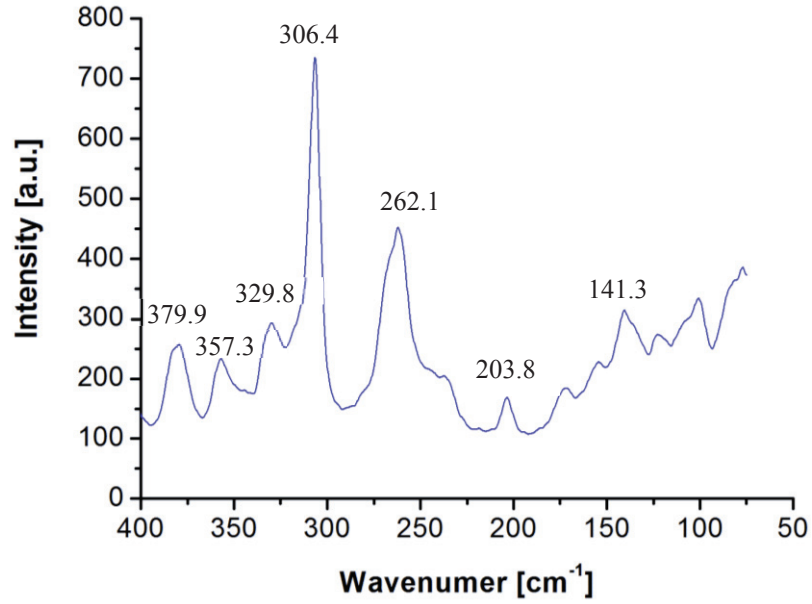

Figure S25. Single-crystal Raman spectrum of **2**.

All compounds with the same R^{Fc} ligands show similar IR spectra in the range 4000-400 cm^{-1}. The IR spectra display weak single C–H stretching bands at about 3080 cm^{-1} besides strong bands at 819-829, 999-1005 and 1105-1134 cm^{-1} that can be assigned to the ferrocene units.[7] The conjugated linker –C=N–N=C–in **1** clearly produces a strong double band (1596 and 1621 cm^{-1}), which in **3** slide together (1618 and 1601 cm^{-1}). In **2** the high-frequency band can just be observed as a shoulder

(1597 cm^{-1}).[9,10] The bands at 360 cm^{-1} in **1** and 374 cm^{-1} in **2** are attributed to the ν(Sn–S) vibrations. The vibrations of Sn–S bonds are also Raman-active. The sharp, intense band at about 306 cm^{-1} in both compounds can be assigned to the ν_s(Sn–Sn–S) vibration, corresponding to the reported value of 310 cm^{-1} in $Na_6Sn_2S_7$.[11] The other sharp band at 356.9 cm^{-1} in **1**, located in the range of the ν_s(Sn–S) vibrations in $Na_4Sn_2S_6 \cdot 14H_2O$,[12] can be attributed to the $\nu_s(SnS_3)$ vibrations (Figures S16 and S17).

7. References for the Supporting Information:

[1] Osborne, A. G.; daSilva, M. W.; Hursthouse, M. B.; Malik, K. M. A.; Opromolla, G.; Zanello, P. *J. Organomet. Chem.* **1996**, *516*, 167.

[2] Hassanzadeh Fard, Z.; Xiong, L.; Müller, C.; Hołynska, M.; Dehnen, S. *Chem. Eur. J.* **2009**, *15*, 6595.

[3] a) Burla, M. C.; Caliandro, R.; Camalli, M.; Carrozzini, B.; Cascarano, G. L.; De Caro, L.; Giacovazzo, C.; Polidori, G.; Spagna, R. *J. Appl. Crystallogr.* **2005**, *38*, 381; b) Sheldrick, G. W. Bruker AXS Inc., Madison WI, **1997**.

[4] Flack, H. D. *Acta Cryst.* **1983**, *A39*, 876.

[5] Bondi, A. *J. Phys. Chem.***1964**, *68*, 441.

[6] Dillon, K. B. and Marshall, A. *J. Chem. Soc., Dalton Trans.* **1987**, 315. Dillon, K. B. and Marshall, A. *J. Chem. Soc., Dalton Trans.* **1984**, 1245.

[7] Kaplan, L.; Kester, W. L.; Katz, J. J. *J. Am. Chem. Soc.* **1952**, *74*, 5531.

[8] You, Z.; Fenske, D.; Dehnen, S. *Dalton Trans.* **2013**, *42*, 8179.

[9] Markopoulos, J.; Markopoulou, O.; Bethell, D.; Nicholls, D. *Inorg. Chim. Acta* **1986**, *122*, L15.

[10] Duan, C. Y.; Tian, Y. P.;Liu, Z. H.; You, X. Z.; Mak, T. C. W. *J. Organomet. Chem.* **1998**, *570*, 155.

[11] Krebs,B.; Schiwy, W. *Z. Anorg. Allg. Chem.* **1973**, 398.

[12] Krebs, B.; Pohl, S.; Schiwy, W. *Angew. Chem.* **1970**, *82*, 884; *Angew. Chem., Int. Ed. Engl.* **1970**, *9*, 897.

3.2 Synthesis of ferrocenyl-substituted organotin selenide and telluride complexes

An alternative way to attach ferrocenyl units to the inorganic chalcogenidotetrelate cages is the treatment of ferrocenyl-substituted tin trichloride ($FcSnCl_3$) with chalcogenide sources, analogous to the formation of binary organo-functionalized chalcogenidotetrelate cages mentioned in the introductory section. The Fc units are then directly attached to the inorganic core, which may change the electrochemical interplay between the Fc units and the inorganic core.

The first investigation into this direction was the treatment of $FcSnCl_3$ with Na_2S to form an AD Fc-functionalized Sn/S cage [$(FcSn)_4S_6$] with only weak electrochemical interaction, as shown by ^{119}Sn Mössbauer spectroscopy.[28] The investigation of Fc-functionalized Sn/S cage were extended in this thesis by treatment of $FcSnCl_3$ with the heavier chalcogenides (E = Se, Te) to generate Fc-functionalized Sn/E complexes. The reactivity with transition metal complex and structures, optical and electrochemical properties of such Sn/E complexes, which were studied in comparison with the [$(FcSn)_4S_6$] cage, are reported in this section.

3.2.1 Ferrocenyl-functionalized Sn/Se and Sn/Te complexes: synthesis, reactivity, optical, and electronic properties

Zhiliang You,[a] Jakob Bergunde,[a] Birgit Gerke,[b] Rainer Pöttgen,[b] and Stefanie Dehnen*[a]

[a]*Fachbereich Chemie and Wissenschaftliches Zentrum für Materialwissenschaften, Philipps-Universität Marburg, Hans-Meerwein-Straße, D-35043 Marburg, Germany*

[b]*Institut für Anorganische und Analytische Chemie, Universität Münster, Corrensstrasse 30, D-48149 Münster, Germany*

Appeared in

Inorg. Chem. **2014**, *53*, 12512–12518.

Author contributions

Z. You conceived the project and carried out the synthesis and characterization, refined and described the crystal structures, wrote the manuscript. J. Bergunde and A. Geese participated in the syntheses. M. Hołyńska helped to refine the crystal structure of **3**. B. Gerke and R. Pöttgen performed the Mössbauer spectroscopic measurements, analyzed the data and inserted their results into the manuscript. S. Dehnen supervised the work and corrected the manuscript.

Abstract

An adamantane-shaped, ferrocenyl-substituted tinselenide complex, $[(FcSn)_4Se_6]$ (**1**; Fc = ferrocenyl), and a ferrocenyl-substituted tintelluride five-membered ring, $[(Fc_2Sn)_3Te_2]$ (**2**), were obtained upon treatment of $FcSnCl_3$ with K_2E (E = Se, Te). **1** further reacts with $Na_2S{\cdot}9H_2O$ and $[Cu(PPh_3)_3Cl]$ to form a ternary complex, $[(CuPPh_3)_6(S/Se)_6(SnFc)_2]$ (**3**). We discuss structures, optical and electrochemical properties as well as Mössbauer spectra.

Inorganic Chemistry

Article

pubs.acs.org/IC

Ferrocenyl-Functionalized Sn/Se and Sn/Te Complexes: Synthesis, Reactivity, Optical, and Electronic Properties

Zhiliang You,[†] Jakob Bergunde,[†] Birgit Gerke,[‡] Rainer Pöttgen,[‡] and Stefanie Dehnen*,[†]

[†]Fachbereich Chemie and Wissenschaftliches Zentrum für Materialwissenschaften, Philipps-Universität Marburg, Hans-Meerwein Strasse, D-35043 Marburg, Germany

[‡]Institut für Anorganische und Analytische Chemie, Universität Münster, Corrensstrasse 30, D-48149 Münster, Germany

Supporting Information

ABSTRACT: An adamantane-shaped, ferrocenyl-substituted tin selenide complex, $[(FcSn)_4Se_6]$ (**1**; Fc = ferrocenyl), and a ferrocenyl-substituted tin telluride five-membered ring, $[(Fc_2Sn)_3Te_2]$ (**2**), were obtained upon treatment of $FcSnCl_3$ with K_2E (E = Se, Te). Complex **1** further reacts with $Na_2S\cdot 9H_2O$ and $[Cu(PPh_3)_3Cl]$ to form a ternary complex, $[(CuPPh_3)_6(S/Se)_6(SnFc)_2]$ (**3**). We discuss structures, optical and electrochemical properties as well as Mössbauer spectra.

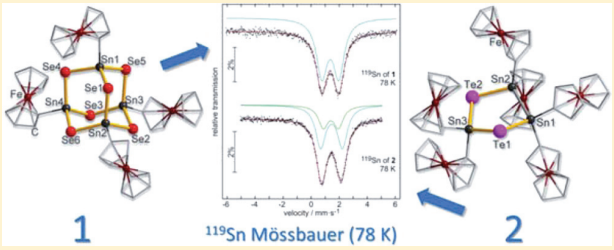

INTRODUCTION

Metalchalcogenides and chalcogenidometalates belong to the most actively investigated inorganic materials. Because of the progress in modern preparative and structural methods, a huge variety of molecular, nanostructured, or mesostructured derivatives with different compositions and diverse structures have been synthesized, showing a broad range of chemical and physical properties.[1] For instance, inorganic chalcogenide cluster-based open frameworks that were synthesized in solvothermal reactions exhibit diverse topologies, which combine high porosity, high surface area, and electrical and ionic conductivity with tunable optoelectronic properties.[2] Molecular species, such as the extensively studied CdE clusters (E = S, Se, and/or Te) are known for showing size-dependent optical and electronic properties.[3] Fine-tuning of optoelectronic and also magnetic properties was furthermore achieved by combination of different transition and/or main-group elements in such systems.[4]

Besides some polymeric structures,[5] organo-decorated metal chalcogenides, especially those of main-group metal chalcogenides, are essentially restricted to the molecular level. Recent developments in this field include new synthetic approaches, reactivity, and further extension of both the inorganic and the organic part of such complexes.[6,7] For this, chalcogenidotetrelate complexes of the general composition $[(RT)_xE_y]$ (R = organic ligand; T = Sn, Ge; E = S, Se, Te), which are based on an adamantane-type (AD) or double-decker-type (DD) inorganic core, that have been known for a long time with nonreactive ligands like Me, Ph, ^{t}Bu, CF_3, C_6F_5, $C(SiMe_3)_3$,[8] were recently decorated with functional organic ligands R^f, such as $R^1(H) = C_2H_4COO(H)$ or $R^2 = CMe_2CH_2C(Me)O$, the latter of which is reactive toward hydrazine, organylhydrazines, hydrazones, or hydrazides.[6a,d,7]

Some examples of Sn/S cages have additionally been reported that were surrounded by mono- (Fc) or bis-functionalized (fC) ferrocenyl units.[9,10] This way, it was possible to study the influence of this specific organometallic ligand on the structural and electrochemical properties of the core.

First investigations were undertaken through the attachment of mono- and bis-substituted ferrocenyl ligands to organo-functionalized precursor DD-type complexes. The resulting Fc-terminated Sn/S complexes, which underwent rearrangement into a larger $[Sn_6S_{10}]$ skeleton during the functionalization reaction, showed intramolecular electronic communication between the different Fc units due to their dynamics in solution.[9] In the case of bis-functionalized ferrocene ligands, the DD inorganic core was retained during ligand attachment, and the more rigid complexes exhibited different electrochemical stabilities as dependent from the mode of linkage between the Sn/S core and the fC unit.[10,11]

An alternative strategy is to directly attach Fc units to the inorganic core. Two different approaches have been reported until now. By treatment of $CdCl_2$ with silylated selenoferrocene (TMSSeFc, TMS = $-SiMe_3$), the Fc-functionalized AD-type Cd/Se complex was synthesized; cyclic voltammetry (CV) measurements, however, indicated instability of the inorganic core during electrochemical treatment.[12] The direct substitution of Sn atoms has been realized in our group by treatment of $FcSnCl_3$ (**A**) with Na_2S in tetrahydrofuran (THF). The resulting AD-type Sn/S complex $[(FcSn)_4S_6]$ (**B**) was investigated by means of ^{119}Sn Mössbauer spectroscopy, which showed a weak electrochemical interplay.[13]

Received: August 21, 2014
Published: November 14, 2014

   dx.doi.org/10.1021/ic502026g | Inorg. Chem. 2014, 53, 12512−12518

Our current work intended to extend the investigations of Fc-functionalized Sn/S complexes by treatment of **A** with the heavier chalcogenides E = Se, Te to generate Fc-functionalized Sn/E complexes. As our first results, we report herein the synthesis of $[(FcSn)_4Se_6]$ (**1**), the heavier homologue of **B**, and $[(Fc_2Sn)_3Te_2]$ (**2**), along with their structures and optical and electrochemical properties. Furthermore, **1** was subject to further extension of the inorganic core to form the multinary, Fc-functionalized cluster $[(CuPPh_3)_6(S/Se)_6(SnFc)_2]$ (**3**).

EXPERIMENTAL SECTION

Syntheses. *General.* All reaction steps were carried out under Ar atmosphere, unless otherwise noted. All solvents were dried and freshly distilled prior to use. Ferrocenyltintrichloride ($FcSnCl_3$), potassium selenide (K_2Se), potassium telluride (K_2Te), and $[Cu(PPh_3)_3Cl]$ were prepared according to the reported methods.[13−15] CuCl and PPh_3 were purchased from Sigma-Aldrich.

*Synthesis and Analysis of $FcSnCl_3$ (**A**).* The precursor $FcSnCl_3$ was prepared according to the reported method.[13] Here, the NMR analyses of $FcSnCl_3$ were carried in deuterated chloroform ($CDCl_3$) instead of deuterated benzene to understand the change of electronic situation on Fc-substituted Sn atoms in comparison with resulting products, because of the influence of solvent effect on the chemical shifts, especially for the ^{119}Sn NMR. ^{1}H NMR: (300 MHz, $CDCl_3$): δ = 4.66, 4.42 (2 × m, 2 × 2H, $Cp_{subst.}$-*H*), 4.37 (s, 5H, $Cp_{unsubst.}$-*H*) ppm; ^{13}C NMR: (75 MHz, $CDCl_3$): δ = 73.1, 72.6, 72.5 ($Cp_{subst.}$-*C*), 70.3 ($Cp_{unsubst.}$-*C*) ppm; ^{119}Sn NMR: (186 MHz, $CDCl_3$): δ = −14.8 ppm.

*Synthesis of $[(FcSn)_4S_6]$ (**B**).* The synthesis of tin sulfide AD-type complex **B** was slightly modified according to the reported synthetic pathway.[13] $FcSnCl_3$ (0.212 g, 0.52 mmol) and Na_2S (0.601 g, 0.77 mmol) were suspended in 18 mL of THF. After 1 d of stirring at room temperature (rt), the solvent was evaporated in vacuum, and the residues were extracted with 10 mL of $CHCl_3$. The yellow extract was layered with *n*-pentane (1:1) and stored in a freezer. Yellow needle-shaped crystals of **B** were obtained within a week. Yield: 0.127 g, 74% (calculated on the basis of $FcSnCl_3$). ^{1}H NMR: (300 MHz, $CDCl_3$): δ = 4.53, 4.42 (2 × m, 2 × 8H, $Cp_{subst.}$-*H*), 4.38 (s, 20H, $Cp_{unsubst.}$-*H*) ppm; ^{13}C NMR: (75 MHz, $CDCl_3$): δ = 75.1, 72.8, 71.6 ($Cp_{subst.}$-*C*), 69.8 ($Cp_{unsubst.}$-*C*) ppm; ^{119}Sn NMR: (186 MHz, $CDCl_3$): δ = 112.1 ppm.

*Synthesis of $[(FcSn)_4Se_6]$ (**1**).* $FcSnCl_3$ (0.201 g, 0.49 mmol) and K_2Se (0.120 g, 0.76 mmol) were suspended in 18 mL of THF. After 2 d of stirring at rt, the solvent was evaporated in vacuum, and the residues were extracted with 10 mL of $CHCl_3$. The red extract was layered with *n*-pentane (1:1) and stored in a freezer. Orange plate-shaped crystals of **1** were obtained within a week. Yield: 0.156 g, 76% (calculated on the basis of $FcSnCl_3$). ^{1}H NMR: (300 MHz, $CDCl_3$): δ = 4.52, 4.43 (2 × m, 2 × 8H, $Cp_{subst.}$-*H*), 4.38 (s, 20H, $Cp_{unsubst.}$-*H*) ppm; ^{13}C NMR: (75 MHz, $CDCl_3$): δ = 74.5, 72.7, 71.3 ($Cp_{subst.}$-*C*), 69.8 ($Cp_{unsubst.}$-*C*) ppm; ^{119}Sn NMR: (186 MHz, $CDCl_3$): δ = −85.8 ppm, $^1J(^{119}Sn^{77}Se)$ = 1470 Hz; ^{77}Se NMR: (95 MHz, $CDCl_3$): δ = −111.0 ppm; ESI-MS(+): *m*/*z* = 1712.1 ($[M + Na]^+$); 1689.1 ($[M]^+$); IR: $\tilde{\nu}/cm^{-1}$ = 3087 (m), 2395 (s), 2340 (s), 2282 (s), 2071 (w), 2043 (w), 2009 (w), 1976 (w), 1780 (w), 1635 (w), 1407 (m), 1376 (m), 1301 (m), 1187 (m), 1138 (s), 1104 (m), 1050 (s), 4018 (s), 996 (s), 898 (m), 871 (m), 819 (s), 757 (m), 732 (m), 630 (m), 593 (m), 481 (s).

*Synthesis of $[(Fc_2Sn)_3Te_2]$ (**2**).* $FcSnCl_3$ (0.153 g, 0.37 mmol) and K_2Te (0.116 g, 0.56 mmol) were suspended in 18 mL of THF. After 2 d of stirring at rt, the solvent was evaporated in vacuum, and the residues were extracted with 8 mL of dichloromethane. The orange-yellow extract was layered with *n*-pentane (1:1), and stored in a freezer. Orange-red block-shape crystals of **2** were obtained within a week. Yield: 0.050 g, 24% (calculated on the basis of $FcSnCl_3$). ^{1}H NMR: (500 MHz, $CDCl_3$): δ = 4.47−4.42 (4 × m, 4 × 4H, $Cp_{subst.}$-*H* in four Fc units connected with a Sn−Sn dumbbell), 4.34, 4.32 (2 × m, 2 × 4H, $Cp_{subst.}$-*H* in two Fc units connected with a Sn(IV) atom), 4.28 (s, 10H, $Cp_{unsubst.}$-*H* in two Fc units connected with a Sn(IV) atom), 4.16 (s, 20H, $Cp_{unsubst.}$-*H* in four Fc units connected with a Sn−Sn dumbbell) ppm; ^{13}C NMR: (125 MHz, $CDCl_3$): δ = 75.1, 75.0, 71.8 ($Cp_{subst.}$-*C* in two Fc units connected to a Sn(IV) atom), 74.4, 71.2, 71.2, 71.0, 70.9, 69.0 ($Cp_{subst.}$-*C* in four Fc units connected to a Sn−Sn dumbbell), 69.4 ($Cp_{unsubst.}$-*C* in two Fc units connected with a Sn(IV) atom), 69.3 ($Cp_{unsubst.}$-*C* in four Fc units connected with a Sn−Sn dumbbell) ppm; ^{119}Sn NMR: (186 MHz, $CDCl_3$): δ = −36.9, −196.9 ppm; ^{125}Te NMR: (158 MHz, $CDCl_3$): δ = −1038.9 ppm; ESI-MS(+): *m*/*z* = 1744.5 ($[M + Na]^+$); IR: $\tilde{\nu}/cm^{-1}$ = 3915 (w, br), 3084 (m, br), 2350 (w), 2050 (w), 1636 (w), 1406 (m), 1373 (m), 1297 (m), 1260 (w), 1181 (m), 1134 (s), 1104 (s), 1049 (m), 1019 (s), 998 (s), 870 (m), 817(vs), 737 (m), 603 (m), 496 (vs), 478 (vs), 405 (m).

*Synthesis of $[(CuPPh_3)_6(S/Se)_6(SnFc)_2]$ (**3**).* To compound **1** (0.0397 g, 0.0235 mmol) and $Na_2S{\cdot}9H_2O$ (0.0349 g, 0.141 mmol), the solvents THF (5 mL) and water (1 mL) were added one after the other. After 15 min of stirring, the generated clear yellow solution was added to the mixture of $[CuCl(PPh_3)_3]$ (0.250 g, 0.282 mmol) in 5 mL of THF. The solution turned to red-brown. It was stirred for 12 h and then filtered. The solution was layered over water (1:1). Light yellow crystals of **3** were obtained within 2 d. Yield: 0.024 g, 33% (calculated on the basis of **1**). ^{1}H NMR: (500 MHz, CD_2Cl_2): δ = 7.75−7.66, 7.60−7.45 (m, 90H, *H*-Ar), 3.74, 1.85 (m, 16H, *H*-THF) ppm. ^{31}P NMR: (202 MHz, CD_2Cl_2): δ = 43.9, 35.9 ppm. ^{119}Sn NMR: (186 MHz, CD_2Cl_2): δ = 153.9, −71.8 ppm. IR: $\tilde{\nu}/cm^{-1}$ = 2963 (w), 2341, 2361 (w, br), 1432 (w), 1477 (w), 1408 (w), 1259 (m), 1084 (br, m), 1013 (s), 868 (w), 792 (s), 743 (m), 689 (m), 563 (w), 482 (m).

NMR Spectroscopy. ^{1}H, ^{13}C, ^{119}Sn, ^{77}Se, and ^{125}Te NMR measurements were carried out using a Bruker DRX 300 or 500 MHz spectrometer at 25 °C. In ^{1}H and ^{13}C NMR spectra, the chemical shifts were quoted in ppm relative to the residual protons of deuterated solvents. In ^{119}Sn, ^{77}Se, and ^{125}Te NMR analyses, Me_4Sn, $(CH_3)_2Se$, and $(CH_3)_2Te$ were used as internal standard, respectively.

Infrared Spectroscopy. Infrared (IR) spectra were recorded on a Bruker TENSOR 37 FT-IR spectrometer.

Raman Spectroscopy. Raman spectra were recorded on a Labram HR 800 Raman spectrometer with a 632.8 nm red laser in the range of 80−3200 cm^{-1}. The beam was focused on the sample through a confocal microscope using a 50× objective lens.

UV−Visible Absorption Spectroscopy. UV−visible absorption spectra were recorded on a PerkinElmer Cary 5000 UV/vis/NIR spectrometer in the range of 800−200 nm, employing the double-beam technique. The samples were prepared as solution in CH_2Cl_2.

Energy-Dispersive X-ray (EDX) Spectroscopy. EDX analyses were performed using the EDX device Voyager 4.0 of Noran Instruments coupled with the electron microscope CamScan CS 4DV. Data acquisition was performed with an acceleration voltage of 20 kV and 100 s accumulation time. For the analyses, multiple single crystals were used, and the data recorded both various times on one single crystal and various times on other single crystals.

Electrospray Ionization (ESI) Mass spectrometry. ESI-MS was performed on a Finnigan MAT 95S. The electrospray ionization ion trap mass spectrometry (ESI-ITMS) spectra were obtained by using solvent as the carrier gas.

^{57}Fe and ^{119}Sn Mössbauer Spectroscopy. $Ca^{119m}SnO_3$ and ^{57}Co/Rh sources were used for the Mössbauer spectroscopic experiments. The measurements were carried out at 78 and 5 K in transmission geometry. The Mössbauer sources were kept at room temperature. Polycrystalline samples of **1** and **2** were diluted with dry SiO_2 and enclosed in small PMMA containers. For the ^{119}Sn measurements a palladium foil of 0.05 mm thickness was used to reduce tin K X-rays concurrently emitted by this source. Fitting of the spectrum was performed with the Normos-90 program system.[16]

Electrochemical Measurements. All electrochemical measurements—cyclic and differential pulse voltammetry (CV and DPV)—were recorded under Ar atmosphere at 25 °C, using 0.1 mol/L $[^nBu_4N][PF_6]$ as the supporting electrolyte. The potentials were referenced internally to ferrocene, added at the end of the experiments.

dx.doi.org/10.1021/ic502026g | Inorg. Chem. 2014, 53, 12512−12518

Table 1. Crystallographic and Refinement Details of 1−3

compound	1	2	3
chemical formula	$C_{40}H_{36}Fe_4Se_6Sn_4$	$C_{60}H_{54}Fe_6Sn_3Te_2$	$C_{136}H_{120}Fe_2Se_{3.25}S_{2.75}Sn_2Cu_6P_6O_4$
formula mass/g·mol^{-1}	1688.61	1721.40	3079.24
crystal color and shape	orange plate	orange-red block	yellow block
crystal size/mm^3	0.22 × 0.15 × 0.08	0.26 × 0.14 × 0.03	0.16 × 0.16 × 0.14
crystal system	orthorhombic	triclinic	monoclinic
a/Å	24.9134(6)	12.5690(4)	42.3467(11)
b/Å	13.2096(4)	12.8600(4)	14.5072(4)
c/Å	27.1065(8)	17.9930(6)	42.7189(11)
α/deg	90	105.6830(10)	90
β/deg	90	95.6560(10)	92.544(1)
γ/deg	90	102.2110(10)	90
V/Å^3	8920.6(4)	2698.98(15)	26217.7(12)
space group	*Pbca*	$P\bar{1}$	*C*2/*c*
Z	8	2	8
radiation type	Mo Kα	Mo Kα	Mo Kα
abs. coefficient, μ/mm^{-1}	8.4	4.0	2.6
abs. correction type	multiscan	multiscan	multiscan
max/min transmission	0.553/0.260	0.889/0.421	0.685/0.663
2θ range/deg	4.4−54.3	4.4−50.0	4.8−50.0
no. of reflections meas.	60 834	45 121	173 710
no. of ind. reflections	9863	9483	22998
R_{int}	0.0923	0.0293	0.074
R_1 ($I > 2\sigma(I)$)/$wR(F^2)$ (all data)	0.0338/0.0841	0.0237/0.0608	0.063/0.189
goodness of fit on F^2	1.041	1.042	1.08
largest diff. peak/hole, e$^-$·Å^{-3}	0.87/−0.95	3.49/−0.78	1.94/−1.20

Scheme 1. Synthesis of Compounds 1 and 2 by Reactions of $FcSnCl_3$ with K_2E (E = Se, Te). By Further Treatment of 1 with $Na_2S·9H_2O$ and Ensuing Reaction with $[Cu(PPh_3)_3Cl]$, the Cluster Compound 3 was Obtained

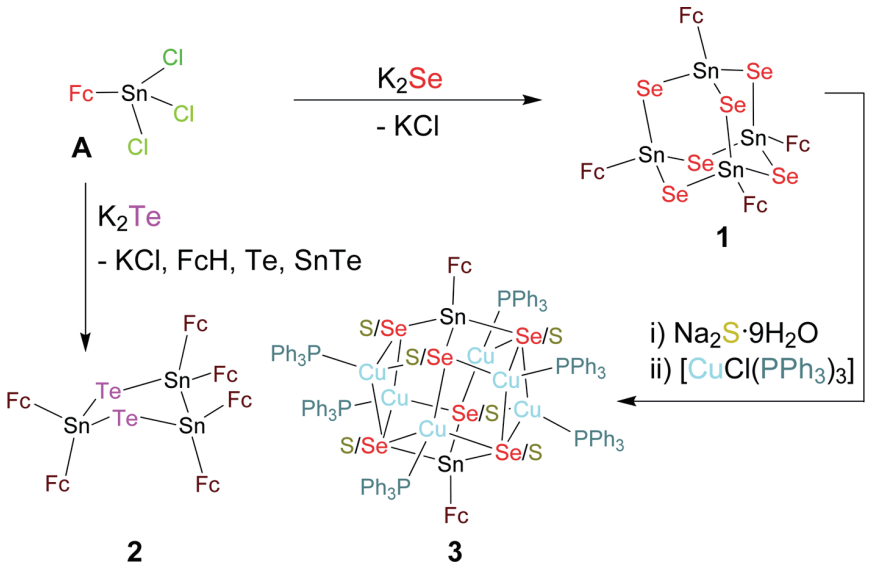

Working and counter electrodes: Pt; scan rate: 200 mV/s; pulse amplitude for DPV: 50 mV.

X-ray Diffraction Measurement, Structure Solution, and Refinement. Data were collected on a diffractometer equipped with a Bruker PHOTON 100 detector system D8 QUEST, using graphite-monochromatized Mo Kα radiation (λ = 0.710 73 Å) at 100 K. The structure solution and refinement were performed by Sir-2004,[17] and full-matrix-least-squares refinement against F^2 was done using the SHELXL-2013 software.[18] Details of the data collections and refinements are given in Table 1. Selected structural parameters are provided in Supporting Information, Tables S6−S10, S12, and S13. S versus Se atomic disorder in compound **3** was modeled by using the PART instruction with EADP during the refinement, ending up with independent positions of both atoms (see Supporting Information, Figure S18 and Table S11). The resulting S/Se ratio (2.71:3.29) is very close to that determined via EDX spectroscopy (2.71:3.25, see Supporting Information, Table S5).

RESULTS AND DISCUSSION

Treatment of **A** with 1.5 equiv of K_2Se in THF yielded a Fc-substituted AD-type Sn/Se complex, $[(FcSn)_4Se_6]$ (**1**), along

dx.doi.org/10.1021/ic502026g | *Inorg. Chem.* 2014, 53, 12512−12518

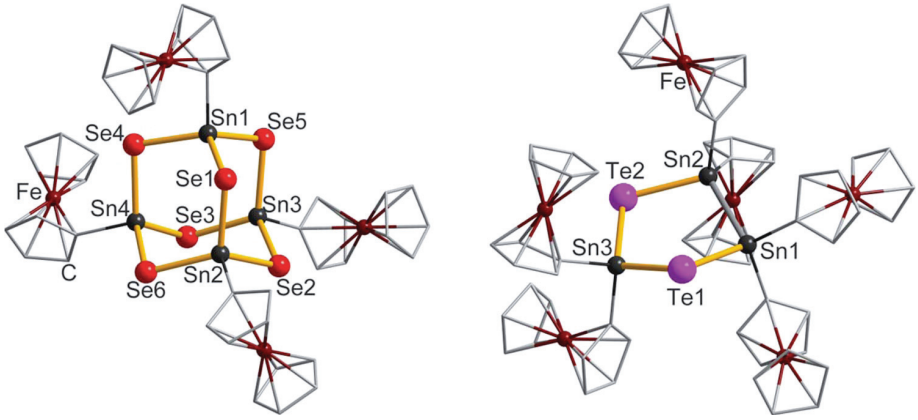

Figure 1. Molecular structures of **1** (left) and **2** (right), without H atoms.

with KCl in a clean reaction. A similar reaction with 1.5 equiv of K_2Te under the same conditions, however, led to the formation of a puckered five-membered Sn/Te ring with bis-substituted Sn atoms, $[(Fc_2Sn)_3Te_2]$ (**2**), besides KCl and a black residue containing Fe, Sn, and Te according to energy dispersive X-ray (EDX) spectroscopy (Supporting Information, Figure S9, Table S4). Owing to a slight excess of Te, we suppose that it comprises a mixture of ferrocene, SnTe, and Te, which is in agreement with an earlier report.[19] Treatment of **1** with 6 equiv of $Na_2S{\cdot}9H_2O$ to initially break up Sn−E bonds, and subsequent reaction of the mixture with 12 equiv of $[CuCl(PPh_3)_3]$ in THF/H_2O, led to the formation of the cluster $[(CuPPh_3)_6(S/Se)_6(SnFc)_2]$ (**3**; Scheme 1). All compounds are air stable in the solid state, well-soluble in chlorinated solvents, and were characterized by standard analytic techniques (see Supporting Information). The molecular structures were determined by single-crystal X-ray diffraction (XRD; see the Experimental Section).

The nearly tetrahedral, AD-type $[Sn_4Se_6]$ core in **1** is decorated by Sn−C-bound Fc units (Figure 1 left), as observed for its sulfide analog **B**. All Sn atoms have the same coordination sphere; they are surrounded by three Se atoms and one Fc unit. Sn−Se bond lengths (2.5130(7)−2.5457(7) Å) and Sn−C bond lengths (2.096(5) and 2.111(5) Å) are in agreement with those reported for the related compound $[(PhSe)_3Sn{-}fC{-}{-}Sn(SePh)_3]$ (2.5058(11)−2.5413(11) Å for Sn−Se; 2.1040(7) Å for Sn−C).[20]

Unexpectedly, the reaction of **A** with the K_2Te did not afford the ubiquitous AD-type cluster topology but the five-membered ring-based Sn/Te complex **2** (Figure 1 right). The ring contains one isolated Sn atom and a Sn−Sn bond, and therefore two types of Sn atoms. This is clearly reflected by two ^{119}Sn NMR signals (−36.9 and −196.9 ppm) with relative intensities close to 2:1 (Supporting Information, Figure S3). Sn1 and Sn2, which are involved in the Sn−Sn bond, are additionally coordinated by two Fc units and one Te atom. Sn3 is bonded to two Fc units and two Te atoms. All Sn atoms therefore adopt nearly tetrahedral coordination geometry. The same inorganic structural motif, however, exhibiting different organic decorations and not only Te, but also S or Se within the ring, $[(R_2Sn)_3E_2]$ (R = ^{t}Bu, Me; E = S, Se, Te), has been independently reported by Puff and Mathiasch.[19,21] Unlike **2**, these compounds were synthesized either by oxidation of cyclic organostannanes (Sn^{II}) or organotin hydrides with elemental chalcogens or through reduction of organotin chalcogenide four-membered rings (Sn^{IV}) with lithium aluminum hydride.[19,21d,22] We assume that the reductive nature of Te^{2-} ($E^\circ_{1/2}$ = −1.143 V)[23] causes Sn−Sn bond formation under production of elemental Te. Ge−Ge bond formation within a telluridogermanate complex was recently observed under similar conditions.[6c] To rationalize the change from a monosubstituted Sn atom in **A** to all bisubstituted Sn atoms, it should be mentioned that the C−Sn bond is known to be labile for C being part of an aryl or a straight-chain alkyl group in the presence of Lewis acids. A prominent example for this is the Kocheshkov redistribution reaction of SnX_4 with $R'SnR_3$ to form $R'SnCl_3$,[24] which allows to explain the findings as a redistribution of Fc units occurring along with the redox reaction. The Sn−Sn bond in **2** (2.7952(3) Å) is slightly shorter than that observed in the related compound $[(^tBu_2Sn)_3Te_2]$ (2.836(2) or 2.843(2) Å),[21d] which might be attributed to the even bulkier ^{t}Bu ligands. The less-affected Sn−Te distances are therefore very similar, ranging from 2.7266(3) to 2.7558(3) Å in both compounds.

The optoelectronic properties of **1** and **2**, and the previously unexplored properties of **B**, were examined by UV−visible absorption spectroscopy in CH_2Cl_2 solutions (Supporting Information, Figure S4). In all three compounds, the absorption bands of the ferrocenyl group were red-shifted with respect to the absorption of pure ferrocene—more significantly as the chalcogenide changed from S through Se to Te. According to the color changes observed for purely inorganic Sn/E complexes,[4a−d] the named variation of the chalcogenide ligands also caused a red shift of the p(E) → s,p(Sn) charge transfer band, even though the structures of the three complexes are not exactly the same and even differ by the number of Sn or E atoms.

To study the impact of both structural changes as well as replacement of one chalcogen by another on the electrochemical properties, cyclic and differential pulse voltammetry (CV and DPV) were run on CH_2Cl_2 solutions of **1**, **2**, and **B**. The voltammograms of **B** and **1** are shown in Figure 2.

Both compounds undergo a single-step oxidation Fe^{2+} → Fe^{3+} in the CV mode (E_{pa} = 450 mV for **B**, 370 mV for **1**), indicating four eqivalent and widely independent redox sites in each compound. The DPV measurements confirm this finding in that only one oxidation peak is observed for each compound; however, the peaks are relatively broad, which is indicative of some communications of the redox sites due to movement of the Fc units in solution. In the case of the sulfide complex **B**, a

dx.doi.org/10.1021/ic502026g | Inorg. Chem. 2014, 53, 12512−12518

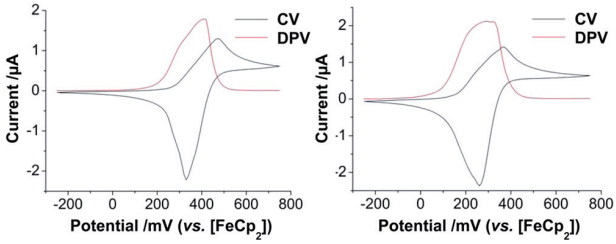

Figure 2. Cyclic and differential pulse voltammograms, recorded at a platinum electrode in CH_2Cl_2 solutions of the sulfide complex **B** (1.60 mM, left) or the selenide complex **1** (1.53 mM, right) in the presence of tetra-*n*-butylammonium hexanfluorophosphate (TBFP) (0.1 M). Scan ranges and rates: CV, −220 to 800 mV, 200 mV/s; DPV, −220 to 800 mV, 10 mV/s. Pulse amplitude 50 mV.

trend toward separation of the peaks is visible, whereas in the case of the selenide complex **1**, both measurements show that the chalcogenide ligand influences the redox properties of the Fc unit, in that the redox potential decreases upon replacing E = S with E = Se, in accordance with a decreased electron withdrawal from the adjacent Sn atoms and consequently slight increase of the electron density within the Cp rings, in turn enabling easier oxidation of the Fe ions. The fact that the cathodic return wave is higher and thinner than the anodic forward wave in both compounds is assumed to be due to an interaction of the Sn/E skeleton with the electrodes in the present case. Different as for nanoparticles bearing ferrocenenyl termini[25] and ferrocene-based Ag/Se clusters,[26] where the effect was reported to be attributed to an adsorption of the ferrocenium form of the complexes onto the electrode, the title compounds here are not terminated by a functional group that would influence the wave shape in CV.[25] The assumption for a contribution of the Sn/E skeleton agrees with the overall tendency of chalcogenides to interact with metal surfaces.[27] Whereas bulkier organic ligands seem to effectively protect the Sn/E complexes from an attachment to the electrode material,[10] the ferrocenyl groups in **1** and **B** do not seem to form a sufficiently protective shield (Supporting Information, Figures S16, S17). Still, the adsorption does not seem to proceed further toward any decomposition of the compounds, as the CV redox waves remained the same after several scans without any intensity drop. The difference between the anodic and cathodic peak potentials (ΔE_p) is slightly shifted from 140 mV in **B** to 110 mV in **1** (Supporting Information, Table S1), suggesting a somewhat stronger interaction of the selenide cluster with the electrode surface as compared to the sulfide cluster.

At first glance, the CV voltammogram of **2** is similar to those of **B** and **1** in that it also exhibits an almost single-step oxidation. However, the oxidation range is even broader and combined with a large and thin cathodic return wave. Additionally, the DPV measurement shows much more complicated oxidation processes going on at the six Fc units in **2**. As indicated by two broad shoulders occurring along the oxidation peak, interactions between the iron centers are very probable here due to the shorter intramolecular Fe···Fe distances (8.30−10.59 Å in **1** and 8.11−9.98 Å in **B** vs 5.53−10.46 Å in **2**; see also Supporting Information, Tables S8−10). Both interactions through the bridging Sn atom of terminal Fc groups and/or through space are thus possible here.

As local probe for the electronic situation of the tin atoms in the cluster core and the iron atoms in the ferrocenyl groups ^{119}Sn and ^{57}Fe Mössbauer spectroscopic measurements were carried out on compounds **1** and **2**. The results are summarized in Figure 3 and Table 2.

Table 2. Fitting Parameters of ^{57}Fe and ^{119}Sn Mössbauer Spectroscopic Measurements of Compounds 1 and 2

T/K	source	δ^a/mm·s^{-1}	$\Delta E_Q{}^b$/mm·s^{-1}	Γ^c/mm·s^{-1}	ratio/%
1					
78	^{119}Sn	1.36(1)	1.21(1)	0.93(1)	100
5	^{57}Fe	0.43(1)	2.39(1)	0.29(1)	100
2					
78	^{119}Sn	1.40(1)	1.08(2)	0.82(3)	33[d]
		1.45(1)	1.55(1)	0.86(1)	67[d]
5	^{57}Fe	0.44(1)	2.39(1)	0.56(1)	100

[a] δ = isomer shift. [b] ΔE_Q = electric quadrupole splitting. [c] Γ = experimental line width. [d] This parameter was kept fixed during the fitting procedure.

The ^{57}Fe and ^{119}Sn spectra of **1** show a great accordance with the spectra of the S analogue **B**. The ^{119}Sn isomer shift of 1.36(1) mm·s^{-1} is slightly increased compared to 1.28(1) mm·s^{-1} of **B** due to a slight decrease in electronegativity when going

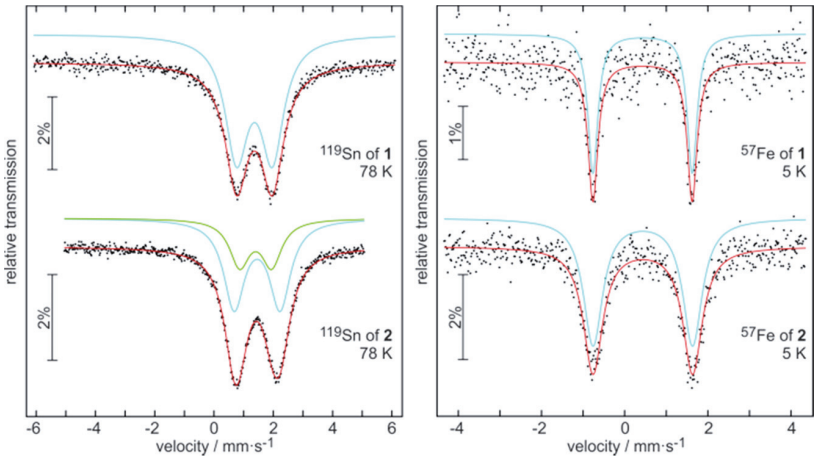

Figure 3. ^{119}Sn (left) and ^{57}Fe (right) Mössbauer spectra of **1** (upper) and **2** (lower).

dx.doi.org/10.1021/ic502026g | Inorg. Chem. 2014, 53, 12512−12518

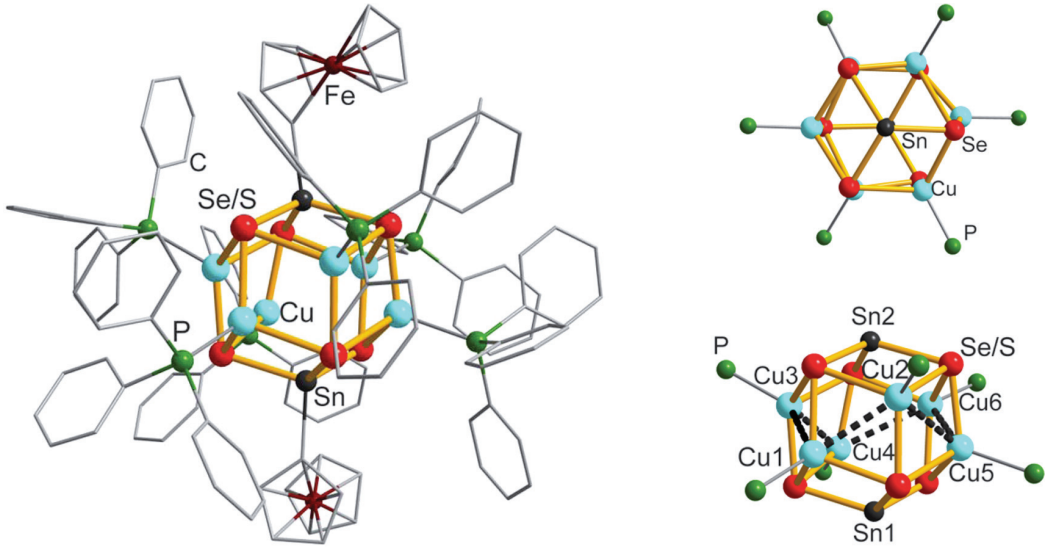

Figure 4. Different views of the molecular structure of **3**, without H atoms (left), further without Fc units and phenyl rings (right), viewed in two different orientations (top and bottom). The chair conformation of six Cu atoms is highlighted by dashed black lines (lower right).

from sulfur to selenium, which results in a higher s-electron density at the tin nucleus. The quadrupole splitting resulting from the noncubic site symmetry of the tin atoms is 1.21(1) mm·s^{-1} and therefore almost identical with the refined splitting of **B**. The ^{57}Fe spectrum was well-reproduced with a single signal, subjected to quadrupole splitting. The single signals of the four crystallographically independent tin atoms superimpose, indicating almost similar electronic situation.

The two tin sites in **2** can be distinguished in the ^{119}Sn spectrum, with those of the Sn−Sn dumbbell showing slightly higher isomer shifts (i.e., slightly higher s-electron density) and enhanced quadrupole splitting (a consequence of the higher site asymmetry). The symmetry of the Sn_3Te_2 core is much lower than that of the adamantane-related Sn_4Se_6 core, leading to larger differences for the six independent ferrocenyl groups. Again, we could reproduce the ^{57}Fe spectrum with a single signal, however, with an enhanced line width accounting for the superposition of six single signals.

Combination of organic binary chalcogenidostannate anions $[SnE^1{}_4]^{4-}$ with chalcogenides like K_2E^2 ($E^1 \neq E^2$) in protic solvents comes along with an exchange of chalcogenide ligands and the formation of mixed chalcogenidometalate anions $[SnE^1{}_{4-x}E^2{}_x]^{4-}$[4f] or $[M_4Sn_4E^1{}_{17-x}E^2{}_x]^{10-}$.[4f,g] However, ternary organotin−metalchalcogenide complexes with different chalcogenides have not been reported so far. To check the availability of the latter, we treated the organotin selenide compound **1** with $Na_2S{\cdot}9H_2O$ first and subsequently with $[CuCl(PPh_3)_3]$ in THF/H_2O, which indeed yielded the mixed-chalcogenide cluster compound **3** (Figure 4), which is isostructural with the known complexes $[(PhSn)_2(CuPMe_2Ph)_6S_6]$ (**C**)[8a] and $[(R^{1,2}T)_2(CuPPh_3)_6S_6]$ (T = Sn, **D**; T = Ge, **E**).[6a] Compound **3** comprises a polynuclear inorganic Cu/Sn/E core, which is shielded by PPh_3 ligands and Fc units attached to the Cu and Sn atoms, respectively.

The $Cu_6Sn_2(S,Se)_6$ architecture represents a rhombic dodecahedron, formed by 2-fold capping of a (nonbonded) chair arrangement of six Cu atoms through two E_3SnFc units. The latter were formed by nucleophilic attack of the AD-type Sn/Se complex in **1** by 6 equiv of S^{2-} anions in aqueous THF solution. According to previously reported NMR studies on chalcogenide exchange reactions, which led to the formation of purely inorganic $[SnSe_xS_{4-x}]^{4-}$ or $[SnSe_xS_{3-x}]^{2-}$ anions,[4g] the two ^{119}Sn MNR signals that were observed for a solution of **3** (δ = 153.9, −71.8 ppm, $\Delta\delta$ = 126 ppm; see Experimental Section) indicate that the initial treatment of **1** has most probably produced two $[FcSnSSe_2]^{3-}$ and two $[FcSnS_2Se]^{3-}$ anions per formula unit of the reactant; this is supported by a spectrum of a fresh mixture of **1** with 6 equiv of $Na_2S{\cdot}9H_2O$ in a 5:1 THF/D_2O mixture at room temperature (as for the synthesis of **3** before addition of the copper complex), which shows two new signals beside that of **1** in a 1:1 ratio (see Supporting Information, Figure S20). Because of mixed occupancy of the chalcogenide positions by S and Se atoms in **3**, their distribution within the molecule could not be rationalized by the crystal structure analysis; however, the assumption is in agreement with the overall S/Se ratio gathered from the crystal structure refinement and observed by means of EDX analyses (Supporting Information, Figure S10; Tables S5, S11), both of which point toward a near 1:1 situation (S/Se = 1:1.2). Disregarding a slight excess of Se atoms, the ratio of heavy atoms in **3** is thus exactly the same as in the reaction mixture. The partial substitution of S with Se atoms clearly influences the bond lengths (Sn−E, 2.4521(12)−2.4919(10) Å; Cu−E, 2.3336(13)−2.8304(15) Å), which are significantly longer than those in the Sn/S or Ge/S compounds **C**, **D**, and **E**. Short Cu···Cu distances (2.7426(11)−2.8093(13) Å) were observed, such as in **C** (2.7634(13)−2.8386(10) Å) and in **D** (2.7322(10)−2.8653(12) Å). In addition, the Sn−Cu distances (3.0260(10)−3.1239(11) Å) are distinctly smaller than the sum of the van der Waals radii (3.60 Å).[28]

CONCLUSION

In conclusion, we have demonstrated that the concept of direct covalent attachment of Fc units to a T/E core (T = Ge, Sn; E = S) can be transferred to E = Se and Te. By treatment of $FcSnCl_3$ with K_2Se and K_2Te, two polynuclear complexes, **1** and **2** were obtained, which possess, however, different Sn/E structures. Further reaction of **1** with $Na_2S{\cdot}9H_2O$ and $[Cu(PPh_3)_3Cl]$ led to the formation of a ternary Cu/Sn/E

dx.doi.org/10.1021/ic502026g | Inorg. Chem. 2014, 53, 12512−12518

(3; E = S and Se) complex containing two Fc units. The optical absorption properties and the electrochemical properties of **1**, **2**, and the previously synthesized sulfide complex **B** were examined by using UV−visible spectroscopy, CV, and DPV and compared. The UV−visible spectra of the three compounds are red-shifted as going from E = S through Se to Te, not only regarding the absorption bands of the Fc units, but also the bands resulting from p(E) → s,p(Sn) charge transfer despite the structural differences. In CV and DPV, all three compounds display slight electronic communication of adjacent Fc units, most notably in the case of **2** with shortest Fe···Fe distances. ^{119}Sn Mössbauer spectra reveal the different tin sites, while ^{57}Fe Mössbauer spectra point to almost similar electronic situation for all ferrocenyl entities, excluding a direct influence of the Sn_4Se_6 or Sn_3Te_2 cores on the metal atom within the ligand.

■ ASSOCIATED CONTENT

Supporting Information

Details on syntheses, ESI mass spectrometry, ^{119}Sn, ^{1}H, and ^{13}C NMR, UV−visible spectroscopy, electrochemical measurements, EDX spectroscopy, IR and Raman spectroscopy, X-ray diffraction, structure analyses, and Mössbauer spectroscopy. Crystallographic data in CIF format. This material is available free of charge via the Internet at http://pubs.acs.org.

■ AUTHOR INFORMATION

Corresponding Author

*E-mail: dehnen@chemie.uni-marburg.de. Fax: +49 6421 2825653. Phone: +49 6421 2825751.

Author Contributions

The manuscript was written through contributions of all authors. All authors have given approval to the final version of the manuscript. All authors contributed equally.

Notes

The authors declare no competing financial interest.

■ ACKNOWLEDGMENTS

This work was supported by the Deutsche Forschungsgemeinschaft (DFG) within the framework of SFB 1083. We are deeply indebted to Dr. M. Hołyńska for valuable help with the X-ray structure analyses, and we also thank A. Geese for his help in the preparation of compound **3**.

■ REFERENCES

(1) (a) Krebs, B. *Angew. Chem., Int. Ed.* **1983**, *22*, 113−134. (b) Dabbousi, B. O.; Bawendi, M. G.; Onitsuka, O.; Rubner, M. F. *Appl. Phys. Lett.* **1995**, *66*, 1316−1318. (c) Murray, C. B.; Kagan, C. R.; Bawendi, M. G. *Science* **1995**, *270*, 1335−1338. (d) Sheldrick, W. S.; Wachhold, M. *Angew. Chem., Int. Ed.* **1997**, *36*, 207−224. (e) Sheldrick, W. S.; Wachhold, M. *Coord. Chem. Rev.* **1998**, *176*, 211−322.

(2) (a) Zheng, N. *Science* **2003**, *299*, 1015−1015. (b) Zheng, N. F.; Bu, X. H.; Feng, P. Y. *Nature* **2003**, *426*, 428−432. (c) Feng, P. Y.; Bu, X. H.; Zheng, N. F. *Acc. Chem. Res.* **2005**, *38*, 293−303.

(3) (a) Soloviev, V. N.; Eichhöfer, A.; Fenske, D.; Banin, U. *J. Am. Chem. Soc.* **2000**, *122*, 2673−2674. (b) Soloviev, N. V.; Eichhöfer, A.; Fenske, D.; Banin, U. *J. Am. Chem. Soc.* **2001**, *123*, 2354−2364. (c) Zheng, N. F.; Bu, X. H.; Lu, H. W.; Zhang, Q. C.; Feng, P. Y. *J. Am. Chem. Soc.* **2005**, *127*, 11963−11965.

(4) (a) Dehnen, S.; Brandmayer, M. K. *J. Am. Chem. Soc.* **2003**, *125*, 6618−6619. (b) Brandmayer, M. K.; Clérac, R.; Weigend, F.; Dehnen, S. *Chem.—Eur. J.* **2004**, *10*, 5147−5157. (c) Zimmermann, C.; Anson, C. E.; Weigend, F.; Clérac, R.; Dehnen, S. *Inorg. Chem.* **2005**, *44*, 5686−5695. (d) Ruzin, E.; Fuchs, A.; Dehnen, S. *Chem. Commun.* **2006**, *46*, 4796−4798. (e) Dehnen, S.; Melullis, M. *Coord. Chem. Rev.* **2007**, *251*, 1259−1280. (f) Lips, F.; Dehnen, S. *Inorg. Chem.* **2008**, *47*, 5561−5563. (g) Ruzin, E.; Zent, E.; Matern, E.; Massa, W.; Dehnen, S. *Chem.—Eur. J.* **2009**, *15*, 5230−5244.

(5) (a) Fard, Z. H.; Clérac, R.; Dehnen, S. *Chem.—Eur. J.* **2010**, *16*, 2050−2053. (b) Fard, Z. H.; Hołyńska, M.; Dehnen, S. *Inorg. Chem.* **2010**, *49*, 5748−5752.

(6) (a) Fard, Z. H.; Xiong, L.; Müller, C.; Hołyńska, M.; Dehnen, S. *Chem.—Eur. J.* **2009**, *15*, 6595−6604. (b) Fard, Z. H.; Müller, C.; Harmening, T.; Pöttgen, R.; Dehnen, S. *Angew. Chem., Int. Ed.* **2009**, *48*, 4441−4444. (c) Heimann, S.; Hołyńska, M.; Dehnen, S. *Chem. Commun.* **2011**, *47*, 1881−1883. (d) Eussner, J. P.; Barth, B. E. K.; Leusmann, E.; You, Z.; Rinn, N.; Dehnen, S. *Chem.—Eur. J.* **2013**, *19*, 13792−13802.

(7) (a) Halvagar, M. R.; Fard, Z. H.; Dehnen, S. *Chem. Commun.* **2010**, *46*, 4716−4718. (b) Fard, Z. H.; Halvagar, M. R.; Dehnen, S. *J. Am. Chem. Soc.* **2010**, *132*, 2848−2849. (c) Halvagar, M. R.; Fard, Z. H.; Dehnen, S. *Chem.—Eur. J.* **2011**, *17*, 4371−4374.

(8) (a) Hauser, R.; Merzweiler, K. *Z. Anorg. Allg. Chem.* **2002**, *628*, 905−906. (b) Dörfelt, C.; Janeck, A.; Kobelt, D.; Paulus, E. F.; Scherer, H. *J. Organomet. Chem.* **1968**, *14*, 22−24.

(9) You, Z.; Dehnen, S. *Inorg. Chem.* **2013**, *52*, 12332−12334.

(10) You, Z.; Fenske, D.; Dehnen, S. *Dalton. Trans.* **2013**, *42*, 8179−8182.

(11) Ferguson, G.; Glidewell, C.; Opromolla, G.; Zakaria, C. M.; Zanello, P. *J. Organomet. Chem.* **1996**, *517*, 183−190.

(12) Lebold, T. P.; Stringle, D. L. B.; Workentin, M. S.; Corrigan, J. F. *Chem. Commun.* **2003**, *12*, 1398−1399.

(13) Pöhlker, C.; Schellenberg, I.; Pöttgen, R.; Dehnen, S. *Chem. Commun.* **2010**, *46*, 2605−2607.

(14) Ruzin, E. Ph.D. thesis, Philipps-Universität Marburg, 2007.

(15) Lippard, S. J.; Ucko, D. *Inorg. Chem.* **1968**, *7*, 1051−1056.

(16) Brand, R. A. *Normos Mössbauer fitting Program;* Universität Duisburg: Duisburg, Germany, 2007.

(17) Burla, M. C.; Caliandro, R.; Camalli, M.; Carrozzini, B.; Cascarano, G. L.; De Caro, L.; Giacovazzo, C.; Polidori, G.; Spagna, R. *J. Appl. Crystallogr.* **2005**, *38*, 381−388.

(18) Sheldrick, G. M. *SHELXL2013;* University of Göttingen: Germany, 2013.

(19) Mathiasch, B. *Z. Anorg. Allg. Chem.* **1977**, *432*, 269−274.

(20) Nayek, H. P.; Hilt, G.; Dehnen, S. *Eur. J. Inorg. Chem.* **2009**, *28*, 4205−4208.

(21) (a) Mathiasch, B. *Synth. React. Inorg. Met.-Org. Chem.* **1977**, *7*, 227−233. (b) Dräger, M.; Mathiasch, B. *Z. Anorg. Allg. Chem.* **1980**, *470*, 45−48. (c) Blecher, A.; Mathiasch, B.; Mitchell, T. N. *J. Organomet. Chem.* **1980**, *184*, 175−180. (d) Puff, H.; Breuer, B.; Schuh, W.; Sievers, R.; Zimmer, R. *J. Organomet. Chem.* **1987**, *332*, 279−288.

(22) Mathiasch, B. *J. Organomet. Chem.* **1976**, *122*, 345−350.

(23) Bratsch, S. G. *J. Phys. Chem. Ref. Data* **1989**, *18*, 1−21.

(24) Davies, A. G. Organotin Halides. In *Organotin Chemistry,* 2nd ed.; Wiley-VCH: New York, 2004; pp 166−167.

(25) Labande, A.; Ruiz, J.; Astruc, D. *J. Am. Chem. Soc.* **2002**, *124*, 1782−1789.

(26) MacDonald, D. G.; Eichhöfer, A.; Campana, C. F.; Corrigan, J. F. *Chem.—Eur. J.* **2011**, *17*, 5890−5902.

(27) (a) Kapusta, S.; Viehbeck, A.; Wilhelm, S. M.; Hackerman, N. *J. Electroanal. Chem.* **1983**, *153*, 157−174. (b) Herrero, E.; Climent, V.; Feliu, J. M. *Electrochem. Commun.* **2000**, *2*, 636−640. (c) Mohtadi, R.; Lee, W. K.; Van Zee, J. W. *Appl. Catal., B* **2005**, *56*, 37−42.

(28) Bondi, A. *J. Phys. Chem.* **1964**, *68*, 441−451.

Ferrocenyl-Functionalized Sn/Se and Sn/Te Complexes: Synthesis, Reactivity, Optical, and Electronic Properties

Zhiliang You,[†] Jakob Bergunde,[†] Birgit Gerke,[‡] Rainer Pöttgen,[‡]
and Stefanie Dehnen[†,*]

[†] Philipps-Universität Marburg, Fachbereich Chemie and Wissenschaftliches Zentrum für Materialwissenschaften, Hans-Meerwein-Strasse, D-35043 Marburg, Germany.
Fax: +49 6421 2825653; Tel: +49 6421 2825751.
E-mail: dehnen@chemie.uni-marburg.de.

[‡] Institut für Anorganische und Analytische Chemie, Universität Münster, Corrensstrasse 30, D-48149 Münster, Germany, E-mail: pottgen@uni-muenster.de

SUPPORTING INFORMATION

1. Supplementary of Mass Spectrometry and NMR Spectroscopy Data

ESI-MS(+) of **1:**

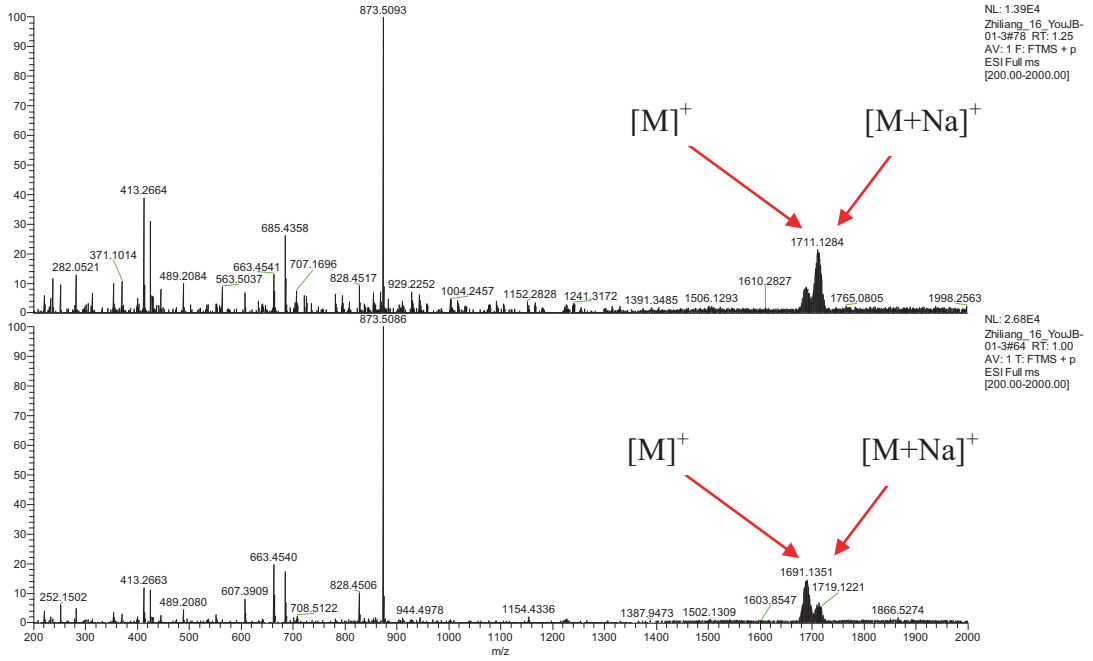

A: Two measurements at different ionization energy

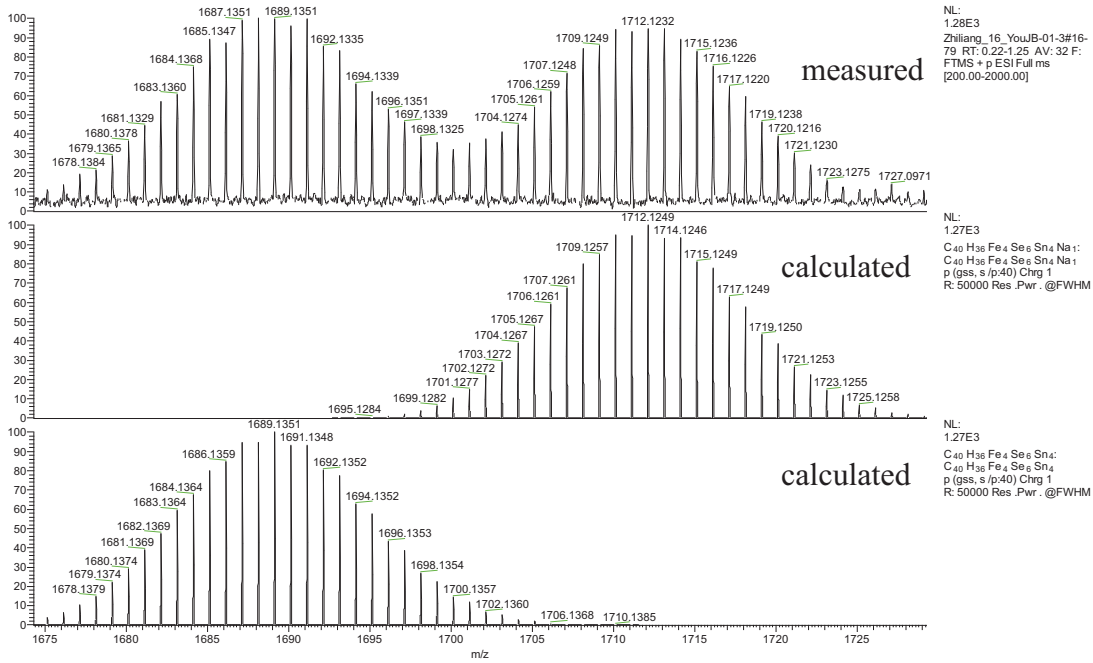

B: $[M]^+$ and $[M+Na]^+$

Figure S1. ESI(+) mass spectrum of **1**, overview of two measurements at different ionization energy (**A**), *m/z* = 1712.1 ($[M+Na]^+$), 1689.1 ($[M]^+$) (**B**).

ESI-MS(+) of **2:**

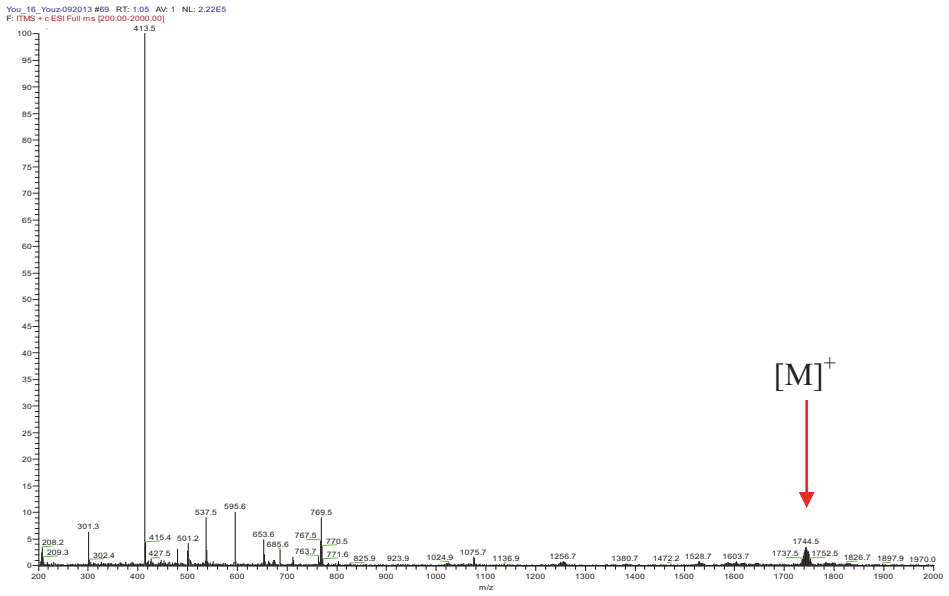

A

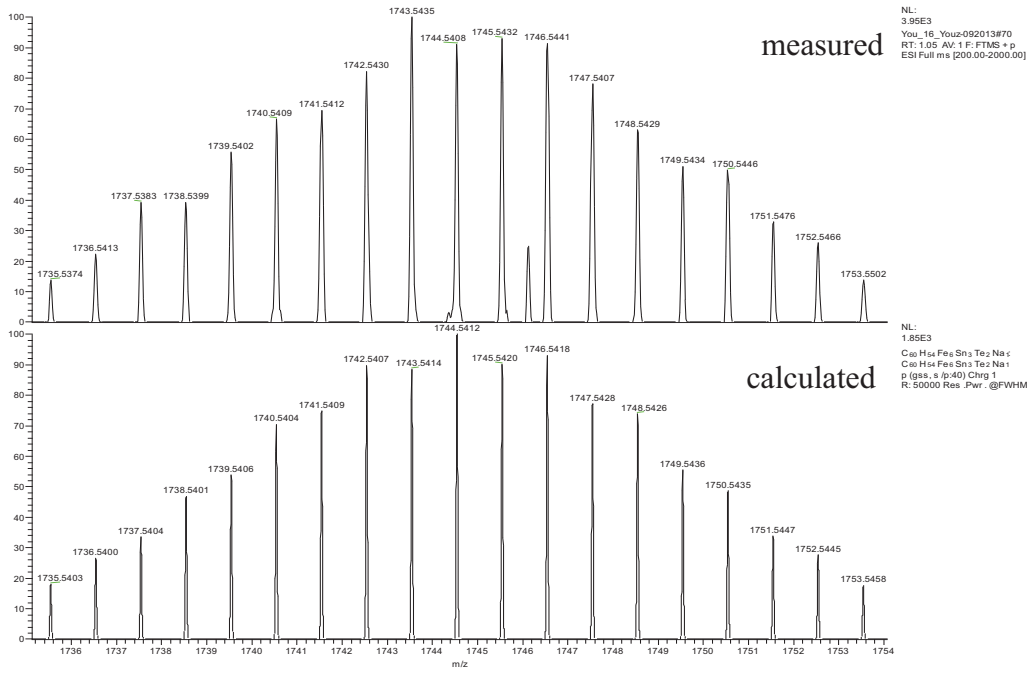

B

Figure S2. ESI(+) mass spectrum of **2**, overview (**A**), *m/z* = 1744.5 ([M]$^+$) (**B**).

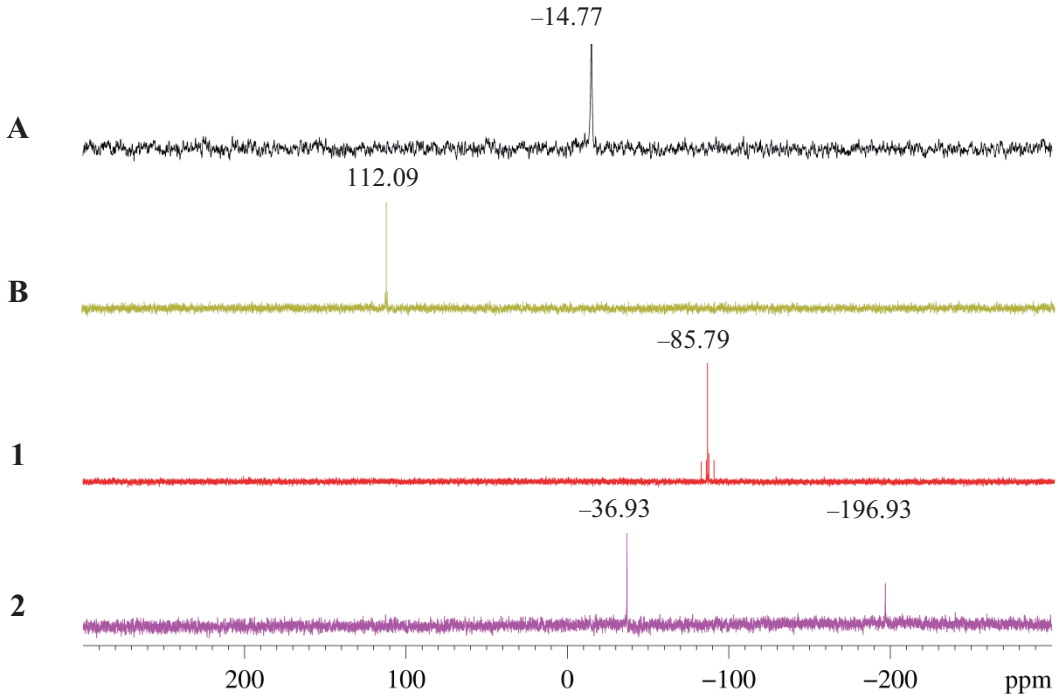

Figure S3 ^{119}Sn-NMR spectra of **A**, **B**, **1**, and **2**.

2. Supplementary UV-Visible Absorption Spectroscopy Data

Figure S4 shows the UV-visible absorption spectra of compounds **B**, **1**, **2**, and $FeCp_2$. Figure S5 shows the UV-visible absorption spectra of compounds **3**, $[Cu(PPh_3)_3Cl]$, and free PPh_3. For better visibility and comparability of the different features, the spectra were adjusted in vertical direction.

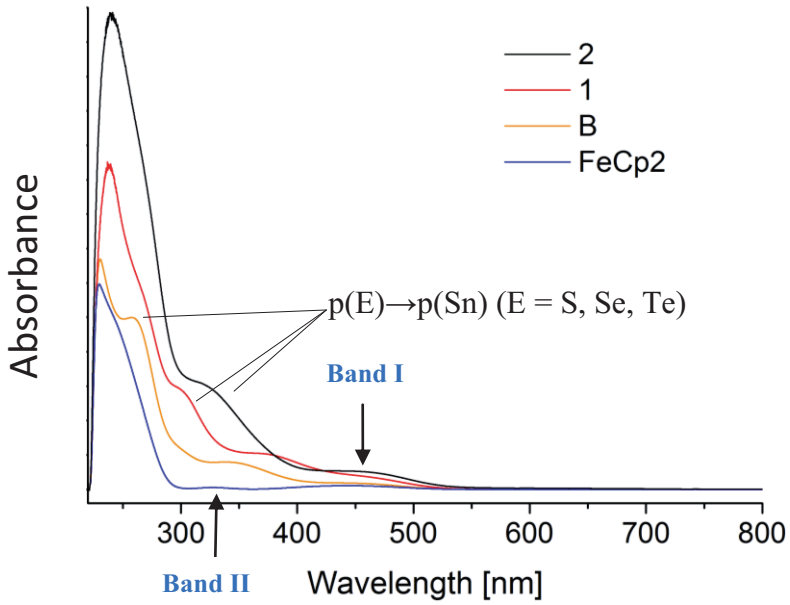

Figure S4. UV-visible absorption spectra of **B** (yellow curve), **1** (red curve), **2** (black curve) and ferrocene ($FeCp_2$, blue curve).

The spectrum of ferrocene (blue curve) displays two significant absorption bands, I around 444 nm, and II around 328 nm, similar to the values recorded in ethanol solution (band I at 400, and II at 325 nm).[1] Besides the two absorption bands, which are slightly (band I) or notably (band II) red shifted, compounds **B** and **1** exhibit an additional absorption (shoulder) at about 262 and 303 nm, respectively, which can be assigned to a p(E)→p(Sn) (E = S, Se) charge transfer of the inorganic E/Sn-core, according to similar reported values.[2-4] In the spectrum of **2**, the p(Te)→p(Sn) charge transfer is reflected by the absorption (shoulder) around 328 nm. As observed, this value is quite similar to the one observed for **2** in spite of the presence of Te atoms instead of Se atoms, since the molecules are smaller. The two typical absorption bands of ferrocenyl groups slide together due to the strong red shift of band II (black curve). Note that the colors of the crystals are much deeper than the solutions, in agreement with reported values for solid state spectra.[2-4]

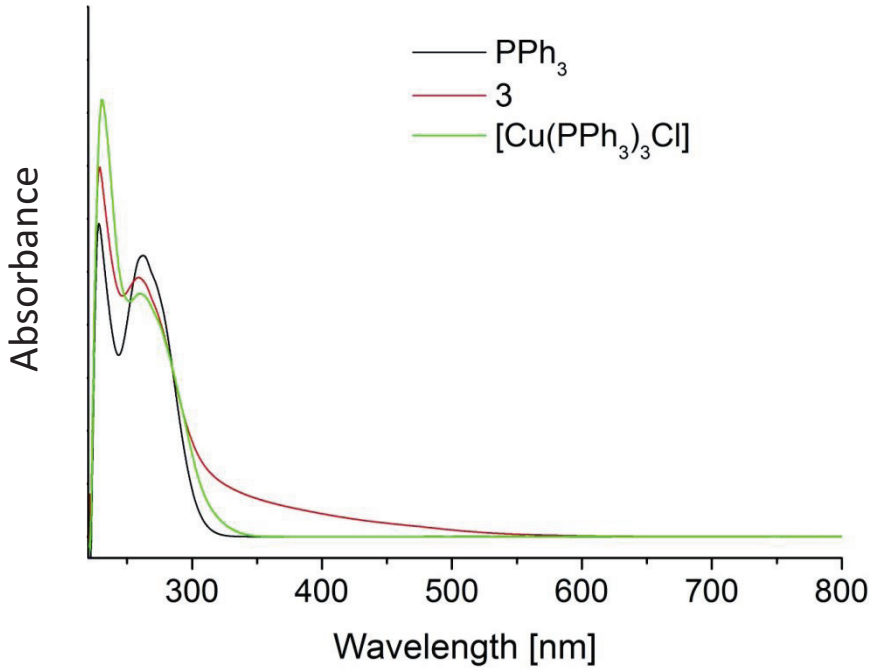

Figure S5. UV-visible absorption spectra of $[Cu(PPh_3)_3Cl]$ (green curve), **3** (red curve), PPh_3 (black curve).

The spectrum observed for compounds **3** similar to those of the reactant $[Cu(PPh_3)_3Cl]$ and the free ligand PPh_3 (Figure S5). All of the three compounds have a strong absorption band around 261 nm, which can be assigned to $\pi \rightarrow \pi^*$ transitions within PPh_3. Yet, the absorption of compound **3** decreases more slowly, producing a tail that ranges from about 300 to 550 nm, which is not visible in the other spectra. This range is in agreement with the absorption bands of ferrocenyl ligands and the p(Se)→p(Sn) charge transfer that was observed in **B**, **1**, and **2**, respectively. The absorption band of the p(S)→p(Sn) charge transfer in **3** was obviously covered by the strong $\pi \rightarrow \pi^*$ absorption.

3. Supplementary Electrochemical Measurement Data

Table S1. Electrochemical characteristics for the redox processes of **B**, **1** and **2** in DCM solution. (Measured at 200 mV/s, *vs*. [$FeCp_2$] in mV)

Complex	E_{pa}	E_{pc}	ΔE_p	$E_{1/2}$
B	450	310	140	380
1	370	260	110	315
2	527	427	100	477

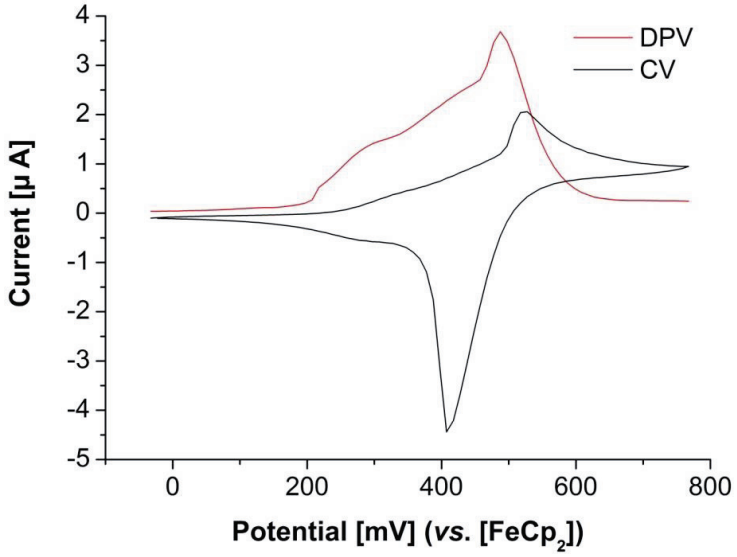

Figure S6. Cyclic and differential pulse voltammograms, recorded at a platinum electrode in a CH_2Cl_2 solution of **2** (1.23 mM) in the presence of TBFP (0.1 M). Scan ranges and rates: CV, –50 to 750 mV, 200 mV/s; DPV, –50 to 750 mV, 10 mV/s. pulse amplitude 50 mV.

As visible in the CV and DPV curves of compounds **B** and **1**, replacement of S with Se decreases the redox potential of neighboring metal atoms, which can be directly derived from the electrochemical experiments, and can be seen indirectly in the Sn-NMR experiments. Moreover, from previous observations made at CV studies of similar compounds and results reported in the literature, we infer that there should additionally be interactions between the E atoms and the metal surfaces, which cause such high and thin cathodic return waves. An effective method to further examine the interactions has been not found until now.

4. Supplementary Energy Dispersive X-ray (EDX) Spectroscopy Data

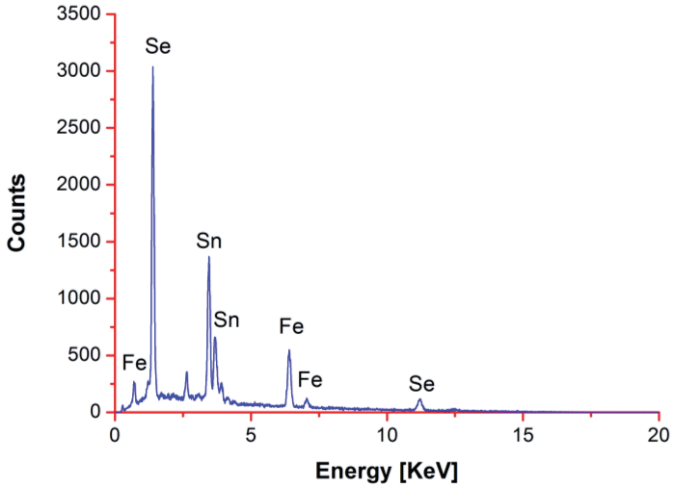

Figure S7. EDX analysis of **1**.

Table S2. EDX analysis of **1**.

Element	k-ratio (calc.)	ZAF	Atom %	Atomic ratio obs. (calc.)	Element Wt %	Wt % Err. (1-Sigma)
Se-L	0.2446	1.677	43.37	6.07 (6)	41.0	+/- 0.3
Sn-L	0.3548	1.123	28.03	3.92 (4)	39.9	+/- 0.6
Fe-K	0.2056	0.931	28.60	4.00 (4)	19.1	+/- 0.5
Total			100	14	100	

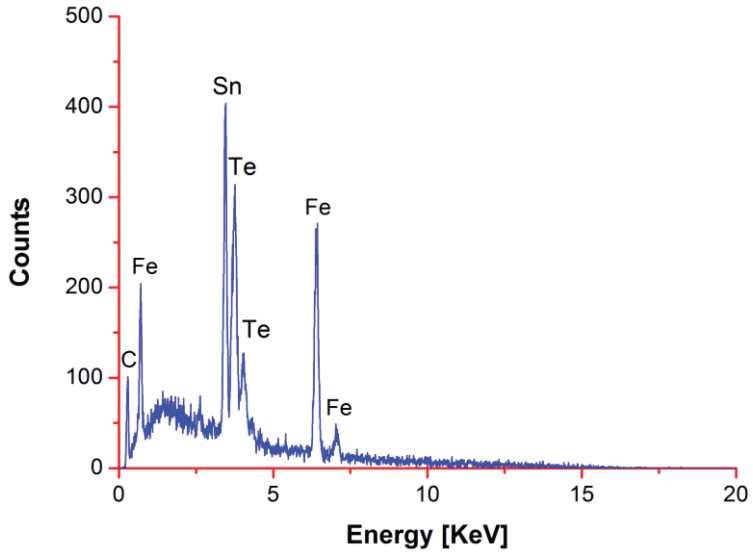

Figure S8. EDX analysis of **2**.

Table S3. EDX analysis of **2**.

Element	k-ratio (calc.)	ZAF	Atom %	Atomic ratio obs. (calc.)	Element Wt %	Wt % Err. (1-Sigma)
Fe-K	0.3747	0.946	54.55	6.00 (6)	35.4	+/- 1.2
Sn-L	0.3644	1.059	27.95	3.07 (3)	38.6	+/- 1.3
Te-L	0.2409	1.078	17.50	1.93 (2)	26.0	+/- 1.6
Total			100	11	100	

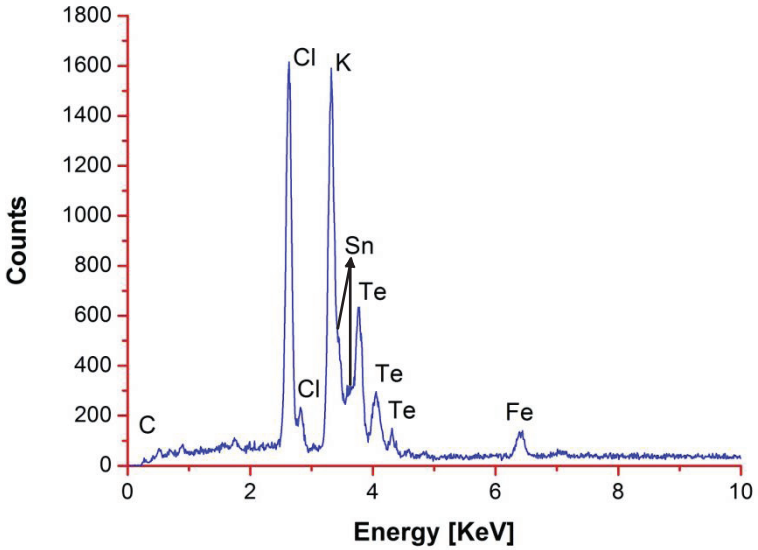

Figure S9. EDX analysis of the black residue of the reaction yielding **2**.

Table S4. EDX analysis of the black residue of the reaction yielding **2**, disregarding the obvious and expected presence of KCl.

Element	k-ratio (calc.)	ZAF	Atom %	Element Wt %	Wt % (1-Sigma) Err.
Te-L	0.5134	1.029	45.3	52.8	+/- 2.8
Sn-L	0.3612	1.009	33.6	36.5	+/- 1.7
Fe-K	0.1160	0.925	21.0	10.7	+/- 0.5
Total			100	100	

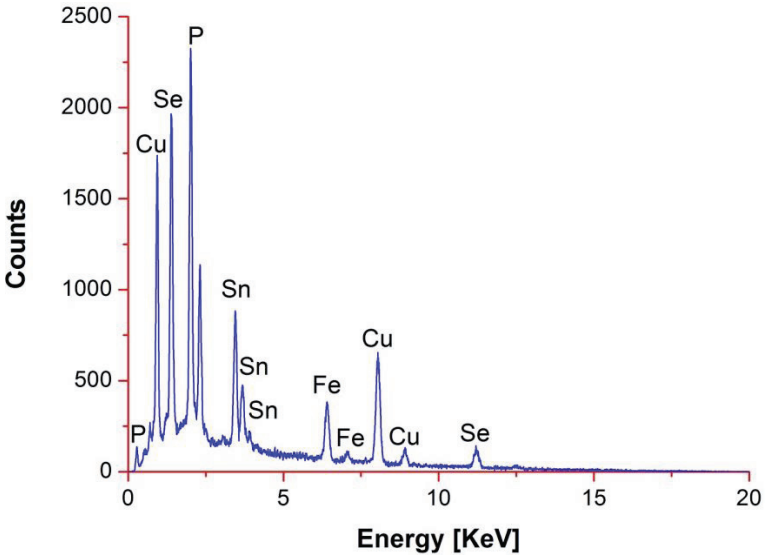

Figure S10. EDX analysis of **3**.

Table S5. EDX analysis of **3**.

Element	k-ratio (calc.)	ZAF	Atom %	Atomic ratio obs. (calc.)	Element Wt %	Wt % Err. (1-Sigma)
Fe-K	0.0557	0.978	5.49	1.23 (2)	5.4	+/- 0.1
S-K	0.0424	1.715	12.78	2.81 (2.75)	7.3	+/- 0.2
Sn-L	0.1200	1.281	7.29	1.60 (2)	15.4	+/- 0.2
P-K	0.0815	1.889	27.97	6.15 (6)	15.4	+/- 0.2
Cu-L	0.1742	2.050	31.62	6.95 (6)	35.7	+/- 0.3
Se-L	0.0843	2.471	14.84	3.26 (3.25)	20.8	+/- 0.2
Total			100	22	100	

5. Supplementary Raman Spectroscopy Data

The infrared (IR) spectra of compounds **1, 2** in the range of 4000-400 cm^{-1} are dominated by vibrational modes of the ferrocenyl (Fc) groups: weak single C–H stretching bands at about 3080 cm^{-1} and strong bands at about 1134, 1104, 999 and 819 cm^{-1}.[1] As an example, we show the Raman spectrum of **2** (Figure S11), exhibiting the Sn–Sn stretching vibration within the five-membered ring.

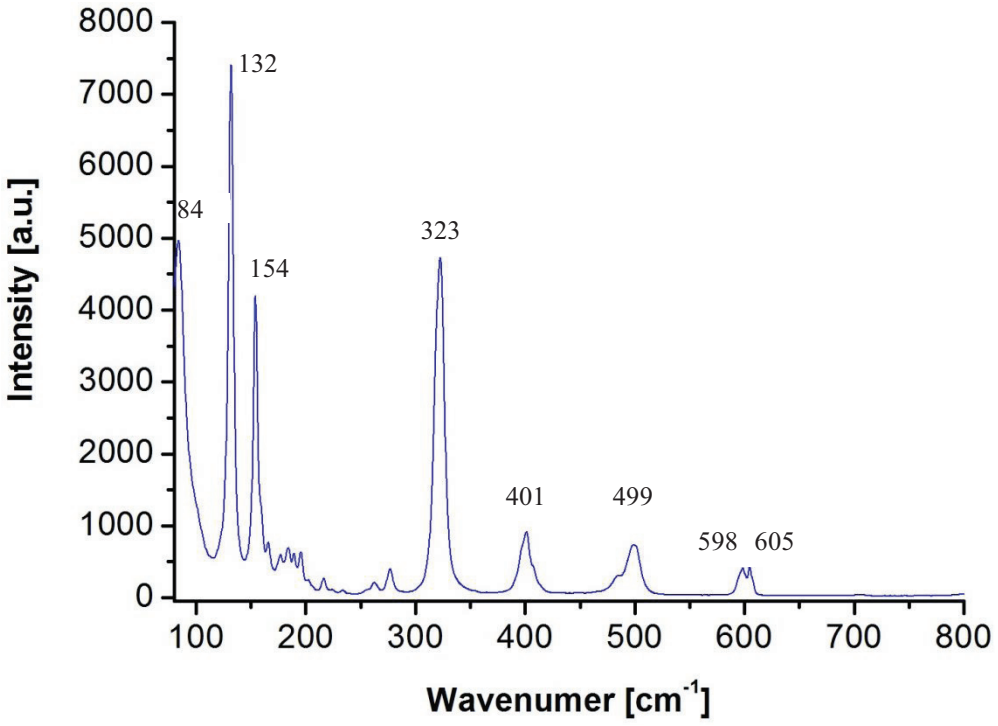

Figure S11. Single-crystal Raman spectrum of **2** in the range of 80-800 cm^{-1}.

The Raman spectrum of **2** exhibits the absorption bands of Fc units at large wave numbers, in agreement with the values reported from the measurement of ferrocene in solid state.[5] At lower wave numbers (80-800 cm^{-1}), one of the two second strongest bands, at 323 cm^{-1}, is assigned to the symmetric $Cp_{\text{-ring}}$-Fe stretching mode of ferrocene, as well.[5] Most of the Raman-active vibrations within the five-membered ring are below 800 cm^{-1}. The Sn–Sn stretching mode, which is IR-inactive but Raman-active, is observed here at 154 cm^{-1}, corresponding to the similar value of 161 cm^{-1} in $Me_8Sn_4Te_2$.[6] The other predominant bands at 132 cm^{-1} and at 84 cm^{-1} are assigned to Sn–Te vibrations.[7,8]

6. Supplementary X-ray Diffraction and Refinement Data

*Compound **1***:

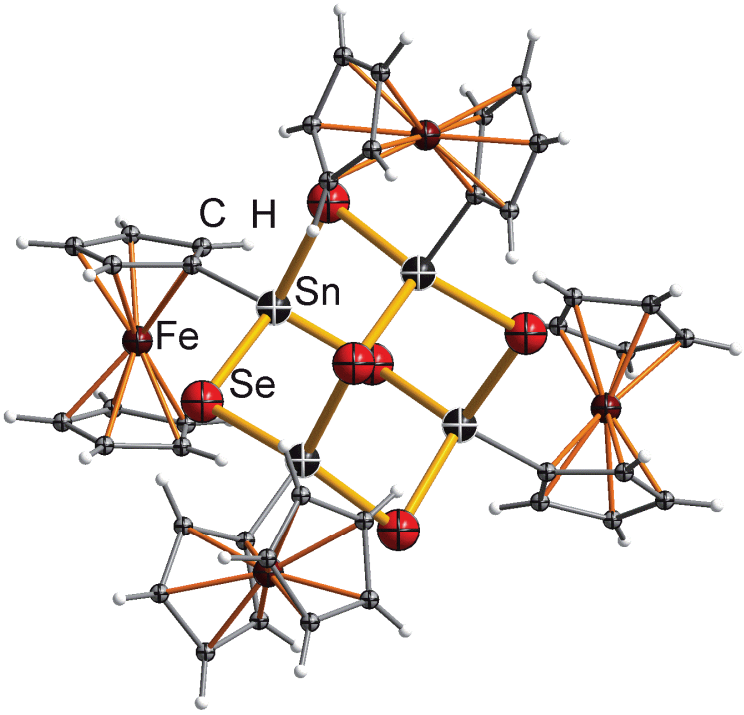

Figure S12. Molecular structure of **1**, viewed along the crystallographic *a* axis.

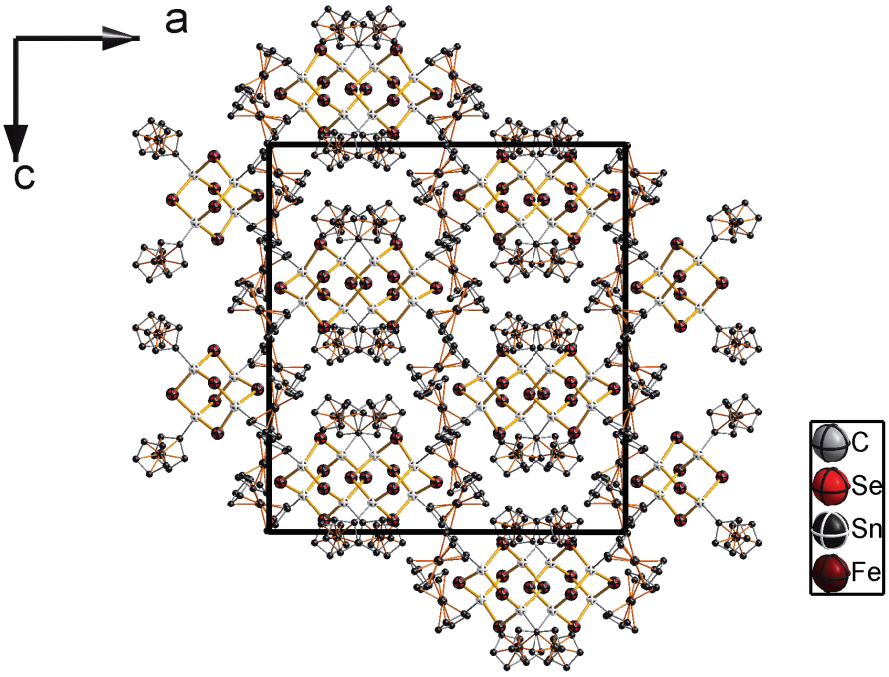

Figure S13. Packing of the molecules of **1** in the crystal, without H atoms, viewed along the crystallographic *b* axis.

*Compound **2***:

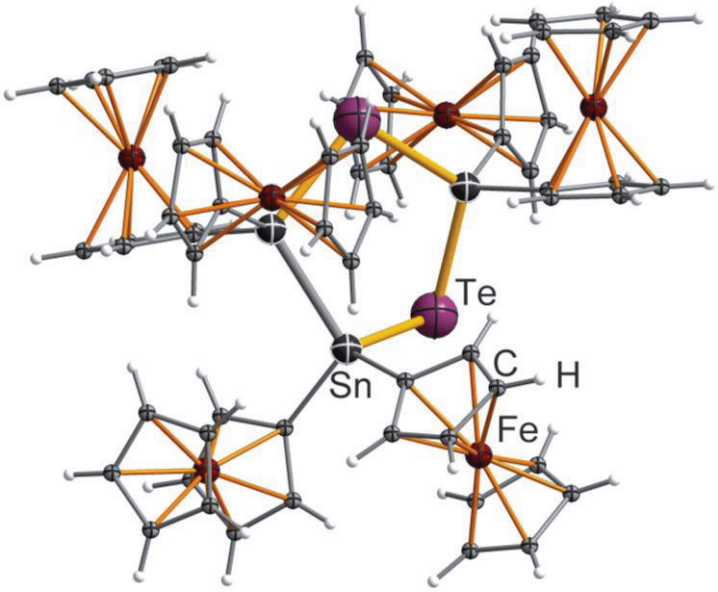

Figure S14. Molecular structure of **2**, viewed along the crystallographic *c* axis.

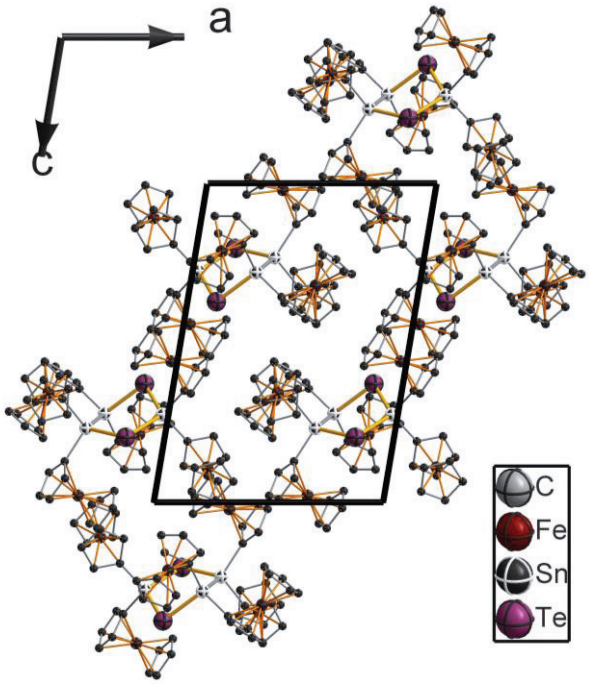

Figure S15. Packing of the molecules of **2** in the crystal, without H atoms, viewed along the crystallographic *b* axis.

Table S6. Selected bond lengths [Å], bond angles [°] in **1**.

Se(1)-Sn(1)	2.5211(7)	Se(6)-Sn(4)	2.5236(7)
Se(1)-Sn(2)	2.5329(7)	Sn(1)-C(1)	2.111(5)
Se(2)-Sn(2)	2.5205(7)	Sn(2)-C(11)	2.109(5)
Se(2)-Sn(3)	2.5393(7)	Sn(3)-C(21)	2.097(5)
Se(3)-Sn(3)	2.5194(7)	Sn(4)-C(31)	2.096(5)
Se(3)-Sn(4)	2.5283(7)	Sn(1)-Se(1)-Sn(2)	101.95(2)
Se(4)-Sn(1)	2.5145(7)	Sn(2)-Se(2)-Sn(3)	101.77(2)
Se(4)-Sn(4)	2.5457(7)	Sn(3)-Se(3)-Sn(4)	102.10(2)
Se(5)-Sn(3)	2.5130(7)	Sn(1)-Se(4)-Sn(4)	101.23(2)
Se(5)-Sn(1)	2.5257(7)	Sn(3)-Se(5)-Sn(1)	102.59(2)
Se(6)-Sn(2)	2.5218(7)	Sn(2)-Se(6)-Sn(4)	103.01(2)

Table S7. Selected bond lengths [Å], bond angles [°] in **2**.

Sn(1)-Sn(2)	2.7952(3)	Sn(2)-C(31)	2.123(4)
Sn(1)-Te(1)	2.7558(3)	Sn(3)-C(41)	2.125(3)
Sn(2)-Te(2)	2.7479(3)	Sn(3)-C(51)	2.124(3)
Sn(3)-Te(2)	2.7266(3)	Te(2)-Sn(2)-Sn(1)	108.572(10)
Sn(3)-Te(1)	2.7302(3)	Te(2)-Sn(3)-Te(1)	113.423(11)
Sn(1)-C(1)	2.112(3)	Sn(3)-Te(1)-Sn(1)	97.060(10)
Sn(1)-C(11)	2.122(3)	Sn(3)-Te(2)-Sn(2)	98.702(10)
Sn(2)-C(21)	2.133(4)		

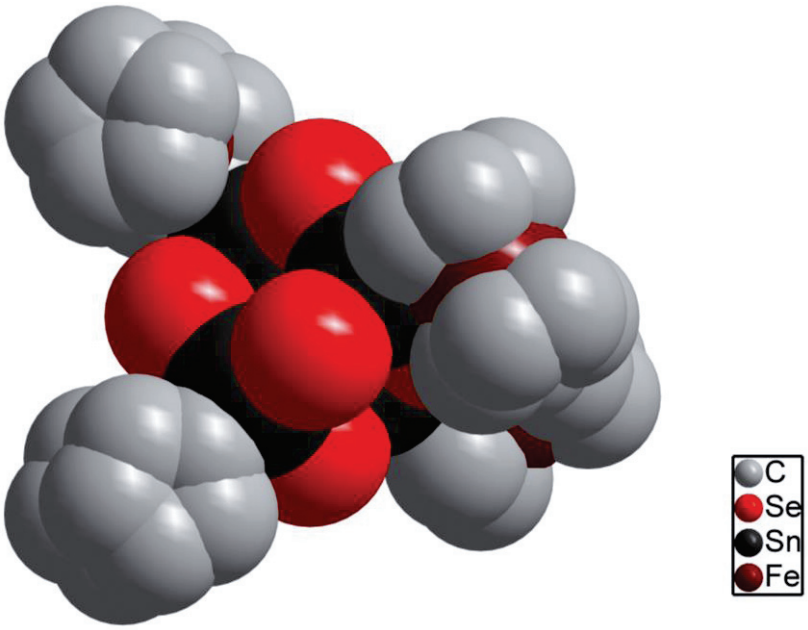

Figure S16. Space-filling model of the molecular structure of **1**, without H atoms, viewed along the crystallographic *b* axis.

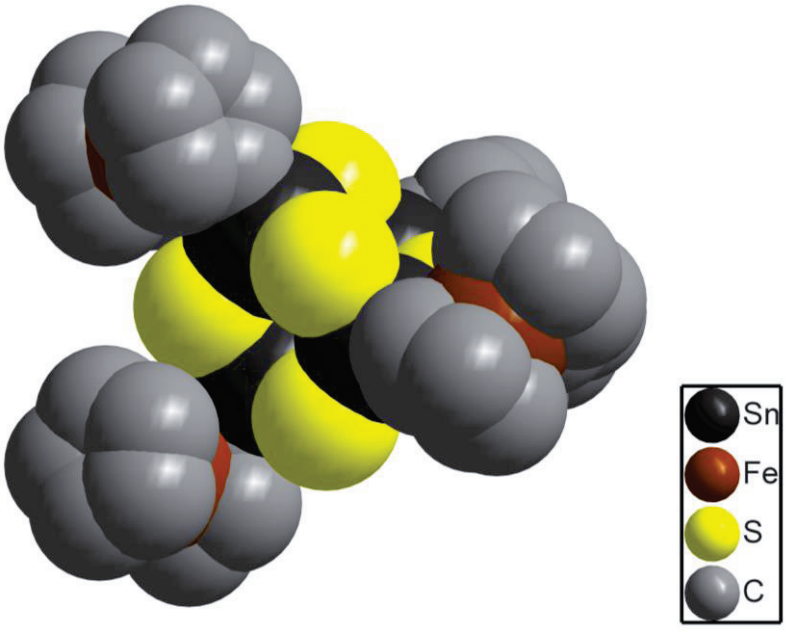

Figure S17. Space-filling model of the molecular structure of the criss-cross type Sn/S complex **B**, without H atoms, viewed along the crystallographic *c* axis.

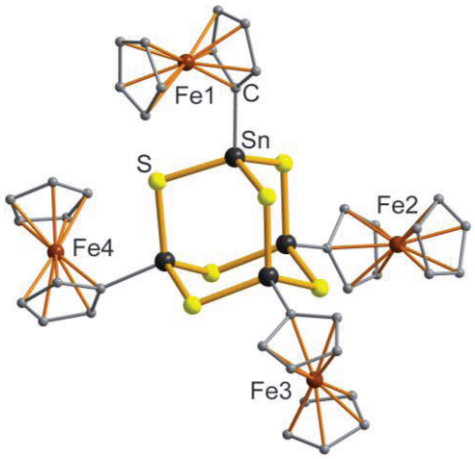

B

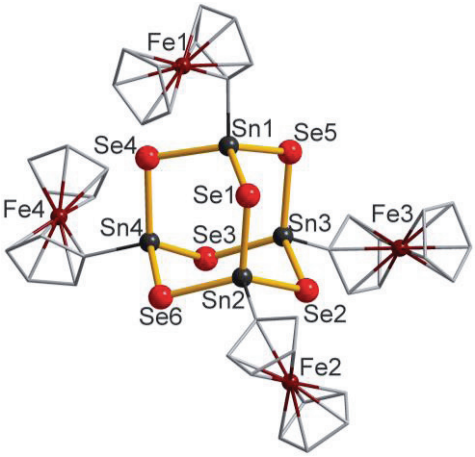

1

Table S8. Fe···Fe distances (Å) in **B**.

Fe1···Fe2	9.98
Fe1···Fe3	9.98
Fe1···Fe4	8.11
Fe2···Fe3	8.11
Fe2···Fe4	9.98
Fe3···Fe4	9.98
Average Fe…Fe distance	9.36

Table S9. Fe···Fe distances (Å) in **1**.

Fe1···Fe2	8.84
Fe1···Fe3	10.27
Fe1···Fe4	8.30
Fe2···Fe3	8.45
Fe2···Fe4	10.59
Fe3···Fe4	9.62
Average Fe…Fe distance	9.35

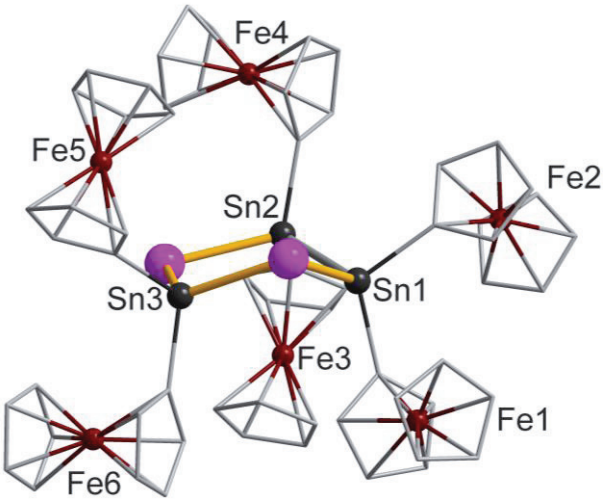

Table S10. Selected Fe···Fe distances (Å) in **2**.

1, iron atoms connected through Sn atom	
Fe1···Fe2	5.5
Fe3···Fe4	6.4
Fe6···Fe5	6.3
2, iron atoms below the Sn/Te ring	
Fe1···Fe3	6.9
Fe1···Fe6	6.3
Fe3···Fe6	7.1
3, iron atoms above the Sn/Te ring	
Fe2···Fe4	6.7
Fe2···Fe5	9.7
Fe4···Fe5	6.8
4, iron atoms on different sides of the Sn/Te ring	
Fe1···Fe4	9.6
Fe1···Fe5	9.1
Fe3···Fe2	6.6
Fe3···Fe5	9.2
Fe6···Fe2	10.5
Fe6···Fe4	9.6

Compound 3

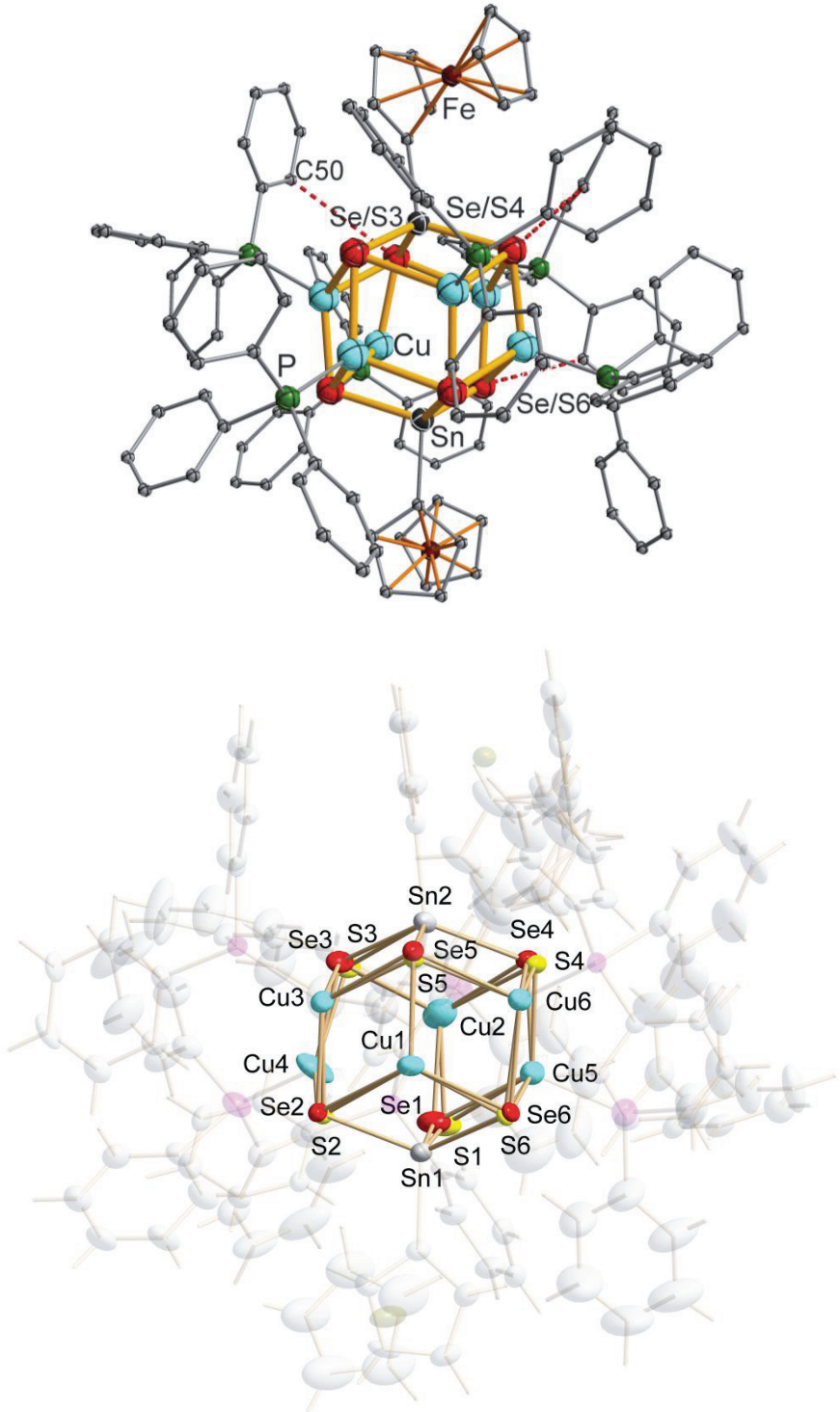

Figure S18. Molecular structure of **3**, viewed along the crystallographic *b* axis with mixed sites (H atoms and solvent molecules are omitted for clarity; red dashed lines indicate the hydrogen bonding of Se/S···H–C; top) and with all atoms (except those of solvent molecules) indicating S/Se atom disorder as well C atom disorder (Fe, P, C, H atoms and according bonds transparent; ellipsoids drawn with 50% probability; bottom).

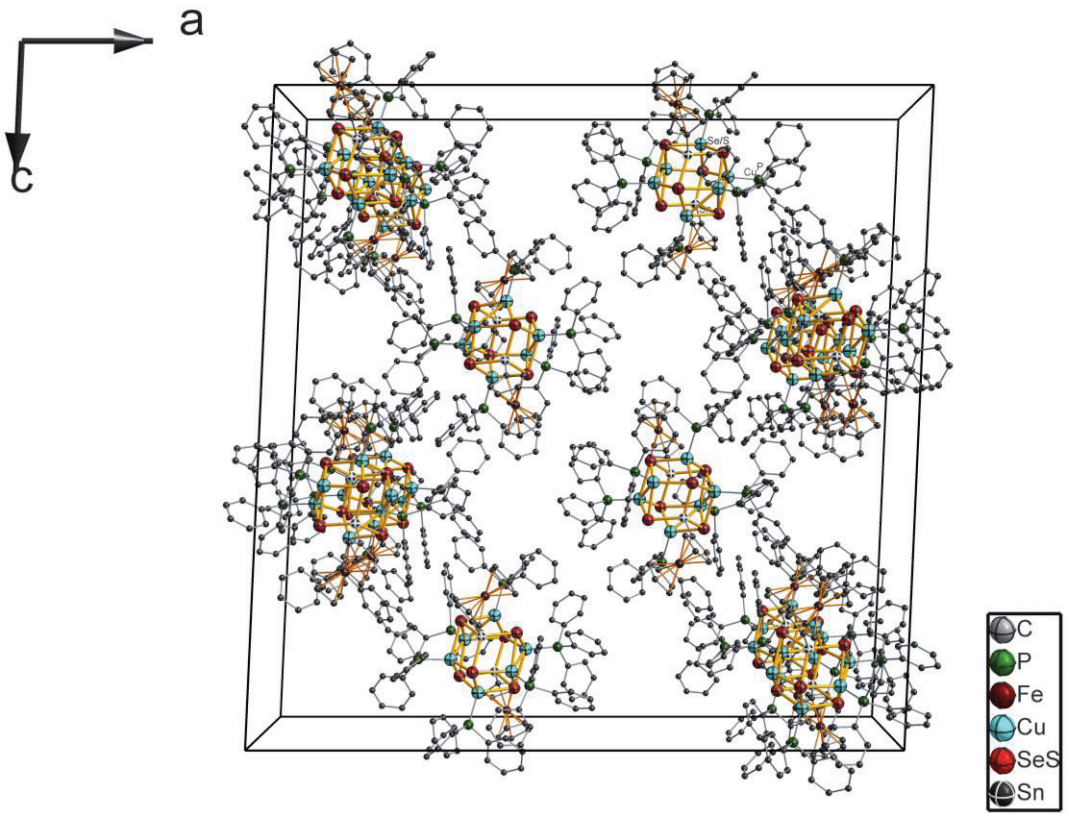

Figure S19. Packing of the molecules of **3** in the crystal, viewed along the crystallographic *b* axis. H atoms and solvent molecules are omitted for clarity.

Table S11. Unit cell and asymmetric unit contents in **3** as resulting from the structure refinement.

	Unit cell	Asymmetric unit
C	1072.00	134.00
H	960.00	120.00
O	52.00	6.50
P	48.00	6.00
S	21.67	2.71
Fe	16.00	2.00
Cu	48.00	6.00
Se	26.33	3.29
Sn	16.00	2.00

Table S12. Selected bond lengths [Å] and angles [°] in **3**, E = Se/S.

Sn(1)-E(1)	2.4788(10)	Cu(4)-E(2)-Cu(1)	114.53(4)
Sn(1)-E(2)	2.4868(10)	Cu(4)-E(3)-Cu(6)	80.26(5)
Sn(1)-E(6)	2.4521(12)	Cu(4)-E(3)-Cu(3)	65.09(4)
Sn(2)-E(3)	2.4683(11)	Cu(6)-E(3)-Cu(3)	110.38(4)
Sn(2)-E(4)	2.4919(10)	Cu(2)-E(4)-Cu(6)	112.27(4)
Sn(2)-E(5)	2.4918(11)	Cu(5)-E(4)-Cu(2)	73.51(4)
Cu(1)-E(5)	2.4307(12)	Cu(5)-E(4)-Cu(6)	65.78(4)
Cu(1)-E(1)	2.5460(12)	Cu(1)-E(5)-Cu(3)	67.42(4)
Cu(1)-E(2)	2.6815(13)	Cu(1)-E(5)-Cu(2)	70.43(4)
Cu(2)-E(1)	2.4277(12)	Cu(3)-E(5)-Cu(2)	112.65(5)
Cu(2)-E(5)	2.5899(12)	Cu(6)-E(6)-Cu(5)	68.53(4)
Cu(2)-E(4)	2.5923(13)	E(1)-Cu(1)-E(2)	103.12(4)
Cu(3)-E(2)	2.3734(11)	E(5)-Cu(1)-E(2)	109.18(4)
Cu(3)-E(5)	2.5098(12)	E(5)-Cu(1)-E(1)	109.33(4)
Cu(3)-E(3)	2.8304(15)	E(1)-Cu(2)-E(5)	108.00(4)
Cu(4)-E(3)	2.3336(13)	E(1)-Cu(2)-E(4)	108.43(4)
Cu(4)-E(2)	2.5105(13)	E(5)-Cu(2)-E(4)	102.04(4)
Cu(5)-E(4)	2.3940(12)	E(2)-Cu(3)-E(5)	117.22(4)
Cu(5)-E(6)	2.6141(15)	E(2)-Cu(3)-E(3)	104.96(4)
Cu(5)-E(1)	2.6954(14)	E(5)-Cu(3)-E(3)	102.22(4)
Cu(6)-E(6)	2.3570(14)	E(3)-Cu(4)-E(2)	117.25(5)
Cu(6)-E(3)	2.5525(15)	E(4)-Cu(5)-E(6)	113.64(5)
Cu(6)-E(4)	2.7463(15)	E(4)-Cu(5)-E(1)	106.17(5)
Cu(1)-E(1)-Cu(5)	113.24(4)	E(6)-Cu(5)-E(1)	99.36(4)
Cu(2)-E(1)-Cu(1)	71.23(4)	E(3)-Cu(6)-E(4)	100.03(5)
Cu(2)-E(1)-Cu(5)	71.14(4)	E(6)-Cu(6)-E(3)	109.76(5)
Cu(3)-E(2)-Cu(4)	70.17(4)	E(6)-Cu(6)-E(4)	110.27(5)
Cu(3)-E(2)-Cu(1)	65.39(3)		

Table S13. Shortest Cu···Cu and Sn···Cu distances [Å] in **3**.

Cu(1)-Cu(3)	2.7426(11)	Sn(1)-Cu(1)	3.0283(10)
Cu(1)-Cu(2)	2.8981(12)	Sn(1)-Cu(5)	3.1239(11)
Cu(2)-Cu(5)	2.9881(13)	Sn(2)-Cu(2)	3.0949(9)
Cu(3)-Cu(4)	2.8093(13)	Sn(2)-Cu(3)	3.0260(10)
Cu(5)-Cu(6)	2.8070(13)	Sn(2)-Cu(6)	3.1225(12)

7. Supplementary NMR Spectroscopy Data

Figure S20 shows the ^{119}Sn NMR spectrum of a fresh mixture of compound **1** with six equivalents of $Na_2S{\cdot}9H_2O$. The signals can be assigned to **1** (–80.9 ppm; mind a slightly different chemical shift with regard to the value given in the Experimental Section of the main manuscript, due to a different solvent used) and to the two newly formed reactants $[FcSnSe_2S]^{3-}$ as well as $[FcSnSeS_2]^{3-}$ (–7.7 and 10.4 ppm, respectively).

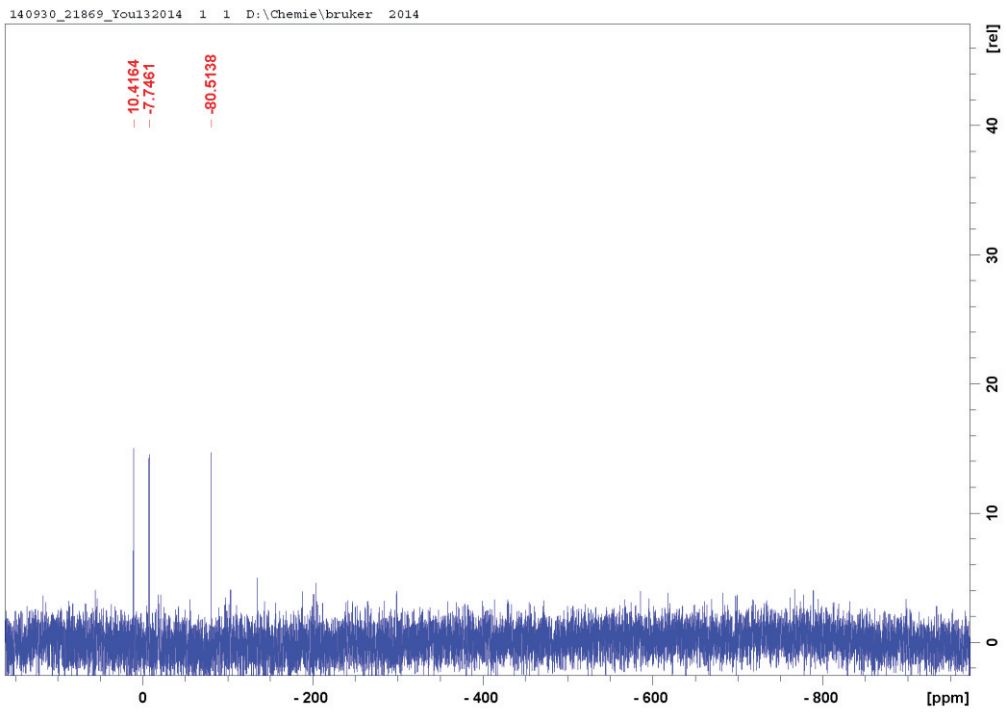

Figure S20. ^{119}Sn NMR spectrum of a fresh reaction solution of compound **1** with six equivalents of $Na_2S{\cdot}9H_2O$, measured under the reported reaction conditions (in a 5:1 THF:D_2O mixture) at room temperature.

8. References for the Supporting Information:

[1] L. Kaplan, W. L. Kester, J. J. Katz, *J. Am. Chem. Soc.* **1952**, *74*, 5531-5532.

[2] Z. You, S. Dehnen, *Inorg. Chem.* **2013**, *52*, 12332-12334.

[3] Z. H. Fard, M. Hołyńska, S. Dehnen, *Inorg. Chem.* **2010**, *49*, 5748-5752.

[4] M. K. Brandmayer, R. Clérac, F. Weigend, S. Dehnen, *Chem. Eur. J.* **2004**, *10*, 5147-5157.

[5] J. Bodenheimer, E. Loewenthal, W. Low, *Chem. Phys. Lett.* **1969**, *3*, 715-716.

[6] B. Mathiasch, *J. Organomet. Chem.* **1980**, *194*, 37-43.

[7] H. Borrmann, J. Campbell, D. A. Dixon, H. P. A. Mercier, A. M. Pirani, G. J. Schrobilgen, *Inorg. Chem.* **1998**, *37*, 6656-6674.

[8] L. J. Brillson, E. Burstein, L. Muldawer, *Phys. Rev. B* **1974**, *9*, 1547-1551.

3.3 Synthesis of organotin-oxido cluster-based multiferrocenyl complexes

The hydrolysis of organotin halides to form tinoxide compounds has been investigated for many years. Clusters with different shapes, including four- and six-membered rings,[32] adamantanes,[33] or mono-, double-, and triple-ladders,[33,34] were reported, and also more complicated compounds with up to twelve tin atoms, such as $[(i\text{PrSn})_9(OH)_6O_8Cl_5]$,[35] $\{[(i\text{PrSn})_{12}(O)_{14}(OH)_6]Cl_2\}$,[36] or $\{[(n\text{BuSn})_{12}(O)_{14}(OH)_6][OH]_2\}$,[37] were obtained by hydrolysis of the monoorganotin compounds. For some of the compounds, the formation mechanisms have been investigated.[38] In contrast, methods starting from the hydrolysis of ferrocenyl-substituted organotin halides have not been reported to date, which is probably due to the difficult synthetic access to ferrocenyl-substituted precursors. In the course of our work on the formation of ferrocenyl-functionalized and -substituted organotin chalcogenide clusters, two ferrocenyl-substituted organotin chlorides $[R^{Fc}SnCl_3\cdot HCl]$ and $FcSnCl_3$, have been synthesized, which are very promising candidates for the formation of tinoxide cluster-based multiferrocenyl compounds.

Thus, the two organotin chlorides were used to form new tinoxide cluster-based multiferrocenyl complexes through hydrolysis reactions. The hydrolysis of $[R^{Fc}SnCl_3\cdot HCl]$ in the presence of NaEPh (E = S, Se) and $[SnCl_6]^{2-}$ led to the formation of screw-shaped multiferrocenyl cations, based on an unprecedented $[Sn_4O_6]$ unit in a one-pot reaction or by stepwise synthesis. A corresponding reaction of $FcSnCl_3$ yielded a multiferrocenyl compound that represents the largest known Fc-decorated Sn/O cluster, containing nine Fc units on its surface.

3.3.1 Organotin-oxido cluster-based multiferrocenyl complexes obtained by hydrolysis of ferrocenyl-functionalized organotin chlorides

Zhiliang You, Robert Möckel, Jakob Bergunde and Stefanie Dehnen*

Fachbereich Chemie and Wissenschaftliches Zentrum für Materialwissenschaften, Philipps-Universität Marburg, Hans-Meerwein-Straße, D-35043 Marburg, Germany

---

Appeared in

Chem. Eur. J. **2014**, *20*, 13491–13496.

Author contributions

Z. You conceived the project and carried out the synthesis and characterization, refined and described the crystal structures, wrote the manuscript. R. Möckel and J. Bergunde participated in the syntheses. M. Hołyńska helped to refine the crystal structure of **1**. S. Dehnen supervised the work and corrected the manuscript.

Abstract

Three organotin-oxido clusters were formed by hydrolysis of ferrocenyl-functionalized organotin chloride precursors in the presence of NaEPh (E = S, Se). [$R^{Fc}SnCl_3$·HCl] (**C**; R^{Fc} = $CMe_2CH_2C(Me)$=N–N=C(Me)Fc) and $[SnCl_6]^{2-}$ formed {($R^{Fc}SnCl_2$)$_3$[$Sn(OH)_6$]}[$SnCl_3$] (**3a**) and {($R^{Fc}SnCl_2$)$_3$[$Sn(OH)_6$]}[$PhSeO_3$] (**3b**), bearing an unprecedented [Sn_4O_6] unit, in a one-pot synthesis or stepwise through [($R^{Fc}SnCl_2$)$_2$Se] (**1**) plus [($R^{Fc}SnCl_2$)SePh] (**2**). A one-pot reaction starting out from $FcSnCl_3$ gave [$(FcSn)_9(OH)_6O_8Cl_5$] (**4**), which represents the largest Fc-decorated Sn/O cluster reported to date.

ChemPubSoc Europe

DOI: 10.1002/chem.201403657

CHEMISTRY
A European Journal
Communication

Tin Chemistry

Organotin–Oxido Cluster-Based Multiferrocenyl Complexes Obtained by Hydrolysis of Ferrocenyl-Functionalized Organotin Chlorides

Zhiliang You, Robert Möckel, Jakob Bergunde, and Stefanie Dehnen*[a]

Abstract: Three organotin–oxido clusters were formed by hydrolysis of ferrocenyl-functionalized organotin chloride precursors in the presence of NaEPh (E = S, Se). [$R^{Fc}SnCl_3$·HCl] (**C**; R^{Fc} = $CMe_2CH_2C(Me)$=N–N=C(Me)Fc) and $[SnCl_6]^{2-}$ formed $\{(R^{Fc}SnCl_2)_3[Sn(OH)_6]\}[SnCl_3]$ (**3a**) and $\{(R^{Fc}SnCl_2)_3[Sn(OH)_6]\}[PhSeO_3]$ (**3b**), bearing an unprecedented $[Sn_4O_6]$ unit, in a one-pot synthesis or stepwise through $[(R^{Fc}SnCl_2)_2Se]$ (**1**) plus $[(R^{Fc}SnCl_2)SePh]$ (**2**). A one-pot reaction starting out from $FcSnCl_3$ gave $[(FcSn)_9(OH)_6O_8Cl_5]$ (**4**), which represents the largest Fc-decorated Sn/O cluster reported to date.

Multiferrocene compounds have been attracting much attention in recent years due to their extraordinary electrochemical properties, which point to potential applications as sensors, optoelectronic materials, or thermotropic liquid crystals.[1] Hence, many different kinds of multiferrocene compounds have been synthesized. These range from fullerenes[2] through polyoxometalates[3] to metal chalcogenide nanoclusters with ferrocenyl decoration,[4] which were obtained by different methods. Of these compounds, tin-oxido cluster-based multiferrocene compounds with (poly)cyclic arrangements of up to six ferrocene units, such as in $[\{fC(COO)_2\}_6Sn_8O_4]$[5] or $[\{BuSn(O)OC(O)Fc\}_6]$,[6] have most commonly been synthesized by the treatment of mono- or bisfunctionalized ferrocenyl carboxylic acids with the corresponding organotin oxide, hydroxide, or chloride.[5–7] Recently, Jurkschat and co-workers have reported a ferrocenyl bridged, mixed Sn/(O,S) ladder-like complex, which was obtained by hydrolysis of a ferrocenyl-functionalized stannylene in the presence of sulfur.[8]

The hydrolysis of organotin halides to form tin oxido compounds without ferrocenyl units has been investigated for many years. Clusters with different shapes, including four- and six-membered rings,[9] adamantanes,[10] or mono-, double-, and triple-ladders,[10,11] were reported, and also more complicated compounds with up to twelve tin atoms, such as in $[(iPrSn)_9(OH)_6O_8Cl_5]$,[12] $\{[(iPrSn)_{12}(O)_{14}(OH)_6]Cl_2\}$,[13] or $\{[(nBuSn)_{12}(O)_{14}(OH)_6][OH]_2\}$,[14] were obtained by hydrolysis of the monoorganotin compounds. For some of the compounds, the formation mechanisms have been investigated.[15]

In contrast, methods starting from the hydrolysis of ferrocenyl substituted organotin halides have not been reported to date, and will thus be presented herein as a rational approach towards tin oxido cluster-based multiferrocenyl compounds.

In the course of our recent work on the formation and derivatization of organofunctionalized Group 14 chalcogenide clusters of the general type $[(R^fT)_xS_y]$, (T = Ge or Sn; R^f = functional organic ligand, such as $R^1 = C_2H_4COOH$, $R^2 = CMe_2CH_2CMeO$, $R^3 = CMe_2CH_2CMeNNH_2$),[16,17] we prepared with the ferrocenyl (Fc)-substituted cluster $[(FcSn)_4S_6]$ by reaction of $FcSnCl_3$ with Na_2S,[18] and upon the treatment of $[(R^fSn)_4S_6]$ ($R_f = R^2$ or R^3) with monosubstituted (Fc) or disubstituted (fC) ferrocenyl moieties. These reactions gave $[(R^{Fc}Sn)_4Sn_2S_{10}]$ (**A**; R^{Fc} = $CMe_2CH_2C(Me)$=N–N=C(Me)Fc) with four terminal Fc units, or $[R^{fC}{}_2Sn_4S_6]$ with two bridging R^{fC} units ($R^{fC1} = \{CMe_2CH_2C(Me) = N–N=C(Me)\}_2fC$ or $R^{fC2} = \{CMe_2CH_2C(Me)=N–NH–C(O)\}_2fC$).[19]

The cluster **A** could be degraded with different amounts of concentrated hydrochloric acid under release of H_2S. By using eight equivalents of HCl, the sulfide-bridged, dinuclear thiostannate complex $[(R^{Fc}SnCl_2)_2S]$ (**B**) and SnS_2 were obtained, whereas a large excess of HCl gave the organotin chloride complex $[R^{Fc}SnCl_3·HCl]$ (**C**) besides hexachloridotin acid [Eq. (1)].[20]

$$[(R^{Fc}Sn)_4Sn_2S_{10}] \rightarrow 4\,[R^{Fc}SnCl_3 \cdot HCl]\,(\mathbf{C}) + 2H_2[SnCl_6] \cdot 6H_2O \quad (1)$$

The product mixture of the latter treatment can be isolated as a dark purple red powder, a solution of which in $[D_6]$DMSO contains about two equivalents of **C** per equivalent of $[SnCl_6]^{2-}$ and minor amounts of acetyl ferrocene, according to ^{119}Sn and ^1H NMR spectra. We have now been able to optimize this reaction by using an HCl ether solution or HCl gas, such that the acetyl ferrocene impurity was removed from the powder (see the Supporting Information).

As outlined in Scheme 1, the treatment of this powder with NaSePh in THF, subsequent evaporation, redissolving in $CHCl_3$, and layering by *n*-pentane for crystallization, gave a mixture of the selenide-bridged, dinuclear complex $[(R^{Fc}SnCl_2)_2Se]$ (**1**) and the phenyl selenide-substituted, mononuclear complex $[(R^{Fc}SnCl_2)SePh]$ (**2**). Upon contact with moisture during storage

[a] Z. You, R. Möckel, J. Bergunde, Prof. Dr. S. Dehnen
Fachbereich Chemie and
Wissenschaftliches Zentrum für Materialwissenschaften (WZMW)
Philipps-Universität Marburg, Hans-Meerwein-Strasse, 35043 (Germany)
Fax: (+49) 6421-282-5653
E-mail: dehnen@chemie.uni-marburg.de

Supporting information for this article is available on the WWW under http://dx.doi.org/10.1002/chem.201403657.

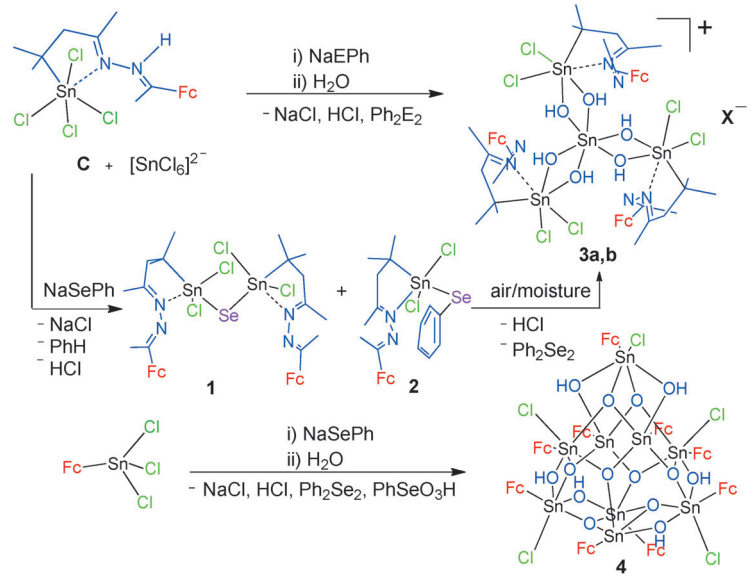

Scheme 1. Synthesis of **3a** and **b** by one-pot reaction (top) or stepwise via **1** and **2** (center), and formation of **4** in a one-pot reaction starting out from $FcSnCl_3$ (bottom). Fc = ferrocenyl; E = S, Se; $X^- = [SnCl_3]^-$ in **3a**, $[PhSeO_3]^-$ for **3b**. The complex molecular structures are shown in Figures 1, 2, and 4, respectively. Indicated by-products were confirmed by standard analytical techniques.

in a freezer, the crystals of **1** and **2** decomposed after two weeks, whereas crystals of the ionic compound $\{(R^{Fc}SnCl_2)_3[Sn(OH)_6]\}[Sn^{II}Cl_3]$ (**3a**) were formed; the counterion seems to evolve from a redox reaction under formation of Ph_2Se_2. By intentional addition of water to the reaction mixture in THF and stirring under air prior to work-up, a related compound $\{(R^{Fc}SnCl_2)_3[Sn(OH)_6]\}[O_3SePh]$ (**3b**) was obtained. This compound **3b** possesses the same cation as **3a**, but a different counterion, $[PhSeO_3]^-$, as an oxidation product of NaSePh. This oxidation did not occur with NaSPh, the corresponding reaction of which gave **3a** again, along with Ph_2S_2.

A more complex tin oxido cluster surrounded by nine Fc units, $[(FcSn)_9(OH)_6O_8Cl_5]$ (**4**), was synthesized by starting out from the precursor $FcSnCl_3$ in a similar one-pot reaction with NaSePh and water. Compounds **1**–**4** were characterized by standard analytic techniques and single-crystal X-ray diffraction analysis (see the Supporting Information).

For the formation of compound **1**, which crystallized as yellow plate-like crystals in the monoclinic space group $P2_1$, NaSePh has served as a selenide source, as known from other reactions.[21] Thus, in the structure, a molecule of benzene is in close proximity to the expected by-product NaCl. The complex is isostructural with the aforementioned sulfide complex **B**; thus, its structure (Figure 1, left) will not be discussed here in detail. Compound **2** crystallized as yellow needles in the triclinic space group $P\bar{1}$, with two molecules in the unit cell. Herein, the expected replacement of Cl^- with $PhSe^-$ took place under release of NaCl and HCl. However, the reaction remained incomplete in that two of the Cl atoms were retained. Together with the organometallic decoration derived from **C**, the Sn atom in **2** possesses nearly trigonal-bipyramidal coordination (Figure 1, right). The observed orientation of the phenyl ring resulted from intramolecular hydrogen bonding Ph(H)···N (3.107 Å), indicated as a gray-blue dashed line in Figure 1.

The ionic compounds **3a** and **b** crystallized in the orthorhombic space group *Pbca*. Both possess the same cation but different counterions, which was additionally confirmed by energy-dispersive X-ray (EDX) spectroscopy (Figures S6 and S7 in the Supporting Information). The anion $[PhSeO_3]^-$ in **3b** was identified by negative-ion electrospray ionization (ESI^-) mass spectrometry at *m/z*: 204.94 (Figure S3 in the Supporting Information). The according ESI^+ mass spectrum exhibited a peak at *m/z* 1758.80, consistent with the molecular weight of the cation $[\{(R^{Fc}SnCl_2)_3Sn(OH)_6\}]^+$. The hydroxyl groups, H atoms of which could not be detected by single-crystal X-ray structure analysis, were confirmed by IR spectroscopy, revealing a broad OH stretching and a sharp OH bending mode at 3632 and 882 cm^{-1}, respectively (see the Supporting Information). All O^{2-} ligands act as μ^3 bridges, whereas all OH^- ligands are μ bridges in the title compounds, in agreement with the overall charge of the anions. The persistence of

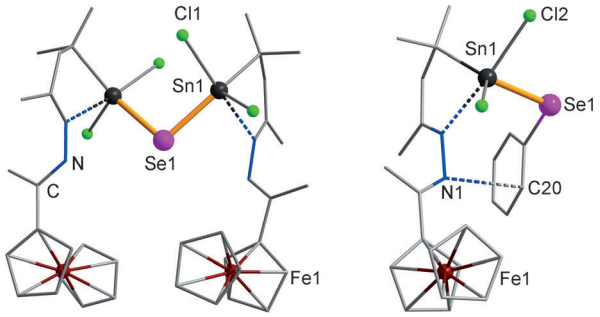

Figure 1. Molecular structures of **1** (one of two independent molecules, left) and **2** (right). Intramolecular hydrogen bonding Ph(H)···N in **2** is indicated by a gray-blue dashed line. The intramolecular N→Sn coordination is given by blue-black dashed lines. Solvent and H atoms are omitted for clarity.

the complexes in solution was confirmed by ^{119}Sn NMR spectroscopy ($\delta = -407.6$ and -210.2 ppm for Sn1 and Sn(2–4), respectively).

In both compounds, cations and anions are closely connected as ion pairs with a common *pseudo*-C_3 axis that runs through Sn5 and Sn1 in **3a** and Se1 and Sn1 in **3b**, respectively (Figure 2, left). The structures of the complex cations in **3a** and **b** (Figure 2, right) are very similar, based on an $[Sn_4O_6]$ architecture. The cations are constructed by a central, spiro-type $[Sn(\mu\text{-}OH)_6Sn_3]$, which is surrounded by three ferrocenyl-terminated ligands. This assembly has been unprecedented in tin chemistry, but it is similar to a subunit in the larger cluster $[\{N(H)(2,6\text{-}i\text{Pr-}C_6H_3)\}_3Sn_{10}O_7Cl_6]$,[22] which was not reproduced to date after its nonrecurring synthesis by hydrolysis in a freezer. The subunit in **3** might have been formed by attachment of three cationic fragments $(R^{Fc}SnCl_2)^+$, which remained upon re-

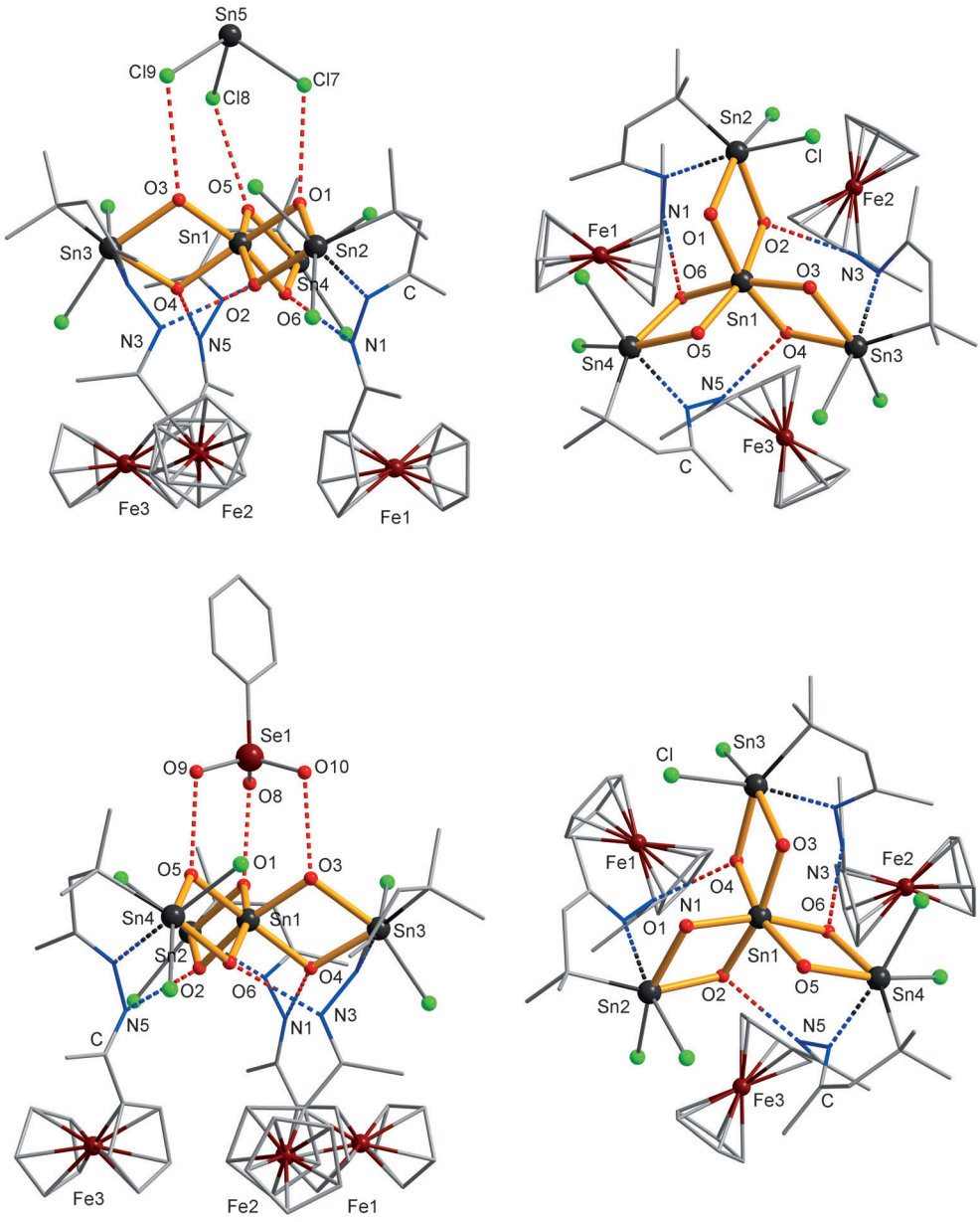

Figure 2. Molecular structures (without hydrogen atoms) of **3a** and **b** viewed perpendicular to the pseudo-C_3 axis (including the anion; left), and along the pseudo-C_3 axis (without the anion; right); only one of the two co-existing enantiomers in both compounds is shown. O(H)···Cl (**3a**) and O(H)···O (**3b**) hydrogen bonds between cation and anion are indicated by red dashed lines (O···Cl 3.117, 3.185, 3.209 Å for **3a**; O···O 2.632, 2.647, 2.695 Å for **3b**); intramolecular hydrogen bonds O(H)···N in the cations are indicated by red-blue dashed lines (O···N 2.701, 2.707, 2.759 Å for **3a** and 2.696, 2.721, 2.749 Å for **3b**). Blue-black dashed lines denote intramolecular N→Sn coordination.

lease of HCl and another Cl^- ligand from **C**, to the central, anionic unit $[Sn(OH)_6]^{2-}$ that were obtained from a reaction of $[SnCl_6]^{2-}$ with water under release of HCl. HCl and Cl^- were trapped by NaEPh, acting as a weak base, as was observed in other basic hydrolysis reactions of monoalkyltin trichlorides.[9,10,12,13] Two screw-shaped cations were formed in both compounds that co-exist in the crystal structures. The enantiomers differ in their helicity; Figure 2 shows the *P*-type for **3a** and the *M*-type for **3b**.

The Sn–O distances within the $[Sn_4(OH)_6]$ unit are very similar in **3a** and **b**. In both clusters, Sn1–O distances (2.032(5)–63(5) Å) are significantly shorter than the organoelement Sn–O bonds (Sn(2–4) –O: 2.072(6)–29(6) Å). The Sn–Cl distances in the cations do not differ notably from those in **C** (2.382(3)–04(3) Å). They vary between 2.391(2) and 2.418(2) Å for **3a** and between 2.395(2) and 2.425(2) Å for **3b**. All Fc units in the cations are placed on the same side of the oblate $[Sn_4(OH)_6]$ unit. The ligands are connected through Schiff-base ligands, in which one of the N atoms of the hydrazone groups maintained the N→Sn coordination that was present in **C**, **1**, and **2**. The second N atom within these groups (N1, N3, or N5, respectively) is involved in additional intramolecular hydrogen bonding with an adjacent OH group each (O2, O4, or O6, respectively), located on the same side of the $[Sn_4(OH)_6]$ "disk". On the other side of the $[Sn_4(OH)_6]$ unit, the anions are connected through O(H)···Cl (**3a**) or O(H)···O (**3b**) hydrogen bonds, respectively, with the three remaining OH groups (O1, O3, O5).

The electronic behavior of **3** has been studied on a CH_2Cl_2 solution of **3a** in the presence of $(nBu_4N)[PF_6]$ (TBFP; 0.1 M) by using cyclic voltammetry (CV; scan rate: 200 mV s^{-1}) at 25 °C. As shown in Figure 4, compound **3a** undergoes a single-step oxidation (**3a**/**3a**$^{3+}$) at E_{pa} = 465 mV with facile electronic communication among the three Fc units. In comparison with our previous investigations on Fc-substituted tin sulfide complexes,[19,20] we can state that the Fc units interact: relatively small Fe···Fe distances (Fe1···Fe2 7.373 Å; Fe1···Fe3 7.279 Å and Fe2···Fe3 7.251 Å) allow sufficient approach of the Fc units in solution. A shoulder at about 341 mV indeed indicates some dynamic of the Fc units. In spite of the big separation of the peak potential (ΔE_p), that is, ΔE_p = 199 mV at 200 mV s^{-1}, the redox process is quasi-reversible, confirmed by analysis of the diagnostic criteria of CV data (see Figure 3 and Table S1 in the Supporting Information).

It was shown in the past that hydrolysis reactions of monoorganotin compounds are influenced by the nature and size of

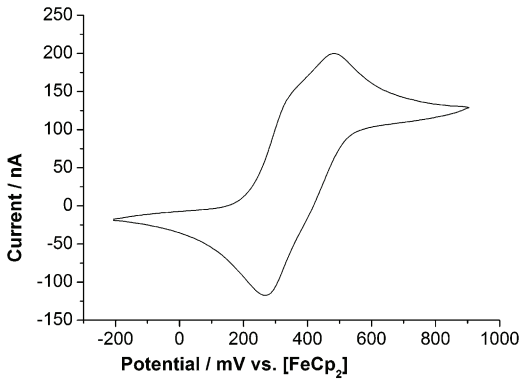

Figure 3. Cyclic voltammogram, recorded at a platinum electrode on a CH_2Cl_2 solution of **3a**, in the presence of tetra-*n*-butylammonium hexafluorophosphate (TBFP; 0.1 M). Scan ranges and rates: CV −200 to +900 mV, 200 mV s^{-1}.

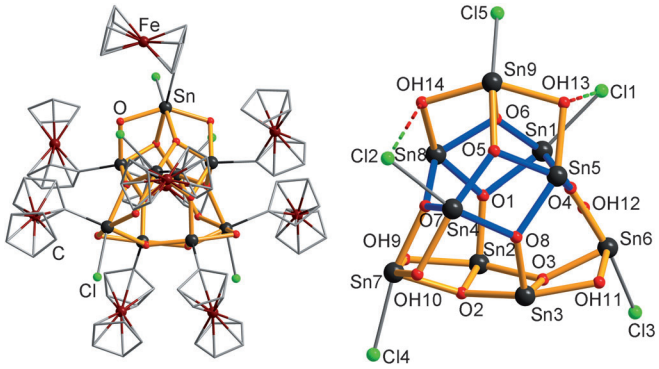

Figure 4. Molecular structure of **4** without H atoms (left) and without Fc units (right). Intramolecular hydrogen bonds O(H)···Cl are indicated by red-green dashed lines (O13···Cl1 3.096 Å; O14···Cl4 3.152 Å).

the organic groups linked to tin atom. Generally, larger tin oxido cages were formed in the presence of less bulky organic groups. For example, with isopropyl substituents, $[(i\text{Pr-Sn})_9(OH)_6O_8Cl_5]$ was formed, which exhibits a pyramidal cage structure. The nine tin atoms possess trigonal-bipyramidal or octahedral coordination, and they are linked by μ^3-O atoms or μ-OH groups.[12] In contrast, sterically more demanding organic ligands inhibited the aggregation of tin oxido units to form large clusters during the hydrolysis. For example, precursors with $(Me_3Si)_3C$-decorated tin atoms led to the formation of cyclic tin oxido trimers only.[9a] The examples of **3a** and **b** given above are consistent with this finding: due to the N→Sn coordination, the organometallic R^{Fc} group possesses a big spatial requirement, which might even hamper the formation of the common Sn_2O_2 four-membered ring; thus, in these cases, the presence of the inorganic hexachloridostannate complex was necessary to trigger the assembly of the $[Sn_4O_6]$ unit with three of these four rings.

The precursor $FcSnCl_3$ has a smaller steric demand, because its coordination to the Sn atom is restricted to the Sn–C bond. Hydrolysis of this species in the presence of NaSePh thus gave the more complex, larger cluster $[(FcSn)_9(OH)_6O_8Cl_5]$ (**4**). The molecular structure of **4**, which crystallized in the monoclinic space group *P*21/*c* with four molecules in the unit cell, is shown in Figure 4. The cluster core consists of nine ferrocenyl-substituted Sn atoms, which are linked by eight μ^3-O atoms and six μ-OH groups in a near-pyramidal shape. Compound **4** is based on the same $[Sn_9O_{14}]$ topology as the quoted compound $[(i\text{PrSn})_9(OH)_6O_8Cl_5]$,[12] with a double-decker-type $[Sn_4O_6]$ unit (highlighted by blue bonds in Figure 4, right), that is side-capped by a mononuclear complex $[RSnCl(OH)_2]$ and a ladder-type complex $[(RSn)_4Cl_2(OH)_4O_2]$, respectively; however, in **4** the organic ligands R are not *i*Pr but Fc groups, thus representing the largest Fc-functionalized Sn/O cluster reported to date that exceeds the number of both tin atoms and ferrocenyl units in comparison with $[\{Fc(COO)_2\}_6Sn_8O_4]$.[5]

The nine ferrocenyl substituted Sn atoms possess three different coordination modes (Table S12 in the Supporting Information): the four Sn atoms (Sn2, Sn3, Sn5, Sn8) that contain no Cl^- ligands show trigonal-bipyramidal coordination by three μ^3-O atoms and one μ-OH group (Sn^O type). The other Sn atoms are octahedrally surrounded. All of them bind to one Cl atom, but they differ in the number of coordinating μ^3-O atoms or μ-OH groups, respectively. Although Sn1 and Sn4 are surrounded by three μ^3-O and one μ-OH ligand (Sn_1^{Cl} type), one of the μ^3-O atoms is replaced by a second μ-OH group in Sn6, Sn7, and Sn9 (Sn_2^{Cl} type).

Overall, the Sn–O/OH distances in the cluster in **4** vary from 1.979(6) to 2.181(6) Å, thus within a smaller range compared to the *i*Pr substituted cluster (Sn–O 1.969(9)–80(11) Å). Of course, the differences are correlated with the different coordination situations at the three types of tin atoms: The five-coordinate Sn^O-type atoms possess the shortest Sn–O distances, 2.029 Å on average for Sn–O, and 2.129 Å on average for Sn–OH. Both of these distances are increased for the Sn_1^{Cl} type atoms with 2.089 Å on average for Sn–O, and 2.166 Å on average for Sn–OH. For the three Sn_2^{Cl}-type atoms, the Sn–O distances are longer on average (2.125 Å), whereas Sn–OH distances (2.126 Å) are similar to those found for the Sn^O type atoms. The Sn–Cl bond lengths also differ with Sn_1^{Cl}–Cl (2.448(2) and 2.463(2) Å) or Sn_2^{Cl}–Cl (2.386(3)–2.427(2) Å), respectively, which is due to the hydrogen-bonding interaction at the Cl^- ligands of the Sn_1^{Cl} type atoms Sn1 and Sn4. The relatively weak intermolecular hydrogen bond between Cl5 and the Fc unit of an adjacent molecule does not affect the Sn9–Cl5 bond in a comparable way; hence, this one is the shortest Sn–Cl bond observed in **4**. Still, the mentioned intermolecular hydrogen bonding leads to a zigzag-type chain arrangement of the clusters, which runs along the crystallographic *a* axis (Figure 5).

In conclusion, we have presented two new tin oxido cluster-based multiferrocenyl complexes, which were formed by an unusual but efficient synthesis route, the hydrolysis of ferrocenyl substituted organotin trichlorides. With diverse counterions, compound **3**, which is based on an unprecedented $[Sn_4O_6]$ unit, has been synthesized either stepwise, via mononuclear and dinuclear compounds **1** and **2**, or in a one-pot reaction from a ferrocenyl-substituted tin chloride complex and $[SnCl_6]^{2-}$. A corresponding reaction of $FcSnCl_3$ led to the formation of **4**, which represents the largest known Fc-decorated Sn/O cluster, containing nine Fc units on its surface.

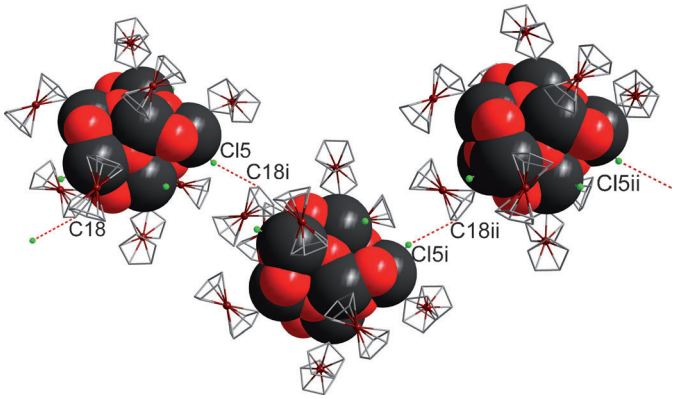

Figure 5. Intermolecular hydrogen bonding to assemble the cluster in **4** into a zigzag-type chain in **4** (without hydrogen atoms). The intermolecular hydrogen bonding Cl5···(H)C18 is indicated by red dashed lines, symmetry code: [i] x, $0.5-y$, $-0.5+z$; [ii] x, y, $-1+z$.

Experimental Section

Synthesis of 1, 2, and 3

The powder containing C and $[SnCl_6]^{2-}$ (0.05 g) was suspended together with NaSePh (0.031 g, 0.172 mmol) in THF (20 mL). After one-day stirring at RT, the solvent was evaporated in vacuum, and the residue was extracted with $CHCl_3$ (8 mL). The red extract was layered with *n*-pentane (1:1), whereupon yellow plate-like crystals of **1** and yellow needle-like crystals of **2** were obtained within a week. In the presence of moisture, the crystals of **1** and **2** decomposed within one week, whereas red plate-like crystals of **3a** were formed. Compounds **3a** and **3b** can be prepared alternatively in a one-pot synthesis by addition of water and into the reaction solution of the powder and NaEPh (E = S, Se) in THF or toluene under air (for details and analyses, see the Supporting Information).

Synthesis of 4

Similar to the one-pot synthesis of **3**, water was added to the reaction solution of $FcSnCl_3$ and NaSePh in THF. After stirring for 12 h, the solvent was evaporated in vacuum; the rest was extracted with $CHCl_3$, and the extract was layered with *n*-pentane (1:1), yellow plate-shaped crystals of **4** were formed within a week (for details and analyses, see the Supporting Information).

X-ray crystallography

Data were collected on a diffractometer equipped with a STOE imaging plate detector system IPDS2T, by using $Mo_{K\alpha}$ radiation with graphite monochromatization (λ=0.71073 Å) at 100 K. The structure solution and refinement were performed by Sir-2004,[21] full-matrix least-squares refinement against $F2$ was done by using SHELXL-2013 software.[22] Details of the data collections and refinements are given in the Supporting Information. Selected bond lengths and bond angles are provided in Tables S8--S11 in the Supporting Information. CCDC-1004575 (**2**·1·2$CHCl_3$), CCDC-1004576 (**2**), CCDC-1004577 (**3a**·$CHCl_3$·0.5C_2Cl_4), CCDC-1004578 (**3b**·4$CHCl_3$), and CCDC-1004579 (**4**·5$CHCl_3$·1.5H_2O) contain the supplementary crystallographic data for this paper. These data can be obtained free of charge from The Cambridge Crystallographic Data Centre via www.ccdc.cam.ac.uk/data_request/cif.

Acknowledgements

This work was supported by Deutsche Forschungsgemeinschaft (DFG) within the framework of SFB 1083. We thank Dr. M. Hołyńska for her help with the structure analysis of compound **1**.

Keywords: cluster compounds · cyclic voltammetry · hydrolysis · organotin compounds · tin

[1] P. Štěpnička in *Ferrocenes: Ligands, Materials and Biomolecules*, Wiley, Chichester, **2008**.

[2] a) D. González-Rodríguez, E. Carbonell, G. D. Rojas, C. A. Castellanos, D. M. Guldi, T. Torres, *J. Am. Chem. Soc.* **2010**, *132*, 16488 – 16500; b) M. Sawamura, Y. Kuninobu, M. Toganoh, Y. Matsuo, M. Yamanaka, E. Nakamura, *J. Am. Chem. Soc.* **2002**, *124*, 9354 – 9355.

[3] a) Y. Yan, B. Li, Q. Y. He, Z. F. He, H. Ai, H. B. Wang, Z. D. Yin, L. X. Wu, *Soft Matter* **2012**, *8*, 1593 – 1600; b) H. S. Xu, L. Zhang, Z. X. Li, X. M. Liu, H. M. Hu, G. L. Xue, *Solid State Sci.* **2010**, *12*, 1332 – 1336; c) Y. J. Niu, X. Y. Ren, B. Yin, D. J. Wang, G. L. Xue, H. M. Hu, F. Fu, J. W. Wang, *J. Organomet. Chem.* **2010**, *695*, 1863 – 1868; d) J. L. Stark, V. G. Young, E. A. Maatta, *Angew. Chem.* **1995**, *107*, 2751 – 2753; *Angew. Chem. Int. Ed. Engl.* **1995**, *34*, 2547 – 2548.

[4] a) D. G. MacDonald, C. Kubel, J. F. Corrigan, *Inorg. Chem.* **2011**, *50*, 3252 – 3261; b) D. G. MacDonald, A. Eichhofer, C. F. Campana, J. F. Corrigan, *Chem. Eur. J.* **2011**, *17*, 5890 – 5902; c) S. Ahmar, D. G. MacDonald, N. Vijayaratnam, T. L. Battista, M. S. Workentin, J. F. Corrigan, *Angew. Chem.* **2010**, *122*, 4524 – 4526; *Angew. Chem. Int. Ed.* **2010**, *49*, 4422 – 4424; d) C. Nitschke, D. Fenske, J. F. Corrigan, *Inorg. Chem.* **2006**, *45*, 9394 – 9401.

[5] G. L. Zheng, J. F. Ma, Z. M. Su, L. K. Yan, J. Yang, Y. Y. Li, J. F. Liu, *Angew. Chem.* **2004**, *116*, 2463 – 2465; *Angew. Chem. Int. Ed.* **2004**, *43*, 2409 – 2411.

[6] V. Chandrasekhar, S. Nagendran, S. Bansal, M. A. Kozee, D. R. Powell, *Angew. Chem.* **2000**, *112*, 1903 – 1905; *Angew. Chem. Int. Ed.* **2000**, *39*, 1833 – 1835.

[7] a) M. Sun, B. Ruan, Q. Zhang, Z. Liu, S. Li, J. Wu, B. Jin, J. Yang, S. Zhang, Y. Tian, *J. Organomet. Chem.* **2011**, *696*, 3180 – 3185; b) V. Chandrasekhar, R. Thirumoorthi, *Eur. J. Inorg. Chem.* **2008**, *29*, 4578 – 4585; c) G. L. Zheng, J. F. Ma, J. Yang, Y. Y. Li, X. R. Hao, *Chem. Eur. J.* **2004**, *10*, 3761 – 3768; d) V. Chandrasekhar, S. Nagendran, S. Bansal, A. W. Cordes, A. Vij, *Organometallics* **2002**, *21*, 3297 – 3300.

[8] M. Henn, M. Schurmann, B. Mahieu, P. Zanello, A. Cinquantini, K. Jurkschat, *J. Organomet. Chem.* **2006**, *691*, 1560 – 1572.

[9] a) D. Dakternieks, B. Zobel, *Organometallics* **2003**, *22*, 1343 – 1345; b) J. Beckmann, M. Henn, K. Jurkschat, M. Schürmann, *Organometallics* **2002**, *21*, 192 – 202; c) J. Janssen, J. Magull, H. W. Roesky, *Angew. Chem.* **2002**, *114*, 1425 – 1427; *Angew. Chem. Int. Ed.* **2002**, *41*, 1365 – 1367; d) J. Beckmann, K. Jurkschat, S. Rabe, M. Schürmann, *Z. Anorg. Allg. Chem.* **2001**, *627*, 2413 – 2419; e) M. A. Edelman, P. B. Hitchcock, M. F. Lappert, *J. Chem. Soc. Chem. Commun.* **1990**, *16*, 1116 – 1118; f) H. Puff, H. Reuter, *J. Organomet. Chem.* **1989**, *364*, 57 – 65; g) H. Puff, W. Schuh, R. Sievers, W. Wald, R. Zimmer, *J. Organomet. Chem.* **1984**, *260*, 271 – 280; h) S. Masamune, L. R. Sita, D. J. Williams, *J. Am. Chem. Soc.* **1983**, *105*, 630 – 631; i) V. K. Belsky, N. N. Zemlyansky, I. V. Borisova, N. D. Kolosova, I. P. Beletskaya, *J. Organomet. Chem.* **1983**, *254*, 189 – 192; j) H. Puff, W. Schuh, R. Sievers, R. Zimmer, *Angew. Chem.* **1981**, *93*, 622 – 623; *Angew. Chem. Int. Ed. Engl.* **1981**, *20*, 591 – 591.

[10] B. Zobel, M. Schurmann, K. Jurkschat, D. Dakternieks, A. Duthie, *Organometallics* **1998**, *17*, 4096 – 4104.

[11] a) J. Beckmann, D. Dakternieks, A. Duthie, F. S. Kuan, K. Jurkschat, M. Schürmann, E. R. T. Tiekink, *New J. Chem.* **2004**, *28*, 1268 – 1276; b) D. Dakternieks, A. Duthie, B. Zobel, *Organometallics* **2002**, *21*, 647 – 652; c) M. Schulte, M. Schurmann, D. Dakternieks, K. Jurkschat, *Chem. Commun.* **1999**, *14*, 1291 – 1292; d) M. Mehring, M. Schurmann, I. Paulus, D. Horn, K. Jurkschat, A. Orita, J. Otera, D. Dakternieks, A. Duthie, *J. Organomet. Chem.* **1999**, *574*, 176 – 192; e) M. Mehring, M. Schurmann, H. Reuter, D. Dakternieks, K. Jurkschat, *Angew. Chem.* **1997**, *109*, 1150 –

1152; *Angew. Chem. Int. Ed. Engl.* **1997**, *36*, 1112 – 1114; f) M. Hill, M. F. Mahon, K. C. Molloy, *Main Group Chem.* **1996**, *1*, 309 – 315; g) J. F. Vollano, R. O. Day, R. R. Holmes, *Organometallics* **1984**, *3*, 745 – 750; h) H. Matsuda, S. Matsuda, N. Kasai, A. Kashiwa, K. Jitsumor, F. Mori, *J. Organomet. Chem.* **1972**, *34*, 341 – 345.

[12] H. Puff, H. Reuter, *J. Organomet. Chem.* **1989**, *368*, 173 – 183.

[13] H. Puff, H. Reuter, *J. Organomet. Chem.* **1989**, *373*, 173 – 184.

[14] a) P. Jaumier, B. Jousseaume, M. Lahcini, F. Ribot, C. Sanchez, *Chem. Commun.* **1998**, *3*, 369 – 370; b) F. Banse, F. Ribot, P. Toledano, J. Maquet, C. Sanchez, *Inorg. Chem.* **1995**, *34*, 6371 – 6379.

[15] A. Davies, M. Gielen, K. H. Pannell, E. R. Tiekink in *Tin Chemistry: Fundamentals, Frontiers, and Applications*, Wiley, Chichester, **2008**, pp. 69 – 90.

[16] a) Z. Hassanzadeh Fard, C. Müller, T. Harmening, R. Pöttgen and S. Dehnen, *Angew. Chem.* **2009**, *121*, 4507 – 4511; *Angew. Chem. Int. Ed.* **2009**, *48*, 4441 – 4444; b) Z. Hassanzadeh Fard, L. Xiong, C. Müller, M. Hołyńska, S. Dehnen, *Chem. Eur. J.* **2009**, *15*, 6595 – 6604.

[17] a) M. R. Halvagar, Z. Hassanzadeh Fard, S. Dehnen, *Chem. Eur. J.* **2011**, *17*, 4371 – 4374; b) Z. H. Fard, M. R. Halvagar, S. Dehnen, *J. Am. Chem. Soc.* **2010**, *132*, 2848 – 2849.

[18] S. Dehnen, C. Pöhlker, I. Schellenberg, R. Pöttgen, *Chem. Commun.* **2010**, *46*, 2605 – 2607.

[19] Z. You, D. Fenske, S. Dehnen, *Dalton Trans.* **2013**, *42*, 8179 – 8182.

[20] a) Z. You, S. Dehnen, *Inorg. Chem.* **2013**, *52*, 12332 – 12334; b) G. Bliznakov, K. Petrov, *Z. Anorg. Allg. Chem.* **1967**, *354*, 307 – 312.

[21] a) H. P. Nayek, G. Hilt, S. Dehnen, *Eur. J. Inorg. Chem.* **2009**, 4205 – 4208; b) L. P. Spencer, P. Yang, B. L. Scott, E. R. Batista, J. M. Boncella, *Inorg. Chem.* **2009**, *48*, 2693 – 2700; c) N. V. Soloviev, A. Eichhofer, D. Fenske, U. Banin, *J. Am. Chem. Soc.* **2001**, *123*, 2354 – 2364.

[22] Z. Padělková, A. Havlík, P. Švec, M. S. Nechaev, A. Růžička, *J. Organomet. Chem.* **2010**, *695*, 2651 – 2657.

[23] M. C. Burla, R. Caliandro, M. Camalli, B. Carrozzini, G. L. Cascarano, L. De Caro, C. Giacovazzo, G. Polidori, R. Spagna, *J. Appl. Cryst.* **2005**, *38*, 381 – 388.

[24] G. M. Sheldrick, *SHELXL2013*, **2013**, University of Göttingen, Germany.

Received: May 23, 2014
Published online on August 27, 2014

CHEMISTRY
A European Journal

Supporting Information

Organotin–Oxido Cluster-Based Multiferrocenyl Complexes Obtained by Hydrolysis of Ferrocenyl-Functionalized Organotin Chlorides

Zhiliang You, Robert Möckel, Jakob Bergunde, and Stefanie Dehnen*[a]

chem_201403657_sm_miscellaneous_information.pdf

1. Experimental Syntheses Details

***General*:** All reaction steps were carried out under Ar atmosphere, unless otherwise noted. All solvents were dried and freshly distilled prior to use. Sodium phenyl sulfide NaSPh, sodium phenyl selenide NaSePh,[1] and ferrocenyltin trichloride $FcSnCl_3$[2] were prepared according to the reported methods. The synthesis of the powder containing **C** and $[SnCl_6]^{2-}$ was slightly modified according to the reported synthetic pathway with HCl gas or HCl ether solution.[3]

^{1}H NMR, ^{13}C NMR and ^{119}Sn NMR measurements were carried out using a Bruker DRX 500 MHz spectrometer at 25ºC. In ^{1}H and ^{13}C NMR spectra, the chemical shifts were quoted in ppm relative to the residual protons of deuterated solvents. In ^{119}Sn NMR, Me_4Sn was used as internal standard.

Infrared (IR) spectra were recorded on a Bruker TENSOR 37 FT-IR spectrometer.

Mass spectrometry (MS) was performed on a Finnigan MAT 95S. The Electrospray Ionisation (ITMS-ESI) spectra were obtained by using solvent as the carrier gas.

*Formation of **1** [($R^{Fc}SnCl_2)_2Se$], **2** [($R^{Fc}SnCl_2$)SePh] (R^{Fc} = [$CMe_2CH_2C(Me)$=N–N=C(Me)]Fc) and synthesis of **3a** {($R^{Fc}SnCl_2)_3[Sn(OH)_6]$}[$SnCl_3$]·$CHCl_3$·0.5$C_2Cl_4$ (**3**·$CHCl_3$·0.5C_2Cl_4)*

The powder containing from **C** and $[SnCl_6]^{2-}$ (0.05 g) was suspended together with NaSePh (0.031g, 0.172 mmol) in THF (20 mL). After 1 day stirring at room temperature, the solvent was evaporated in vacuum, and was extracted with 8 mL $CHCl_3$. The red extract was layered with *n*-pentane (1:1), and stored in a freezer. Yellow plate-shape crystals of **1** and yellow needle-shape crystals of **2** were obtained within a week. After two weeks, the crystals of **1** and **2** disappeared, whereas red, plate-like crystals of **3a** formed.

3a could be also synthesized by a one-pot reaction. Like the formation of **1** and **2**, the powder (2 g, ca. 2.65 mmol Sn) and NaSPh (0.908, 6.88 mmol) were first suspended in THF. After 1 day stirring at room temperature, water (0.32 mL, 17.8 mmol) was added, and then stirred for 12 h in an open air atmosphere. The solvent was evaporated in vacuum; the residue was extracted with $CHCl_3$. Crystals of **3a** were formed within a week by layering the extract with *n*-pentane (1:1).

Analyses of **3a**:

^{1}**H** NMR (500 MHZ, CD_2Cl_2, 25°C): δ/ppm = 1.27, 1.46 (2xs, 18H; ***Me***2C), 2.19 (s, 9H; ***Me***(Cp)C=N), 2.25 (s, 9H, ***Me***C=N), 2.87 (dd, 6H, C***H***2), 4.15 (s, 15H, $Cp_{unsubst.}$-***H***), 3.90-4.81 (m, 12H, $Cp_{subst.}$-***H***), 7.32 (s, 2H, C***H***Cl_3), 7.56, 7.61 (2xt, 2H, Sn-O***H***), 8.03 (d, 1H, Sn-O***H***), 8.52 (s, 3H, Sn-O***H***); ^{13}**C** NMR (126 MHZ, CD_2Cl_2, 25°C): *δ/ppm* = 20.32 (N=C***C***H_3), 22.15 (N=C***C***H_3(Cp)), 26.63 ((***C***H3)$_2$C), 41.85 (***C***Me_2), 49.90 (***C***H_2), 68.37, 69.92, 71.21, (H***C***-Cp)), 77.95 (***C***HCl_3), 81.54 (-***C***-Cp), 163.22 (Cp(H)***C***=N), 165.85 (Me(CH2)***C***=N); ^{119}**Sn** NMR (186 MHz, CD_2Cl_2): *δ/ppm* = –407.62 (Sn1), –210.15 (Sn2-Sn4).

IR: ῡ/cm^{-1} = 3728.7 (w, br), 3625.7 (w, br), 3597.6 (w, br), 3087.1 (w, br), 2960.08 (m, br), 2851.4 (m, br), 2351.1 (s), 2328.7 (s), 2255.7 (w), 2108.3 (w), 1985.9 (w), 1786.8 (w), 1632.0 (w), 1590.1 (s), 1477.4 (m), 1436.9 (s), 1370.3 (m), 1336.7 (s), 1302.1 (m), 1283.2 (m), 1216.5 (w), 1125.3 (s), 1027.5 (m), 1001.1 (w), 946.8 (w), 891.9 (m), 823.5 (s), 757.6 (s), 724.1 (w), 689.4 (m), 656.8 (w), 496.4 (vs), 474.4 (vs).

Synthesis of ***3b*** *{($R^{Fc}SnCl_2)_3[Sn(OH)_6]$}$[O_3SePh]\cdot 4CHCl_3$ (**3**$\cdot CHCl_3\cdot 0.5C_2Cl_4$ and **3**$\cdot 4CHCl_3$; R^{Fc} = $[CMe_2CH_2C(Me)=N–N=C(Me)]Fc$)*

The powder (2 g, ca. 2.65 mmol Sn) and NaSePh (1.24 g, 6.88 mmol) were suspended in THF. After 1 day stirring at room temperature, water (0.32 mL, 17.8 mmol) was added, and then stirred for 12 h in an open air atmosphere. The solvent was evaporated in vacuum; the residue was extracted with $CHCl_3$. The crystals of **3b** were formed within a week by layering the extract with *n*-pentane (1:1).

MS-ESI(+): *m/z* = 1758.80 ($[M\text{-}O_3SePh]^+ = \{(R^{Fc}SnCl_2)_3[Sn(OH)_6]\}^+$)

MS-ESI(-): *m/z* = 204.94 ($[PhSeO_3]^-$)

IR: ϋ/cm^{-1} = 3732.4 (w, br), 3632.3 (w, br), 3093.3 (w, br), 2958.0 (w, br), 2856.9 (w, br), 2344.8 (s), 2299.6 (m), 2255.5 (w), 1635.8 (w), 1589.6 (m), 1470.2 (m), 1373.4 (m), 1336.3 (m), 1300.6 (m), 1252.6 (w), 1216.8 (w), 1119.0 (m), 1006.6 (m), 942.1 (w), 882.6 (s), 830.1 (s), 746.7 (vs), 688.9 (vs), 647.1 (vs), 578.4 (s), 473.1 (s).

As expected, the NMR data of **3a** and **3b** are the same, except the signals for the $[PhSeO_3]$ group: ^{1}**H** NMR (500 MHZ, CD_2Cl_2, 25°C): δ/ppm = 7.59, 7.65, 8.25 (3xm, 5H, Ph-***H***); ^{13}**C** NMR (126 MHZ, CD_2Cl_2, 25°C): *δ/ppm* = 127.80, 133.53, 135.21, 161.33 (Ph-***C***).

Synthesis of ***4*** *$[(FcSn)_9Cl_5(OH)_6O_8]\cdot 5CHCl_3$, {**4**$\cdot 5CHCl_3$, Fc = $H_4C_5FeC_5H_5$}*

The precursor $FcSnCl_3$ (0.79 g, 1.90 mmol) and NaSePh (0.753 g, 4.18 mmol) were suspended in THF. After 1 day stirring at room temperature, water (0.23 mL, 12.8 mmol) was added, and the mixture was stirred for 12 h in an open air atmosphere. The solvent was evaporated in vacuum; the rest was extracted with $CHCl_3$. The plate-shape yellow crystals of **4** were formed within a week by layering the extract with *n*-pentane (1:1).

^{1}**H** NMR (500 MHZ, $CDCl_3$, 25°C): δ/ppm = 4.16, 4.25 (m, m, 45H, $Cp_{unsubst.}$-***H***) 4.19, 4.21-4.22, 4.36, 4.55 (4xm, 36H, $Cp_{subst.}$-***H***); ^{13}**C** NMR (126 MHZ, $CDCl_3$, 25°C): *δ/ppm* = 69.31, 69.37, ($Cp_{unsubst.}$-***C***); 75.11, 75.03, 74.41, 71.20, 71.16, 71.03, 70.90, 69.04 ($Cp_{subst.}$-***C***); ^{119}**Sn** NMR (186 MHz, $CDCl_3$): *δ/ppm* = –324.11 (Sn^O), –329.97 (Sn^O), –337.55 (Sn^O), –452.17 (Sn_1^{Cl}), –477.36 (Sn_2^{Cl}).

IR: ϋ/cm^{-1} = 3921.5 (w, br), 3596.2 (w, br), 3550.7 (w, br), 3354.1 (w, br), 3093.5 (w, br), 2960.9 (w, br), 2923.9 (w, br), 2854.6 (w, br), 2361.0 (w), 2344.4 (w), 2324.2 (w), 2164.2 (w), 2037.3 (w), 1980.4 (w), 1647.8 (w, br), 1411.2 (w), 1379.9 (w), 1304.4 (w), 1260.9 (m), 1140.5 (s), 1105.43 (s), 1021.1 (s), 1002.0 (s), 815.1 (s), 703.4 (s), 630.9 (s), 591.3 (s), 563.8 (s), 477.0 (vs), 436.6 (s).

2. Spectrometry and Spectroscopy

^{1}H- and ^{119}Sn-NMR spectra were recorded of the degradation powder of **A** containing **C** and $[SnCl_6]^{2-}$ (Figure S1).

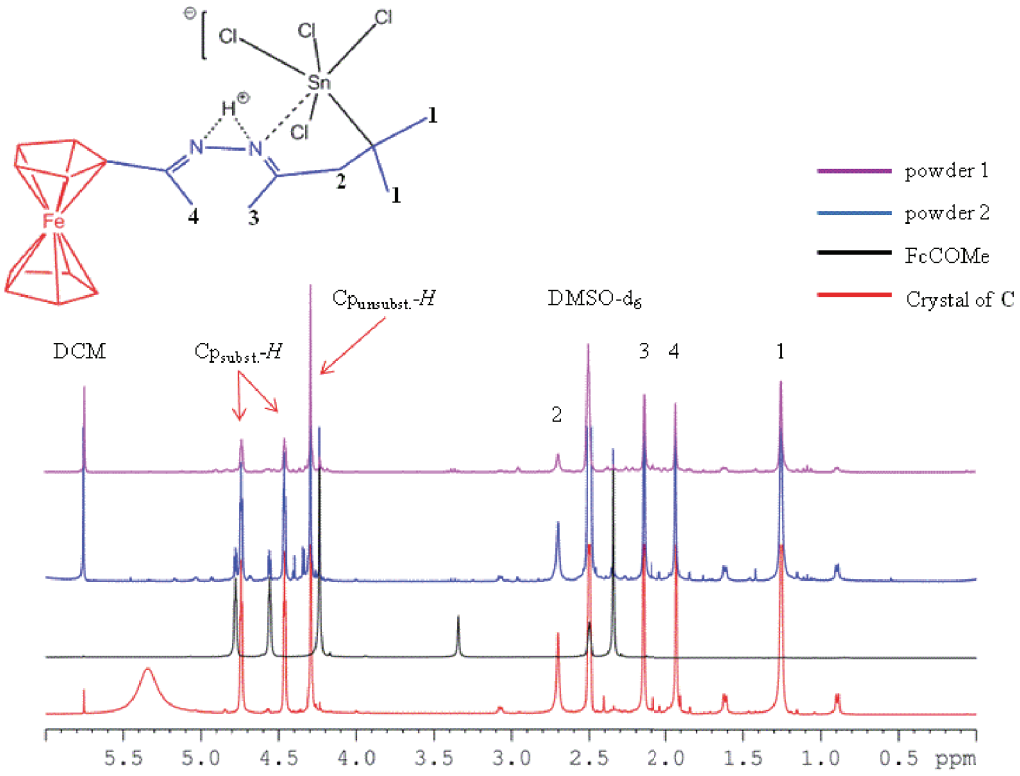

Figure S1. ^{1}H-NMR spectrum of degradation powder 1, obtained by the degradation of **A** with HCl ether-solution (purple curve), in comparison with powder 2 by degradation with concentrated hydrochloric acid (37% HCl, blue curve), acetylferrocene (FcCOMe, black curve) and crystals of **C** (red curve).

ESI (+) mass spectrum of **3b** (Figure S2)**:**

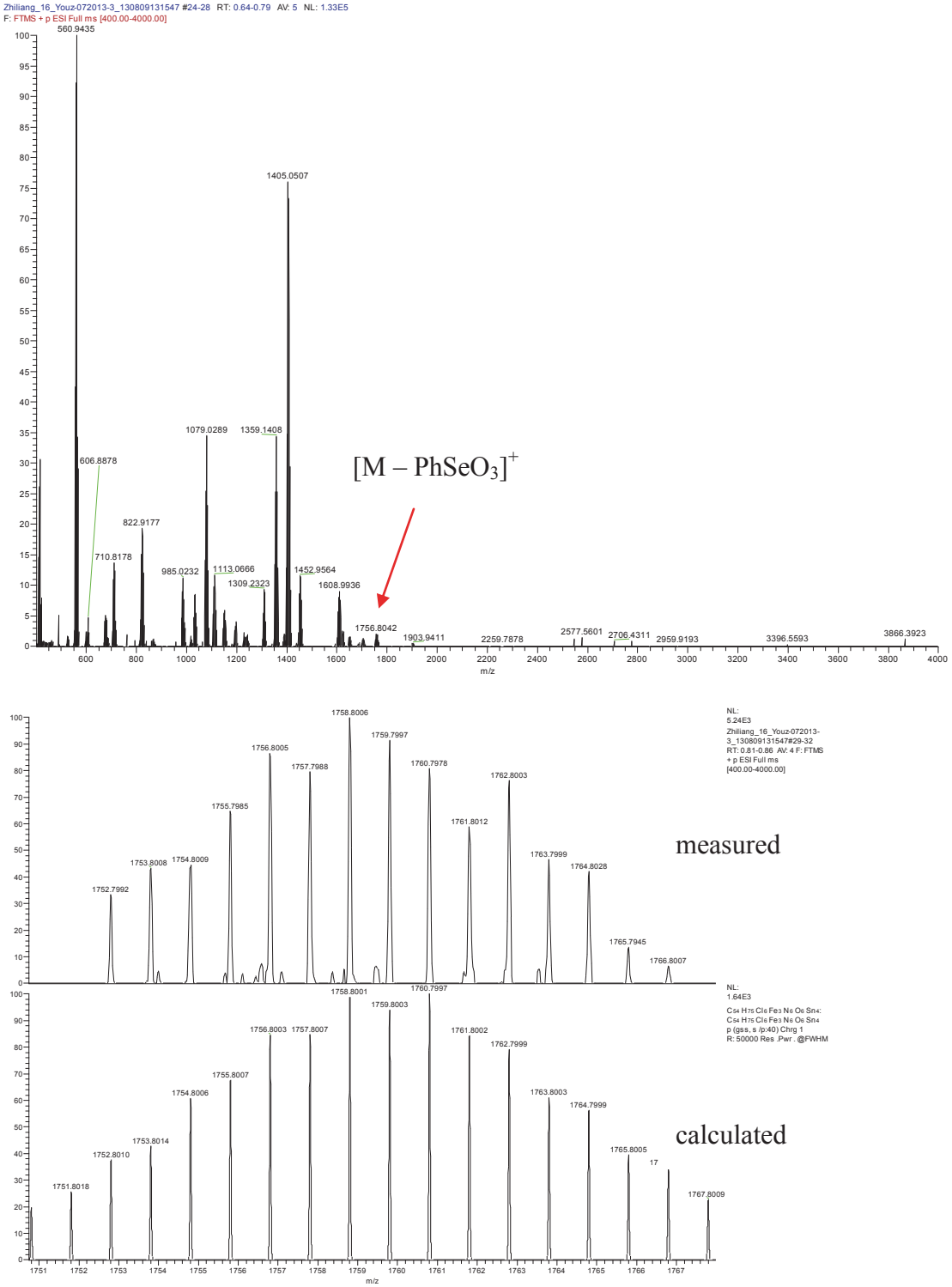

Figure S2. ESI mass spectrum of **3b**: overview (**A**), *m/z* = 1758.80 ($\{(R^{Fc}SnCl_2)_3[Sn(OH)_6]\}^+$) (**B**).

ESI (-) mass spectrum of **3b** (Figure S3)**:**

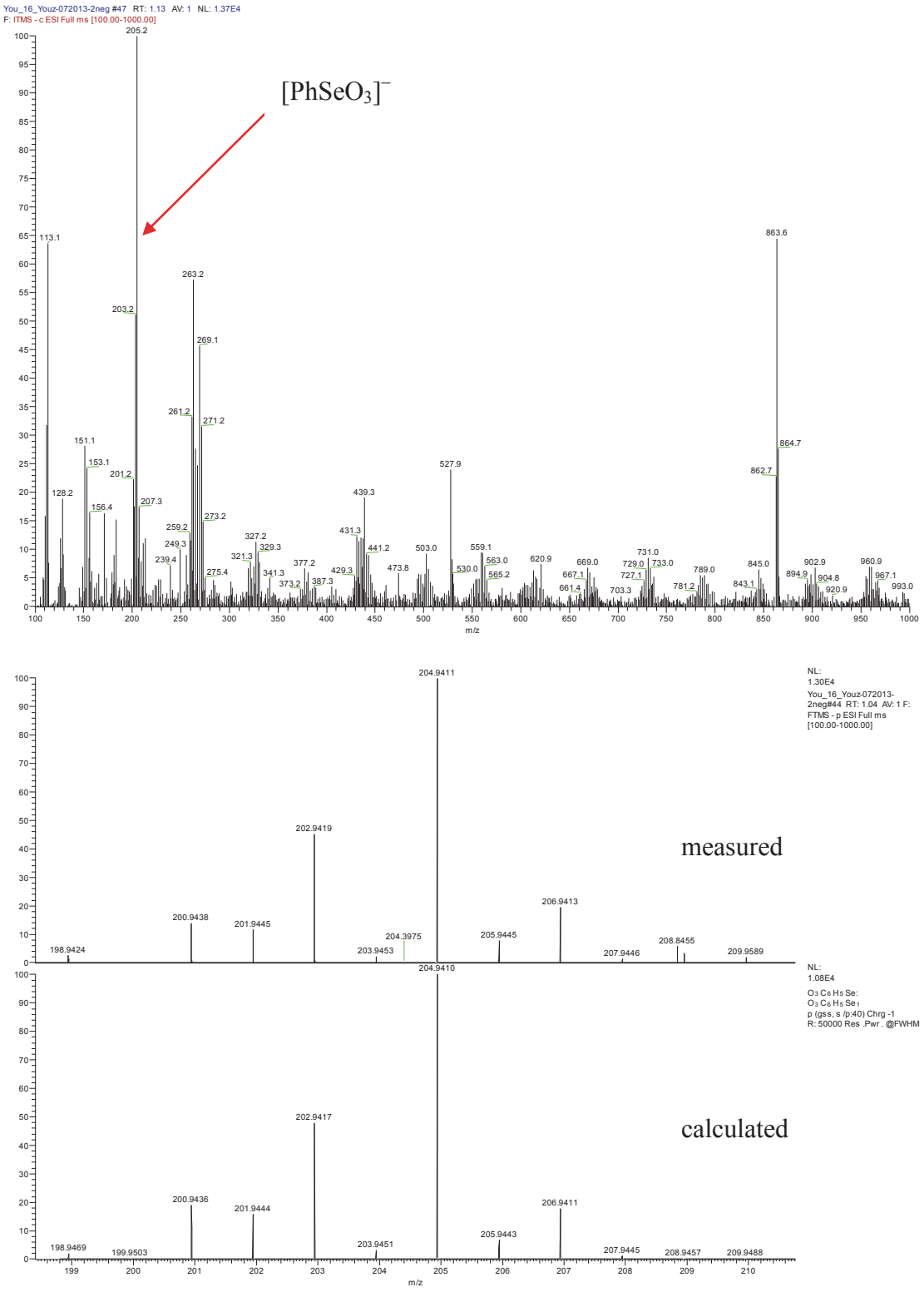

Figure S3. ESI(-) mass spectrum of **3b**: overview (**A**), *m/z* = 204.94 ([$PhSeO_3$]¯) (**B**).

3. Electrochemical measurements

Electrochemical measurements – cyclic voltammetry (CV) – were recorded under Ar atmosphere at 25°C, using 0.1 mol/L [nBu$_4$N][PF$_6$] as the supporting electrolyte. The potentials (Table S1) were referenced internally to ferrocene, added at the end of the experiments. Working and counter electrodes: Pt.

Table S1. Electrochemical characteristics for the oxidation process of **3a** in DCM solution. (scan rate varying from 100 up to 600 mV/s, *vs*. [FeCp$_2$] in mV)

Scan rate	E_{pa}	E_{pc}	$E_{1/2}$	ΔE	i_{pa}/i_{pc}
100	448	250	349	198	0.87
200	465	266	366	199	0.84
300	474	273	374	201	0.83
400	472	276	374	196	0.82
500	466	270	368	196	0.81
600	472	270	371	202	0.80

4. Energy dispersive X-ray (EDX) spectroscopy

EDX analyses were performed using the EDX device Voyager 4.0 of Noran Instruments coupled with the electron microscope CamScan CS 4DV. Data acquisition was performed with an acceleration voltage of 20 kV and 100 s accumulation time. For the analyses, multiple single crystals were used and the data recorded both various times on one single crystal and various times on other single crystals. Figures S4-S8 show the EDX spectra, Tables S2-S6 summarize the data.

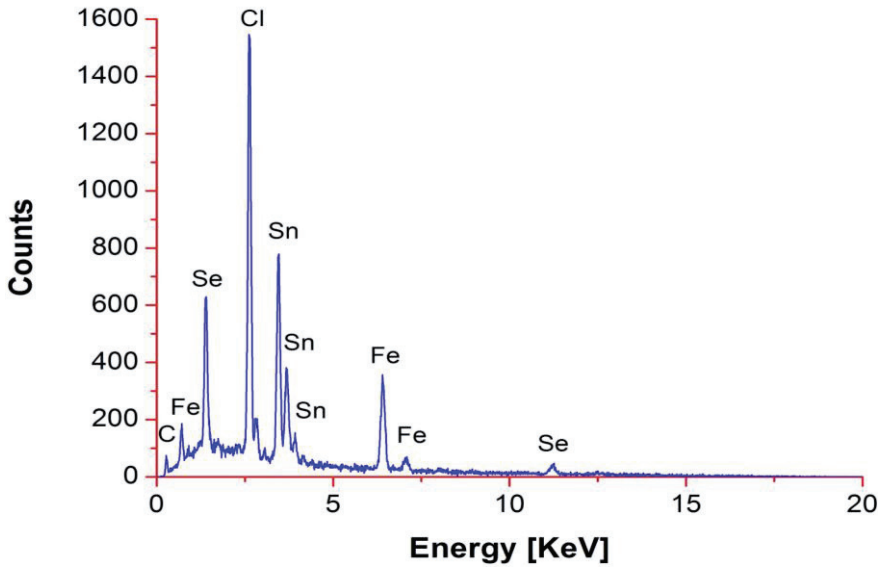

Figure S4. EDX analysis of **1**.

Table S2. EDX analysis of **1**.

Element	k-ratio (calc.)	ZAF	Atom %	Atomic ratio obs. (calc.)	Element Wt %	Wt % Err. (1-Sigma)
Se-L	0.1062	2.301	26.90	1.34 (1.00)	24.43	+/- 0.39
Sn-L	0.4895	1.103	39.54	1.98 (2.00)	54.00	+/- 0.62
Fe-K	0.2160	0.997	33.56	1.68 (2.00)	21.57	+/- 0.68
Total			100	5	100	

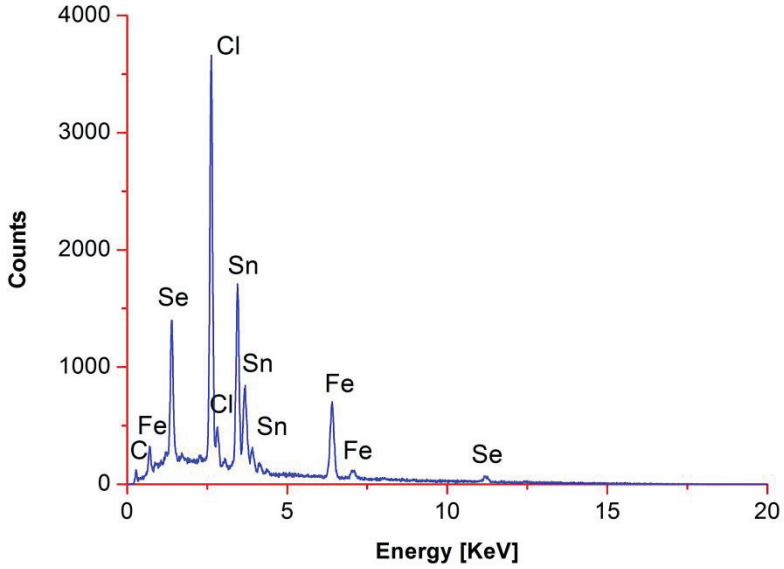

Figure S5. EDX analysis of **2**.

Table S3. EDX analysis of **2**.

Element	k-ratio (calc.)	ZAF	Atom %	Atomic ratio obs. (calc.)	Element Wt %	Wt % Err. (1-Sigma)
Sn-L	0.4469	1.118	36.40	1.09 (1.00)	49.97	+/- 0.74
Fe-K	0.1966	0.991	30.17	0.91 (1.00)	19.49	+/- 0.44
Se-L	0.1397	2.185	33.43	1.00 (1.00)	30.54	+/- 0.49
Total			100	8	100	

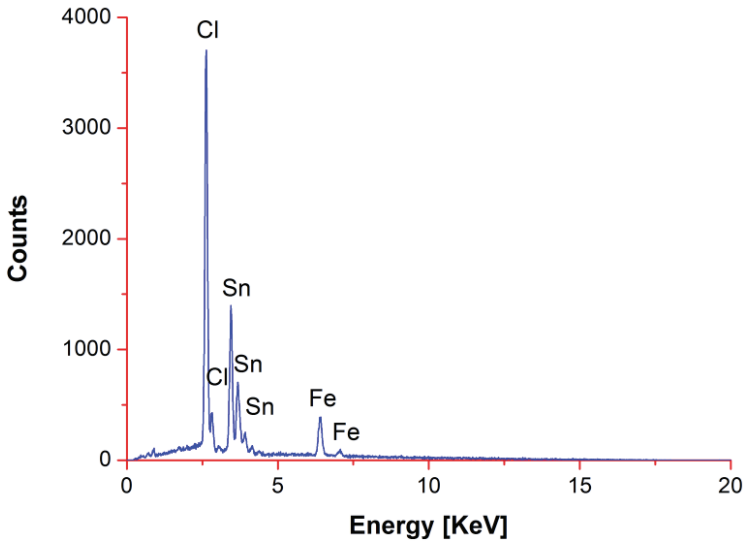

Figure S6. EDX analysis of **3a**.

Table S4. EDX analysis of **3a**.

Element	k-ratio (calc.)	ZAF	Atom %	Atomic ratio obs. (calc.)	Element Wt %	Wt % Err. (1-Sigma)
Sn-L	0.7517	1.034	62.16	5.00 (5.00)	77.74	+/- 1.22
Fe-K	0.2179	1.022	37.84	3.00 (3.00)	22.26	+/- 0.77
Total			100	8	100	

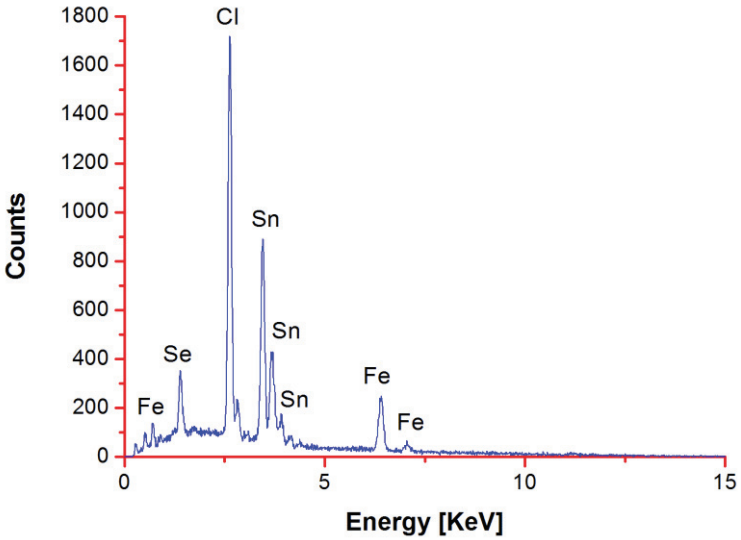

Figure S7. EDX analysis of **3b**.

Table S5. EDX analysis of **3b**.

Element	k-ratio (calc.)	ZAF	Atom %	Atomic ratio obs. (calc.)	Element Wt %	Wt % Err. (1-Sigma)
Se-L	0.0543	2.025	12.65	1.01 (1.00)	11.00	+/- 0.31
Sn-L	0.6272	1.063	51.03	4.08 (4.00)	66.67	+/- 1.31
Fe-K	0.2380	0.938	36.32	2.91 (3.00)	22.33	+/- 0.97
Total			100	8	100	

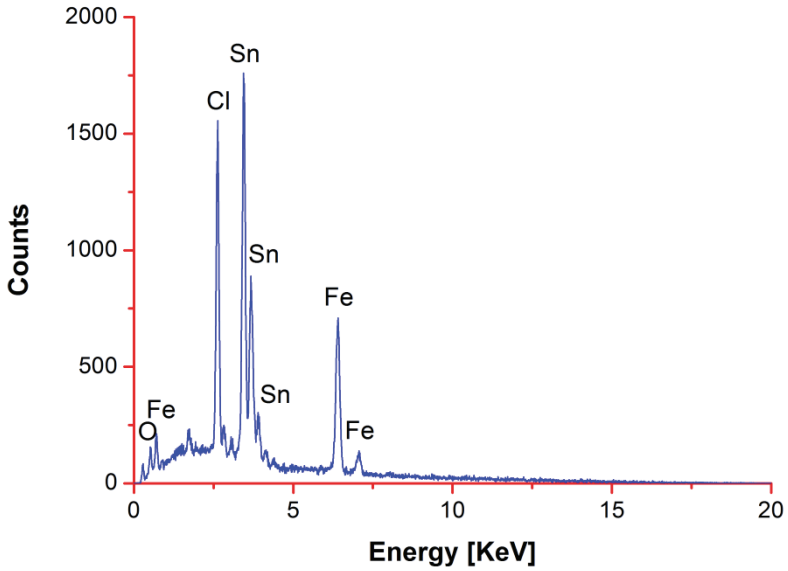

Figure S8. EDX analysis of **4**.

Table S6. EDX analysis of **4**.

Element	k-ratio (calc.)	ZAF	Atom %	Atomic ratio obs. (calc.)	Element Wt %	Wt % Err. (1-Sigma)
Fe-K	0.3641	0.95	52.93	9.53 (9.00)	34.60	+/- 0.77
Sn-L	0.6167	1.060	47.07	8.47 (9.00)	65.40	+/- 0.93
Total			100	18	100	

5. Raman Spectroscopy

Raman spectrum was recorded on a Labram HR 800 Raman spectrometer with a 632.8 nm red laser in the range of 80-2000 cm^{-1}. The beam was focused on the sample through a confocal microscope using a 50× objective lens (Figure S9).

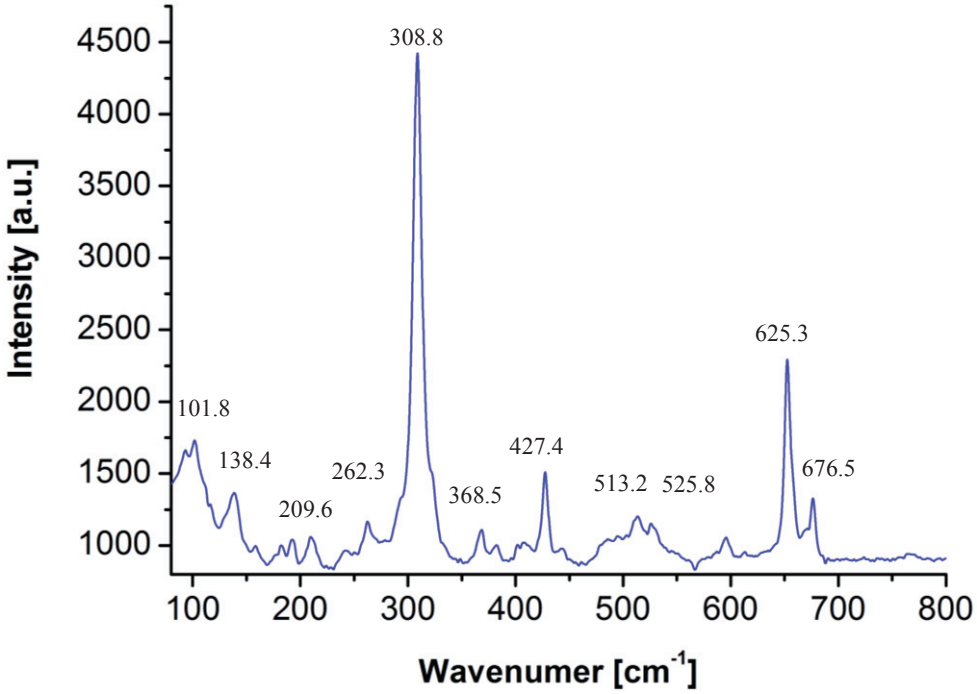

Figure S9. Single-crystal Raman spectrum of **3b** in the range of 80-800 cm^{-1}.

All two compounds of **3** contain the same tin-oxido cluster-based mutiferrocenyl cation, thus they should exhibit the same dominate vibrations in infrared (IR) as well as in Raman spectra. As an example, IR and Raman spectroscopy has been carried out on crystalline **3b**. Like other previously reported compounds with the R^{Fc} ligand, the IR spectrum of **3b** exhibits the typical absorption bands of Fc units at 3093.3, 1119.0, 830.1, 942.1 cm^{-1} and the conjugated –C=N–N=C– groups at 1635.8, 1598.6 cm^{-1}.[3] Moreover, the asymmetric stretching and bending vibrations of the OH groups result in the bands at 3632 and 882 cm^{-1}, respectively, which are in agreement with such reported values in R_3SnOH (R = alkyl) [4,5] and [*i*-$Pr_4Sn_2OCl(OH)_2$].[6] The band at 746.7 cm^{-1} can be assigned to the asymmetric stretching mode of Sn–O–Sn.[4,7] The Raman spectrum of **3b** is dominated by the absorption bands of Fc units, which are most in agreement with the observed values by the measurement of ferrocene in solid state.[8] In the range of 80-800 cm^{-1}, the strongest bands at 308.8 cm^{-1} belong to Fc units, showing the symmetric $Cp_{\text{-ring}}$-Fe stretching. [8] The second strongest band at 625.3 cm^{-1} can be probably assigned to the ν_s(Sn–O), and the ν_s(Sn–O–Sn) can be located at 427.4 cm^{-1} as a sharp medium intensity band.[7]

6. X-ray diffraction measurement, structure solution and refinement details

Data were collected on a diffractometer equipped with a STOE imaging plate detector system IPDS2T, using MoKα radiation with graphite monochromatization (λ = 0.71073 Å) at 100 K. The structure solution and refinement was performed by Sir-2004,[9] full-matrix-least-squares refinement against F^2 was done using SHELXL-2013 software.[10] Details of the data collections and refinements are given in Table S7. Selected bond lengths and bond angles are provided in Tables S8-11. CCDC 1004575-1004579. Structural details are illustrated in Figures S10-S19.

Table S7. Crystal and structure refinement data.					
Compound	2·**1**·3$CHCl_3$	**2**	**3a**·$CHCl_3$·0.5C_2Cl_4	**3b**·4$CHCl_3$	**4**·5$CHCl_3$·1.5O
Chemical formula	$C_{75}H_{95}Cl_{17}Fe_4N_8Se_2Sn_4$	$C_{24}H_{28}Cl_2FeN_2SeSn$	$C_{56}H_{70}Cl_{14}Fe_3N_6O_6Sn_5$	$C_{64}H_{77}Cl_{18}Fe_3N_6O_9Se_1Sn_4$	$C_{95}H_{86}Cl_{20}Fe_9O_{15.5}Sn_9$
Formula Mass/g·mol^{-1}	2567.31	668.68	2180.48	2433.69	3702.32
Crystal color and shape	Yellow plate	Yellow needle	Red plate	Orange block	Yellow plate
Crystal size /mm^3	0.21 x 0.17 x 0.09	0.40 x 0.06 x 0.05	0.17 x 0.08 x 0.06	0.23 x 0.18 x 0.06	0.15 x 0.14 x 0.03
Crystal system	Monoclinic	Triclinic	Orthorhombic	Orthorhombic	Monoclinic
a/Å	16.379(2)	7.319 (15)	24.473 (1)	23.984 (2)	26.4003 (11)
b/Å	17.877(2)	13.269 (2)	24.303 (11)	24.345 (2)	17.8810 (6)
c/Å	17.488(2)	14.651 (3)	25.549 (12)	30.584 (3)	25.3471 (9)
α/°	90.0	68.404 (5)	90.0	90.0	90.0
β/°	115.803(5)	88.527 (7)	90.0	90.0	104.384 (2)
γ/°	90.0	74.506 (6)	90.0	90.0	90.0
V/Å3	4610.1(9)	1270.7 (4)	15195.7 (12)	17858.0 (3)	11590.4 (7)
Space group	$P2_1$	$P\bar{1}$	*Pbca*	*Pbca*	$P\ 2_1/c$
Z	2	2	8	8	4
Abs. coefficient, *μ*/mm^{-1}	3.00	3.21	2.71	2.572	3.472
Abs. correction type	Numerical	Multi-Scan	Multi-Scan	Multi-Scan	Multi-Scan
min/max transmission	0.546/0.765	0.358/0.866	0.656/0.854	0.861/0.589	0.624/0.903
2θ range /deg	4.6 to 50.0	5.4 to 50.0	4.0 to 50.0	4.0 to 50.0	3.9 to 50.0
No. of reflections measured	79239	17049	86335	384484	172135
No. of independent refl.	31907	4447	13364	15729	20391
Flack x parameter [11]	0.08(3)	–	–	–	–
R_{int}	0.228	0.130	0.0835	0.115	0.121
R_1 ($I > 2\sigma(I)$) / $wR(F^2)$ (all data)	0.101/0.226	0.082/0.199	0.058/0.157	0.058/0.151	0.050/0.134
Goodness of fit on F^2	0.96	1.00	1.03	1.06	1.06
Largest diff. peak/hole /e$^-$·Å^{-3}	1.45/–1.55	3.28/–1.74	3.30/–2.00	2.70/–2.32	2.91/–2.48

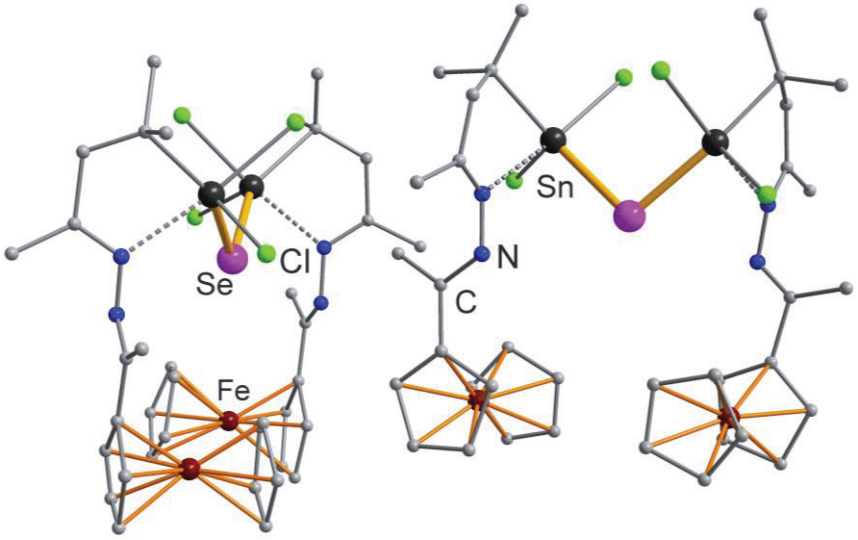

Figure S10. Molecular structures of the two independent molecules in **1**. Solvents and H atoms are omitted for clarity.

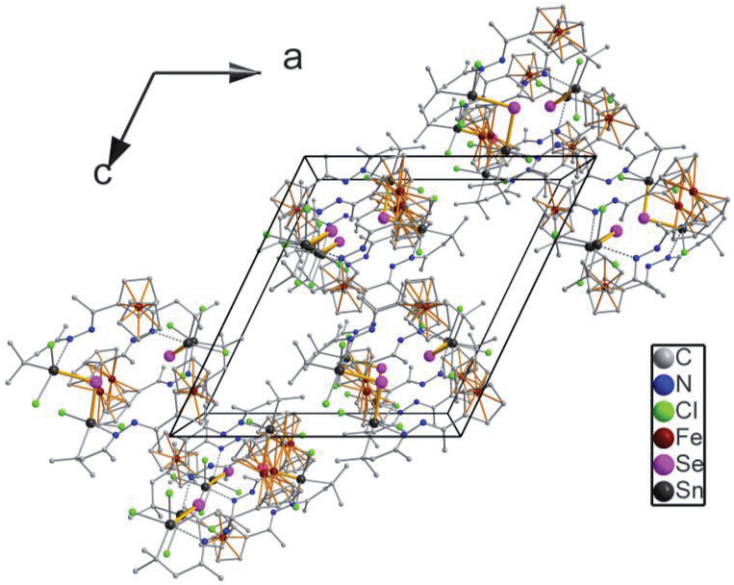

Figure S11. Packing of the molecules of **1** in the crystal, viewed along the crystallographic *b* axis. Solvents and H atoms are omitted for clarity.

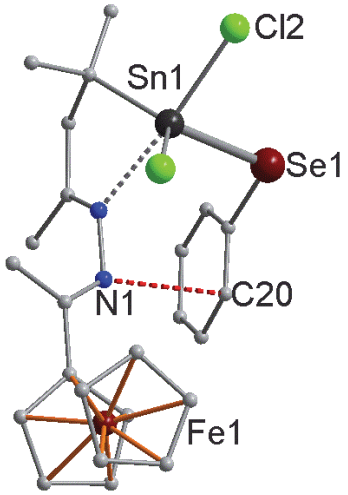

Figure S12. Molecular structure of **2**. Intramolecular hydrogen bond (red dashed lines) between N1 and Ph-ring is illustrated. H atoms are omitted for clarity.

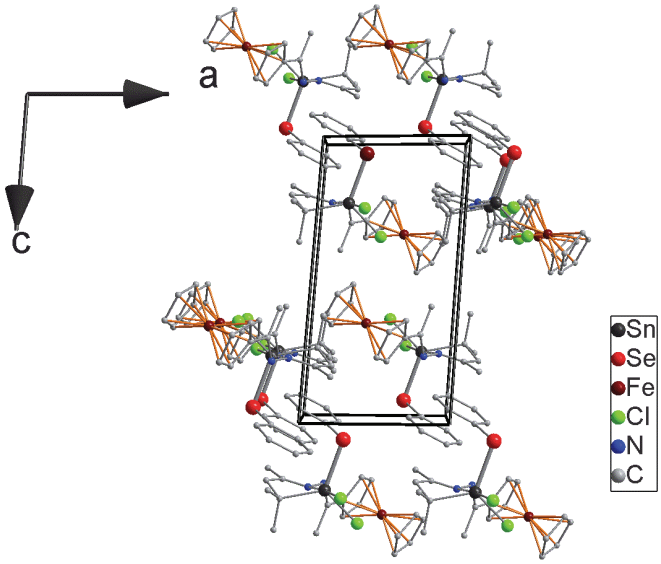

Figure S13. Packing of the molecules of **2** in the crystal, viewed along the crystallographic *b* axis. H atoms are omitted for clarity.

Table S8. Selected bond lengths [Å], bond angles [°] in **2**.

Sn(1)-Se(1)	2.5342(19)	N(2)-Sn(1)-Se(1)	95.2(3)
Sn(1)-Cl(1)	2.362(4)	C(16)-Sn(1)-Cl(1)	123.4(4)
Sn(1)-Cl(2)	2.436(4)	N(2)-Sn(1)-Cl(1)	85.5(3)
Sn(1)-C(16)	2.166(15)	C(16)-Sn(1)-Cl(2)	101.4(4)
Sn(1)-N(2)	2.352(13)	N(2)-Sn(1)-Cl(2)	174.6(3)
Cl(1)-Sn(1)-Se(1)	114.45(11)	Cl(1)-Sn(1)-Cl(2)	92.34(13)
Cl(2)-Sn(1)-Se(1)	90.24(10)	C(16)-Sn(1)-N(2)	75.8(5)
C(16)-Sn(1)-Se(1)	120.1(4)	C(19)-Se(1)-Sn(1)	102.8(4)

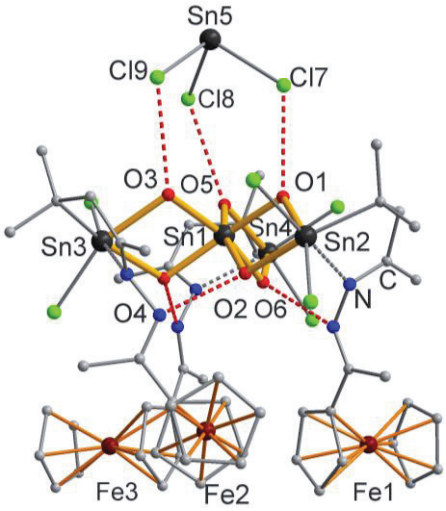

Figure S14. Molecular structure of **3a**. Intramolecular hydrogen bonds are illustrated as red dashed lines. Solvents and H atoms are omitted for clarity.

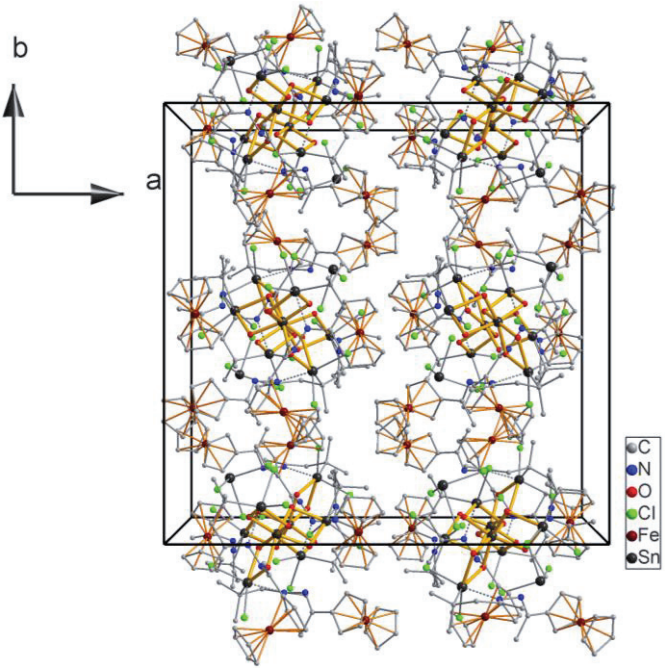

Figure S15. Packing of the molecules of **3a** in the crystal, viewed along the crystallographic *c* axis. Solvents and H atoms are omitted for clarity.

Table S9. Selected bond lengths [Å], bond angles [°] in **3a**.

Sn(1)-O(1)	2.042(6)	Sn(2)-N(2)	2.327(7)
Sn(1)-O(2)	2.047(6)	Sn(3)-N(4)	2.325(7)
Sn(1)-O(3)	2.035(6)	Sn(4)-N(6)	2.334(7)
Sn(1)-O(4)	2.053(5)	N(1)-N(2)	1.407(10)
Sn(1)-O(5)	2.026(6)	N(3)-N(4)	1.405(10)
Sn(1)-O(6)	2.063(5)	N(5)-N(6)	1.424(11)
Sn(2)-O(1)	2.207(6)	O(1)-Sn(1)-O(2)	75.4(2)
Sn(2)-O(2)	2.083(6)	O(3)-Sn(1)-O(4)	75.7(2)
Sn(3)-O(3)	2.229(6)	O(5)-Sn(1)-O(6)	75.4(2)
Sn(3)-O(4)	2.078(6)	O(1)-Sn(2)-O(2)	71.2(2)
Sn(4)-O(5)	2.216(6)	O(3)-Sn(3)-O(4)	71.2(2)
Sn(4)-O(6)	2.072(6)	O(5)-Sn(4)-O(6)	71.2(2)
Sn(2)-Cl(1)	2.394(2)	Cl(1)-Sn(2)-Cl(2)	95.33(8)
Sn(2)-Cl(2)	2.396(2)	Cl(3)-Sn(3)-Cl(4)	95.48(9)
Sn(3)-Cl(3)	2.391(3)	Cl(5)-Sn(4)-Cl(6)	94.26(9)
Sn(3)-Cl(4)	2.418(2)	Cl(8)-Sn(5)-Cl(9)	93.15(10)
Sn(4)-Cl(5)	2.402(2)	Cl(8)-Sn(5)-Cl(7)	93.51(10)
Sn(4)-Cl(6)	2.410(2)	Cl(9)-Sn(5)-Cl(7)	93.22(10)
Sn(5)-Cl(7)	2.472(3)	C(19)-Sn(2)-N(2)	76.7(3)
Sn(5)-Cl(8)	2.465(3)	C(37)-Sn(3)-N(4)	75.8(3)
Sn(5)-Cl(9)	2.471(3)	C(1)-Sn(4)-N(6)	77.1(3)

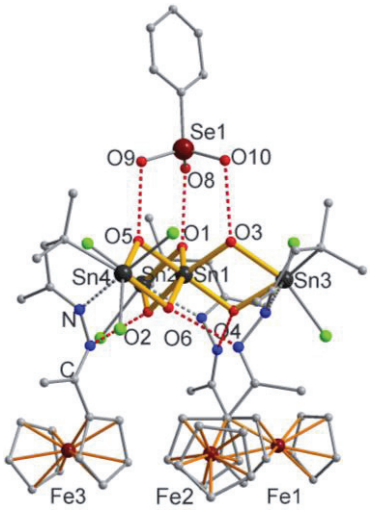

Figure S16. Molecular structure of **3b**. Intramolecular hydrogen bonds are illustrated as red dashed lines. Solvents and H atoms are omitted for clarity.

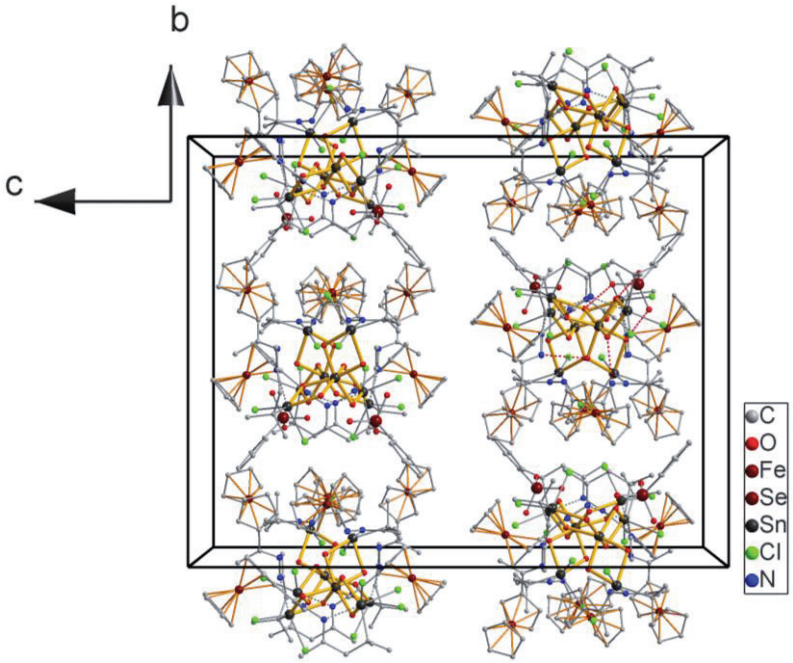

Figure S17. Packing of the molecules of **3b** in the crystal, viewed along the crystallographic *a* axis. Solvents and H atoms are omitted for clarity.

Table S10. Selected bond lengths [Å], bond angles [°] in **3b**.

Sn(1)-O(1)	2.032(5)	Sn(2)-N(2)	2.346(6)
Sn(1)-O(2)	2.058(5)	Sn(3)-N(4)	2.313(6)
Sn(1)-O(3)	2.034(5)	Sn(4)-N(6)	2.339(6)
Sn(1)-O(4)	2.050(5)	N(1)-N(2)	1.407(8)
Sn(1)-O(5)	2.034(5)	N(3)-N(4)	1.415(9)
Sn(1)-O(6)	2.047(5)	N(5)-N(6)	1.413(9)
Sn(2)-O(1)	2.169(5)	O(1)-Sn(1)-O(2)	76.4(2)
Sn(2)-O(2)	2.079(5)	O(3)-Sn(1)-O(4)	76.8(2)
Sn(3)-O(3)	2.186(5)	O(5)-Sn(1)-O(6)	75.88(19)
Sn(3)-O(4)	2.089(5)	O(1)-Sn(2)-O(2)	73.1(2)
Sn(4)-O(5)	2.150(5)	O(3)-Sn(3)-O(4)	72.72(19)
Sn(4)-O(6)	2.076(5)	O(5)-Sn(4)-O(6)	72.82(19)
Sn(2)-Cl(1)	2.398(2)	Cl(1)-Sn(2)-Cl(2)	93.03(8)
Sn(2)-Cl(2)	2.413(2)	Cl(3)-Sn(3)-Cl(4)	94.83(7)
Sn(3)-Cl(3)	2.395(2)	Cl(5)-Sn(4)-Cl(6)	93.01(7)
Sn(3)-Cl(4)	2.414(2)	O(8)-Se(1)-O(10)	109.8(4)
Sn(4)-Cl(5)	2.399(2)	O(9)-Se(1)-O(10)	113.5(4)
Sn(4)-Cl(6)	2.425(2)	O(8)-Se(1)-O(9)	112.7(4)
Se(1)-O(8)	1.625(7)	C(16)-Sn(2)-N(2)	76.0(3)
Se(1)-O(9)	1.638(7)	C(34)-Sn(3)-N(4)	76.6(3)
Se(1)-O(10)	1.624(7)	C(52)-Sn(4)-N(6)	76.9(3)

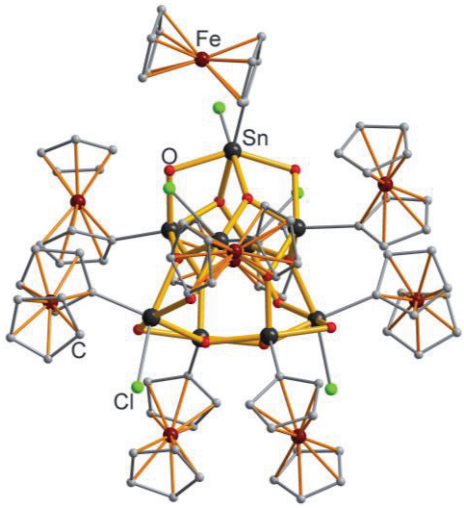

Figure S18. Molecular structure of **4**. Solvents and H atoms are omitted for clarity.

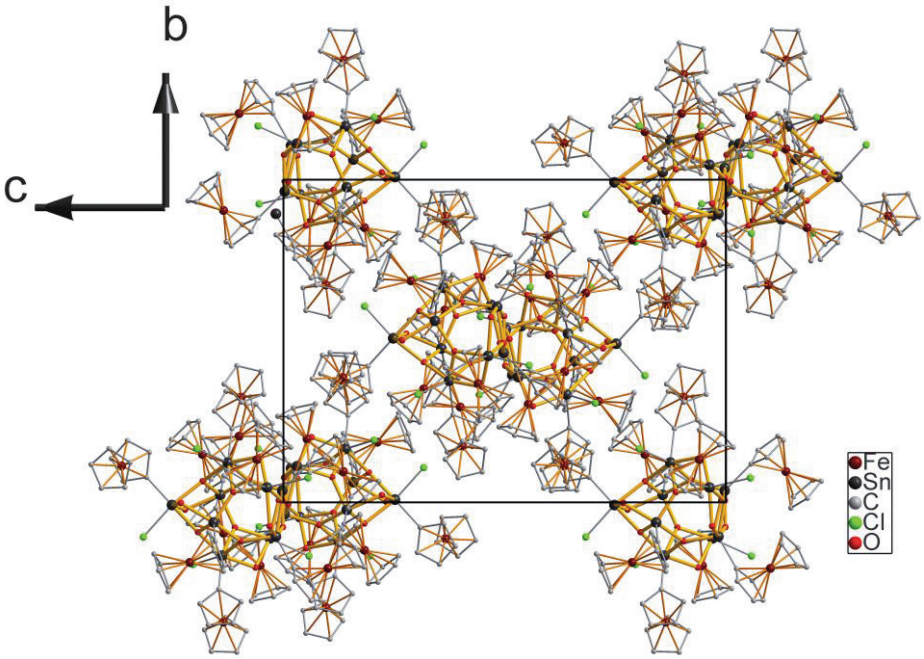

Figure S19. Packing of the molecules of **4** in the crystal, viewed along the crystallographic *a* axis. Solvents and H atoms are omitted for clarity.

Table S11. Selected bond lengths [Å] in **4**.

Sn(1)-O(4)	2.056(6)	Sn(6)-O(12)	2.072(6)
Sn(1)-O(6)	2.086(6)	Sn(6)-O(11)	2.174(6)
Sn(1)-O(1)	2.117(6)	Sn(6)-O(4)	2.185(6)
Sn(1)-O(12)	2.166(6)	Sn(7)-O(2)	2.079(6)
Sn(2)-O(1)	1.977(6)	Sn(7)-O(10)	2.082(6)
Sn(2)-O(2)	2.017(6)	Sn(7)-O(7)	2.155(5)
Sn(2)-O(3)	2.082(6)	Sn(7)-O(9)	2.155(5)
Sn(2)-O(9)	2.135(6)	Sn(8)-O(7)	1.997(5)
Sn(3)-O(8)	1.981(6)	Sn(8)-O(6)	1.998(6)
Sn(3)-O(3)	2.024(6)	Sn(8)-O(1)	2.091(5)
Sn(3)-O(2)	2.084(6)	Sn(8)-O(14)	2.113(5)
Sn(3)-O(11)	2.145(6)	Sn(9)-O(6)	2.117(5)
Sn(4)-O(7)	2.060(5)	Sn(9)-O(13)	2.130(6)
Sn(4)-O(5)	2.071(6)	Sn(9)-O(14)	2.148(6)
Sn(4)-O(8)	2.146(6)	Sn(9)-O(5)	2.162(6)
Sn(4)-O(10)	2.163(6)	Sn(1)-Cl(1)	2.447(2)
Sn(5)-O(4)	1.984(6)	Sn(4)-Cl(2)	2.461(2)
Sn(5)-O(5)	2.009(6)	Sn(6)-Cl(3)	2.411(2)
Sn(5)-O(8)	2.102(6)	Sn(7)-Cl(4)	2.426(2)
Sn(5)-O(13)	2.121(6)	Sn(9)-Cl(5)	2.386(2)
Sn(6)-O(3)	2.064(6)		

Table 12. Different types of Sn atoms in **4**.

Sn type	*c. n.*[a]	*c. s.*[b]	*c. a.*[c]	Sn atom
Sn^{O}	5	trigonal bipyramidal	3 μ_3-O,1 μ-OH	Sn2, Sn3, Sn5, Sn8
Sn_1^{Cl}	6	octahedral	3 μ_3-O,1 μ-OH, 1 Cl	Sn1, Sn4
Sn_2^{Cl}	6	octahedral	2 μ_3-O, 2 μ-OH, 1 Cl	Sn6, Sn7 Sn9

[a] *c. n.*: coordination number; [b] *c. s.*: coordination sphere; [c] *c. a.*: coordination atom and number.

7. References for the Supporting Information:

[1] L. P. Spencer, P. Yang, B. L. Scott, E. R. Batista, J. M. Boncella, *Inorg*. *Chem*. **2009**, *48*, 2693-2700.

[2] C. Pohlker, I. Schellenberg, R. Pottgen, S. Dehnen, *Chem*. *Commun*. **2010**, *46*, 2605-2607.

[3] Z. You, S. Dehnen, *Inorg*. *Chem*. **2013**, *52*, 12332-12334.

[4] J. M. Brown, A. C. Chapman, P. J. Smith, R. Harper, A. G. Davies, D. J. Mowthorp, *J. Chem*. *Soc*. *Dalton Trans*. **1972**, *3*, 338-341.

[5] H. Kriegsmann, H. Hoffmann, S. Pischtschan, *Z*. *Anorg*. *Allg*. *Chem*. **1962**, *315*, 283-290.

[6] H. Puff, I. Bung, E. Friedrichs, A. Jansen, *J*. *Organomet*. *Chem*. **1983**, *254*, 23-32.

[7] C. Belin, M. Chaabouni, J. L. Pascal, J. Potier, J. Roziere, *J*. *Chem*. *Soc*. *Chem*. *Commun*. **1980**, *3*, 105-106.

[8] J. Bodenheimer, E. Loewenthal, W. Low, *Chem*. *Phys*. *Lett*. **1969**, *3*, 715-716.

[9] M. C. Burla, R. Caliandro, M. Camalli, B. Carrozzini, G. L. Cascarano, L. De Caro, C. Giacovazzo, G. Polidori, R. Spagna, *J*. *Appl*. *Crystallogr*. **2005**, *38*, 381-388.

[10] G. M. Sheldrick, (2013). *SHELXL2013*. University of Göttingen, Germany.

[11] S. Parsons and H. Flack, *Acta Cryst.* **2004**, *A60*, 61.

4 Summary and Outlook

In this thesis, two synthetic pathways of attachment of ferrocenyl units to organotin chalcogenide clusters have been introduced with the aim at a deeper understanding and control of the synthesis, reactivity, and structural properties of organo- and organometal-functionalized chalcogenide complexes, and to study the possible physicochemical properties of the resulting hybrid compounds that derive from the combination of chalcogenide complexes or clusters with metallocene decoration or linkage.

The first synthetic access succeeded by extending the organic ligand shell of the well known DD clusters $[(R^fSn)_4S_6]$ (**A**, $R^f = R^2$; **B**, $R^f = R^3$) through condensation reactions with mono- (Fc) and bis-substituted (fC) ferrocenyl ligands, yielding three compounds **DT-1**, **DT-2** and **IC-1** with two types of Sn/S topologies, respectively. The inorganic cores maintained their DD topology in **DT-1** and **DT-2** during the reactions. However, they are slightly different in detail due to the two different modes of linkage, which also cause different electrochemical stabilities of both compounds. Differently, the Sn/S core undergoes a complete re-arrangement into a DSC topology in **IC-1**. The surrounding four Fc units in **IC-1** show different ligand dynamics in solution than in the solid state, as confirmed by NMR spectroscopy, and by CV and DPV. A controlled degradation of **IC-1** was realized by addition of different amounts of HCl, yielding binuclear or mononuclear species **IC-2** and **IC-3**, the latter of which can act as a precursor to formation/recovery of **IC-2** or **IC-1**, respectively (Scheme 4.1).

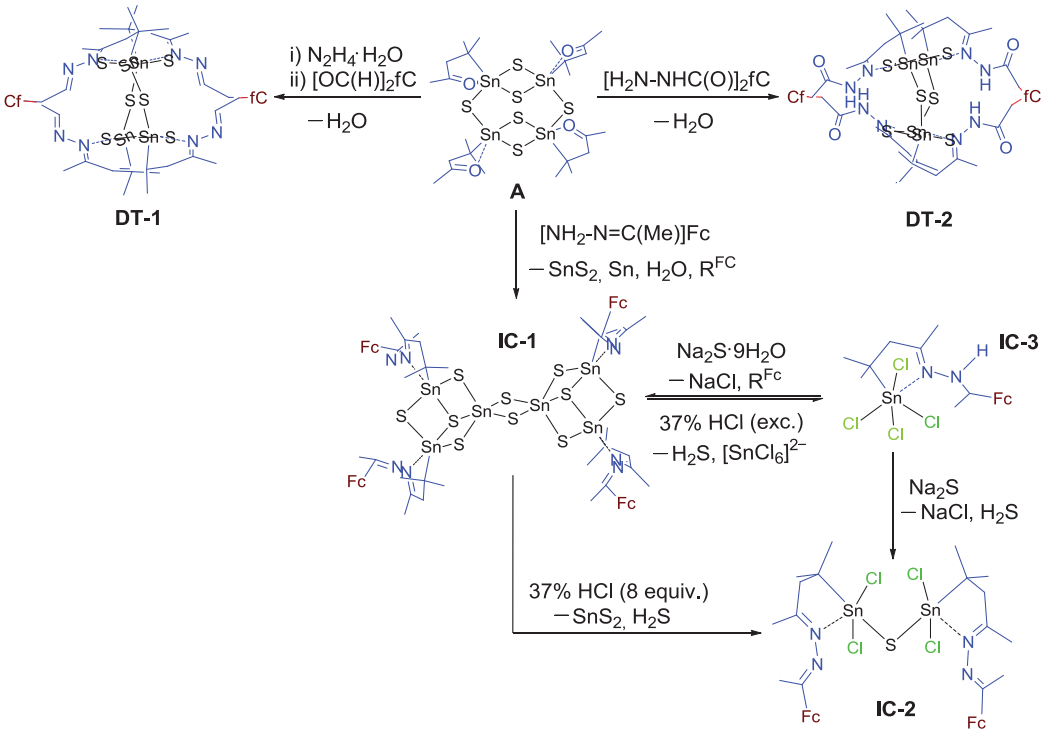

Scheme 4.1 Synthesis of **IC-1** and **DT-(1,2)** with mono- and bis-substituted ferrocenyl units (Fc or fC, respectively). Degradation of **IC-1** to **IC-2** and **IC-3** by HCl addition and formation/recovery of **IC-1** or **IC-2** by reaction of **IC-3** with Na_2S.

The second synthetic approach was the treatment of ferrocenyl-substituted tin trichloride ($FcSnCl_3$) with chalcogenide sources, enabling a direct functionalization of the inorganic core with Fc units. The treatment of $FcSnCl_3$ with the heavier chalcogenides E = Se, Te yielded **S-1**, a homologue of the previously reported AD Sn/S complex $[(FcSn)_4S_6]$[28] and a puckered five-membered Sn/Te ring in **S-2**. An extension of the inorganic core of **S-1** could be realized by treatment with $Na_2S{\cdot}9H_2O$ and ensuing reaction with $[CuCl(PPh_3)_3]$ to form the multinary, Fc-functionalized cluster **S-3** (Scheme 4.2). The optical absorption properties and the electrochemical properties of **S-1**, **S-2** and the afore-synthesized sulfide complex $[(FcSn)_4S_6]$ were examined by means of UV-visible spectroscopy, CV and DPV, and compared with each other. The UV-visible spectra of the three compounds are red-shifted as going from E = S through Se to Te, regarding both the absorption bands of the Fc units, and the bands resulting from p(E)→s,p(Sn) charge transfer despite the structural differences. According with CV and DPV, all three compounds display slight electronic communication of adjacent Fc units, most notably in the case of **S-2** with shortest Fe···Fe distances. ^{119}Sn Mössbauer spectra reflect the different tin sites, while ^{57}Fe Mössbauer spectra point to almost similar electronic situation for all ferrocenyl entities, excluding a direct communication behavior of the $[Sn_4Se_6]$ or $[Sn_3Te_2]$ cores with the metal atom within the ligand.

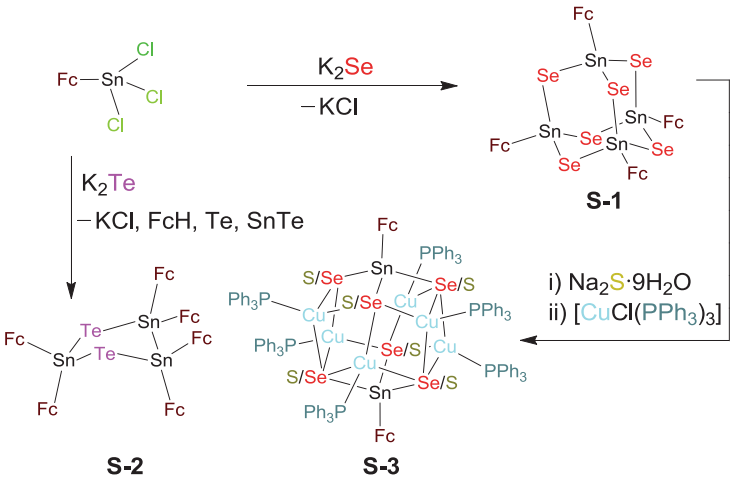

Scheme 4.2 Synthesis of **S-1** and **S-2** by reactions of $FcSnCl_3$ with K_2E (E = Se, Te). By further treatment of **S-1** with $Na_2S{\cdot}9H_2O$ and ensuing reaction with $[Cu(PPh_3)_3Cl]$, the cluster compound **S-3** was obtained.

The two organotin chlorides mentioned above (**IC-3** and $FcSnCl_3$) are suitable precursors for the formation of new types of tinoxide cluster-based multiferrocenyl complexes through hydrolysis reaction. The hydrolysis of **IC-3** in the presence of NaEPh (E = S, Se) and $[SnCl_6]^{2-}$ – either in a one-pot reaction or stepwise *via* mono- and dinuclear compounds **EC-1** and **EC-2** – afforded two screw-shaped multiferrocenyl cations within ionic compounds **EC-3a**,**b** with different counterions, both based on an unprecedented $[Sn_4O_6]$ unit. A corresponding reaction of $FcSnCl_3$ succeeded to

yield a multiferrocenyl compound **EC-4** that represents the largest known Fc-decorated Sn/O cluster, containing nine Fc units on its surface (Scheme 4.3).

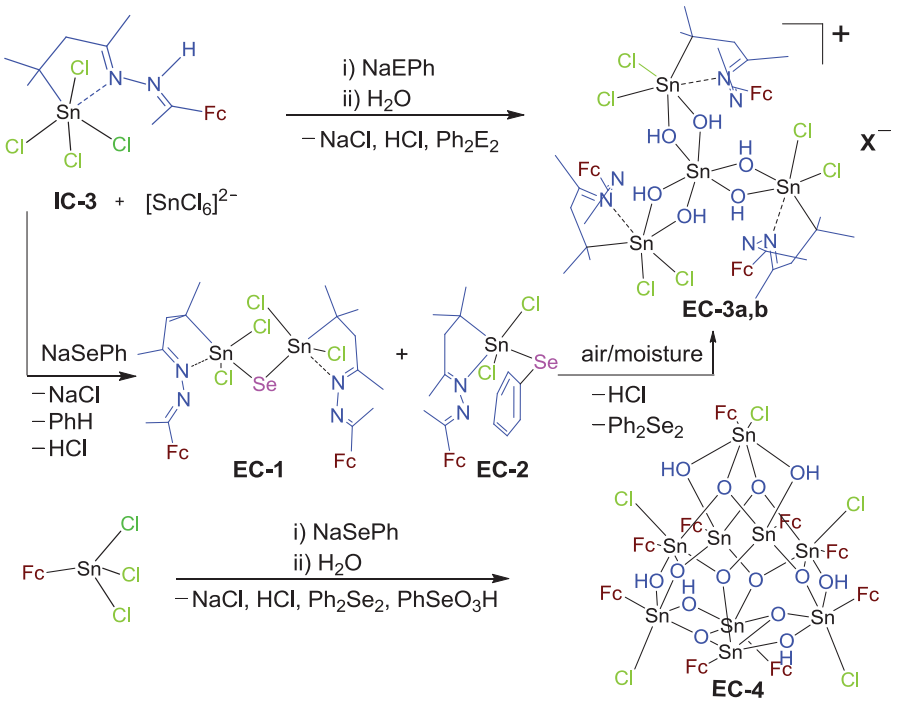

Scheme 4.3 Synthesis of **EC-3a**,**b** by one-pot reaction (top) or stepwise *via* **EC-1** and **EC-2** (center), and formation of **EC-4** in a one-pot reaction starting out from $FcSnCl_3$ (bottom). Fc = ferrocenyl; E = S, Se; X^- = $[SnCl_3]^-$ in **EC-3a**, $[PhSeO_3]^-$ for **EC-3b**.

The results reported herein pointed toward a large synthetic potential of Fc- or fC-decorated Sn/E complexes and clusters. Future investigations may thus focus on further extension of the inorganic cores of the known ferrocenyl-functionalized chalcogenide compounds through reactions with transition metal complexes. It is very probable that the investigation of the physicochemical properties of the resulting compounds will bear many new interesting features.

4 Zusammengfassung

In dieser Arbeit wurden zwei synthesechemische Routen zum Anbinden von Ferrocenyl-Einheiten an Organozinnchalkogenid-Cluster etabliert, um ein tieferes Verständnis bzw. eine bessere Kontrolle über Synthese, Reaktivität und strukturelle Eigenschaften von organo- und organometall-funktionalisierten Chalkogenid-Komplexen zu erlangen. Auch die chemischen und physikalischen Eigenschaften der resultierenden Hybridverbindungen, die sich aus der Kombination von Chalkogenid-Komplexen oder Chalkogenid-Clustern mit Metallocen-Dekorationen oder Metallocen-Linkern ergeben, wurden studiert.

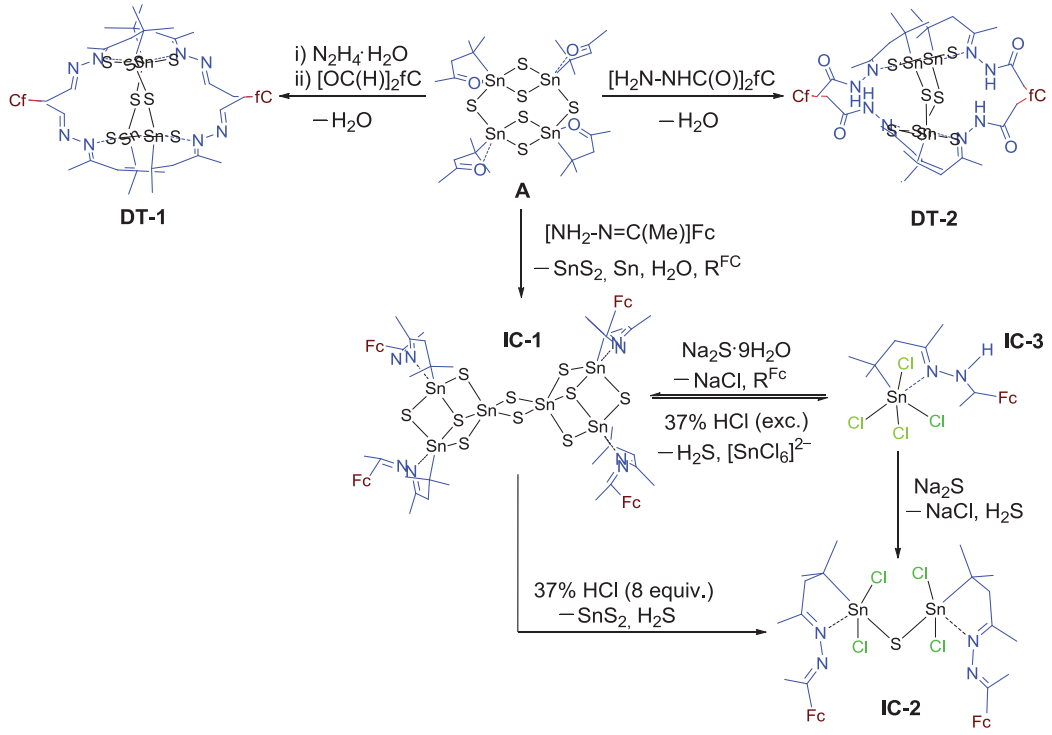

Schema 4.1 Synthese von **IC-1** und **DT-(1,2)** mit mono- (Fc) oder bis-substituierten (fC) Ferrocenyl-Einheiten. Abbau von **IC-1** zu **IC-2** und **IC-3** durch HCl-Zugabe und Bildung/Rückgewinnung von **IC-1** oder **IC-2** durch Umsetzung von **IC-3** mit Na_2S.

Dem ersten der beiden Wege folgend gelang die Einführung von Ferrocenyl-Einheiten durch Erweiterung der organischen Ligandenhülle der bekannten DD-Cluster $[(R^fSn)_4S_6]$ (**A**, $R^f = R^2$, **B**, $R^f = R^3$) in Kondensationsreaktionen mit mono- (Fc) oder bis-substituierten (fC) Ferrocenyl-Liganden. Es wurden die drei Verbindungen **DT-1**, **DT-2** und **IC-1** hergestellt, in denen zwei unterschiedliche Sn/S-Topologien auftreten. Die anorganischen Clusterkerne in **DT-1** und **DT-2** behielten die DD-Topologie während der Reaktionen; aufgrund unterschiedlicher Formen der Verknüpfung mit den Liganden sind beide Cluster jedoch im Detail verschieden, was auch zu unterschiedlichen elektrochemischen Stabilitäten der beiden Verbindungen führt. In **IC-1** hingegen erfuhr der Sn/S-Kern eine komplette Umlagerung zu einer DSC-Topologie. Die vier

umgebenden Fc-Einheiten im **IC-1** zeigen in Lösung und im festen Zustand eine unterschiedliche Ligand-Dynamik auf, was durch NMR-Spektroskopie, und mittels CV- und DPV-Messungen bestätigt werden konnte. Ein kontrollierter Abbau der Verbindung **IC-1** wurde durch die Zugabe unterschiedlicher Mengen von HCl realisiert, wodurch es zur Bildung der zweikernigen bzw. einkernigen Spezies **IC-2** bzw. **IC-3** kam. Letztere Verbindung kann als Präkursor für die Bildung/Rückgewinnung von **IC-2** bzw. **IC-1** fungieren (Schema 4.1).

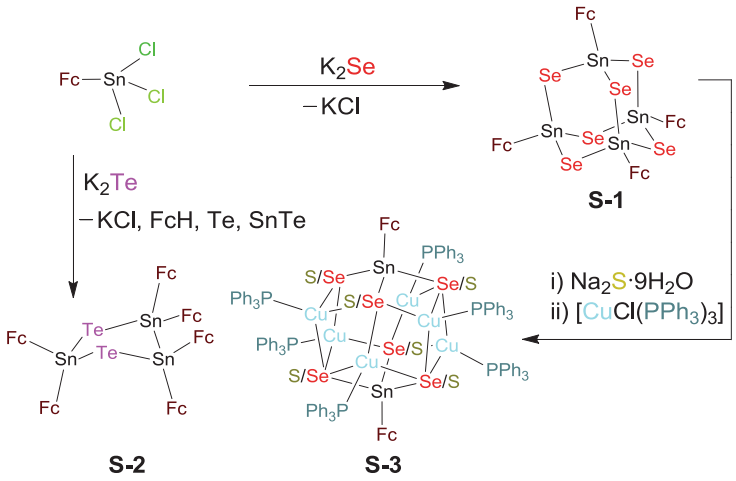

Schema 4.2 Synthese von **S-1** und **S-2** durch Reaktionen von $FcSnCl_3$ (Fc = Ferrocenyl) mit K_2E (E = Se, Te). Durch weitere Umsetzung von **S-1** mit $Na_2S{\cdot}9H_2O$ und anschließender Reaktion mit $[Cu(PPh_3)_3Cl]$ entstand die Clusterverbindung **S-3**.

Bei der zweiten synthesechemischen Route wurde Ferrocenyl-substituiertes Zinntrichlorid ($FcSnCl_3$) direkt mit Chalkogenid-Quellen umgesetzt, so dass eine direkte Funktionalisierung des anorganischen Kerns mit Fc-Einheiten möglich war. Reaktionen von $FcSnCl_3$ mit schwereren Chalkogeniden (E = Se, Te) führten zur Bildung von **S-1**, einer dem zuvor beschriebenen AD-artigen Sn/S-Komplex $[(FcSn)_4S_6]$[28] homologen Verbindung, und zur Bildung eines gewellten, fünfgliedrigen Sn/Te-Rings in **S-2**. Eine Erweiterung des anorganischen Kerns von **S-1** konnte durch Umsetzung mit $Na_2S{\cdot}9H_2O$ und anschließender Reaktion mit $[Cu(PPh_3)_3Cl]$ realisiert werden, wobei der multinäre, Fc-funktionalisierte Cluster **S-3** entstand (Schema 4.2). Die optischen Absorptionseigenschaften und die elektrochemischen Eigenschaften von **S-1**, **S-2** und der zuvor synthetisierten Sulfid-Verbindung $[(FcSn)_4S_6]$ wurden mittels UV-Vis-Spektroskopie, CV- und DPV-Messungen untersucht und miteinander verglichen. Die UV-Vis-Banden der drei Verbindungen werden beim Übergang von E = S über Se zu Te in den roten Spektralbereich verschoben; dies gilt sowohl für die Absorptionsbanden der Fc-Einheiten als auch für die Banden des p(E)→s,p(Sn)-Charge-Transfer-Übergangs – trotz der strukturellen Unterschiede. Gemäß der CV- und DPV-Studien zeigen alle drei Verbindungen eine merkliche elektronische Kommunikation benachbarter Fc-Einheiten, vor allem im Fall von **S-2** mit kürzesten Fe···Fe-Distanzen. ^{119}Sn-

Mössbauer-Spektren spiegeln die unterschiedlichen Positionen der Zinnatome in den Mehrkernkomplexen wider, während ^{57}Fe-Mößbauer-Spektren eine fast gleiche elektronische Situation für alle Fc-Einheiten aufzeigen. Eine direkte Kommunikation der $[Sn_4Se_6]$- oder $[Sn_3Te_2]$-Kerne mit den Metallatomen in den Liganden wurde durch die Untersuchungen weitgehend ausgeschlossen.

Die beiden oben erwähnten Organozinnchloride (**IC-3** und $FcSnCl_3$) sind zudem geeignete Präkursoren für die Bildung neuartiger, Zinnoxid-Cluster-basierter Multiferrocenyl-Komplexe, die über Hydrolysenreaktionen zugänglich sind. Die Hydrolyse von **IC-3** in Gegenwart von NaEPh (E = S, Se) und $[SnCl_6]^{2-}$ – entweder in einer Eintopfreaktion oder schrittweise über die ein- bzw. zweikernigen Verbindungen **EC-1** und **EC-2** – lieferte die beiden ionischen Verbindungen **EC-3a**,**b** mit den gleichen Multiferrocenyl-Kationen neben unterschiedlichen Gegenionen. Die Kationen in **EC-3a**,**b** basieren auf einer ungewöhnlichen, Schaufelrad-artigen $[Sn_4O_6]$-Einheit. Eine entsprechende Reaktion von $FcSnCl_3$ führte zur Bildung der Multiferrocenyl-Verbindung **EC-4**, die den größten bisher bekannten, Fc-dekorierten Sn/O-Cluster mit neun Fc-Einheiten auf der Oberfläche darstellt (Schema 4.3).

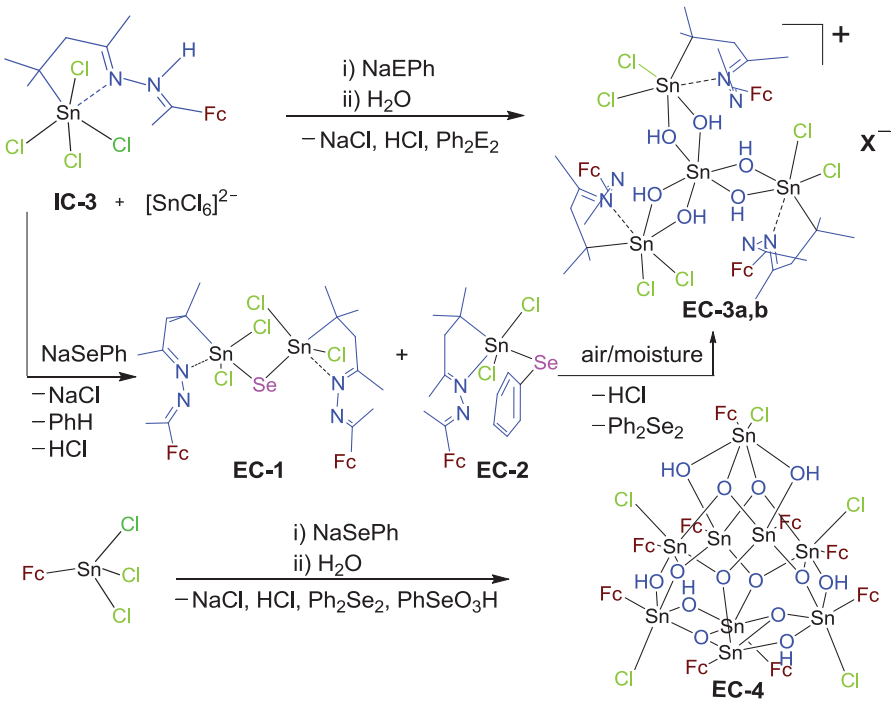

Schema 4.3 Synthese von **EC-3a**,**b** durch Eintopfreaktion (oben) oder schrittweise über **EC-1** und **EC-2** (Mitte), und die Bildung von **EC-4** in einer Eintopfreaktion ausgehend von $FcSnCl_3$ (unten). Fc = Ferrocenyl; E = S, Se; X = $[SnCl_3]^-$ in **EC-3a**, $[PhSeO_3]^-$ für **EC-3b**.

Die Ergebnisse, über die hier berichtet wurde, zeigen eine große Vielfalt von Fc- oder fC-dekorierten Sn/E-Komplexen und Sn/E-Clustern auf. Zukünftige Untersuchungen können auf dem

benannten Synthesepotential der verschiedenen Präkursoren und der Produkte selbst aufbauen. So ist beispielsweise zu erwarten, dass durch weitere Reaktionen mit Übergangsmetallkomplexen neue und noch komplexere Erweiterungen der anorganischen Clusterkerne dieser Ferrocenyl-funktionalisierten Chalkogenid-Verbindungen möglich sind. Es ist sehr wahrscheinlich, dass auch die Untersuchung der physikalischen und chemischen Eigenschaften der so zu erhaltenen Verbindungen noch viele weitere interessante Erkenntnisse hervorbringen wird.

5 References

[1] a) Yuhas, B. D.; Smeigh, A. L.; Samuel, A. P. S.; Shim, Y.; Bag, S.; Douvalis, A. P.; Wasielewski, M. R.; Kanatzidis, M. G. *J. Am. Chem. Soc.* **2011**, *133*, 7252. b) Yuhas, B. D.; Prasittichai, C.; Hupp, J. T.; Kanatzidis, M. G. *J. Am. Chem. Soc.* **2011**, *133*, 15854. c) Devika, M.; Reddy, K. T. R.; Reddy, N. K.; Ramesh, K.; Ganesan, R.; Gopal, E. S. R.; Gunasekhar, K. R. *J. Appl. Phys.* **2006**, *100*, 023518-1. d) Llanos, J.; Mujica, C.; Sanchez, V.; Pena, O. *J. Solid State Chem.* **2003**, *173*, 78. e) Evenson, C. R.; Dorhout, P. K. *Z. Anorg. Allg. Chem.* **2001**, *627*, 2178. f) Gitzendanner, R. L.; DiSalvo, F. J. *Inorg. Chem.* **1996**, *35*, 2623. g) Bowes, C. L.; Ozin, G. A. *Adv. Mater.* **1996**, *8*, 13. h) Parise, J. B.; Ko, Y. H.; Rijssenbeek, J.; Nellis, D. M.; Tan, K. M.; Koch, S. *J. Chem. Soc., Chem. Comm.* **1994**, *4*, 527.

[2] a) Sheldrick, W. S.; Wachhold, M. *Coord. Chem. Rev.* **1998**, *176*, 211. b) Sheldrick, W. S.; Wachhold, M. *Angew. Chem., Int. Ed.* **1997**, *36*, 207. c) Krebs, B. *Angew. Chem. Int. Ed.* **1983**, *22*, 113.

[3] a) Heine, J.; Dehnen, S. *Z. Anorg. Allg. Chem.* **2012**, *638*, 2425. b) Haddadpour, S.; Melullis, M.; Staesche, H.; Mariappan, C. R.; Roling, B.; Clérac, R.; Dehnen, S. *Inorg. Chem.* **2009**, *48*, 1689. c) Tsamourtzi, K.; Song, J. H.; Bakas, T.; Freeman, A. J.; Trikalitis, P. N.; Kanatzidis, M. G. *Inorg. Chem.* **2008**, *47*, 11920. d) Dehnen, S.; Melullis, M. *Coord. Chem. Rev.* **2007**, *251*, 1259.

[4] a) Jiang, T.; Lough, A.; Ozin, G. A.; Bedard, R. L.; Broach, R. *J. Mater. Chem.* **1998**, *8*, 721. b) Jiang, T.; Lough, A.; Ozin, G. A.; Bedard, R. L.; Broach, R. *J. Mater. Chem.* **1998**, *8*, 721.

[5] Ding, N.; Kanatzidis, M. G. *Nat. Chem.* **2010**, *2*, 187.

[6] Cooper, E. R.; Andrews, C. D.; Wheatley, P. S.; Webb, P. B.; Wormald, P.; Morris, R. E. *Nature* **2004**, *430*, 1012.

[7] Lin, Z. J.; Wragg, D. S.; Warren, J. E.; Morris, R. E. *J. Am. Chem. Soc.* **2007**, *129*, 10334.

[8] Guloy, A. M.; Ramlau, R.; Tang, Z. J.; Schnelle, W.; Baitinger, M.; Grin, Y. *Nature* **2006**, *443*, 320.

[9] Lin, Y. M.; Massa, W.; Dehnen, S. *J. Am. Chem. Soc.* **2012**, *134*, 4497.

[10] a) Bag, S.; Trikalitis, P. N.; Chupas, P. J.; Armatas, G. S.; Kanatzidis, M. G. *Science* **2007**, *317*, 490. b) Yaghi, O. M.; Sun, Z.; Richardson, D. A.; Groy, T. L. *J. Am. Chem. Soc.* **1994**, *116*, 807.

[11] a) Chen, X.; Huang, X. Y.; Fu, A. H.; Li, J.; Zhang, L. D.; Guo, H. Y. *Chem. Mater.* **2000**, *12*, 2385. b) Albertelli, G. D.; Cowen, J. A.; Hoff, C. N.; Kaplan, T. A.; Mahanti, S. D.; Liao, J. H.; Kanatzidis, M. G. *Phys. Rev.* B **1997**, *55*, 11056.

[12] a) Ruzin, E.; Fuchs, A.; Dehnen, S. *Chem. Commun.* **2006**, *46*, 4796. b) Zimmermann, C.; Anson, C. E.; Weigend, F.; Clérac, R.; Dehnen, S. *Inorg. Chem.* **2005**, 44, 5686. c) Brandmayer, M. K.; Clérac, R.; Weigend, F.; Dehnen, S. *Chem. -Eur. J.* **2004**, *10*, 5147.

[13] a) Halvagar, M. R.; Fard, Z. H.; Dehnen, S. *Chem. -Eur. J.* **2011**, *17*, 4371. b) Fard, Z. H.; Halvagar, M. R.; Dehnen, S. *J. Am. Chem. Soc.* **2010**, *132*, 2848. c) Halvagar, M. R.; Fard, Z. H.; Xiong, L.; Dehnen, S. *Inorg. Chem.* **2009**, *48*, 7373. d) Fard, Z. H.; Xiong, L.; Müller, C.; Hołyńska, M.; Dehnen, S. *Chem. -Eur. J.* **2009**, *15*, 6595.

[14] a) Hauser, R.; Merzweiler, K. *Z. Anorg. Allg. Chem.* **2002**, *628*, 905. b) Dorfelt, C.; Janeck, A.; Kobelt, D.; Paulus, E. F.; Scherer, H. *J. Organomet. Chem.* **1968**, *14*, 22.

[15] Unno, M.; Kawai, Y.; Shioyama, H.; Matsumoto, H. *Organometallics* **1997**, *16*, 4428.

[16] a) Eussner, J. P.; Barth, B. E. K.; Leusmann, E.; You, Z.; Rinn, N.; Dehnen, S. *Chem. -Eur. J.* **2013**, *19*, 13792. b) Fard, Z. H.; Müller, C.; Harmening, T.; Pottgen, R.; Dehnen, S. *Angew. Chem. Int. Ed.* **2009**, *48*, 4441.

[17] Heimann, S.; Hołyńska, M.; Dehnen, S. *Chem. Commun.* **2011**, *47*, 1881.

[18] Fard, Z. H.; Clérac, R.; Dehnen, S. *Chem. -Eur. J.* **2010**, *16*, 2050.

[19] a) Tranchemontagne, D. J.; Mendoza-Cortes, J. L.; O'Keeffe, M.; Yaghi, O. M. *Chem. Soc. Rev.* **2009**, *38*, 1257. b) Czaja, A. U.; Trukhan, N.; Muller, U. *Chem. Soc. Rev.* **2009**, *38*, 1284. c) Britt, D.; Tranchemontagne, D.; Yaghi, O. M. *Abstr. Pap. Am. Chem. Soc.* **2009**, *237*, 0065-7727. d) Dinca, M.; Long, J. R. *Angew. Chem., Int. Ed.* 2008, 47, 6766. e) Feng, P. Y.; Bu, X. H.; Zheng, N. F. *Acc. Chem. Res.* **2005**, *38*, 293. f) Zheng, N. F.; Bu, X. H.; Feng, P. Y. *Nature* **2003**, *426*, 428. h) Zheng, N. *Science* **2003**, *299*, 1015. l) Yaghi, O. M.; Li, H. L.; Davis, C.; Richardson, D.; Groy, T. L. *Acc. Chem. Res.* **1998**, *31*, 474. m) Yaghi, O. M.; Li, H. L.; Davis, C.; Richardson, D.; Groy, T. L. *Acc. Chem. Res.* **1998**, *31*, 474. n) Murray, C. B.; Kagan, C. R.; Bawendi, M. G. *Science* **1995**, *270*, 1335.

[20] Zheng, S. T.; Zhang, H.; Yang, G. Y. *Angew. Chem. Int. Ed.* **2008**, *47*, 3909.

[21] Zheng, N. F.; Bu, X. H.; Lauda, J.; Feng, P. Y. *Chem. Mater.* **2006**, *18*, 4307.

[22] Togni, A.; Hayashi, T. in *Ferrocenes: Homogeneous Catalysisi, Organic Synthesis, Materials Science* Wiley-VCH, New York, 1st. ed., **1995**.

[23] Li, M. X.; Cai, P.; Duan, C. Y.; Lu, F.; Xie, J.; Meng, Q. J. *Inorg. Chem.* **2004**, *43*, 5174.

[24] Chandrasekhar, V.; Thirumoorthi, R. *Dalton Trans.* **2010**, *39*, 2684.

[25] Kang, J. H.; Nelson, J. A.; Lu, M.; Xie, B. H.; Peng, Z. H.; Powell, D. R. *Inorg. Chem.* **2004**, *43*, 6408.

[26] a) Zheng, G. L.; Ma, J. F.; Su, Z. M.; Yan, L. K.; Yang, J.; Li, Y. Y.; Liu, J. F. *Angew. Chem. Int. Ed.* **2004**, *43*, 2409. b) Chandrasekhar, V.; Nagendran, S.; Bansal, S.; Kozee, M. A.; Powell, D. R. *Angew. Chem. Int. Ed.* **2000**, *39*, *12*, 1833.

[27] a) Ahmar, S.; MacDonald, D. G.; Vijayaratnam, N.; Battista, T. L.; Workentin, M. S.; Corrigan, J. F. *Angew*. *Chem*. *Int*. *Ed*. **2010**, *49*, 4422. b) Lebold, T. P.; Stringle, D. L. B.; Workentin, M. S.; Corrigan, J. F. *Chem*. *Commun*. **2003**, 1398.

[28] Dehnen, S.; Pöhlker, C.; Schellenberg, I.; Pöttgen, R. *Chem*. *Commun*. **2010**, *46*, 2605.

[29] Osborne, A. G.; daSilva, M. W.; Hursthouse, M. B.; Malik, K. M. A.; Opromolla, G.; Zanello, P. *J*. *Organomet*. *Chem*. **1996**, *516*, 167.

[30] a) Top, S.; Vessieres, A.; Jaouen, G. *J*. *Chem*. *Soc*., *Chem*. *Comm*. **1994**, *4*, 453. b) Song, Q. B.; Lu, Z. L.; Wu, X. L.; Ma, Y. X. *Transit*. *Metal*. *Chem*. **1994**, *19*, 503.

[31] Connell, A.; Holliman, P. J.; Butler, I. R.; Male, L.; Coles, S. J.; Horton, P. N.; Hursthouse, M. B.; Clegg, W.; Russo, L. *J*. *Organomet*. *Chem*. **2009**, *694*, 2020.

[32] a) Dakternieks, D.; Zobel, B. *Organometallics* **2003**, *22*, 1343; b) Beckmann, J.; Henn, M.; Jurkschat, K.; Schürmann, M. *Organometallics* **2002**, *22*, 192; c) Janssen, J.; Magull, J.; Roesky, H. W. *Angew*. *Chem*. **2002**, *114*, 1425; *Angew*. *Chem*. *Int*. *Ed*. **2002**, *41*, 1365; d) Beckmann, J.; Jurkschat, K.; Rabe, S.; Schürmann, M. *Z. Anorga. Allg. Chem.* **2001**, *627*, 2413; e) Edelman, M. A.; Hitchcock, P. B.; Lappert, M. F.; *J*. *Chem*. *Soc*., *Chem*. *Comm*. **1990**, *16*, 1116; f) Puff, H.; Reuter, H. *J*. *Organomet*. *Chem*. **1989**, *364*, 57; g) Puff, H.; Schuh, W.; Sievers, R.; Wald, W.; Zimmer, R. *J*. *Organomet*. *Chem*. **1984**, *260*, 271; h) Masamune, S.; Sita, L. R.; Williams, D. J. *J*. *Am*. *Chem*. *Soc*. **1983**, *105*, 630; i) Belsky, V. K.; Zemlyansky, N. N.; Borisova, I. V.; Kolosova, N. D.; Beletskaya, I. P. *J*. *Organomet*. *Chem*. **1983**, *254*, 189; j) Puff, H.; Schuh, W.; Sievers, R.; Zimmer, R. *Angew*. *Chem*. **1981**, *93*, 622; *Angew*. *Chem*. *Int*. *Ed*. **1981**, *20*, 591.

[33] Zobel, B.; Schürmann, M.; Jurkschat, K.; Dakternieks, D.; Duthie, A. *Organometallics* **1998**, *17*, 4096.

[34] a) Beckmann, J.; Dakternieks, D.; Duthie, A.; Kuan, F. S.; Jurkschat, K.; Schürmann, M.; Tiekink, E. R. T. *New J. Chem*. **2004**, *28*, 1268; b) Dakternieks, D.; Duthie, A.; Zobel, B. *Organometallics* **2002**, *21*, 647; c) Schulte, M.; Schürmann, M.; Dakternieks, D.; Jurkschat, K. *Chem*. *Commun*. **1999**, *14*, 1291; d) Mehring, M.; Schürmann, M.; Paulus, I.; Horn, D.; Jurkschat, K.; Orita, A.; Otera, J.; Dakternieks, D.; Duthie, A. *J*. *Organomet*. *Chem.* **1999**, *574*, 176; e) Mehring, M.; Schürmann, M.; Reuter, H.; Dakternieks, D.; Jurkschat, K. *Angew*. *Chem*. **1997**, *109*, 1150; *Angew*. *Chem*. *Int*. *Ed*. **1997**, *36*, 1112; f) Hill, M.; Mahon, M. F.; Molloy, K. C. *Main Group Chem*. **1996**, *1*, 309; g) Vollano, J. F.; Day, R. O.; Holmes, R. R. *Organometallics* **1984**, *3*, 745; h) Matsuda, H.; Matsuda, S.; Kasai, N.; Kashiwa, A.; Jitsumor, K; Mori, F. *J*. *Organomet*. *Chem*. **1972**, *34*, 341.

[35] Puff, H.; Reuter, H. *J*. *Organomet*. *Chem*. **1989**, *368*, 173.

[36] Puff, H.; Reuter, H. *J*. *Organomet*. *Chem*. **1989**, *373*, 173.

[37] a) Jaumier, P.; Jousseaume, B.; Lahcini, M.; Ribot, F.; Sanchez, C. *Chem*. *Commun*. **1998**, *3*, 369; b) Banse, F.; Ribot, F.; Toledano, P.; Maquet, J.; Sanchez, C. *Inorg*. *Chem*. **1995**, *34*, 6371.

[38] Davies, A.; Gielen, M.; Pannell, K. H.; Tiekink, E. R. in *Tin Chemistry*: *Fundamentals, Frontiers, and Applications*, John Wiley & Sons Ltd., Chichester, **2008**, pp. 69-90.

6 Acknowledgments

The research presented in this thesis would not have been possible without the generous help and support of many people. In this section I would like to thank and acknowledge all of them.

Firstly, I would like to thank my supervisor Prof. Dr. Stefanie Dehnen for her intellectual and professional guidance, for the opportunity to work in an exciting research group, for introducing me to the preparation of scientific manuscripts, and especially for allowing me a large degree of independence and creative freedom to explore a wide range of synthetic aspirations.

I am grateful to Prof. Dr. Jörg Sundermeyer, who commented on my research and reviewed the thesis. For all the productive discussions and supports for the difficult time at the beginning of my Ph.D. I am thankful to Dr. Reza Halvagar and Dr. Zohreh Hassanzadeh Fard. Furthermore, I would also like to express my thanks to all colleagues, external collaborators and students, for support and approval of this thesis:

Dr. Małgorzata Hołyńska and Dr. Klaus Harms for helping me at crystal structure analyses and Michael Marsch and Radostan Riedel for collecting single crystal data.

Dr. Istemi Kuzu, who provided me with valuable Raman spectroscopy analyses.

The NMR department, especially Cornelia Mischke, for help with the measurements.

Dr. Yumei Lin and Michael Hellwig for teaching me how to measure EDX.

The ESI-MS department for help with the measurements.

Collaborators Prof. Dr. Rainer Pöttgen and Birgit Gerke from Universität Münster for the Mössbauer measurements and Prof. Dr. Dieter Fenske from KIT for external XRD measurement.

Students, especially Robert Möckel and Jakob Bergunde, for their valuable contributions to the experimental work.

Surely, also Frau Ursula Siepe for her appreciated help, and all the group members of AK Dehnen.

I wish to thank all my friends for we got to know each other in Marburg, for all the help and nice moments.

Finally, loving thanks to my parents and whole my family for the endless, groundless support and caring.

Lebenslauf

Zhiliang You

Persönliches

Studium

07/2010 – 12/2014 **Promotion am Fachbereich Chemie der Philipps-Universität Marburg**

- Titel der Promotion: Untersuchungen Ferrocenyl-funktionalisierter Organozinnchalkogenid und -oxid Komplexes
- Betreuer: Prof. Dr. Stefanie Dehnen
- Note: **1,2**

10/2005 – 03/2010 **Diplomstudiengang in Chemie, Philipps-Universität Marburg**

- Makromolekulare Chemie als Wahlpflichtfach
- Titel der Diplomarbeit: Synthese und Charakterisierung Ferrocenyl-substituierter und Ferrocenyl-verbrückter Organozinnsulfid-Komplexe
- Betreuer: Prof. Dr. Stefanie Dehnen

10/2004 – 09/2005 **Sprachkurs an der Universität Erfurt**
Deutsch Sprachprüfung für den Hochschulzugang (DSH)

09/2000 – 07/2004 **Bachelorstudiengang Chemietechnik und -technologie**
Universität für Forstwirtschaft Nanjing, China

- Titel der Bachelorarbeit (**mit Auszeichnung**): Studie zur Synthese von Polyphenol-Epoxidharz aus Gallussäure
- Betreuer:
  Prof. Dr. Xin-nan An (Universität für Forstwirtschaft Nanjing)
  Dr. Zhen-wu Kong (Institut für Chemische Industrie der Forstprodukts)

Berufliche Qualifikation

07/2010 - 10/2014 **Wissenschaftlicher Mitarbeiter der Philipps-Universität Marburg**

- Verantwortung für elektrochemische Analysen in der Arbeitsgruppe
- Betreuung von Praktikanten im Masterstudium und Studierenden im Rahmen des Grundpraktikums am Fachbereich Chemie der Philipps-Universität Marburg

04/2013 **Teilnahme am Fortbildungstag der DECHEMA:**

- Cyclovoltammetrie, Grundlagen, Interpretation und Fehlerquellen

Vorträge und Posterpräsentationen

07/2014 **Vortrag:**
Mitarbeiterseminar für Arbeitsgruppen der Anorganischen Chemie,
Philipps-Universität Marburg
Titel: Ferrocenyl-Functionalized Organotin Chalcogenide and Oxide Complexes

07/2013	**Posterpräsentation:** 14th International Conference on the Coordination and Organometallic Chemistry of Germanium, Tin and Lead / ICCOC-GTL2013 in Baddeck, Cape Breton, Nova Scotia, Canada
09/2012	**Teilnahme und Posterpräsentation:** 16. Vortragstagung der Wöhler-Vereinigung, Göttingen
08/2011	**Teilnahme und Vortrag:** Wisschenschaftliches Kolloquium für Arbeitsgruppen der Anorganischen Chemie, Hirschegg, Österreich Titel: The Modification of Organotin Sulfide Compounds with Mono- and Disubstituted Ferrocenyl-Ligands
09/2011	**Teilnahme und Posterpräsentation:** 8th International Conference on Inorganic Chemistry AGICHEM 2011 Heidelberg
09/2010	**Teilnahme an der Veranstaltung:** 150. Weltkongress der Chemie in Karlsruhe

Zusätzliche Qualifikationen

Sprachen	**Chinesisch**: Muttersprache **Deutsch**: verhandlungssicher **Englisch**: konversationssicher
EDV	**Microsoft Office**: gut **NMR-Software Topspin**: gut **XRD-Software, z.B X-Area, WinGx, ShelXTL und Diamond**: sehr gut

Persönliches

Ich bin	positiv, sportlich, fleißig, leistungsbereit, begeisterungsfähig und hilfsbereit.
Ich Kann	Probleme lösen, präsentieren, kommunizieren, Kompromisse eingehen, unterstützen und Hilfestellung leisten, analytisch denken, mich in neue oder fremde Aufgabenstellungen schnell einarbeiten, ein Team führen, im Team arbeiten, Leistungen anderer anerkennen, aus Niederlagen lernen, Menschen ein- und wertschätzen, Entscheidungen treffen und dafür Verantwortung übernehmen.

Publikationen

1. Z. W. Kong,* H. Huang, **Z. You**, X. N. An, "Study on synthesis of polyphenol type epoxy resin from gallic acid", *Chemistry and Industry of Forest Products* **2005**, *25*, 33.
2. **Z. You**, D. Fenske, S. Dehnen,* "Modification of Sn/S cages with bisfunctional ferrocenyl ligands", *Dalton Trans.* **2013**, *42*, 8179 (**Front Cover**).
3. J. P. Eußner, B. E. K. Barth, E. Leusmann, **Z. You**, N. Rinn, S. Dehnen,* "Functionalized organotin chalcogenide complexes exhibiting defect-heterocubane scaffolds: formation, synthesis and characterization", *Chem. Eur. J.* **2013**, *19*, 13792.
4. **Z. You**, S. Dehnen,* "Directed formation of a ferrocenyl-decorated organotin sulfide complex, its controlled degradation", *Inorg*. *Chem*. **2013**, *52*, 12332.
5. **Z. You**, R. Möckel, J. Bergunde, S. Dehnen,* "Organotin-oxido cluster-based multiferrocenyl complexes by hydrolysis of ferrocenyl-functionalized organotin chlorides", *Chem. Eur. J.* **2014**, *20*, 13491.
6. **Z. You**, J. Bergunde, B. Gerke, R. Pöttgen, S. Dehnen,* "Ferrocenyl-functionalized Sn/Se and Sn/Te complexes: synthesis, reactivity, optical and electronic properties", *Inorg*. *Chem*. **2014**, *53*, 12512.
7. G. Thiele, **Z. You**, S. Dehnen,* "Molecular chevrel-like clusters $[(RhPPh_3)_6Se_8]$ and $[Pd_6Te_8]^{4-}$", **2014**, *submitted.*
8. K. M. Poole, M. Korabik, A. Fournet, M. Shiddiq, **Z. You**, G. Christou, S. Hill and M. Hołyńska,* "A new offset isomer of the classical oxime-bridged $[Mn^{III}_6]$ SMMs", **2014**, *submitted*.
9. **Z. You**, K. Harms, S. Dehnen,* "Acid or base induced re-arrangments of ferrrocenyl-decorated organotin sulfide cages", **2014**, *in preparation*.
10. **Z. You**, S. Dehnen,* "Solvents-dependent syntheses to a series of ferrocenyl-terminated Sn/Se compounds", **2014**, *in preparation*.

Marburg, 5. Januar 2015